

STABLE AND METASTABLE SOLIDIFICATION

OF CAST IRON

A thesis submitted in supplication

for the degree of

DOCTOR OF PHILOSOPHY

by

STEPHEN BRUCE JONES, B.Sc.

DEPARTMENT OF INDUSTRIAL METALLURGY

UNIVERSITY OF BIRMINGHAM

October 1971.

UNIVERSITY OF  
BIRMINGHAM

**University of Birmingham Research Archive**

**e-theses repository**

This unpublished thesis/dissertation is copyright of the author and/or third parties. The intellectual property rights of the author or third parties in respect of this work are as defined by The Copyright Designs and Patents Act 1988 or as modified by any successor legislation.

Any use made of information contained in this thesis/dissertation must be in accordance with that legislation and must be properly acknowledged. Further distribution or reproduction in any format is prohibited without the permission of the copyright holder.

## SYNOPSIS

The stable to metastable eutectic transition was studied in three cast irons with carbon equivalents of 4.0 and silicon contents of 1.00%, 2.04% and 2.43%. Castings were produced in sand moulds containing a solid steel chill as well as in heated and unheated ceramic moulds, cooled at one end by a water cooled copper chill. Structural variations obtained were analysed with reference to physical conditions of cooling within the castings and compositional differences between the alloys.

Transformations in white and mottled structures during freezing or near the freezing temperature were studied by rapid solidification and isothermal treatments in heated metal moulds. Castings produced in a polished copper chill mould had plane surfaces enabling study of nucleation and growth processes under chill conditions. The 2.04% Si alloy was used as a base for the addition of a range of pure elements to study structural variations in heated ceramic mould castings.

Thermal analysis, macrostructures and microstructural examinations indicate that metastable eutectic may partly or fully decompose during the cooling of a casting. Microstructural examinations by optical and scanning electron microscopes provide evidence of such decomposition. Etching in alkaline sodium picrate or bromine solution was found valuable for this purpose.

Amounts of carbide decomposition increased with increasing silicon content and transformation temperature, and decreased as post-solidification cooling rates increased. Solidification of hypoeutectic alloys at chill surfaces may produce areas containing primary cementite needles.

## ACKNOWLEDGEMENTS

The author wishes to thank Professor E.C. Rollason for providing the facilities of the Aitchison Laboratories, and Dr. V. Kondic for the encouragement and guidance given under his supervision.

Acknowledgements are also due to the Science Research Council for financial support and to the British Cast Iron Research Association for their supply and analysis of the alloys used as melting stock. The author wishes to thank the staff and students of the Department of Industrial Metallurgy for many valuable discussions during the course of this investigation.

Finally, sincere thanks are due to Mrs. P.A. Jones and Mrs. M.L. Spriggs for their help in the preparation and typing of this thesis.

# C O N T E N T S

<u>Section</u>		<u>Page</u>
1	INTRODUCTION	
2	REVIEW OF PREVIOUS WORK	1
2.1	Stable and Metastable Equilibria	1
2.2	The Nature of Liquid Cast Iron	3
2.3	Nucleation in Cast Irons	5
2.4	Growth in Cast Irons	7
2.5	The Iron-Graphite Stable Eutectic System	9
	2.5.1 Crystal Structure and Morphology of Graphite	
	2.5.2 Stable Eutectic Formation	10
2.6	The Metastable Eutectic System	14
	2.6.1 Cementite Crystal Structure	14
	2.6.2 Metastable Eutectic Structure and Growth	15
2.7	Mottled Structures	17
2.8	Indirect Graphite Formation	19
2.9	Conclusions and Outline of the Present Work	24
3	EXPERIMENTAL PROCEDURE	27
3.1	Alloy Preparation	27
3.2	Ceramic Shell Mould Production	27
3.3	Ceramic Mould Experiments	28
	3.3.1 Melting Unit	28
	3.3.2 Ceramic Mould Preheating Furnace	29
	3.3.3 Casting Procedure	30
	3.3.4 Thermal Analysis in Ceramic Moulds	31
3.4	Chill-Sand Castings	32
3.5	Metal Mould Experiments	33
	3.5.1 Cylindrical Moulds	33
	3.5.1.1 Melting Procedure	34

<u>Section</u>	<u>Page</u>
3.5.2 Cruciform Plate Castings	35
3.5.3 Plate Castings	36
3.6 Chill Casting Experiments	37
3.6.1 Melting and Casting Procedure	37
3.6.2 Initial Treatments	38
3.7 Heated Ceramic Mould Alloying Experiments	38
3.8 Metallography	39
3.9 Scanning Electron Microscopy	40
3.10 Microprobe Analysis	41
3.11 Hardness Tests	41
<b>4 EXPERIMENTAL RESULTS</b>	<b>42</b>
4.1 Ceramic Mould Cooling Conditions	42
4.1.1 Thermal Analysis Results	42
4.1.2 Superheat	45
4.1.3 Summary of Thermal Analyses	45
4.2 Ceramic Mould Structures	45
4.2.1 Macrostructures	46
4.2.2 Microstructural Measurements	47
4.2.3 Microstructures	48
4.2.3.1 1.00% Silicon Alloy	48
4.2.3.2 2.04% Silicon Alloy	51
4.2.3.3 2.43% Silicon Alloy	54
4.2.3.4 Summary	56
4.3 Chill/Sand Castings	57
4.3.1 Thermal Analysis Results	57
4.3.2 Chill/Sand Casting Macrostructures	58
4.3.3 Chill/sand Casting Microstructures	58
4.3.3.1 1.00% Silicon Alloy	58
4.3.3.2 2.04% Silicon Alloy	60

<u>Section</u>	<u>Page</u>
4.3.3.3 2.43% Silicon Alloy	61
4.3.4 Summary	63
4.4 Heated Metal Mould Experiments	64
4.4.1 Introduction	64
4.4.2 Physical Conditions	64
4.4.3 Microstructures	66
4.4.3.1 1.00% Silicon Alloy	66
4.4.3.2 2.04% Silicon Alloy	69
4.4.3.3 2.43% Silicon Alloy	71
4.5 Chill Casting Experiments	75
4.5.1 Physical Conditions	75
4.5.2 Macrostructures	76
4.5.3 Microstructures	77
4.5.4 Alloying Effects in Chill Castings	80
4.5.4.1 Macrostructures	80
4.5.4.2 Microstructures	80
4.6 Heated Ceramic Mould Experiments: Alloying Effects	81
4.6.1 Introduction	81
4.6.2 Microstructural Measurements	82
4.6.3 Hardness Test Results	82
4.6.4 Microstructures	83
4.6.4.1 Aluminium	83
4.6.4.2 Magnesium	84
4.6.4.3 Bismuth	84
4.6.4.4 Titanium	84
4.6.4.5 Strontium	85
4.6.4.6 Calcium	85
4.6.4.7 Tellurium	86
4.6.5 Summary	88

<u>Section</u>	<u>Page</u>
5	DISCUSSION 89
5.1	Introduction 89
5.2	Factors Affecting Cast Iron Structure 93
5.3	Mottle Formation 93
5.4	Physical Factors 95
5.4.1	Introduction 95
5.4.2	Physical Influences in Solidification 95
5.4.3	Post-Solidification Processes 97
5.5	Compositional Influences on Solidification 98
5.5.1	Introduction 98
5.5.2	The Effect of Silicon 99
5.5.3	Solidification in Ceramic and Chill/Sand Moulds 101
5.5.4	Solidification in Heated Metal Moulds 104
5.6	Indirect Graphite Formation 105
5.6.1	Introduction 105
5.6.2	Cementite Decomposition 106
5.6.3	Compositional Effects 107
5.6.4	Graphite Nucleation 109
5.6.5	Graphite Growth 110
5.6.6	Summary 115
5.7	Influence of Solute Elements other than Silicon 116
5.8	Nucleation and Growth at Chill Surfaces 119
	CONCLUSIONS 121
	REFERENCES
	ACKNOWLEDGEMENTS

INTRODUCTION

Research in the metallurgy of cast irons has been widespread over the past fifty years, indicating their general application in engineering. In recent years, cast iron solidification has been closely investigated, both in attempts to understand basic solidification mechanisms and to enable closer structural control. An important aspect of this work has been the introduction of controlled solidification techniques, which have enabled isolation of some aspects of growth in cast irons. Commercial methods of structural control are centred on casting conditions and alloy composition, using chills, pouring and superheating temperatures, inoculants and alloying additions.

An important feature of cast iron is the possibility of transition between stable and metastable eutectics, either within a given casting or between castings differing in composition or cooling system. The macro- and microstructural response of a given alloy to a range of cooling conditions is of interest from both practical and theoretical points of view. Considerable amounts of work have been carried out using chill/sand or wedge castings which impose variable but reproducible cooling conditions in the solidifying alloy. The position and the nature of the transitions between stable and metastable structures under such conditions and the extent of mottle under such conditions may give information on many aspects of stable and metastable eutectic nucleation and growth.

The present research is concerned with the influence of alloy composition and thermal variables on structural transitions which occur in typical castings. An attempt has been made to view the casting process as an integral whole, consisting of both solidification and post-solidification processes. Heated and unheated ceramic moulds with a water cooled copper chill at the base produced castings for comparison with chill/sand castings. Rapid solidification of

(ii)

thin section castings followed by isothermal treatments in heated metal moulds enabled study of high temperature transformation processes in white and mottled structures without cooling and reheating. The use of a polished chill mould produced castings with plane surfaces, enabling direct examination of nucleation and growth under chill conditions. Structural effects of a small range of pure element additions were investigated in heated ceramic mould castings of one of the alloys.

## 2. REVIEW OF PREVIOUS WORK

As the literature on cast irons is too extensive for overall detailed treatment, the following review will be confined to the major problems concerning the solidification of cast irons with white or flake graphite microstructures. Attention will be concentrated on microstructural differences and their dependence on physical and chemical variables.

### 2.1 STABLE AND METASTABLE EQUILIBRIA

Phase equilibria of the pure iron-carbon and iron-carbon-silicon systems may be used as an approximate guide to the solidification of commercial cast irons, provided that the influences of chemical and physical variables on the less pure alloy are borne in mind.

The binary iron-carbon equilibrium diagram due to Hillert<sup>(1)</sup> (Fig. 1), combines experimental results (thin lines) with data from thermodynamic analysis (thick lines). The diagram indicates a stable austenite-graphite eutectic, narrowly separated from a metastable austenite-cementite eutectic system which lies at a lower temperature.

The free-energy/composition relationships resulting from Hillert's binary diagram have been derived at various temperatures by Brigham et al<sup>(2)</sup> (Fig. 2). The liquid solubility lines intersect at a stable eutectic undercooling of approximately 11°C. At this temperature, the carbide phase becomes more stable than graphite with respect to the liquid. This may result in carbide nucleation and overgrowth of graphite in the solidifying melt to give a transition in structure. Following sections will enlarge on the importance of this feature in the production of the wide structural variety of iron-carbon alloys.

Commercial cast irons contain silicon, and their behaviour may be followed by using the ternary iron-carbon-silicon system. Solidification

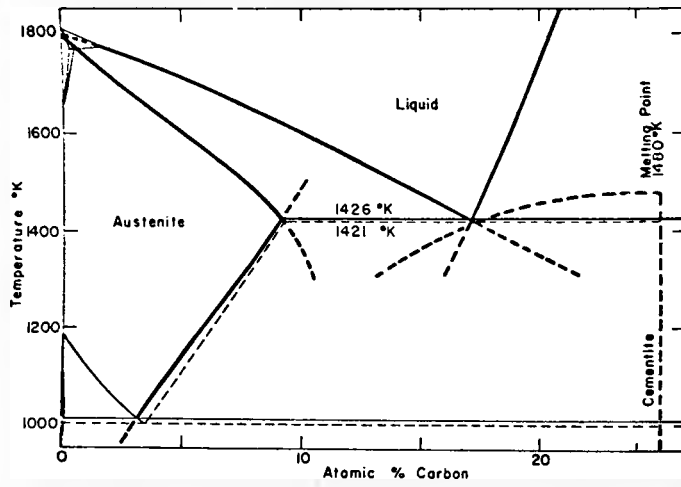


FIG. 1. The iron-carbon constitution diagram after HILLERT.<sup>[1]</sup> The full lines represent the Fe-C system and the dashed, the Fe-Fe<sub>3</sub>C system. All thick lines, full and dashed, were calculated.

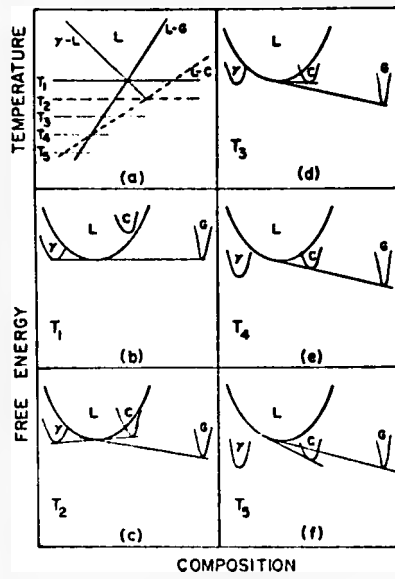


FIG. 2. Free energy-composition diagrams of the iron-carbon system at various undercoolings.

Brigham et al. (2)

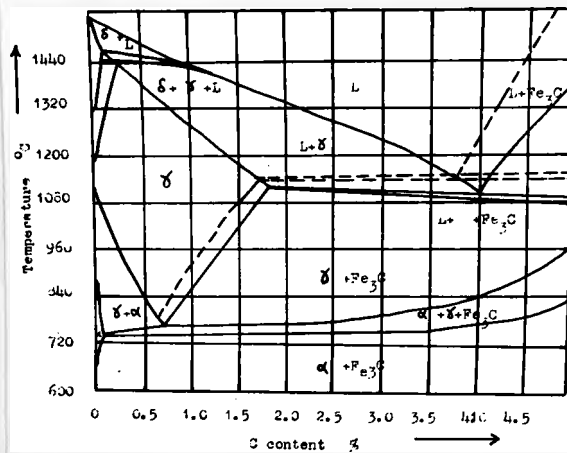


FIG. 3. Section Through The Fe-C-Si Equilibrium Diagram At 2% Si (Levi & Stamenov (3))

sequences can be understood from quasi-binary sections through the ternary diagram. Levi and Stamenov<sup>(3)</sup> produced a diagram representing a section through the ternary system at 2% silicon (Fig. 3), which exhibits several changes from the binary system. The invariant eutectic crystallisation temperature is replaced by a freezing range which is raised by increasing carbon content in the case of the stable system (dotted lines), and lowered in the case of the metastable system (thick lines). The eutectoid transformation is also replaced by a temperature range which expands and rises to higher temperatures as the carbon content increases.

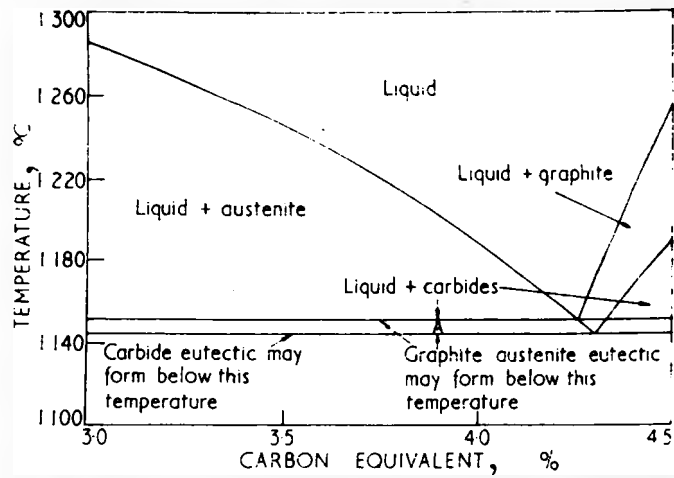
Sections at constant carbon content were produced by Oldfield<sup>(4)</sup>, who correlated cooling curves with microstructure and extrapolated to zero cooling rates to obtain equilibrium stable and metastable freezing temperatures. The results using a range of silicon additions to a given iron-carbon alloy are shown in Fig. 4, indicating that silicon reduces the metastable eutectic equilibrium freezing temperature and increases the region in which stable eutectic crystallisation is favoured.

Variations in microstructure produced by elements such as silicon and phosphorus, which are common in commercial cast irons, may be expressed by the concept of a carbon equivalent concentration:

$$\text{Carbon Equivalent} = \% \text{ Carbon} + \frac{1}{3}(\text{silicon} + \text{Phosphorus})\%$$

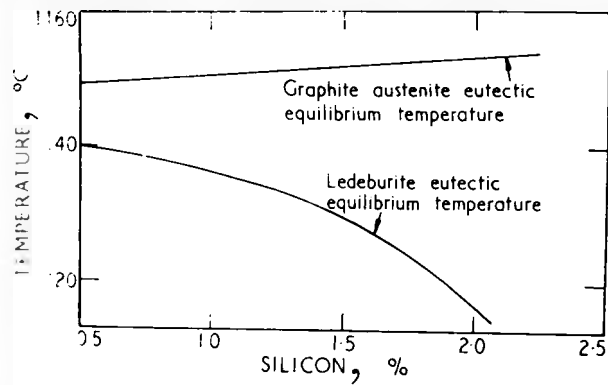
This is utilised in the iron-carbon equivalent diagram of Oldfield<sup>(5)</sup> (Fig. 5), which forms a useful basis for the discussion of commercial alloy solidification.

Isothermal solidification diagrams for iron-carbon-silicon alloys at varying silicon contents, have been constructed by Snagovski et al<sup>(6)</sup>. These show that the sequences of separation of the primary and eutectic phases under isothermal conditions depends on the previous treatment, composition, and the degree of undercooling of the melt. In Fig. 6, the lines for separation



**Fe-C equivalent double diagram**

FIG.4. Oldfield. (4)



**Effect of silicon on eutectic equilibrium freezing temperatures**

FIG.5. Oldfield. (5)

of austenite (OZ), stable eutectic (BF) and metastable eutectic (NI) are shown for alloys with the compositions shown in the accompanying table (Table 1).

Anisothermal solidification behaviour has been predicted by Drapal<sup>(7)</sup>, who superimposed cooling rate curves on the isothermal diagram, Fig. 7. From such a construction, he was able to predict chill, mottle and grey solidification regions in chill/sand test castings.

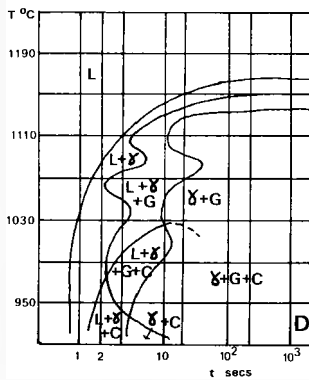
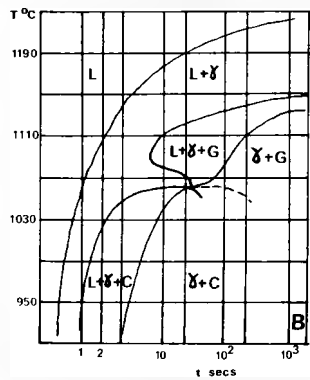
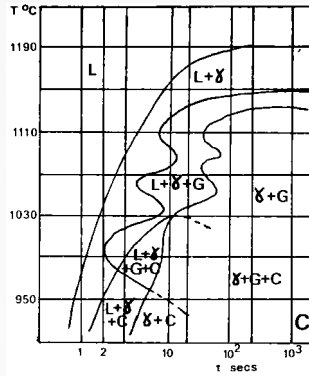
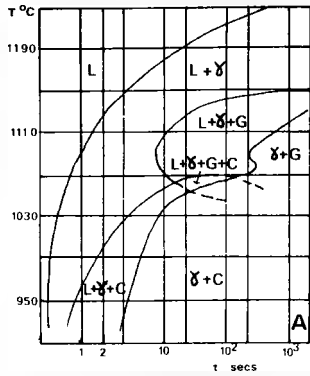
General patterns of cast iron solidification have been also followed using thermal analysis techniques, accompanied by rapid quenching of the freezing melt to disclose crystallisation sequences and morphologies at various stages of solidification. Cooling curves corresponding to typical eutectic structures are shown in Fig. 8<sup>(8)</sup>.

At compositions differing from the eutectic, solidification in the stable system begins with primary phase deposition (austenite for hypoeutectic, graphite for hypereutectic melts). Stable eutectic nucleation on or near the primaries follows after a period of primary growth, when the eutectic composition is reached. Eutectic colonies forming directly from the liquid develop on spherical growth fronts. The growth morphology of these phases is governed by cooling variables as well as by the history and composition of the melt.

Any conditions which encourage undercooling below the metastable eutectic equilibrium temperature, increase the possibility of forming white or mottled structures. Solidification according to the metastable system may arise from one or more of the following conditions: reduction in the degree of graphite eutectic nucleation or in the rate of graphite eutectic cell growth; narrowing of the separation between the stable and metastable eutectic equilibrium temperatures; and increases in cooling rate.

## 2.2 THE NATURE OF LIQUID CAST IRON

The structure and properties of liquid cast iron are of fundamental importance in determining solidification behaviour, especially during nucleation.



Alloy	%C	%Si
A	3.54	0.67
B	3.65	0.94
C	3.63	2.14
D	3.58	2.94

FIG. 6. Isothermal Transformation Diagrams for Fe-C-Si Alloys. Snagovski & Luchin. (6)

Table 1.

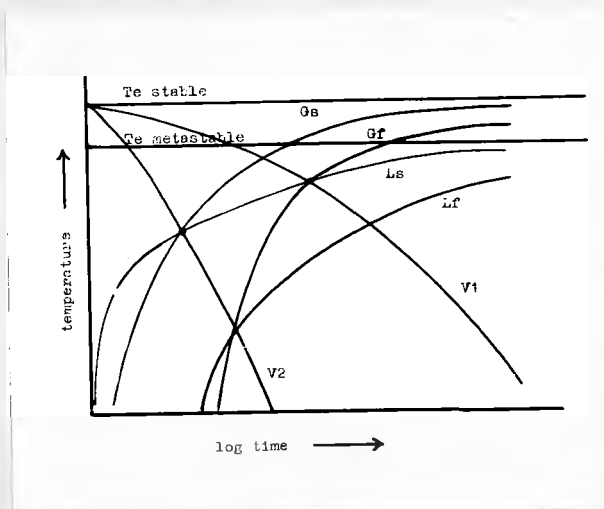


FIG. 7. Fe-C Eutectic Transformation Diagram with Superimposed Cooling Curves. Drapel. (7).

It is therefore important to examine the evidence available in this field.

Conventional x-ray and electron diffraction techniques have been found too limited for extensive study of liquid iron carbon alloy structure. Theories of carbon distribution in the liquid originated from studies of other fluids and examination of structure-sensitive properties of cast iron. (9.10)

In the experiments of Vertman and Samarin<sup>(11)</sup>, centrifuging of liquid cast iron at temperatures 30-50°C above the melting point produced non-uniform carbon distributions on solidification. Their calculations revealed the presence of carbon microgroups of the order of  $10^{-6}$  cm in diameter: a particle size characteristic of colloidal disperse systems which have a high stability (in particular, their particles do not settle under the influence of gravity). This suggests that molten cast iron is a microheterogeneous system, consisting of microgroups of carbon suspended in carbon saturated iron.

The concept of liquid cast iron as a colloidal disperse system helps to explain variations in viscosity, density, surface tension, electrical resistivity and magnetic susceptibility which occur with changes in carbon content and temperature. Viscosity measurements by Nakagawa et al<sup>(12)</sup> indicate differences between the liquids formed from white and grey cast irons of the same chemical composition. This has been attributed to a greater concentration of carbon microgroups in the grey melt than are present in the white. The phenomenon of heredity, whereby castings of the same composition, subject to the same casting variables, give different structures, is well known. Williams<sup>(13)</sup> showed that white melting stock gave castings with consistently greater chill depths than similar castings produced from grey stock of the same composition. Boyes and Fuller<sup>(14)</sup> reported that the differences between the melting stocks lay in nucleation from the liquid. This view was shared by Patterson<sup>(15)</sup>. Heredity effects appear to be due to differences in solid structure which affect the nature of the melt and the mode of nucleation during solidification.

Liquid metal treatments which alter the physical nature of liquid cast iron are important in controlling solidification structures. Piworwarski<sup>(6)</sup> demonstrated that superheating refined graphite eutectic structures and encouraged metastable solidification by increasing undercooling. He concluded that the effect of superheat lay in the dissolution of graphite nuclei. More recently, Ivanov<sup>(10)</sup> reported that graphite cluster concentration in cast iron decreases with increasing superheat, becoming undetectable above 1700°C. This tendency was confirmed by the viscosity measurements of Nakagawa et al<sup>(12)</sup>. If the clusters act as the forerunners of the nuclei of the solid phase, their refinement and dispersion by superheating renders graphite eutectic nucleation more difficult and causes greater undercooling. The structure of liquid cast irons therefore appears to be closely related to nucleation of the stable eutectic.

### 2.3 NUCLEATION IN CAST IRONS

Cast iron nucleation has been extensively studied, especially in the development of commercially important inoculants for the stable eutectic. While it is generally agreed that cast irons nucleate heterogeneously<sup>(17)</sup>, the nature of the nuclei involved has been the subject of much speculation. Commercial cast irons contain large quantities of impurities some of which may be responsible for heterogeneous nucleation of the stable eutectic. The effectiveness of a nucleation substrate depends on a number of factors, including particle size and geometry; surface energy; lattice structure and epitaxial relationships; thermal and chemical stability; and the degree of equilibrium under which solidification takes place.

A wide variety of nuclei have been postulated for the grey iron eutectic. Internucleation of austenite and graphite has been considered, but results are not in agreement: Lakeland<sup>(18)</sup> proposed austenite as a nucleant for graphite, while Koves and Mondolfo<sup>(19)</sup> who studied small iron-carbon droplets, solidified in vacuum, were unable to prove the internucleating ability of either phase.

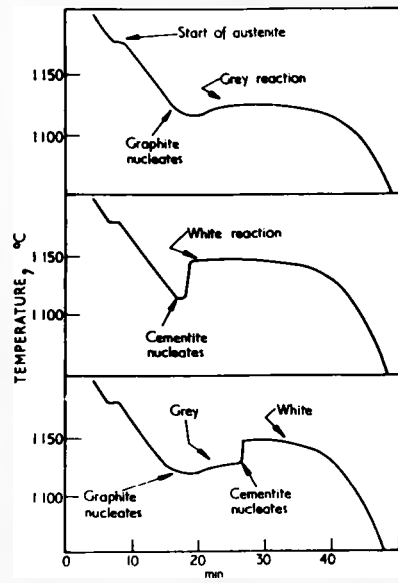
Foundry experience with commercial alloys<sup>(20)</sup> has shown that undercoolings are maximum near the eutectic composition. This implies that the presence of one or other primary phase in hypo- or hypereutectic melts aids eutectic nucleation. The conflict of these results with those from pure alloy melts<sup>(19)</sup>, suggests that the presence of Si, Mn, S, P and other impurities affects the suitability of proeutectic phases as sites for eutectic nucleation.

Proeutectic phases apart, suggestions for stable eutectic nuclei have included retained or colloidal graphite;<sup>(16.21)</sup> dissolved gases;<sup>(21.22)</sup> silicon segregates;<sup>(23.24)</sup> silicate slimes;<sup>(25)</sup> salt-like carbides;<sup>(24.26.27)</sup> oxides<sup>(28)</sup> and sulphides.<sup>(29.30)</sup> Morrogh<sup>(31)</sup> concluded that specific nucleation mechanisms are unknown, and that graphite or metal lattice residues or atomic irregularities in the austenite-liquid interface could equally form a basis for graphite eutectic nucleation.

As shown in the previous section, physical treatments, especially superheating, affect liquid structures and subsequent solidification, presumably through nucleation. Patterson and Ammann<sup>(32)</sup> found that the relationship between superheat and undercooling in cast irons was discontinuous (Fig. 9). They postulated the presence of various types of nuclei in the melt which were selectively deactivated by increasing superheat. The nuclei involved were not identified.

Gittus<sup>(33)</sup>, and later Patterson and Brand<sup>(34)</sup>, examined variations in stable eutectic solidification in vibrated and unvibrated castings. They concluded that the overall effect of vibration was to increase stable eutectic cell numbers via enhanced nucleation. Recent work<sup>(35)</sup> on the effects of pressure on solidification and solid state graphitisation has indicated promotion of spheroidal graphite forms and reduction in first stage graphitisation times.

Apart from physical treatments, certain alloying additions may suppress the stable eutectic by destroying nuclei. Mascre<sup>(36)</sup> cited magnesium as an



Cooling curves for grey, white, and mottled iron

FIG.8. Hultgren et al. (8).

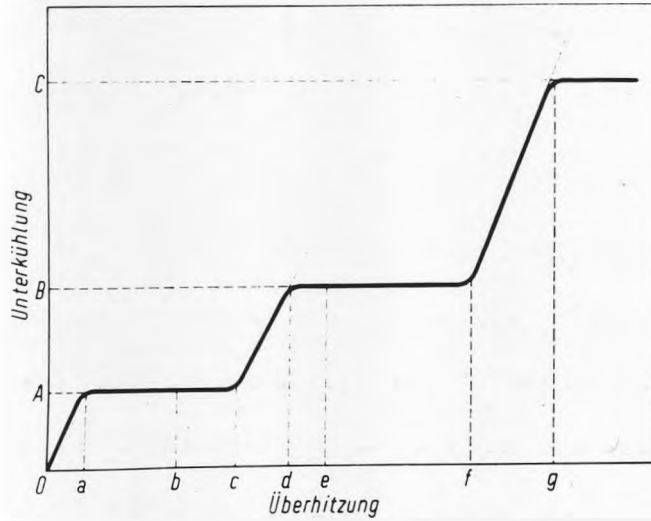


FIG.9. Patterson & Ammann. (32).



FIG.10. Cementite plates.  
Hillert & Steinhauser. (38).

"antinucleant" of the stable eutectic; taking effect by destroying the more effective graphite nuclei (possibly FeS).

Calculations by Hillert<sup>(1)</sup>, assuming homogeneous nucleation, showed that graphite is the favoured phase for nucleation at all undercoolings. This is at variance with results for superheated and degassed melts, where cementite has been found to nucleate preferentially<sup>(19,37)</sup>; probably because of the destruction or neutralisation of the stable eutectic heterogeneous nuclei.

Cementite may be nucleated on or near proeutectic austenite after undercooling below the metastable eutectic equilibrium temperature<sup>(37)</sup>. Once nucleated, it develops as plates which grow rapidly, spreading to other parts of the melt independently of the primary austenite. Plate multiplication into characteristic fan-shaped clusters (Fig. 10) suggests brittleness at growth temperatures, causing fragmentation and self nucleation under thermal stresses and turbulence. Hillert and Steinhauser<sup>(38)</sup>, showed that each primary cementite plate may form the basis of a eutectic colony.

#### 2.4 GROWTH IN CAST IRONS

Before considering specific growth relationships and morphologies in later sections, it is possible to examine certain growth theories common to both stable and metastable eutectics.

Changes in eutectic morphology are governed by many factors including structural bonding of phases; form and distribution of the nuclei; melt undercooling; heat extraction rates; temperature and concentration gradients at the solid-liquid interface; diffusion of solid and impurities in the melt and solid; adsorption of impurities on growing phases; interfacial energies and the relative undercoolings of the phases at the growth front. Although structural bonding (in the absence of impurities) is ideally invariant, all other factors result from, or are affected by the degree of non-equilibrium under which

solidification occurs. The growth process is therefore governed by a series of interdependent variables which alter with the state of non-equilibrium.

Rapid cooling reduces the time available for solidification and increases the activation energy for diffusion of atoms to growing heterogeneous nuclei. The melt undercools, solidification occurring via increased nucleation at lower temperatures, where the energy required to form new surfaces is less. The effects of increasing cooling rates are also seen in increased temperature and concentration gradients, higher growth rates and slower diffusion in liquid and solid states.

Relating these parameters as in Jackson and Chalmers' equation for normal eutectic growth<sup>(39)</sup>:

$$\lambda = \text{const} \sqrt{\frac{D \cdot \sigma_{\alpha\beta} \cdot T_e}{C_e \cdot R}}$$

where D = diffusion coefficient in the liquid

$\sigma_{\alpha\beta}$  = interfacial energy between  $\alpha/\beta$  lamellae

$T_e$  = eutectic equilibrium temperature

$C_e$  = eutectic concentration

R = eutectic growth rate

$\lambda$  = interlamellar spacing

From this equation it follows that:

$$\lambda \propto R^{-1/2}$$

and since  $\Delta T \propto \frac{1}{L \lambda}$

$$\Delta T \propto R^{1/2}$$

It can be seen that if growth rate increases while diffusion in the liquid decreases, the net result of increasing non-equilibrium is to refine the interlamellar spacing. In the less ideal grey eutectic, this effect is reflected by the change from A to D graphite with increased undercooling.

Oldfield<sup>(5)</sup> considered the heat balance of eutectic cell growth and obtained the equation:

$$\frac{dq}{dt} = 4 R^2 N^3 L \frac{dr}{dt}$$

where N = number of liquid-solid interfaces per unit length

dr/dt = radial growth rate

dq/dt = rate of heat extraction per unit volume

L = latent heat of fusion per unit volume

R = growth rate

In practice, the rate of heat evolution (R.H.S.) is balanced by heat extraction at a given undercooling. If the heat extraction rate is increased, the melt undercools until balance is reached at a lower temperature with higher nucleation. Boyes and Fuller<sup>(14)</sup> have summarised the effects of nucleation and growth rate variation on graphite morphology, chilling tendency, and mottle formation (Fig. 11).

## 2.5 THE IRON-GRAPHITE STABLE EUTECTIC SYSTEM

### 2.5.1 CRYSTAL STRUCTURE AND MORPHOLOGY OF GRAPHITE

Graphite in iron-carbon alloys forms with a hexagonal layer lattice similar to that of natural graphite (Fig. 12)<sup>(40)</sup>. The spacing of the carbon atoms within the layers is much closer than the interlayer spacing, reflecting the relative strength of the covalent bonding within the layers and the weak homopolar bonding between the layers. The strength of the covalent bonds within the graphite layers is thought to be responsible for the persistence of carbon microgroupings in molten cast iron.

Graphite crystal growth on an atomic scale has been envisaged<sup>(41)</sup> as occurring by layer addition at re-entrant twin planes (Fig. 13). This mechanism produces graphite flakes by a-direction propagation, which in normal grey cast irons is

Summary of effects of variations in degree of nucleation  
and cell growth rate on graphite structure, chilling  
tendency and mottling characteristics

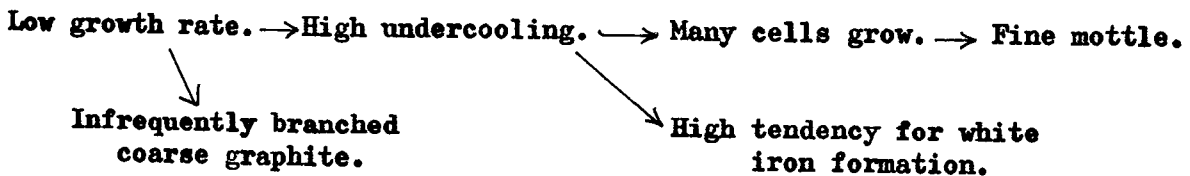
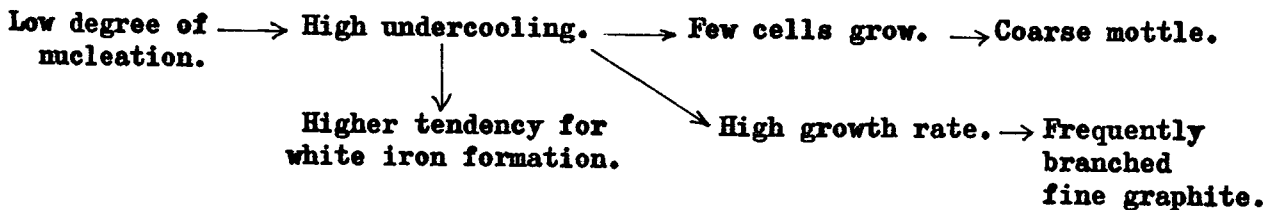
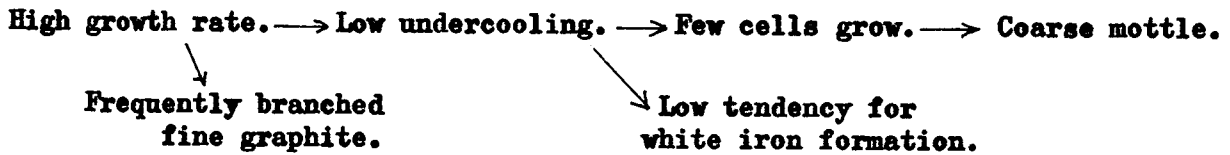
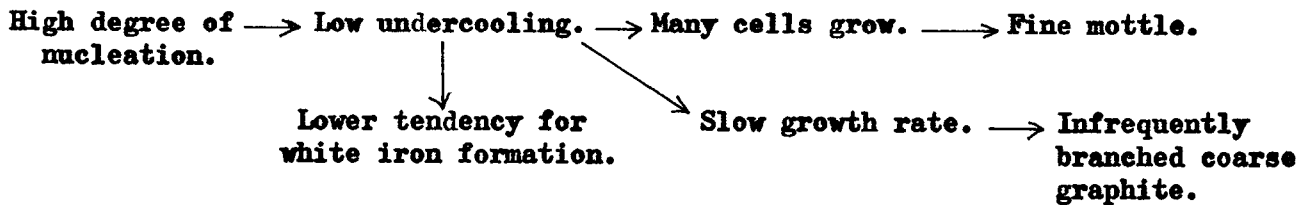


FIG. 11. Boyes & Fuller. (14)

considerably faster than c-direction growth, produced by the addition of atoms to screw dislocations (Fig. 14).

These growth mechanisms have been used<sup>(42)</sup> to explain interactions of solute elements with graphite crystals. Three main classes of interaction have been proposed:

- (a) adsorption on growing surface steps, which 'poisons' the growth mechanism and leads to alternative morphologies (Mg, rare earths),
- (b) elements may segregate to form boundary layers which cause instability (B),
- (c) elements may affect the edge energy of (0001) planes, producing co-operative growth along the c-axis under certain conditions (e.g. Se).

The colloidal disperse theory implies graphite growth by microgroup addition to growing flakes. This viewpoint does not appear to be fully reconciled with the atomic-scale growth theories just outlined.

As the direction of slowest growth in normal grey cast irons is the c-axis, flakes are ideally bounded by large (0001) surfaces. Branching takes place by the formation of irregularities in the (1010) direction. In hypoeutectic grey cast irons, the flakes are commonly curved and deformed. High mobility during growth results from the weak nature of the homopolar bonds between the hexagonal planes.

### 2.5.2 STABLE EUTECTIC FORMATION

Controlled solidification experiments<sup>(18.37)</sup> with pure iron-carbon alloys have produced lamellar austenite-graphite eutectic forms at slow growth rates. Under these conditions the constant  $n$ , in the equation  $\lambda = AR^n$ ,  $n = 0.49$ <sup>(18)</sup>, suggesting that the eutectic is normal (for normal eutectics,  $n = 0.34$  to  $0.5$ ). In commercial cast irons, impurity adsorption and segregation tends to disturb planar growth interfaces and parallel flake growth is hampered, even at very low growth rates.

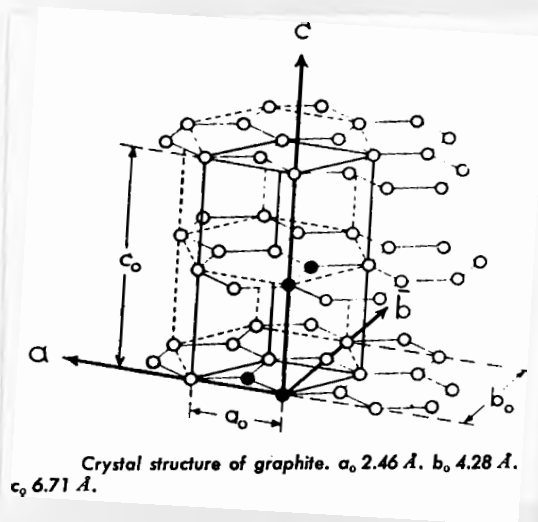


FIG.12. Wilkinson & Hellowell (40).

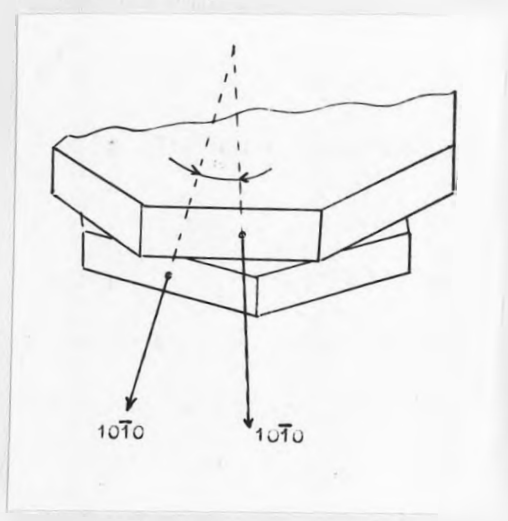


FIG.13. Steps On  $(10\bar{1}0)$  Surfaces Formed By A Rotation Boundary: Active Sites In Flake Graphite Growth. Minkoff & Lux. (42).

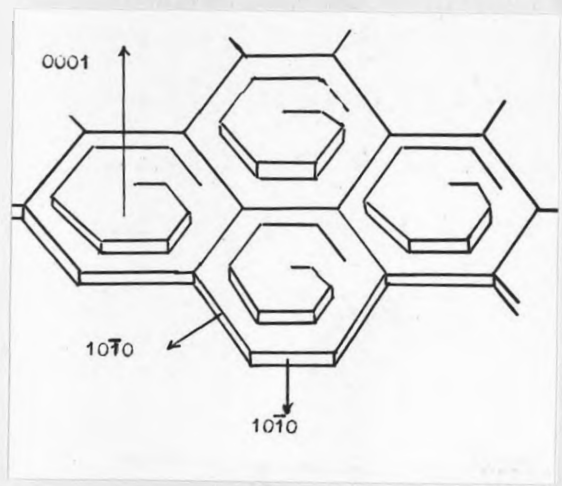


FIG.14. C-Direction Growth From An Array Of Screw Dislocations Entering A Graphite Crystal. Minkoff & Lux (42).



FIG.15. Morrogh. (48).

Under normal solidification conditions, eutectic growth is less co-operative<sup>(43)</sup> and branching and flake deformation occur. Hughes<sup>(17)</sup> considered graphite branching to be due to the difficulty of forming preferred low energy interfaces between austenite and the graphite basal planes. Koves and Mondolfo<sup>(19)</sup> described the branched eutectic as degenerate, but Lakeland and Hogan<sup>(44)</sup> believed it to be normal since a degree of co-operation between the two phases is maintained in all flake growth forms.

All types of the graphite eutectic which form directly from the melt during the solidification of normal castings, grow radially with graphite in contact with the liquid. The eutectic is divided into colonies, each of which is believed to result from a single nucleation event. Repeated sectioning and polishing<sup>(45,46)</sup>, deep etching<sup>(47)</sup> and more recently, scanning electron microscopy<sup>(48,49)</sup>, have suggested that the graphite within each colony is interconnected (Fig. 15)

Graphite eutectic morphologies are commonly classified using the A.S.T.M. system<sup>(50)</sup> (Fig. 16), which depends on variations in the state of graphite division, branching and deformation. The drawback with the A.S.T.M. classification is that it only accounts for changes within the eutectic cell, and neglects allied variations in nucleation. A more complete classification system has been suggested by Gunnarson<sup>(51)</sup>, in which the cell numbers are related to the graphite types within the cells.

Changes in eutectic morphology result from variations in eutectic nucleation and growth rate. These parameters are in themselves affected by complex relationships between undercooling, composition, segregation and cooling variables.

Hillert<sup>(43)</sup>, studying pure iron-carbon alloys, demonstrated that increases in growth rate reduced directionality and tended to stabilise the undercooled eutectic. Fig. 17 shows the effect of a sudden increase in growth rate on the

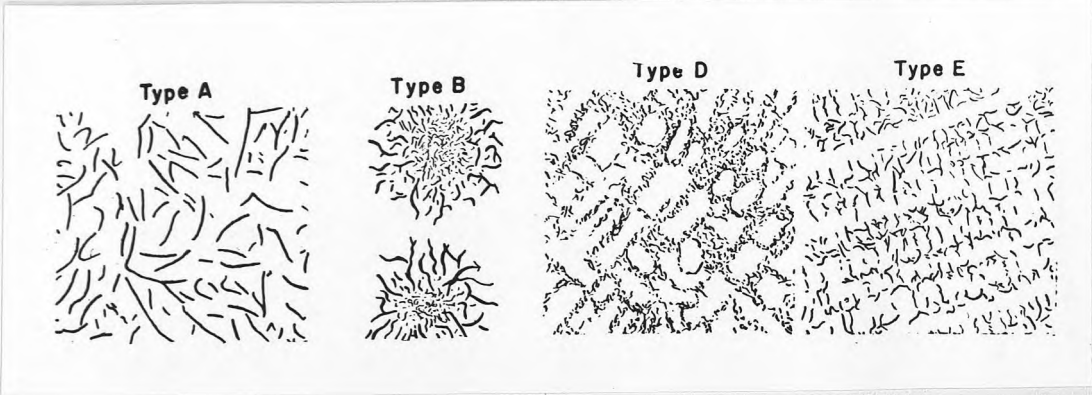


FIG.16. A.S.T.M. Graphite Classification. (50)



FIG.17. Hillert & Subba Rao. (43)

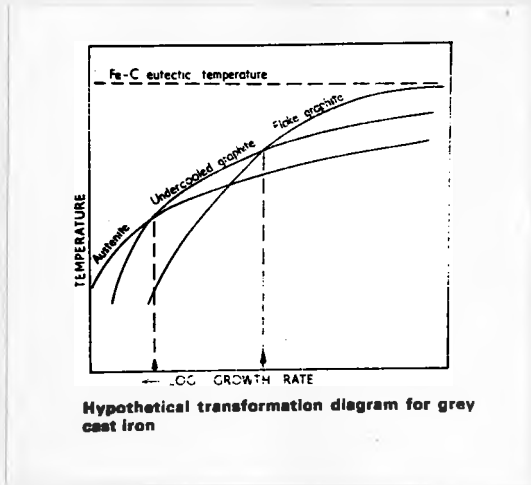


FIG.18. Hillert & Subba Rao. (43)

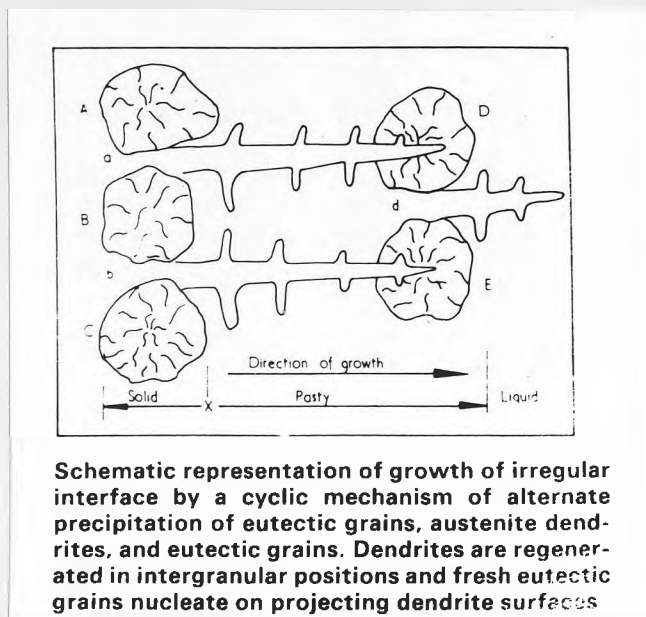


FIG.19. Lakeland & Hogan. (44)

structure of a unidirectionally solidified melt. The presence of austenite dendrites at high growth rates was explained using the hypothesis that graphite is the leading phase at small undercoolings, while austenite formation is increasingly favoured as the temperature falls (Fig. 18). The undercooled or 'D'-type graphite structure was believed to form with a greater degree of co-operation between the two phases than the A-type eutectic.

Djidjev<sup>(52)</sup> considered the effects of cooling rate on the stable eutectic and concluded that the main factor determining graphite morphology is the relationship of the mean radial growth rates of austenite and graphite. The mean radial rate of eutectic growth increases with undercooling, thus favouring austenite as the leading phase, since the growth rate of austenite increases more rapidly than that of graphite with undercooling. When the rate of graphite growth is greater than that of austenite, types A and B eutectic are obtained, while for D and E eutectics, austenite is the leading phase.

In commercial cast irons, solute rejection and adsorption at the growing interface can exert great influence on graphite nucleation, growth rate and form. The degree of segregation of a given element is governed the composition of the alloy, distribution and diffusion coefficients, degree of nucleation, and growth rate (as determined by section size and cooling conditions).

Charbonnier and Margerie<sup>(53)</sup> report that in castings of up to 10 cm. dia., chemical heterogeneities on a microscopic scale are much greater than macro-segregation. Segregation is most commonly found as concentration gradients across primary austenite dendrites, or from the centre to edge of eutectic cells.

Merchant<sup>(54)</sup> suggested that the segregation of elements with low distribution and diffusion coefficients should be high. Using this criterion, sulphur should have the most significant segregation influence in eutectic cell boundaries; phosphorus and manganese would segregate only moderately, while silicon

and carbon would be depleted at cell edges. These tendencies were confirmed by experiment.

It is reported that elements which decrease the activity of carbon in liquid cast iron have segregation coefficients less than 1 and vice versa<sup>(55)</sup>. Elements which segregate to colony boundaries are often eutectic carbide stabilisers (Cr, V, Mn, Mo), while graphitisers tend to segregate to colony centres (Si, Al, Ni, Cu). This may also account for the formation of carbides or pearlite at cell boundaries. The addition of elements such as Ag, Bi, Cd or Pb to cast iron results in their almost complete segregation to eutectic cell boundaries, because they are virtually insoluble in liquid cast iron.

Segregation may hinder carbon deposition from the melt, retarding growth and causing changes in eutectic morphology. Djidjev<sup>(52)</sup> explained the variation in graphite distribution across B-type eutectic colonies by referring to silicon segregation at the colony centres. The increased silicon concentration reduced carbon diffusivity and led to fine graphite; coarser graphite forming at the cell boundaries where the silicon content was less. Lakeland<sup>(18)</sup> explained the same phenomenon by suggesting increased sulphur adsorption on growing graphite flakes during eutectic solidification. The coarsening of the graphite from the colony centre to the periphery was said to be due to retardation of austenite growth by sulphur segregation in the liquid<sup>(56)</sup>.

Any factors which inhibit the transport of carbon atoms to the graphite-liquid interface will tend to retard eutectic growth rates and may enable sufficient undercooling for metastable solidification. Heisterkamp and Lohberg<sup>(57)</sup> showed that the diffusion of carbon atoms above the eutectic temperature is retarded by sulphur. This mechanism was tentatively extended to the case of tellurium by Nieswaag and Zuithoff<sup>(58)</sup>.

Lakeland and Hogan<sup>(59)</sup> proposed a cyclic growth mechanism for pure Fe-C-S alloys which could easily apply to commercial cast irons (Fig. 19). Solidification of eutectic colonies leads to sulphur segregation and "constitutional"

undercooling in the intercolony areas. Austenite may nucleate in these areas forming dendrites. Carbon segregation at the dendrite peripheries causes local supersaturation of the melt and leads to graphite nucleation and eutectic cell growth.

## 2.6 THE METASTABLE EUTECTIC SYSTEM

### 2.6.1 CEMENTITE CRYSTAL STRUCTURE

Lipson and Petch<sup>(60)</sup> studied the structure of cementite using X-ray diffraction. In their model (Fig. 20) each carbon atom is located near the centre of a prism formed by six iron atoms. Within the unit cell, the mean Fe-C distance is  $2.03\text{\AA}$ . There are, however, two more iron atoms within  $2.31\text{\AA}$  of each carbon, and it may be that these also have some influence on carbon environment. Bonding between iron atoms is metallic and Petch<sup>(58)</sup> suggested that the carbon is linked to the iron by resonating covalent bonds. In commercial cast irons, cementite composition may not adhere strictly to the formula  $\text{Fe}_3\text{C}$ . Petch<sup>(61)</sup> discussed the bonding in the Lipson and Petch<sup>(60)</sup> cementite model and recognised the possibility of bond variation due to alloying. This idea was followed by Brown and Hawkes<sup>(62)</sup>, who considered the effects of atoms substituted in the iron lattice and held by intermetallic bonds or present as interstitials in the crystal structure (Fig. 21). Carbide stabilisation was discussed in terms of weakening of the Fe-C resonance bond by atoms which distend the lattice (nickel, cobalt), or strengthening by lattice contraction (chromium, manganese). Interstitials not held by metallic bonding (sulphur, boron) would presumably reinforce the resonance bond and stabilise the structure. This model does not hold for all elements: aluminium and silicon are predicted as carbide stabilisers, when they are in fact graphitisers.

### 2.6.2 METASTABLE EUTECTIC STRUCTURE AND GROWTH

Wilkinson and Hellowell<sup>(40)</sup>, and later Brigham<sup>(63)</sup>, produced lamellar forms of the metastable eutectic in which  $\lambda = AR^{-0.34}$ . This factor, together with the discovery of an orientation relationship between cementite and austenite<sup>(64)</sup>

suggests that ledeburite is a 'normal' eutectic under controlled growth conditions.

The metastable eutectic has two main growth forms (Fig. 22). Co-operative growth at low undercoolings between nearly-parallel austenite rods, with cementite as the matrix phase gives the 'normal' eutectic. Each cell of this eutectic has been shown to consist of continuous austenite and cementite forming two inter-twining crystals<sup>(38)</sup>. At greater undercoolings, an acicular or platelike eutectic forms, in which the cementite occurs as plates, similar to the proeutectic type. Fuller and Hughes<sup>(65)</sup> showed that the nucleation and growth of the two eutectic forms differs. Normal ledeburite forms in a columnar manner, while the acicular eutectic appears to nucleate and grow simultaneously at a great number of points.

Hillert and Subba Rao<sup>(43)</sup> suggest that if the eutectic reaction is diffusion controlled, and if surface energy requirements are met, the normal growth form with rod-like austenite should predominate. As cooling rates increase, the cementite has a tendency to form plates similar to proeutectic  $Fe_3C$ . The superiority of the edgewise growth form as non-equilibrium increases indicates departure from diffusional and surface energy control. Hillert and Steinhauser<sup>(38)</sup> explained the block structure of ledeburite colonies in terms of the relative growth velocities perpendicular and parallel to the nucleating cementite platelet (Fig. 23). Edgewise progress is favoured, overtaking the sideways growth to give a stepped structure (Fig. 24). Bunin<sup>(66)</sup> demonstrated the superiority of edgewise growth at high cooling rates by showing that the step angle decreased with increasing cooling rate until sideways growth was totally eliminated.

The formation of acicular ledeburite is much less frequent than that of the normal or stepped structures. With increasing degrees of non-equilibrium, mixtures of normal eutectic with non-co-operative edgewise growth forms give rise to 'degenerate' structures.

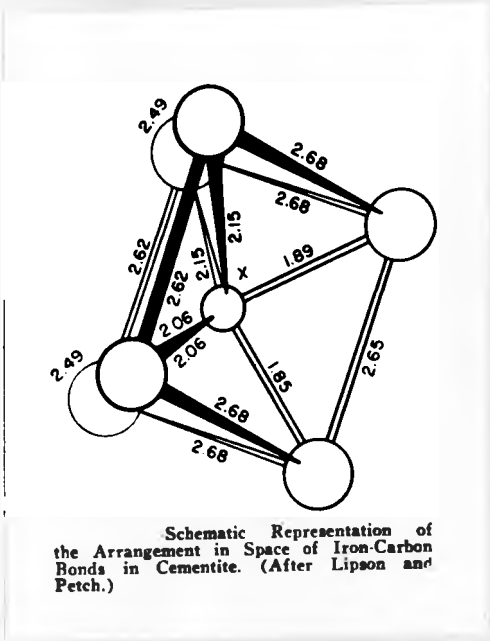


FIG.20. Lipson & Petch. (60)

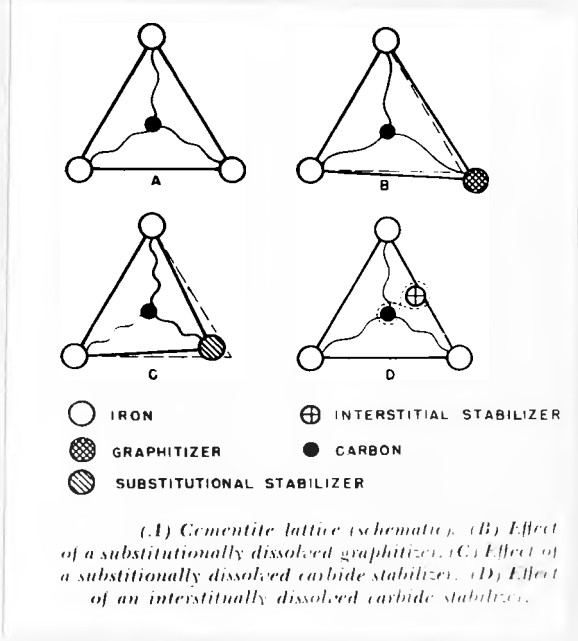


FIG.21. Brown & Hawkes. (62)



FIG.22. 'Normal' and 'Acicular' Metastable Eutectic. Rickard & Hughes. (70)

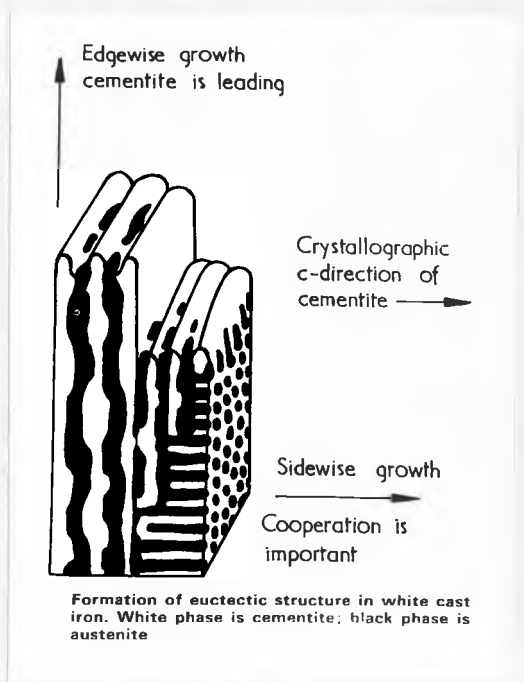


FIG.23. Hillert & Subba Rao. (43)

Thermal non-equilibrium may not be the only factor in the formation of the degenerate structure. It may be encouraged by close spacing of the primary cementite plates, which limits sideways co-operative growth giving a coarse eutectic<sup>(38)</sup>. Compositional effects are of obvious importance, as surface energy and diffusion appear to govern the occurrence of edgewise growth. Phosphorus<sup>(67)</sup>, sulphur, oxygen and manganese<sup>(68)</sup> have been shown to produce massive degenerate carbide forms.

The acicular eutectic is characterised by the absence of sideways growth. The platelike structure was found to solidify after a greater degree of undercooling than that required for the normal or degenerate eutectics<sup>(68.70)</sup>. Rapid cooling, which causes greater undercooling, favours platelike growth. Scheil and Pohl<sup>(69)</sup> managed to eliminate sideways growth and produce an acicular structure by reducing the silicon content of the alloy under study.

Work on segregation in white cast irons was reviewed by Merchant<sup>(55)</sup>, who concluded that carbide stabilising elements segregate to cementite, while graphite promoters are found in the austenite. Redistribution of the elements on solidification is dependant on the diffusion rates of the partitioning elements in the solidifying melt. Partitioning has been shown to decrease as cooling rate increases, except in the case of elements such as silicon and aluminium (and presumably gases), which have comparatively high diffusion rates in the liquid phase. Levi and Stamenov<sup>(71)</sup> considered silicon segregation in white cast irons from the point of view of phase equilibria. They produced a model of silicon segregation (Fig. 25), which predicts substantial silicon enrichment in the peripheral austenite-ledgeburite interface zones during eutectic crystallisation. This was said to lead to localised fluctuations in carbon concentration, forming graphite micro-nuclei at the austenite cementite interfaces. The overall picture of silicon segregation in ledgeburite was confirmed by Malinockha et al<sup>(72)</sup>, using microprobe analysis and special etching techniques.

## 2.7 MOTTLED STRUCTURES

Hillert<sup>(1)</sup> studied the nucleation and growth kinetics of the stable and metastable eutectics, concluding that while graphite nucleated preferentially, cementite had a considerable growth advantage over the stable eutectic. These factors, coupled with the closeness of the two eutectic equilibrium temperatures, may lead to the presence of the stable and metastable eutectics in the same region, forming a mottled structure. The conditions for mottle production vary according to alloy composition and the cooling system.

In sand castings, mottle is usually the result of a critical cooling rate (Fig. 8), such that when the casting undercools into the metastable region graphite growth and recalescence is insufficient to prevent cementite nucleation in the undercooled liquid. Once cementite nucleates, its growth advantage is such that it rapidly overtakes and engulfs the stable colonies to produce a mottled structure.

Another cause of mottle in foundry situations is the chill wave effect described by Hughes<sup>(73)</sup> for chill/sand test castings. Thermal sequences in chill/sand test castings are complex, depending on pouring temperature and the thermal characteristics of the chill or mould. A two-dimensional representation of the time-temperature distribution in a metal mould (Fig. 26) shows that the chilling effect of the mould walls moves into the casting with time. This may be shown in terms of a chill effect line x-y. In a composite chill/sand mould, the chill wave interacts with the normal process of sand mould solidification. The chill wave travels axially up the casting, causing undercooling and enabling cementite growth to follow the chill wave. Graphite colonies are overgrown by the fast moving white eutectic to give mottled structures similar to those of sand castings. Superimposition of the chill effect line on the eutectic solidification area (Fig. 27) enables a graphical interpretation. Chill/sand test results may be qualitatively extended to cover the effects of chills (whether external, internal, surface or thin sections) in normal castings.

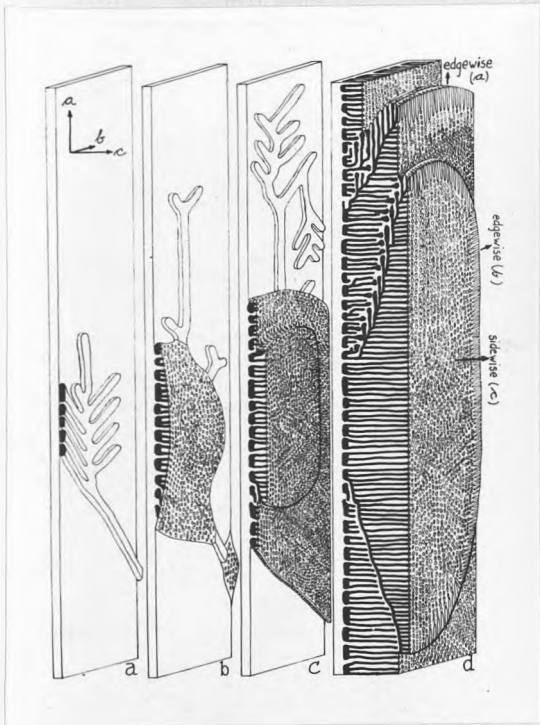


FIG.24. Ledeburite Growth. (38)  
Hillert & Steinhauser.

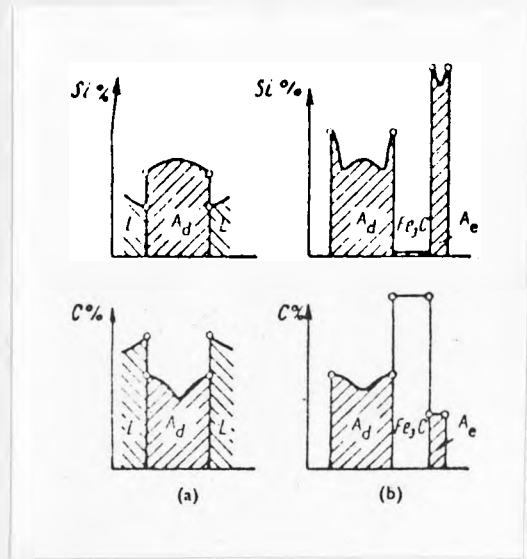


FIG.25. Segregation in Ledeburite. (71)  
Levi & Stamenov.

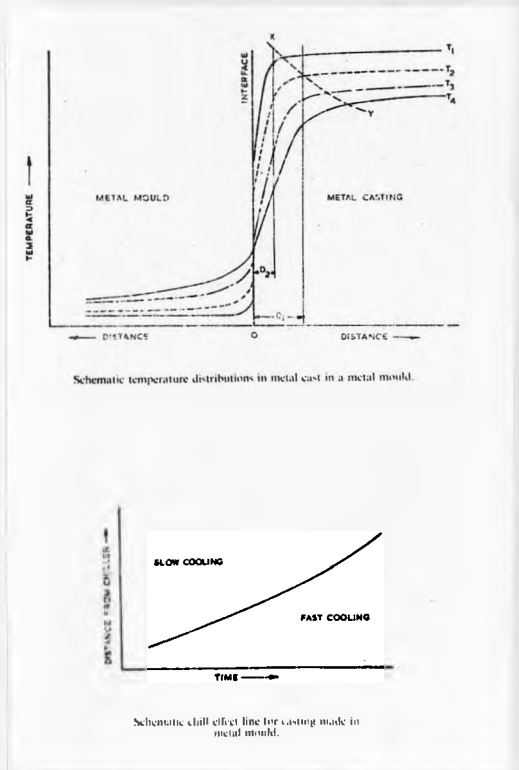


FIG.26. Hughes. (73)

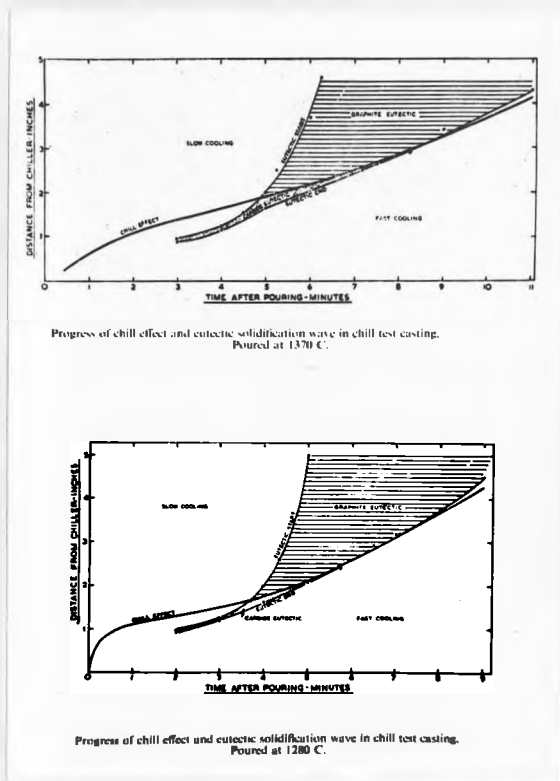


FIG.27. Hughes. (73)

In all these cases, there is the possibility of chill wave propagation and hence mottling.

The extent of mottle, whether produced by a critical cooling rate within the casting, or induced by chilling, is obviously dependant on metal composition. The effects of variation in stable eutectic nucleation potential and growth rate on mottling have been summarised by Boyes and Fuller<sup>(14)</sup> (Fig. 11). Another factor in determining the degree of mottle in a given casting is the degree of separation of the two eutectics: this has been shown to be very sensitive to composition (4.74). In general, the introduction of elements which widen the separation of the eutectic equilibrium temperatures will enlarge the region of preferred graphite growth and decrease the likelihood of mottling.

The influence of segregation on mottling has already been mentioned in connection with the concentration of carbide-stabilising elements at stable cell boundaries<sup>(55)</sup>, which may lead to metastable crystallisation in these regions. A similar mechanism was postulated by Kamensky and Piskor<sup>(75)</sup> to explain the occurrence of aligned graphite streamers between columnar ledeburite colonies in chilled iron rolls (Fig. 28). Microprobe analysis of the streamer regions revealed nickel and silicon segregation into the graphitic areas and concentrations of the carbide stabilising elements chromium and vanadium in the surrounding ledeburite. These segregates were said to balance the relative nucleation and growth stabilities of the two eutectic forms, enabling parallel columnar growth under the conditions of high temperature gradient inherent in the permanent mould process.

The streamer graphite formations noted by Kamensky and Piskor<sup>(75)</sup> are included in the range of structures covered by the term 'indefinite chill'. Loper and Heine<sup>(76)</sup> defined three main types of graphite formed by low temperature nucleation and growth, all of which may occur with the metastable eutectic to give indefinite chill. These structures form a continuous series from those

solidifying directly from the melt to those formed by the solid state decomposition of cementite. Their structures and modes of formation will be discussed in detail in the section on indirect graphite formation.

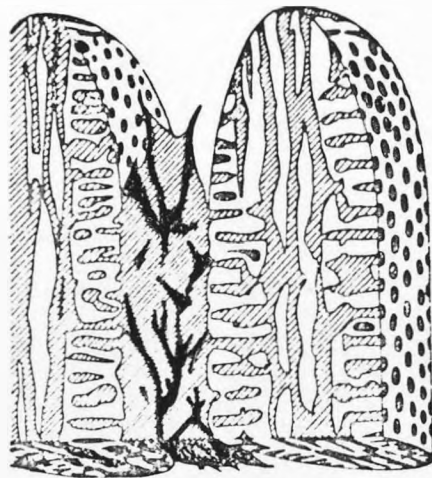
## 2.8 INDIRECT GRAPHITE FORMATION

Mottled or completely graphitic structures may be formed by the solid state decomposition of metastable eutectic at high temperatures to give austenite and graphite. At lower temperatures, deposition of carbon from supersaturated austenite may lead to further graphitisation.

The decomposition of cementite involves destruction of the orthorhombic lattice by carbon diffusion to a suitable nucleation substrate and the reformation of the iron atoms into F.C.C. austenite, saturated with carbon at the temperature in question. The kinetics and product morphologies of the decomposition process are highly temperature dependent for a given alloy. Small compositional differences caused by basic constitution or segregation can lead to wide variations in decomposition behaviour. As mentioned in a previous section, variations in cementite stability with alloy composition have been accounted for by citing interatomic bond strengths in the crystal lattice<sup>(62)</sup>, or micronuclei<sup>(71)</sup>. In spite of these theories, and wide knowledge of the effects of alloying additions, the actual mechanisms by which alloying may affect cementite stability remain largely unknown.

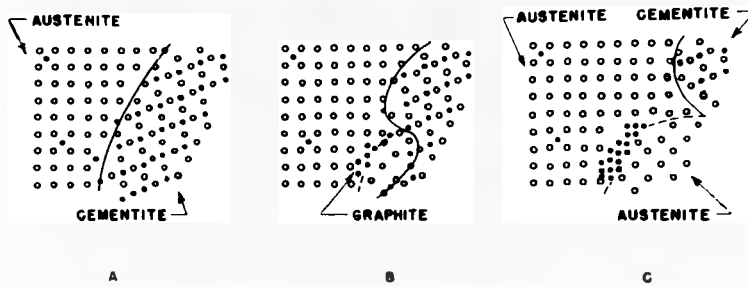
The work of Brown and Hawkes<sup>(62)</sup> showed that the decomposition process was one of nucleation and growth. The process was depicted on an atomic scale as in Fig. 29. This shows that graphite nucleation takes place at an austenite-cementite interface, while subsequent growth occurs by diffusion of carbon atoms through the surrounding austenite.

The nucleation of temper carbon at austenite-cementite interfaces was noted by Walker and Kondic<sup>(77)</sup> and ascribed to the preferred energy state of these



Correct indefinite chill structure  
for cast iron rolls according to  
Kamensky and Piskor.

FIG.28. Kamensky & Piskor. (75).



Mechanism of gamma-range graphitization (schematic), showing how growth of the graphite lattice (array of solid circles) ultimately must proceed by diffusion of carbon (solid circles) through austenite: (A) at some favorable area between austenite (left) and cementite (right), carbon atoms collect (B) to

form the nucleus of the graphite lattice; the corresponding iron atoms of the decomposing cementite form austenite which soon surrounds the graphite. Further deposition of carbon from the cementite (right, C), can only take place by diffusion of carbon through the intervening austenite.

FIG.29. Brown & Hawkes. (62).

sites. Russian workers<sup>(78.79)</sup> have confirmed these findings; considering interfaces, grain boundaries and free surfaces as sites where the dissipation of the strain energy induced by graphite deposition is easiest. The strain dissipation theory would account for the increase in solid state graphite nucleation after mechanical deformation or quenching which increases the number of flaws in the lattice.

Burke and Swindells<sup>(80)</sup> defined the rate determining processes during solid-state graphite growth:

1. solution of cementite in austenite
2. carbon diffusion through austenite
3. precipitation of carbon on to a suitable nucleus
4. removal of iron and solute atoms from the moving interface  
(strain energy term)

The relative importance of these steps in a given situation will depend on temperature and alloy composition<sup>(81)</sup>.

Hultgren and Ostberg<sup>(82)</sup> showed that the morphology of graphite formed by decomposition is not dependant on nucleation so much as on the subsequent growth conditions, which in turn depend on the temperature composition and the annealing atmosphere. High temperatures promote flake or flake aggregate forms in which graphite nucleates with the basal plane of the hexagonal lattice aligned with the nucleating surface. At lower temperatures, and in the presence of surface active elements such as sulphur<sup>(83)</sup>, the tendency is towards more compact aggregates.

Commercial malleable castings are cast completely white and annealed to develop a grey structure in various matrices. They are usually cooled below the  $AC_3$  transformation after casting before reheating to cause decomposition. The reason for this procedure, apart from ease of handling, is that the cooling process induces flaws in the cementite structure which aids graphite nucleation<sup>(78.79)</sup>. Another factor in improving the graphitisation of commercial malleable castings is that pearlite formed during cooling does not entirely re-dissolve on heating:

sufficient remains in the form of spheroids to greatly increase the nucleation-active austenite-cementite interface area. The nucleation characteristics of normal malleable irons are therefore different from those of white irons which decompose during continuous cooling after casting, or which are annealed without cooling below  $AC_3$ .

Apart from the deliberate exploitation of the metastable nature of cementite in malleableising, there exists another field involving the same mechanism: that of graphitisation in normal castings after solidification without reheating. Hughes<sup>(84)</sup>, in reviewing the development of a theory of grey cast irons, showed that cementite decomposition after solidification was at one time widely held to give rise to all the types of flake graphite encountered in cast irons. The indirect formation theory was discarded in the case of A and B graphite at an early stage. The mechanism of D-type graphite formation has been the subject of more recent controversy.

Eash<sup>(23)</sup>, using inoculation and quenching, concluded that the undercooled eutectic formed indirectly as a result of solid-state carbide decomposition. This view was shared by Morrogh and Williams<sup>(29)</sup>, who used an interrupted quench technique. Hultgren et al<sup>(8)</sup> disagreed with the cooling curve interpretations previously put forward and proposed direct formation from the liquid. Morrogh<sup>(85)</sup> later accepted the conclusions of Hultgren<sup>(8)</sup> and reinterpreted his results in terms of the direct formation mechanism.

The work of Berman and Kondic<sup>(86)</sup> demonstrated that the time required for cementite decomposition at temperatures close to the eutectic was of the same order as that of graphite formation on cooling. Later, Harris and Kondic<sup>(87)</sup> suggested that the formation of graphite by decomposition near eutectic temperatures could give rise to graphite similar in form to that of the undercooled eutectic.

Oldfield's experiments on ledeburitic irons<sup>(88)</sup>, quenched after rapid

heating to temperatures between the stable and metastable eutectics, produced a 'quasi-flake' graphite. This was unlike undercooled graphite, and led to his dismissal of the indirect formation theory. Recent work by Gadgil and Kondic<sup>(49)</sup> and also Fredriksson and Hillert<sup>(89)</sup>, suggests that some of the graphite in the cast structure, (especially 'streamers') may result from cementite decomposition. The origin of the streamer graphite noted by Kamensky and Piskor<sup>(75)</sup> may therefore be open to question.

The indirect formation mechanism has been put forward to account for the occurrence of several types of graphite found in cast irons affected by alloying elements. Morrogh<sup>(90)</sup> in 1941 reported the presence of graphite films distributed around areas of cementite and 'pre-existing' cementite in the mottled regions of cast irons containing titanium and sulphur and zinc and sulphur. Later investigation<sup>(91)</sup> of alloys with nickel and sulphur and copper and sulphur revealed similar features in which the graphite tended to be interconnected, forming continuous membranes around carbide. It was suggested<sup>(91)</sup> that these structures arose because the iron solidified in a white form and then graphitised. The mechanism proposed for cementite decomposition relied on the influence of temperature on the reaction:



This reaction proceeds to the right as temperatures fall, causing a reduction of the amount of FeS and a lessening of carbide stability, since sulphur has a neutral effect when combined in MnS. Williams<sup>(68)</sup> observed similar forms of graphite in manganese-free irons, and attributed the structures to the influence of sulphur.

Loper and Heine<sup>(76)</sup> defined the main classes of graphite which occur in regions of indefinite chill as follows:

1. Compact graphite formed in certain as-cast malleable irons (and graphite steels) where the carbon equivalent was just below the solubility of carbon in austenite (C.E. = 2.0). The compact form was said to be identical

to temper carbon in malleable irons, except that it was formed during cooling. The alloy known as 'Centra-steel' would seem to fall into this category<sup>(92)</sup>.

2. Film graphite formed when the carbon equivalent was slightly higher. Carbide films were initially formed, subsequently decomposing to produce long graphite filaments.

3. Lacy graphite was found at still higher carbon equivalents, when the amount of initial carbide was still greater.

Compact graphite formation was believed to occur in the solid state by cementite decomposition and carbon precipitation from supersaturated austenite. Continuous growth by diffusion and precipitation was made possible by a gradually decreasing temperature between the solidus and the  $AC_3$  transformation temperature. Film, lacy and Widmanstätten graphite were said to form in the last stages of eutectic freezing, or by carbide decomposition just after solidification. The indirect mechanism was found to be sensitive to alloying additions, especially tellurium and bismuth.

Boyes and Fuller<sup>(14)</sup> reviewed the formation of mottled structures where these graphite types occur. They pointed out that the characteristic mottled appearance was not the only form possible: simultaneous growth of grey and white eutectics might give structures in which the two eutectics were not discretely separated. In spite of this reminder, there is as yet no quantitative theory which could account for the matching of stable and metastable eutectic growth rates, or alternatively for sequential growth, presumably enabled by segregation, to cause close-coupled mottling.

An instance of 'indirect' graphite formation which is common to nearly all cast irons except those quenched immediately after solidification is that of deposition from supersaturated austenite during cooling below the eutectic temperature. The amount and extent of the graphite formed by this reaction will vary with the alloy composition, cooling rate and nature of the eutectic graphite

which acts as a nucleation substrate. Nevertheless, the fact remains that in the great majority of cast irons, eutectic graphite flakes are enveloped by an outer graphite layer formed in the solid state.

Djidjev<sup>(52)</sup> noted graphite concentrations at primary austenite-graphite eutectic interfaces, suggesting graphite deposition from supersaturated austenite, after complete solidification. This observation, together with the 'envelope' theory outlined above is interesting in the light of recent scanning electron microscope studies<sup>(41.42)</sup>, which explain graphite growth in terms of surface structures. Clearly, more work is necessary to establish the relationships between growth substrate structure, temperature and graphite morphology for carbon deposition from both liquid and solid states.

## 2.9 CONCLUSIONS AND OUTLINE OF THE PRESENT WORK

The wide structural variations possible in cast irons have been shown to result from the influence of a complex series of interdependent variables on nucleation and growth in the liquid and solid states. It appears that in many instances the full implications of possible physical and chemical interactions have not been appreciated. Instances of incomplete knowledge appear in all aspects of solidification of Fe-C-Si alloys from the liquid state, to solid-state reactions.

Various methods have been devised for studying the relative importance of interdependent variables in determining cast iron structure. Controlled solidification experiments which produce steady state growth conditions have been used by many investigators. The disadvantage of these methods is that they are restricted to growth studies, and cannot easily cover the complex range of nucleation-growth interactions encountered in real castings.

In commercial castings, the common methods of structural control are centred on variations in nucleation (alloy composition and liquid metal treatments), cooling rate and post-solidification heat-treatment. This field may be

studied using production or specially-designed castings, applying control by means of composition and casting variables. Random variation of growth rate and direction in such cases makes determination of solidification sequences and nucleation and growth stabilities difficult.

The first part of the present series of experiments was designed to control the conditions of nucleation and growth in a test casting by directional and reproducible heat extraction, and thus improve the normal casting or chill-test casting methods of investigation. For this purpose, three alloys with a range of carbon and silicon contents, but standard carbon equivalents, were cast in heated ceramic moulds cooled at one end by a water-cooled copper chill (thus avoiding solidification from the mould sides). The cooling conditions gave a continuous range of solidification forms; from those found at slow cooling rates, to the high degree of non-equilibrium at the chill. It was hoped that by relating structures to the thermal conditions under which they formed, a clearer picture of the stable-metastable eutectic transition in liquid and solid states might emerge. These experiments were supplemented by steel chill/sand test castings in all three alloys to relate the structures formed under controlled conditions to those encountered in foundry practice.

An extension of this work examined solidification and high temperature solid state behaviour of mottled and white structures. Thin plate and rod sections were cast in heat resistant metal moulds, maintained at temperatures close to those of solidification of Fe-C -Si alloys for varying times before water quenching. This technique produced white or mottled structures by rapid cooling through the metastable eutectic temperature and enabled study of decomposition processes under near-isothermal conditions without cooling below  $AC_3$  and reheating. These conditions are likely to occur in large castings where chills are present; especially those of the solid variety with fixed thermal mass.

In order to extend the range of cooling rates even further, solidification under extreme non-equilibrium conditions was studied by casting one of the alloys

into chill moulds using very small specimens. These experiments gave information about the nucleation and growth of the white eutectic.

The same alloy was used to study the effect of a range of alloying elements on phase morphologies and interdependence of growth forms under the solidification conditions present in the heated ceramic moulds.

### 3. EXPERIMENTAL PROCEDURE

#### 3.1 ALLOY PREPARATION

The alloys used in these experiments were based on typical commercial cast irons with carbon equivalents of 4.0. Alloys were prepared as 75 kg melts in an acid-lined H.F. furnace using oxygen-blown vanitit, armco iron, silicon metal, ferromanganese and ferrous sulphide. Melt additions were made to vary the carbon and silicon contents, while keeping the other elements constant. The compositions of the three irons produced are given in Table 2.

The melting stock was sand cast as bars 18 cm long and 6.5 cm dia. These bars were sectioned into 1 kg billets which were used in the series of ceramic mould experiments. Furnace charges for the heated metal mould experiments were made by remelting the stock alloy in a rapid melt electric induction furnace, casting at 1550°C into steel chill moulds as cylinders 2.5 cm dia. The white iron rods were sectioned using a slitting wheel to give pieces suitable for remelting in small crucibles. Grey iron for the chill experiments was cast at 1300°C in ceramic shell moulds, giving bars 2.5 cm diameter.

#### 3.2 CERAMIC SHELL MOULD PRODUCTION

Ceramic shell moulding was extensively used in these experiments for the production of moulds, crucibles, pouring basins and runners, and as a means of producing accurate metal moulds. Although the designs of the ceramic shells varied widely, the methods by which they were made were similar.

In all cases, wax patterns were made by casting molten wax into silicone-lubricated duralumin moulds. Component parts of the pattern were assembled by welding with a hot knife. Completed patterns were degreased in trichloroethylene and then dipped in a solution of detergent to aid wetting.

Ceramic shells were built up using primary coats of slurry and subsequent layers of coarser refractory material (Table 3). After primary coating, a

ALLOY	C	Si	Mn	S	P
M 85	3.57	1.00	0.21	0.031	0.015
M 89	3.37	2.04	0.22	0.034	0.015
M 91	3.23	2.43	0.22	0.034	0.015

TABLE 2. Composition of Alloys (%) supplied by B.C.I.R.A.

Primary slurry		Secondary slurry	
Syton 2X	100ml.	Ethyl Alcohol	43ml.
Lissapol	0.5ml.	Shellac	1gm.
n-Octanol	1.0ml.	Water	6ml.
Zircon Flour	400gm.	Conc HCl	0.2ml.
		Silester O.S.	56ml.
		F.F.Sillimanite	160gm.

TABLE.3. Composition of Primary and Secondary Slurries for Ceramic Shell Moulds.

fluidised bed of 30-80 grade aluminium silicate gave an initial stucco coating which was allowed to dry in air for six hours before a second primary coat was applied. The secondary layers, which followed the primary coats after twelve hours, were applied by dipping the pattern into an acidified (pH 2-3) ethyl silicate solution, followed by coating with 16-30 grade molochite using a fluidised bed. Suspension of the pattern in an ammonia-filled container for three minutes gelled and hardened the ethyl silicate binder. Coats were applied at ten minute intervals to extend the useful life of the binding solution by allowing ammonia evaporation from the pattern. Five coats of secondary stucco gave a shell approximately 8 mm thick which was allowed to dry overnight before dewaxing.

To counteract mould cracking on dewaxing, the moulds were placed in a muffle furnace at 1000°C. The thermal shock gave a thin layer of molten wax at the mould wall, which cushioned the brittle refractory during the subsequent wax expansion. Mould firing at 1100°C for 1 hour strengthened the refractory and removed any carbon left from the dewaxing process.

### 3.3 CERAMIC MOULD EXPERIMENTS

The object of these experiments was to produce a widely varying range of structures within one test bar. Cylindrical ceramic shell moulds 25 cm long and 2.5 cm dia were produced (Fig. 30), having an enlarged cavity at the base to accept a chill. A mould preheating furnace limited nucleation at the mould walls while solidification took place under the influence of the water cooled copper chill at the mould base. Melting and mould conditions were varied to investigate the effects of casting variables such as pouring temperature and mould temperature.

#### 3.3.1 MELTING UNIT

1 kg cylindrical charges were melted in a 10 Kc/S E.M.A. induction heating unit, supplied by a 50 Kw middle frequency generator operating at 420-440 V.

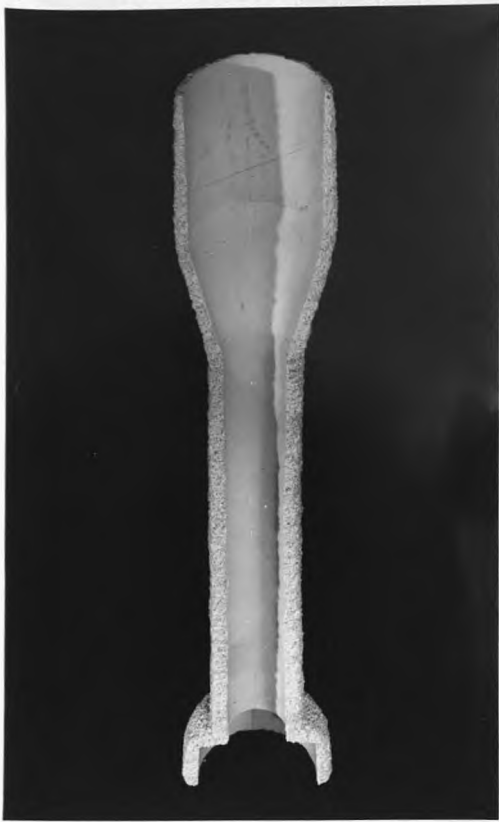


FIG. 30. Ceramic Investment Mould and Wax.



FIG. 31. General View of the Melting Unit with the Mould Heating Furnace in Position.

The advantage of the unit was that melting and pouring could be carried out in 2-3 minutes. During melting, the charge was contained in a zircon sand-sodium silicate-CO<sub>2</sub> bonded crucible. The melt was retained in the crucible by a cylindrical plug of cast iron or steel 2.5 cm dia and 0.6 cm thick, situated out of the immediate inductive range of the coil. The plug was melted by the molten charge. As soon as the plug melted, the charge drained rapidly through the 1 cm hole in the crucible base into the mould below. Fig. 31 shows a general view of the melting unit.

### 3.3.2 CERAMIC MOULD PREHEATING FURNACE

The preheating furnace consisted of 14 silicon carbide resistance elements arranged in two circuits, one of six bars being connected through a variac and ammeter, while the eight bar assembly was used for automatic temperature control via a Pt/Pt 13% Rh thermocouple and temperature recorder/controller. The controlling thermocouple was inserted through the side of the furnace so that its hot junction touched the mould surface half way along the test bar. A sillimanite or stainless steel tube between the mould and elements ensured an even heat supply to the mould. The water cooled copper chill was positioned below the furnace body so that its face was level with the furnace baseplate (Fig. 32).

Moulds were fitted over the copper chill and centralised in the furnace. The furnace top was closed by shaped sillimanite refractory bricks which reduced convection and stabilised the mould at the furnace centre. All gaps at the mould base and furnace top were filled with asbestos wool to limit convection and guard against metal entering the furnace or leaking from the join between the mould and chill.

A mould temperature of 1150<sup>0</sup>C was found to minimise eutectic solidification from the mould walls, and the preheat furnace was maintained at that temperature for all the heated mould experiments. The working temperature of 1150<sup>0</sup>C could be attained within 45 minutes, and in practice a further 15 minutes were

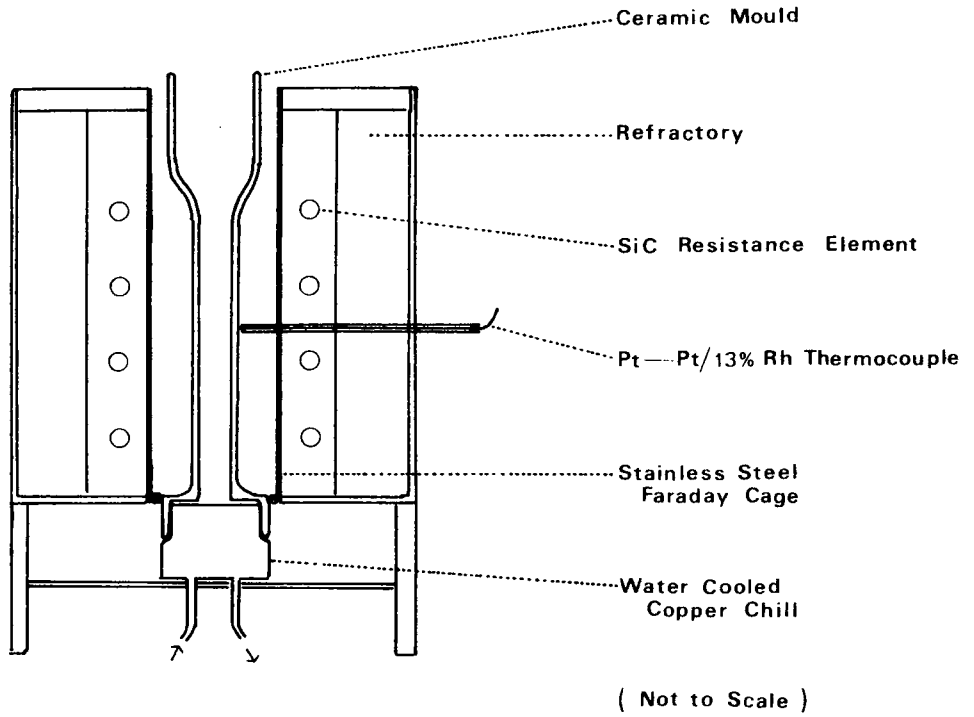


**FIG. 32** Preheating Furnace, Ceramic Mould and Chill.

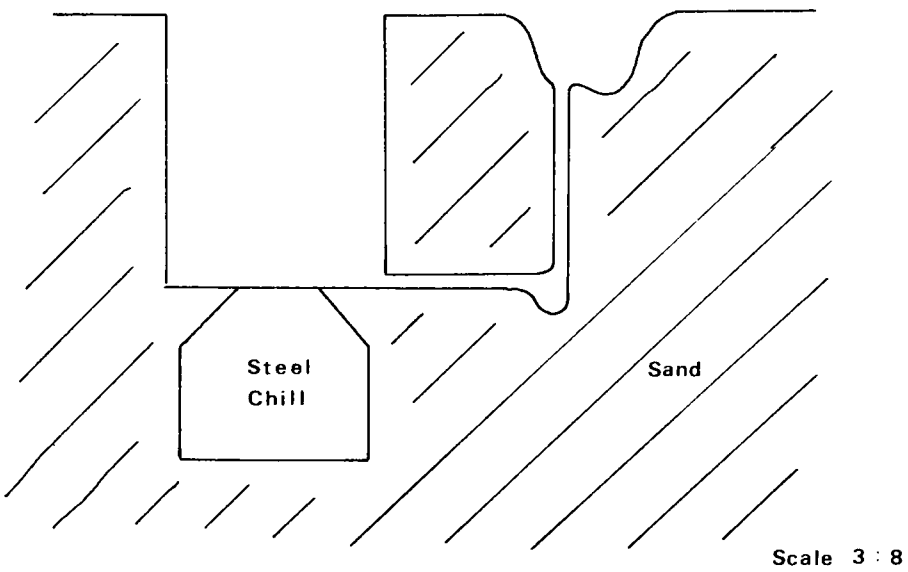


**FIG. 33** Chill/Sand Mould.

allowed for temperature stabilisation before pouring. Any tendency for water condensation on the chill was reduced by using only minimal water circulation until 2 minutes before pouring, when full pressure was applied.

### 3.3.3 CASTING PROCEDURE

Pouring temperatures were attained accurately by varying crucible plug material, using cast iron discs at low superheats, and similar steel plugs at higher temperatures. The relative masses of the charge and plugs were such that negligible compositional differences resulted from the use of steel plugs. Control of the power input during melting and pouring gave a maximum temperature equal to that desired for pouring. Once this was achieved the input was maintained until pouring took place. The temperature of the melt was measured in the crucible by means of a silica-sheathed Pt/Pt 13% Rh thermocouple, connected to an 'Xactrol' temperature recorder.

After pouring, the preheat furnace was left on for 30 minutes, during which time solidification took place under the action of the chill. The furnace temperature was found to rise to 1200-1220°C after pouring, falling to 1150°C after about 10 minutes. Water circulation in the chill was maintained after switching the furnace off until the mould reached 300°C, when the mould could be removed.

All three alloys were cast at 1440°C into ceramic moulds preheated to 1150°C. The effect of superheat was investigated in the 2.04 Si alloy by casting into an 1150°C mould at 1290°C. The effect of mould temperature on chill and mottle formation was studied by repeating the 1440°C superheat series of castings with the furnace at room temperature.

After mould stripping, the chill flash was removed and retained. The castings were then sectioned longitudinally using a slitting wheel mounted on a travelling bed surface grinder. Sections were surface ground and then polished using water lubricated silicon carbide papers. This treatment formed the basis of subsequent examinations.

### 3.3.4 THERMAL ANALYSIS IN CERAMIC MOULDS

Attempts were made to establish thermal sequences within the mould during solidification using Pt/Pt 13% Rh thermocouples and a high speed multipen recorder. Before use, all thermocouples were calibrated against a sub-standard Pt/Pt 13% Rh thermocouple at temperatures of 700 and 1000°C. A tolerance of  $\pm 2^{\circ}\text{C}$  at 1000°C was allowed in the thermocouples used in these experiments.

Thin silica sheaths were set in the wax patterns at measured distances from the chill. On investment and dewaxing they projected into the mould cavity so that the thermocouple tips when inserted were in the central axis of the cylindrical casting. The twin-bore recrystallised alumina thermocouple insulators were secured to the mould sides with thin chromel wire to support their weight at high temperature. The thermocouple junctions with the compensating leads were passed through the top of the furnace into a water cooled copper cylinder filled with alumina wool. This arrangement prevented overheating and inaccuracy at the compensating lead connections. The compensating leads were connected to a 'Rikadenki' 5-pen recorder, the temperature at the terminals being measured by a mercury in glass thermometer.

As the number of recording pens was limited, temperature measurements were made in two series for each set of casting conditions. The thermal sequences in each casting were examined at four positions, and each set of casting conditions was therefore covered by eight analyses at distances between 0.5 and 16 cm from the chill.

Initial experiments showed substantial A.C. pickup by the thermocouples from the inductive fields of the preheat furnace elements. This was reduced by using a stainless steel Faraday cage around the mould, and by encasing the compensating cables in a copper braided sheath. The cage, cold junction enclosure and braided sheath were in electrical contact and earthed to a cold water main. In spite of the extensive shielding, the thermocouple traces still showed signs of disturbance. This made thermal recording impossible with the preheat furnace in operation.

Two series of castings were produced in the 2.04% Si alloy with temperature measurement in operation, using a 1440°C pouring temperature in both cases. In the first set, the mould was at room temperature, the preheat furnace being switched off throughout. In the second series, preheating of the mould to 1150°C was discontinued as soon as pouring took place. In this way, interference-free cooling curves were obtained for the heated mould. Thermal conditions identical to the previous experiments were not achieved. Heavy insulation of the preheat furnace reduced heat losses in the heated mould experiments, and enabled a comparison of the relative effects of chill and mould environment under the two sets of casting conditions.

### 3.4 CHILL-SAND CASTINGS

The nature of the cooling process in the ceramic mould experiments made correlation with chill-sand mould solidification desirable. This was especially necessary in view of the use of 'dynamic' water cooled copper chills, as opposed to the 'static' type of solid chill found in normal practice.

A solid steel chill was inserted in a bromsgrove red/plumbago sand mould (Fig. 33) to simulate a typical industrial chill situation. The steel chill was coated with a thin layer of graphite to prevent metal adhesion.

Thermal analysis was carried out using 0.25 mm Pt/Pt-13% Rh thermocouples enclosed in silica tubes, drawn out to give a thin wall at the hot junctions. The tubes were bound together with fine chromel wire and clamped vertically at fixed distances above the chill surface. Temperature records were obtained in the same way as for the ceramic mould experiments.

2.5 Kg billets of all three alloys were melted in the 50 Kw induction furnace and bottom poured into chill-sand moulds at 1400°C. The resulting bars were sectioned longitudinally, one face being surface ground for macro examination, while the other portion was further sectioned and ground for microstructural studies.

### 3.5 METAL MOULD EXPERIMENTS

A feature of cast iron solidification is the possibility of structural changes in the solid state during or immediately after the completion of freezing. These processes were examined by casting thin section samples into heated metal moulds. Rapid cooling of the molten metal resulted in metastable solidification, while the elevated temperature of the moulds enabled study of transformation processes at temperatures near the eutectic.

Initial experiments with copper and steel moulds indicated the feasibility of the technique, but brought to light properties required of the mould material: heat, oxidation and melt reaction resistance, coupled with good conduction at elevated temperatures. The first alloy chosen as a mould material was Ni-20% Cr, used for the production of cylindrical moulds. Moulds for later experiments with thin plate castings were made in AISI type 310 stainless steel (55% Fe, 25% Cr, 20% Ni) for ease of machining and casting extraction.

#### 3.5.1 CYLINDRICAL MOULDS

Ni-20% Cr alloy was prepared by direct alloying in an induction furnace and cast into 1 cm bars in steel chill moulds. The billets were cut into 4 cm lengths and drilled longitudinally to give a cylindrical mould cavity which just penetrated the mould base to allow air escape on casting. Mould tops were machined to produce a thin projecting tube of metal which located the silica down runner of the melting crucible (Fig. 34). A length of heat resistant nickel alloy strip, spot welded to the mould, served as a lifting rod and thermocouple support. Moulds were produced with a range of internal diameters (4 mm, 3 mm and 2 mm), giving a variety of cooling conditions.

0.25 mm Pt/Pt-13% Rh thermocouples were introduced into the mould cavity through 2 mm holes drilled in the side of the mould 1 cm from the base. 28 S.W.G. chromel-alumel thermocouples inserted into blind holes in the mould wall monitored mould temperature. Compensating leads from the thermocouples were welded to copper wires connected to a 'Rikadenki' 5-pen recorder. The



FIG.34. Ni/20%Cr Cylindrical Mould.

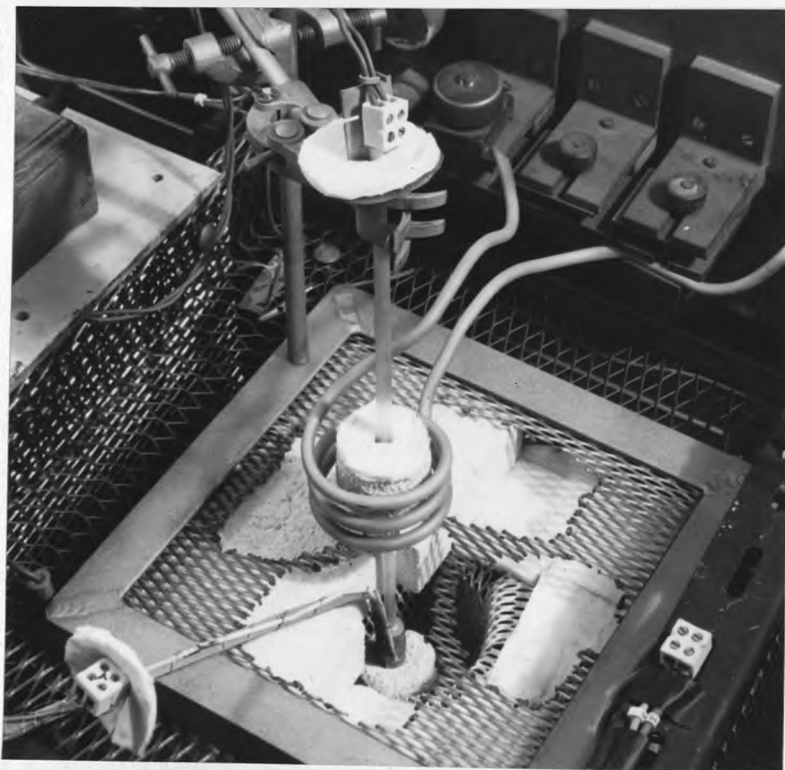


FIG.35. Heated Metal Mould Casting Apparatus.

cold junctions were insulated with plastic and sealed in oil-filled glass tubes maintained at 0°C in crushed ice.

### 3.5.1.1 MELTING PROCEDURE

The melting unit consisted of a 6-9 Kw Delapena h.f. generator operating at 400-440 V, supplying a 5 cm dia water cooled coil at 375 Kcs/sec. Furnace charges of approx. 50 gms (the minimum for accurate temperature control) were contained in ceramic shell crucibles 2.7 cm dia and 3 cm high, supported beneath the coils by a silica tube resting on the preheat furnace top (Fig. 35).

A hollow silica stopper rod sealed a 5 mm hole in the crucible base. Melt temperatures were measured using a Pt/Pt-13% Rh thermocouple inserted into the stopper rod so that the hot junction coincided with the melt centre. On melting, the temperature of the charge was monitored via the thermocouple and a potentiometer. When the pouring temperature was reached, removal of the stopper rod allowed rapid pouring of the charge through a 5 mm silica tube moulded into the base of the crucible and attached to the lip of the metal mould in the preheat furnace below.

The mould preheat furnace consisted of six silicon carbide resistance elements in series, set in sillimanite refractory bricks. Temperatures were controlled via a central Pt/Pt-13% Rh thermocouple, variac and a temperature recorder-controller. A.C. pickup, which had been a problem in the larger ceramic mould preheat furnace, was entirely eliminated by the use of a stainless steel mesh Faraday cage which totally isolated the furnace elements. The exterior of the furnace, variac and temperature-controlling relays were shielded with earthed steel mesh.

As moulds were heated by the solidifying metal, mould preheat temperatures were some degrees lower than the temperatures at which the castings ceased to cool rapidly. The magnitude of the mould temperature rise varied with the internal diameter of the mould. Castings were produced in all three alloys at a range of mould temperatures with a constant pouring temperature of 1300°C (Table 4).

EXPT.	ALLOY	MOULD DIAMETER mm.	MOULD TEMPERATURE °C.	TIME TO QUENCH mins.
A	1.00%Si	3	1015	0.55
B	1.00%Si	3	1015	8.00
H	2.04%Si	3	1017	0.50
J	2.04%Si	3	1017	8.00
K	2.04%Si	3	1033	0.40
L	2.04%Si	3	1039	4.40
M	2.43%Si	2	1006	0.25
N	2.43%Si	2	1015	2.00

TABLE 4. Ni/20%Cr Cylindrical Mould Casting Conditions.

EXPT.	ALLOY	MOULD TEMP. °C. (mean)	TIME TO QUENCH, mins.			
			1	2	3	4
R	2.43%Si	1060	0.5	1.5	-	6
S	2.43%Si	1065	0.5	1.5	3	6
T	2.43%Si	1070	0.5	1.5	-	-
V	2.43%Si	1083	0.5	1.5	3	6

TABLE 5. '301' Stainless Steel Cruciform Mould Casting Conditions.

After casting, moulds were withdrawn after measured intervals and quenched in water (Fig. 36). As casting extraction was impossible, both mould and casting were sectioned longitudinally using a liquid-cooled grinding wheel to expose the iron specimen. The resulting section was prepared for metallography in the normal way.

### 3.5.2 CRUCIFORM PLATE CASTINGS

Cruciform plate castings 1.5 cm x 0.5 cm with arms 2 mm, 1.5 mm, 1.0 mm and 0.5 mm thick were produced in '301' stainless steel divided moulds (Fig. 37). The moulds themselves were cast by the ceramic investment process using a duralumin die for wax injection.

Mould halves were bored with 2 mm registering holes and clamped together using stainless steel locating pins. Thermocouple support and mould handling was enabled by spot welding a length of nickel alloy strip to one half of the mould (Fig. 38). Optimum filling was obtained by mounting the moulds vertically and using the 1.5 mm plate as a sprue.

Metal was directed into the mould cavity by means of a ceramic pouring cup produced by investing a wax pattern joined to an alumina insulating bead. These were attached to the moulds using pyruma cement, which was hardened by baking at 200°C for  $\frac{1}{2}$  hour. The alumina bead tended to insulate the mould from the metal solidifying in the pouring cup and therefore reduced mould heating.

Mould temperatures were monitored using 28 SWG chromel alumel thermocouples inserted in blind holes drilled in between the arms of the mould cavity. Cooling curves were obtained from 0.25 mm Pt/Pt-13% Rh thermocouples sited in the mould cavities at the plate centres. All thermocouples were bound to the supporting strip using thin chromel wire.

Study of the time dependence of high temperature transformation processes demanded careful standardisation of casting and mould conditions. For this

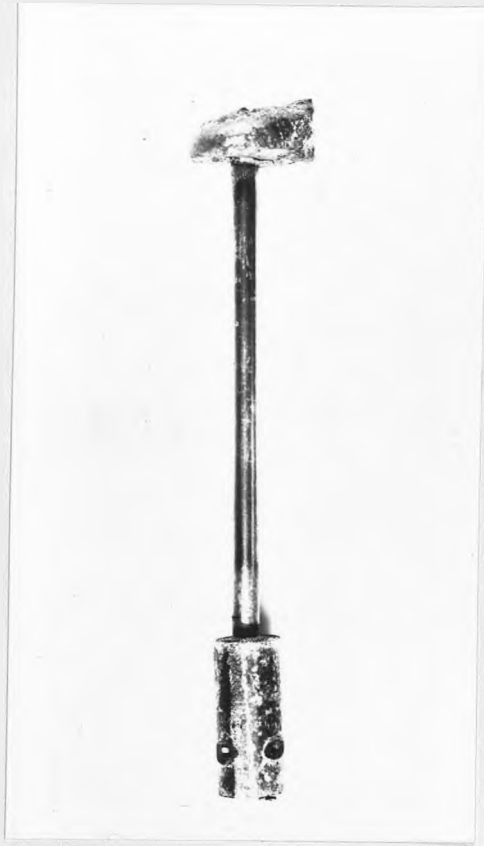


FIG.36. Cylindrical Mould with Casting in Situ.



FIG.37. Cruciform Mould with Casting in Situ.



FIG.38. Cruciform Mould Assembly with Pouring Cup.

reason a four-way crucible/melt distributor was designed and produced by the investment process (Fig. 39). This enabled casting of four equal amounts of metal of the same composition and superheat into four moulds maintained at equal temperature in the preheat furnace.

The preheat furnace in this series of experiments was the same as that for the cylindrical moulds. The furnace top was modified to provide four entry and withdrawal ports for the moulds, in addition to the central hole for the crucible-distributor. A projection half way down the distributor shaft located it in the preheat furnace top at the correct level relative to the induction coil and moulds.

In practice, after setting the distributor in place, the furnace top was insulated using alumina matting and an earthed heat resistant mesh shield, both pierced for mould withdrawal. The moulds were inserted and positioned with their pouring basins under the spouts of the distributor. The holes in the furnace top were then heavily insulated with alumina matting to minimise heat loss.

Mould preheating, melting and pouring procedures were the same as for the cylindrical moulds, except that charges of 100 grams were employed. After pouring, moulds were withdrawn at pre-set intervals and quenched in a water bath.

Castings were made in the 2.4% Si and 1.0% Si alloys, pouring at 1600°C with a variety of mould temperatures (Table 5). After cooling, the steel clamping pins were removed and the castings extracted by lifting from the mould cavity (Fig. 40). Plate arms were sectioned longitudinally and transversely and thermoplastic-mounted for metallography.

### 3.5.3 PLATE CASTINGS

In view of the possibility of interaction between the thermal fields of the different plates in the cruciform castings, the '301' stainless steel moulds were redesigned to produce plate castings of a single 1 mm thickness (Fig. 41).

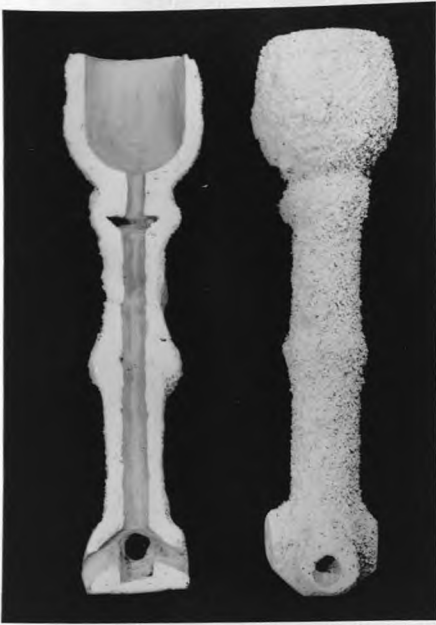


FIG.39. Four-way Melt Distributor.



FIG.40. Extracted Cruciform Casting.



FIG.41. Extracted 1mm. Plate Casting.

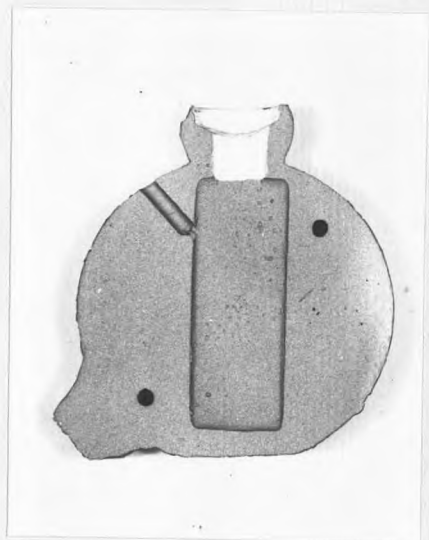


FIG.42. 1mm. Plate Mould.

All the features of the cruciform mould experimental technique were otherwise retained. 0.25 mm Pt/Pt-13% Rh thermocouples were introduced into the mould cavity via a 2 mm hole bored on the mould parting line (Fig. 42).

Castings were again produced in the 2.4% Si and 1.0% Si alloys using the superheat/pouring temperature of 1600°C with preheated moulds at a range of temperatures (Table 6). After stripping, the castings were sectioned longitudinally and transversely for micro examination.

### 3.6 CHILL CASTING EXPERIMENTS

Both ceramic and shell mould casting processes involved 'chill' solidification. Microstructures indicated certain differences from normal hypoeutectic metastable solidification, and it was hoped that controlled chill casting might give information about metastable eutectic nucleation and growth. The chill casting experiments were designed to produce the highest possible cooling rates using conventional casting processes.

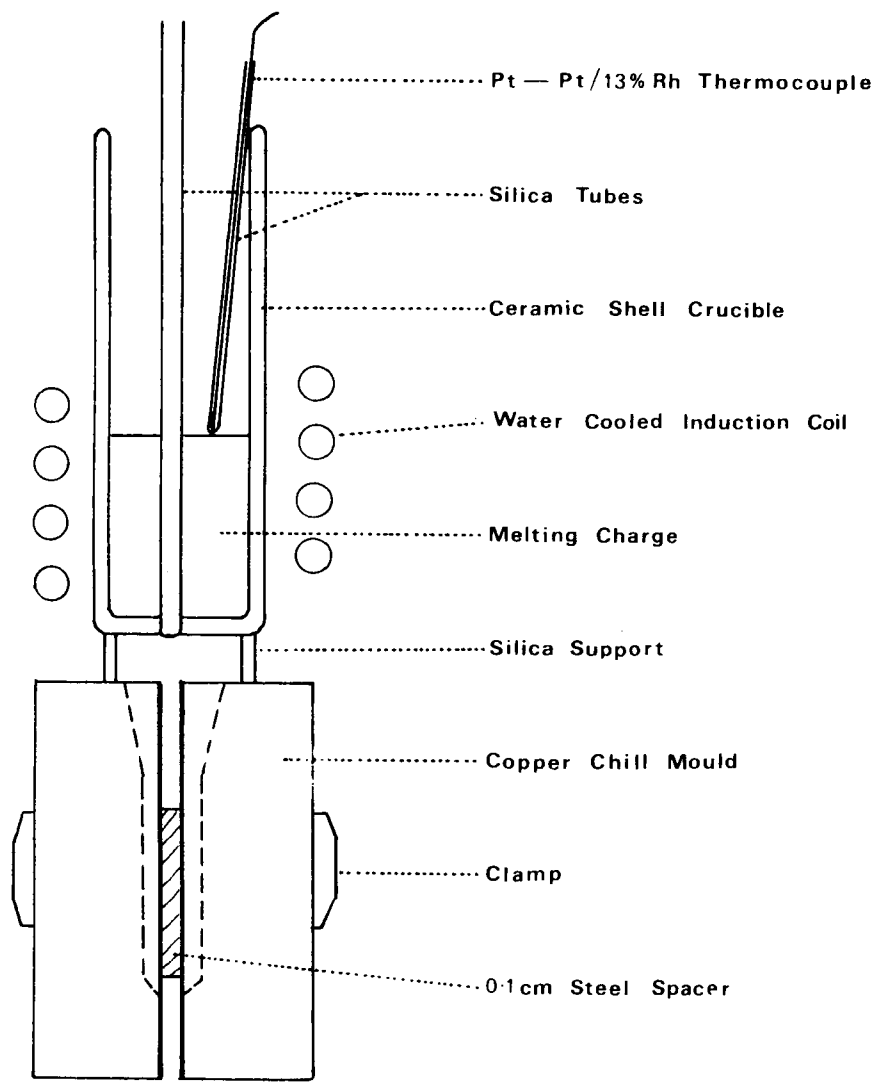
#### 3.6.1 MELTING AND CASTING PROCEDURE

The melting unit and controlled bottom pouring crucible technique were the same as used in the heated mould experiments. 3.5 cm sections were cut from 2.5 cm diameter bars of the 2.04% Si alloy cast in ceramic shell moulds. Each billet was drilled with an axial 4 mm hole for the crucible stopper rod, giving furnace charges of 80-90 gms. These were melted in ceramic shell crucibles 2.7 cm diameter x 7 cm high, supported beneath the induction coils by a silica tube. Chill specimens 1 cm diameter x 6 cm long were cast in a massive copper chill mould situated below the crucible (Fig. 43). The range of solidification conditions was increased by introducing 1 mm steel spacers between the flat mould faces, producing a gap in which metal could solidify as a rapidly cooled flash. The body of the cylindrical casting provided information on solidification at lower cooling rates.

Nucleation at the mould walls was examined after polishing the chill mould

EXPT.	ALLOY	MOULD TEMP. °C. (mean)	TIME TO QUENCH, (mins)			
			1	2	3	4
C	1.00%Si	1036	-	0.85	11.4	21.0
D	1.00%Si	1060	1.2	4.2	6.3	26.5
E	1.00%Si	1092	2.0	14.0	25.0	36.0
F	1.00%Si	1100	1.3	7.0	14.0	30.0
G	1.00%Si	1115	2.5	7.5	14.0	32.0
O	2.43%Si	991	1.0	2.4	5.0	10.0
P	2.43%Si	1040	1.9	3.9	6.9	9.9
Q	2.43%Si	1050	0.8	3.0	-	13.0
U	2.43%Si	1063	0.9	2.1	3.0	10.0

TABLE 6. '301' Stainless Steel 1mm. Plate Mould Casting Conditions.



( Not to scale )

FIG. 43 Chill Casting Apparatus.

with "Sylvo". Flash specimens from the polished mould could be examined at a magnification of up to 1250 times by optical microscopy without metallographic preparation.

Chill castings were made in the 2.04% Si alloy, pouring at a range of temperatures (1160; 1200; 1300; 1400; 1500; and 1600°C) to investigate the effect of superheat. Alloying additions of 0.2 atomic % aluminium, <sup>magnesium</sup> and tellurium were made to castings produced at 1400°C to study their influence on chill structures. Alloying additions were introduced by packing the required amount of the pure granulated element into 2 mm holes drilled longitudinally into the billets. These holes were sealed with rammed cast iron drillings before melting, thus minimising losses during melting.

### 3.6.2 INITIAL TREATMENTS

Transverse sections for metallography were cut from the cylindrical chill bars. These, together with longitudinal and transverse flash sections, were hot mounted in P.V.C. (I.C.I. "CORVIC" P.V.C. D60/13), which provided a closely adhering matrix and resisted rounding and acid infiltration at the specimen edges. Flash specimens produced in the polished mould were examined without polishing, both in the as-cast condition and after heat tinting and etching. Heat tinting was carried out in air, using an electric hotplate at 350-450°C until the desired surface colour was obtained. Prolonged etching in 5% picral for up to 2 hours revealed surface detail.

### 3.7 HEATED CERAMIC MOULD ALLOYING EXPERIMENTS

The series of heated ceramic mould experiments was extended by making 0.2 atomic % additions of Al, Mg, Bi, Ti, Sr, Ca and Te, to the 2.04% Si alloy. Alloying additions were packed into 5 mm holes drilled longitudinally into the 1 Kg furnace charges to different depths at various positions. The holes were then sealed with cast iron drillings. This method ensured even distribution of additions and reduced air melting losses.

Castings were poured at 1440°C with moulds at 1150°C to determine the

effects of graphite promoters and carbide stabilisers on the stable-metastable transition and individual phase morphologies under the conditions of solidification imposed in the heated moulds. Compositions of additions are given in Table 7

### 3.8 METALLOGRAPHY

Macro examinations were carried out after etching surface-ground specimens for 2 minutes in 20% nital. Macrostructures were darkened before photography with 30% hydrochloric acid.

All sections for micro examination were ground on water lubricated silicon carbide paper down to 600 grade. This was followed by alternate etch-polishing with 5% picral and a rotating 1 micron diamond lap, until all grinding marks disappeared. Final etching and polishing on a 0.25 micron diamond lap was repeated twice before further treatment.

A variety of etchants was employed in microstructural examinations. 2% nital and 5% picral were used for normal white and grey microstructures. For examination of cementite decomposition, it was necessary to use etches which revealed the boundaries of decomposed cementite colonies. Hultgren<sup>(93)</sup> reported the use of alkaline sodium picrate for this purpose in steels and it has since been shown to be effective for cast irons<sup>(53)</sup>. The use of sodium picrate was extended by using a double etching process, etching for 30 secs in boiling alkaline sodium picrate, drying, and then re-etching in 2% nital for 15 secs. The nital stripped off the surface film left by the first etch and gave good graphite and matrix definition, while retaining the cementite colouration. During the course of this work bromine was found to be a useful etch for showing segregation and decomposed cementite areas. A  $\frac{1}{2}\%$  solution of bromine in methanol was applied to the polished specimen surface and washed off after  $\frac{1}{2}$ -1 second with hot water, followed by acetone. This etch could also be used with nital for greater matrix definition.

Zeiss Ultraphot and Universal microscopes were used for examination and recording of representative microstructures in all specimens. Microstructural

Element	Purity %	Form
Al	99.993	Cast Bar
Mg	98.5	"
Bi	99.97	"
Ti	99.9	Wire
Sr	99.99	Cast Bar
Ca	99.5	Borings
Te	99.5	Cast Bar

TABLE 7 . Composition of Alloying Additions .

features in the ceramic mould specimens were related to overall structure by measuring their position relative to the chill face. Distances were recorded using the vernier attachment on the microscope stage.

### 3.9 SCANNING ELECTRON MICROSCOPY

Selected areas (maximum 1 cm square) were cut from polished samples and deep etched in 10% hydrochloric acid in alcohol for 12 hours. As the alloys contained silicon, a few drops of hydrofluoric acid were added to the etchant to improve its action. An alternative etch which was useful in exposing carbide structure was a 5% solution of bromine in methyl alcohol, applied for up to 12 hours. After etching, specimens were cleaned in boiling acetone and dried in a hot air stream.

All specimens were mounted on aluminium carriers using 'Durofix' flue with silver dag to provide a conducting path from specimen to stub. This prevented charge build up on the specimen which may cause image fogging.

The scanning electron microscope used in this investigation was a Cambridge Stereoscan Mk II. This instrument enabled surface examinations with a greatly increased depth of focus. The best resolution obtainable is about 200 Å, but this is dependent on the morphology and atomic number of the materials concerned. After selective deep etching treatments, the technique gives stereoscopic views of the unattacked phases. The method is of obvious use in the study of graphite in cast irons, and has been employed by several investigators.

The object of scanning electron microscopy in this series of experiments was to examine the form and continuity of graphite and cementite in test specimens. Results are accompanied by an angle, representing the angle between the normal to the specimen surface and the electron beam.

### 3.10 MICROPROBE ANALYSIS

Microprobe investigations were carried out using a Cambridge Microscan Mk IIA microanalyser. This equipment is suitable for semiquantitative and qualitative analysis of inclusions and segregation, and is capable of detecting elements above sodium in the periodic table.

Specimen surfaces were prepared by the techniques used in normal metallography, polishing to 0.25 micron after mounting in conducting bakelite. Surfaces were lightly etched in 1% picral to enable specimen orientation under the electron beam. Heavy etching was avoided as this can lead to topographical and leaching effects which may influence results.

### 3.11 HARDNESS TESTS

Hardness testing was used as a guide to overall structural variation between heated ceramic mould specimens with pure element additions. A standard Vickers testing machine, with 10 Kg load and mounted with an adjustable vernier table, gave hardness values at intervals of 0.5 mm along the central axis of each specimen using the chill as reference zero.

## 4. EXPERIMENTAL RESULTS

### 4.1 CERAMIC MOULD COOLING CONDITIONS

The heated mould experiments were designed to inhibit eutectic nucleation and growth from the mould walls, while permitting directional solidification under the influence of the water cooled copper chill at the mould base. The technique is a development of the conventional chill/sand test casting, with modifications introduced by the use of a different mould material and a water cooled chill. In view of the sensitivity of cast iron to solidification conditions, it is of importance to investigate thermal processes in heated and unheated ceramic moulds.

#### 4.1.1 THERMAL ANALYSIS RESULTS

Cooling curve data from the room temperature and heated mould experiments was analysed to determine the influence of mould temperature on the severity and extent of the chill effect. The methods used in cooling curve analysis were similar to those of Hughes<sup>(73)</sup>.

Curves showing the progress of eutectic solidification with respect to bar position were plotted from eutectic arrest data (Fig. 44). Isochrone plots of temperature distribution vs distance from the chill (Fig. 45) showed discontinuities corresponding to the passage of 'chill waves'. The points of discontinuity were joined to define the path of the chill waves AB, A'B', which move from the chill along the casting axis with time. The lines AB and A'B' were replotted on distance-time axes and superimposed on the eutectic solidification curves (Fig. 44) to indicate sections of the castings subject to chill influence during solidification.

The positions of the chill effect lines can only be obtained by extrapolation once eutectic solidification starts, since the temperature distribution lines become compressed. Extrapolated portions are shown by dotted lines.

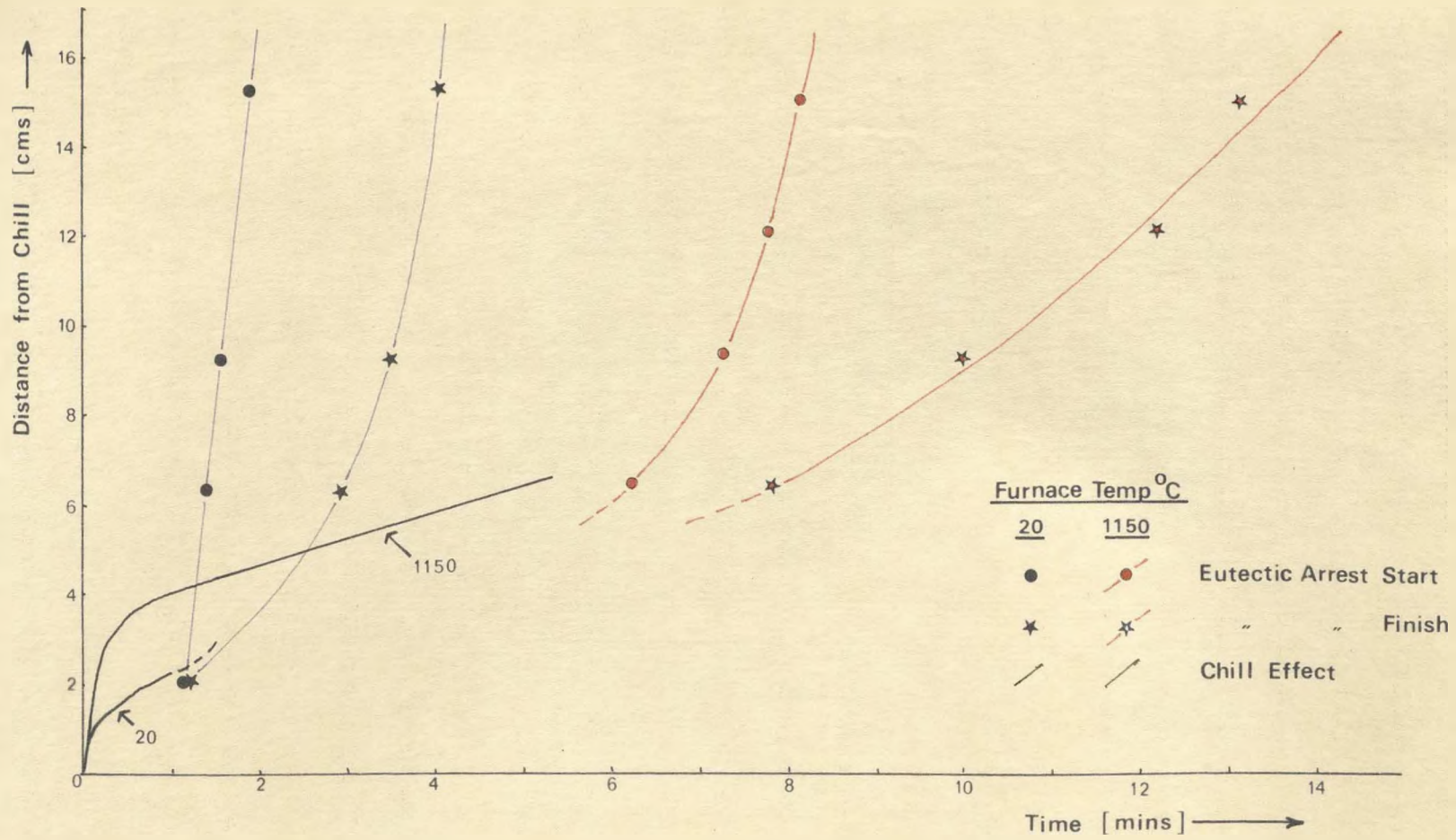
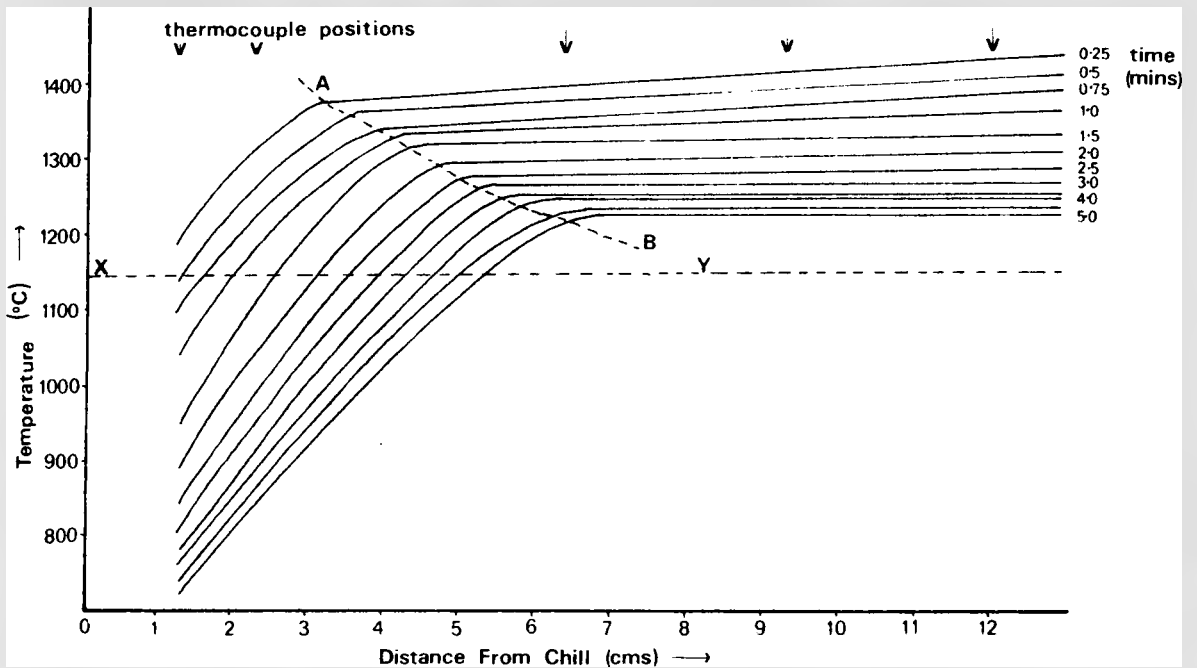
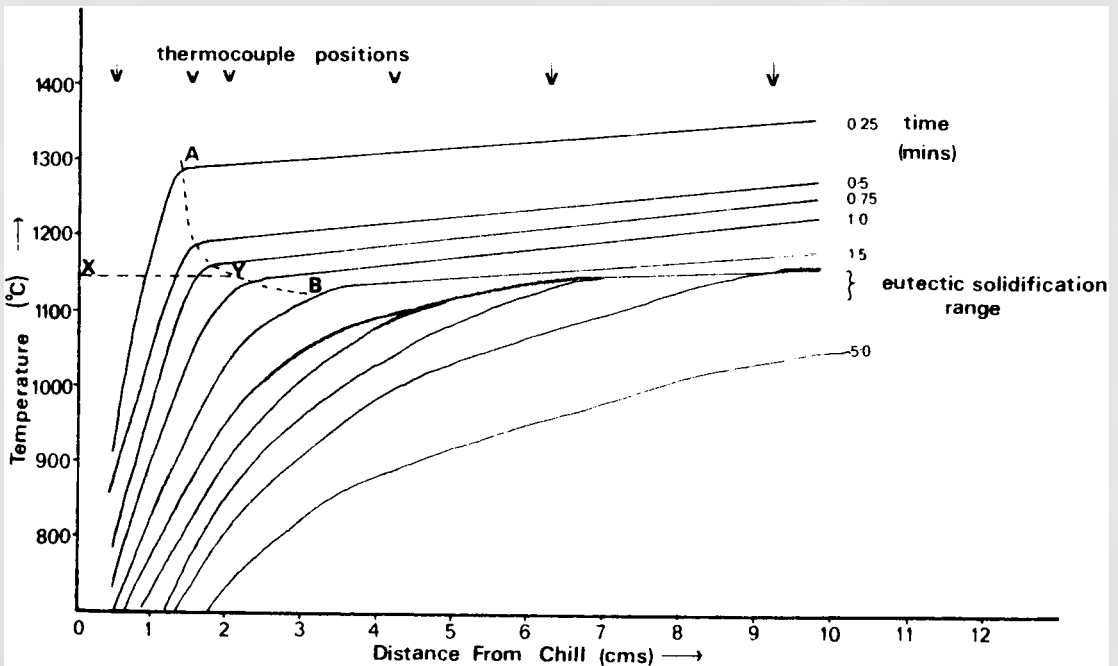


FIG 44. Progress of Chill Effect and Eutectic Solidification in Heated Ceramic Mould Experiments.  
 2.04% Si Alloy. Poured at 1440°C.



a). mould preheated to 1150 c



b). room temperature mould

FIG 45 2.04% Si Alloy: Temperature Distributions In Ceramic Moulds

It may be seen from Fig. 44 that solidification near the chill took place after the passage of the chill wave and was therefore subject to chill influence at all stages of freezing. At distances more removed from the chill, solidification due to heat loss through the mould walls was already in progress when the chill wave arrived. Still further from the chill, solidification was complete on arrival of the chill wave.

Preheating the mould to  $1150^{\circ}\text{C}$  retarded the start of eutectic solidification at a given distance from the chill while increasing its duration. The positions of the chill effect lines indicate an increase in chill penetration on mould heating. These effects result from reduction in heat loss through the mould walls and inhibition of eutectic nucleation and growth at positions remote from the chill.

The increase in chill effect penetration with mould heating may be understood by reference to Fig. 45 which give temperature distributions for heated and room temperature moulds for a series of times from 0.25 mins. after casting. The position the chill effect line reaches before solidification is indicated by the distance X-Y. In both cases, this distance is governed by the balance between the mould walls and chill as means of heat extraction. Where heat losses through the mould walls are high, as in the room temperature mould, the gradient of the chill effect line is high and the distance X-Y is small. Heat conservation in the  $1150^{\circ}\text{C}$  mould results in close spacing of the isochrones, reduces the chill effect line gradient, and increases the penetration of the chill effect at any given time.

Close spacing of the temperature distribution lines in the heated mould implies lower cooling rates than are experienced in the room temperature mould. This is confirmed by cooling rate results (Fig. 46). The assumption that the chill wave always produces cooling rates sufficiently rapid for metastable solidification may not be correct if temperature distribution lines are too close together. For this reason, the increase in chill wave penetration with

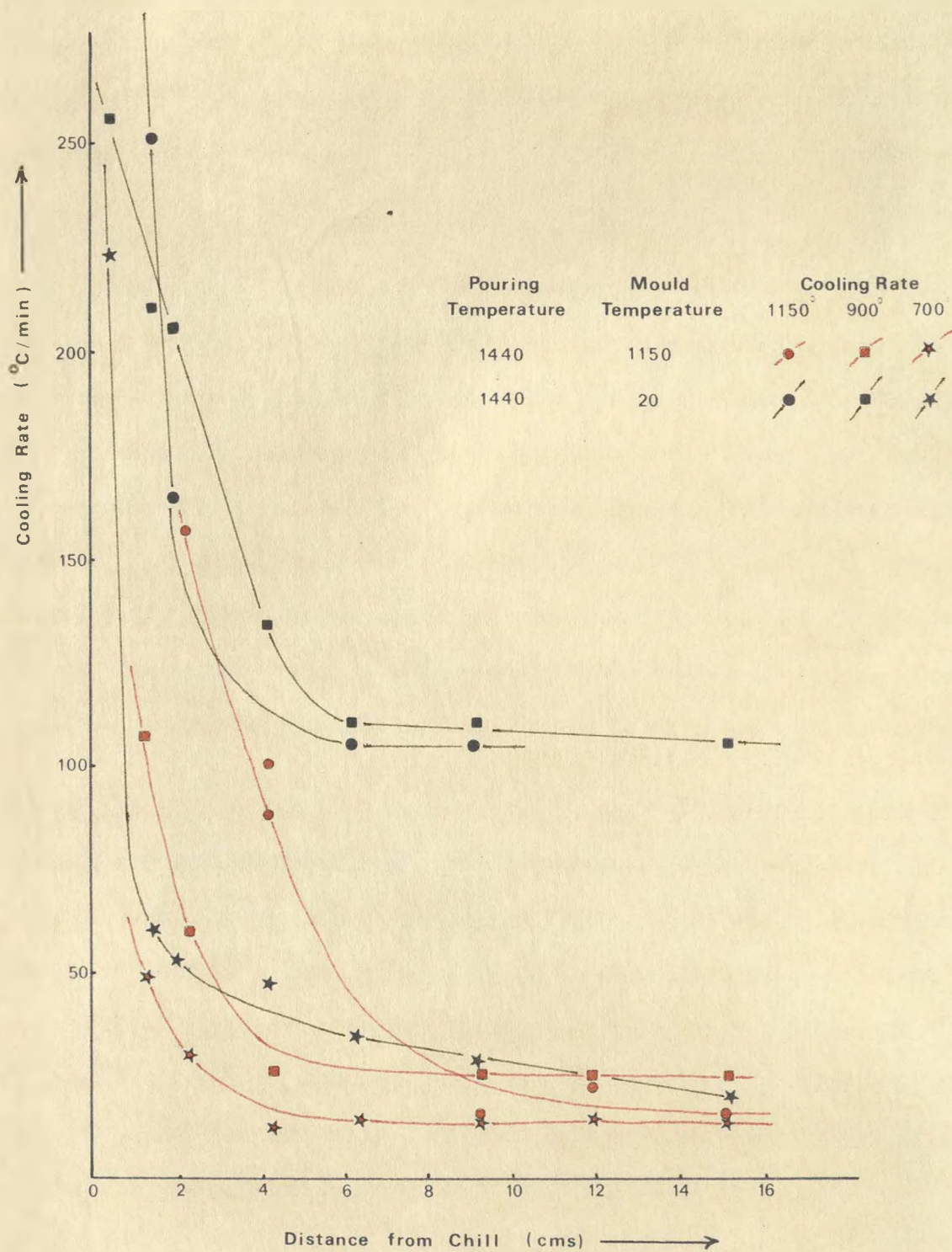


**FIG 46** Variation in Cooling Rate with Distance from the Chill  
 CERAMIC MOULD EXPERIMENTS

mould heating does not necessarily imply a greater depth of white or mottled structure. The liquid metal may instead be subject to continuously falling cooling rates which soon become non-critical through the eutectic solidification range, decreasing with distance from the chill until very slow furnace cooling conditions are reached.

Consideration of cooling rates at  $1150^{\circ}$ ,  $900^{\circ}$  and  $700^{\circ}\text{C}$  (Fig. 46) is important in understanding final solidification structures. Cooling rates are highly variable with distance from the chill, the relative differences between chill and remote positions being maintained as temperatures fall. The figure shows cooling rates to be consistently lower in heated mould specimens. Cooling rate variation during solidification and subsequent solid-state transformations is increased by raising mould temperature, producing a greater range of solidification conditions. Chill effects at  $1150^{\circ}\text{C}$  are rapidly attenuated in the room temperature mould castings, being undetectable after 6 cm from the chill. Mould heating to  $1150^{\circ}\text{C}$  increases the extent of chill influence, which is apparent at up to 8 cm from the chill.

The effect of mould temperature on solidification under such complex casting conditions will depend on the nucleation and growth characteristics of the stable and metastable eutectics. These in turn vary with alloy composition. Solid-state transformations after solidification are also affected by chill/mould thermal interactions. Cooling rate curves for  $900^{\circ}$  and  $700^{\circ}\text{C}$  show that the chill effect tendencies apparent during solidification are present during subsequent cooling. Heated mould cast structures must therefore be interpreted in the light of their solid-state cooling rates.

From these results we may draw some conclusions regarding thermal conditions in the series of experiments where moulds were maintained at  $1150^{\circ}\text{C}$  for  $\frac{1}{2}$  hr. after casting. Inhibition of mould wall heat losses will result in greater chill effect penetration than in the castings where mould heating was discontinued on

pouring. Cooling rates in such castings will be still further reduced at regions remote from the chill. Structures will represent solidification processes over a continuous range from the extreme values at the chill to the slow cooling conditions near the top of the casting. Prolonged mould heating is likely to extend the range of test bar structures, since the delay in eutectic solidification caused by mould heating enables solidification under chill influence at cooling rates not normally encountered in castings as small as the test piece.

#### 4.1.2 SUPERHEAT

Increasing the pouring temperature will displace the temperature distribution lines of Fig. 45 upwards, together with the chill effect lines AB and A'B'. This will extend the region of chill influence over solidification in both room temperature and heated moulds. The use of a water cooled copper chill eliminates thermal saturation, which might be a significant effect of superheat in a casting with a solid chill of limited heat capacity.

#### 4.1.3 SUMMARY OF THERMAL ANALYSES

Increasing the mould temperature to 1150°C results in delayed eutectic solidification coupled with greater chill wave penetration and reduced cooling rates at all temperatures in all parts of the test bar. Resulting macro- and microstructures will depend on the relative nucleation and growth kinetics of the stable and metastable eutectics of the alloy in question, together with the stability of growth structures during subsequent solid-state cooling. Increasing pouring temperature results also in greater chill effect penetration.

#### 4.2 CERAMIC MOULD STRUCTURES

Cast iron structures produced in the study of chill effects in sand test castings are normally investigated by inspection of fracture surfaces. This method is of limited sensitivity, as important structural effects occur on a microscopic scale and cannot be detected by macroexamination, even of polished

and etched samples. The extent of mottle is difficult to define from macro-examination, since graphite colonies are encountered well into the zone which would appear white on fracture. The use of the terms "clear chill" and "mottle" clarifies the position, clear chill being defined as metastable eutectic with no graphite present on a microscopic scale. Macrostructural examination is valuable in determining overall nucleation and growth patterns, but detailed information on the interdependence of growth forms can only be obtained from a study of both macro- and microstructures.

#### 4.2.1 MACROSTRUCTURES

Macrostructures of the ceramic mould castings are shown in Figs. 47 and 48. Amounts of chill and mottle are highly variable with casting temperature and alloy composition.

Increasing the mould temperature to 1150°C enhances chill and mottle formation in the 1% Si alloy, while coarsening the mottle zone. Chill and mottle penetration in the heated mould is roughly parallel to the chill, while mottle in the room temperature mould occurs as an inverted V-shaped zone along the bar axis. The effect of increasing mould temperature is not followed in the higher silicon alloys, where greatest chill and mottle penetration and coarsest mottle is found in the room temperature moulds.

Heated mould castings show mottle refinement and reduction in chill and mottle with increasing silicon. Although specimens from room temperature moulds show similar trends with respect to chill and mottle, mottle densities and distribution are not so regular. Mottle is finest in the 1% Si alloy. Graphite cells in the mottle zone are coarser in the other alloys, the mottle in the 2.43% Si alloy specimen coarsening appreciably as the mottle/grey transition is approached.

A decrease in pouring temperature from 1440°C to 1290°C with the mould at

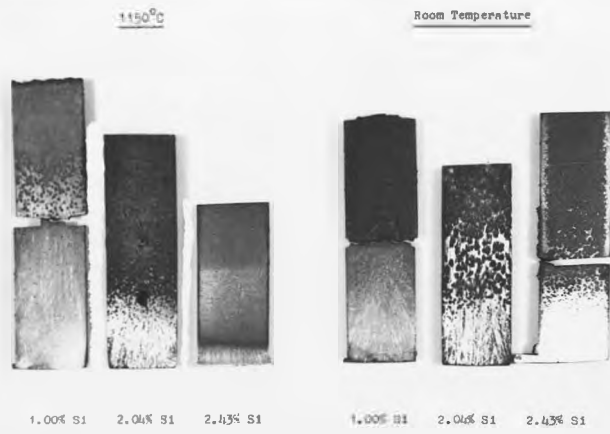


FIG. 47a VARIATION IN CERAMIC MOULD MACROSTRUCTURES WITH TEMPERATURE.

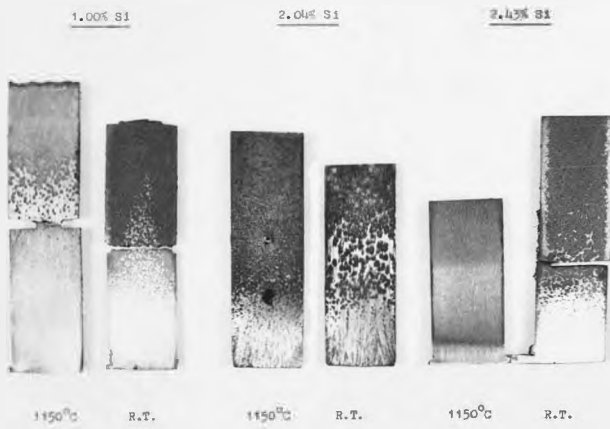


FIG. 47b VARIATION IN CERAMIC MOULD MACROSTRUCTURES WITH COMPOSITION.

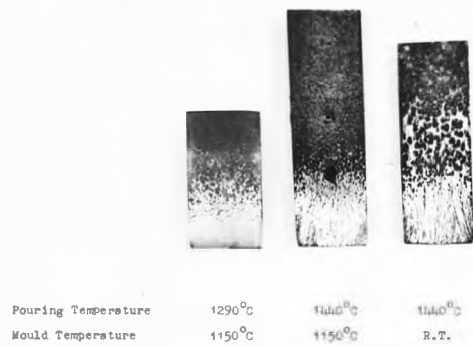


FIG. 48 2.04% Si ALLOY CERAMIC MOULD CASTING MACROSTRUCTURES.

1150°C decreases the depth of clear chill in the 2.04% Si alloy (Fig. 48). Graphite colonies are found very close to the chill in the 1290° casting, while graphite in the 1440° specimen appears further from the chill and coarsens less rapidly. Chill and mottle in the 1440° casting penetrates further into the specimen, although the amount of mottle is less than in the 1290° casting.

#### 4.2.2 MICROSTRUCTURAL MEASUREMENTS

Structural comparisons may be made by means of microstructural measurements shown in Figs. 49a and 49b. In these figures, the many structural factors which make up chill and mottle are summarised by the following three measurements made along the bar axis with the chill face as reference zero:

1. the first appearance of graphite in the microstructure
2. the first 'B'-type graphite rosettes
3. the last eutectic cementite

The distance from the first graphite to the last cementite in the microstructure may be taken as a measure of the amount of mottle. The appearance of rosette graphite is an indication of the relationship of the mottled region to graphite morphology, which changes with distance from the chill.

Fig. 49a shows solidification patterns with changing Si content for room temperature and heated ceramic moulds. Equivalent points in the different alloy castings are joined to clarify structural relationships.

The trends in chill and mottle formation noted from the macrostructures are maintained in the microstructural measurements. Changes in graphite morphology from undercooled fine flakes to radial cells with coarser graphite are noted for the 2.04% and 2.43% silicon alloys. Graphite colonies in the 1.00% silicon alloy were centered on radial flakes which coarsened gradually, showing no sudden transition.

The effect of pouring temperature on chill depth of 2.04% silicon alloy castings is shown in Fig. 49b. Reductions in pouring temperature in the heated

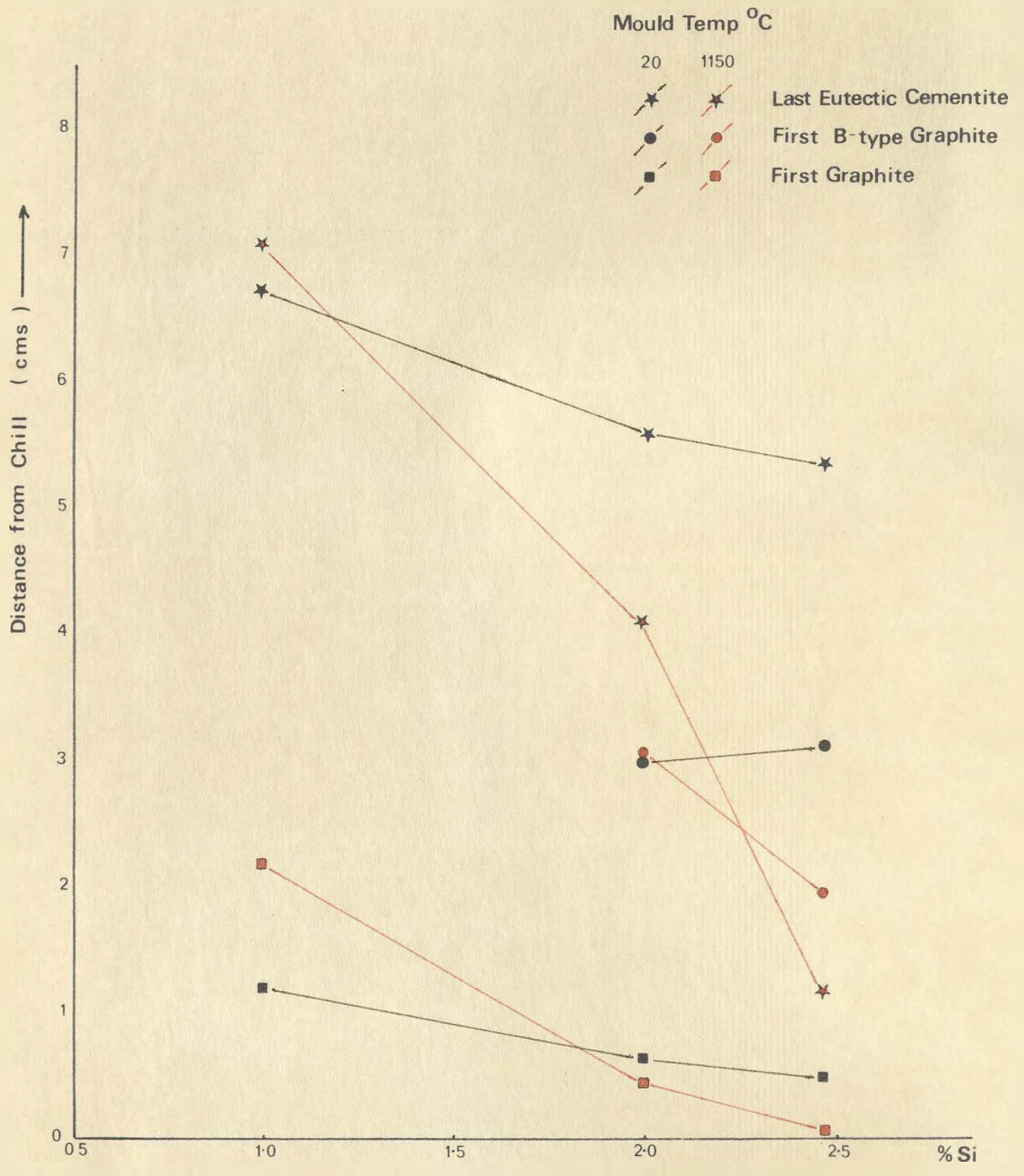


FIG. 49a. Ceramic Mould Experiments ; Microstructural Measurements

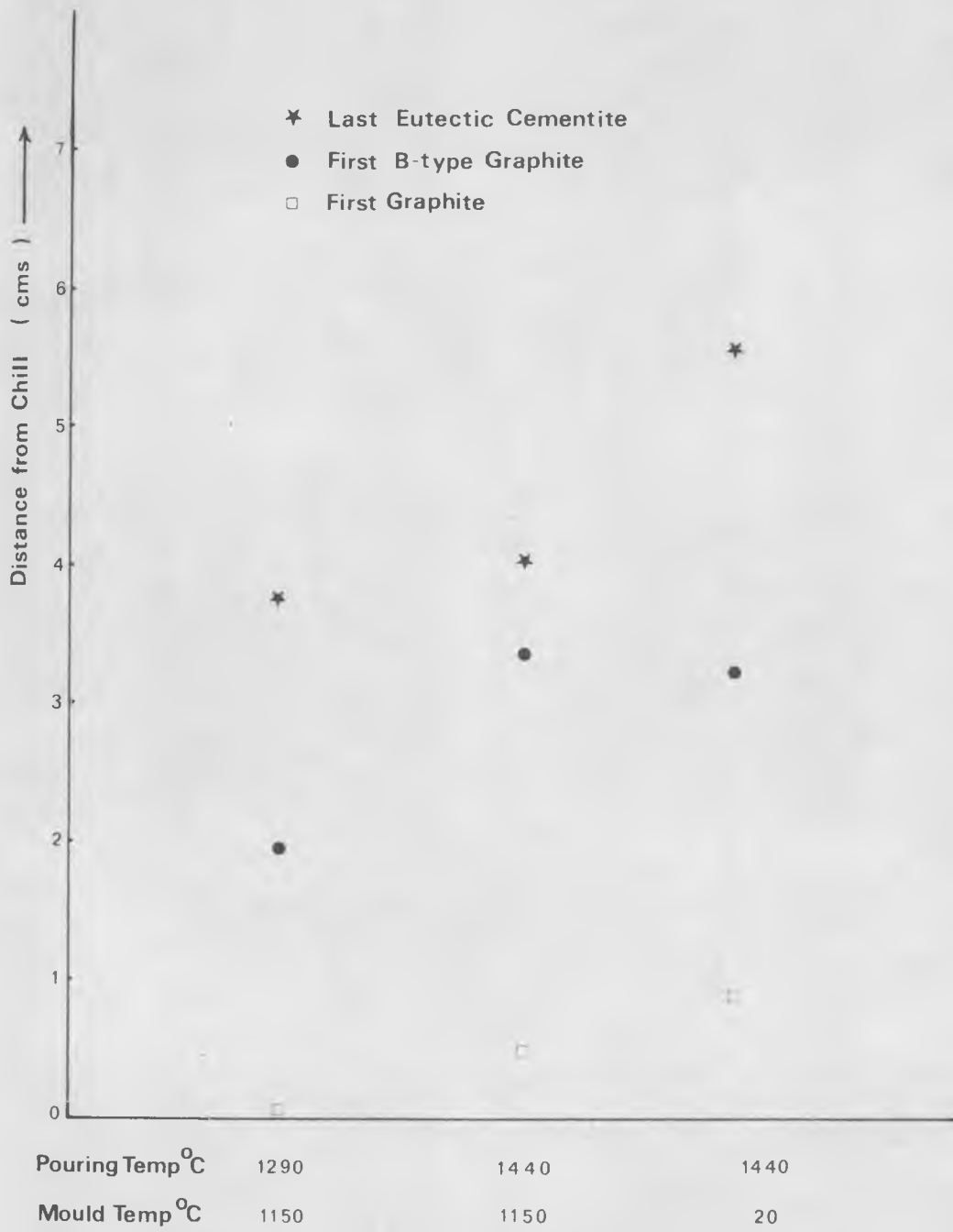


FIG. 49 b.

2.04 % Si Alloy. Microstructural Measurements

CERAMIC MOULD EXPERIMENTS

mould casting reduce chill and mottle penetration, while decreasing the amount of clear chill. Coarse B-type graphite occurs nearer the chill in the low superheat casting.

#### 4.2.3 MICROSTRUCTURES

Clear chill zone structures were the same in all three alloys studied, although the extent and distribution of metastable eutectic forms varied along the bar axis with temperature and composition. The sequences observed in the ceramic mould experiments also occurred in the chill/sand castings and chill cast specimens. As metastable eutectic structures are considered in detail in the section on chill casting experiments, description of microstructures of ceramic mould and chill/sand castings will begin with the first appearance of graphite in the microstructure. Distances quoted with the following microstructures refer to their position along the bar axis relative to the chill.

##### 4.2.3.1 1.00% SILICON ALLOY

The first graphite in the heated mould castings (Fig. 50) took the form of short thick flakes; forming circular colonies with projections loosely aligned in the direction of growth along the bar axis. A feature of these colonies was the apparent lack of a coherent boundary between the stable and metastable eutectics, many points of contact occurring between graphite and cementite. In some areas (Fig. 51) graphite flakes followed the contours of cementite, both on boundaries with austenite dendrites and within the ledeburite structure itself. When graphite occurred within a ledeburite colony, the normal cementite matrix/austenite rod structure was often disrupted, austenite becoming the matrix phase enclosing dispersed cementite filaments (Fig. 52).

With increasing distance from the chill, graphite colonies became more extensive and numerous, beginning to impinge on one another. Graphite flakes in the colony centres coarsened and became more clearly radial, while the streamer arms which contained the finer flakes grew longer. Close contact with the metastable eutectic was maintained at colony borders, the two structures

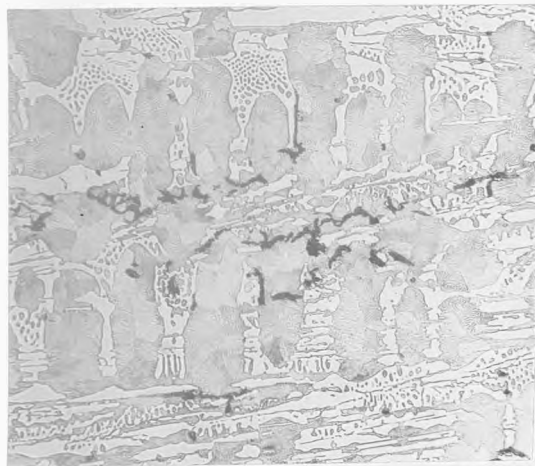


FIG.50. 1%Si. 1150° ceramic mould.  
Nital. 21mm. x160.  
First graphite.

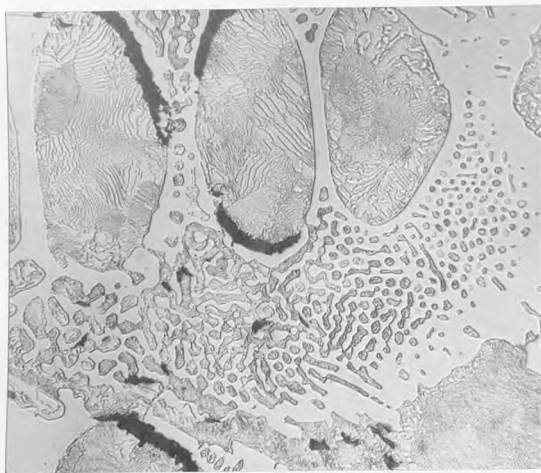


FIG.51. 1%Si. 1150° ceramic mould.  
Nital. 23.4mm. x400.  
Outlining graphite.

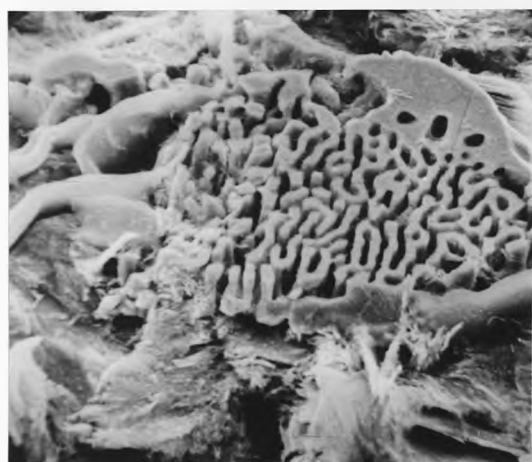


FIG.52. 1%Si. 1150° ceramic mould.  
Br<sub>2</sub>. Stereo @ 45°. x1290.  
Graphite/ledeburite border.



FIG.53. 1%Si. 1150° ceramic mould.  
Nital. 68.5mm. x160.  
Dissociated ledeburite.

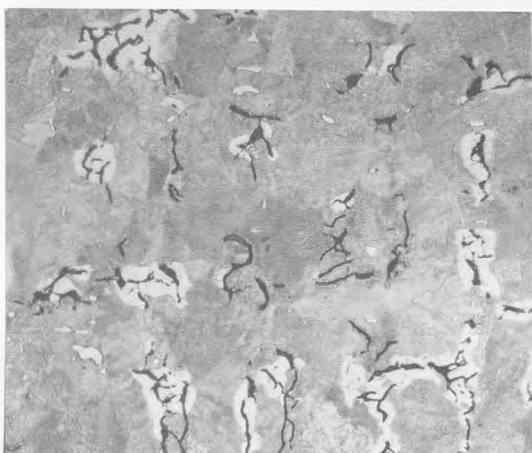


FIG.54. 1%Si. 1150° ceramic mould.  
Nital. 76.3mm. x160.  
Isolated cementite particles.

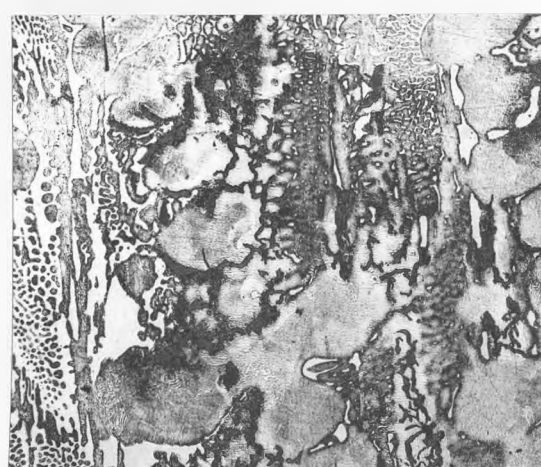


FIG.55. 1%Si. 1150° ceramic mould.  
Br<sub>2</sub>. 57.5mm. x160.  
Dissociated ledeburite  
and networks.

becoming increasingly mixed. Ledeburite colonies in border areas exhibited extensive dissociation of the matrix cementite (Fig. 53). Cementite laths, continuous with ledeburite areas, appeared to penetrate graphite colony boundaries, giving needle-shaped spaces in the flake structure. The amount of cementite in the ledeburite and needle areas decreased with increasing distance from the chill, until only isolated cementite particles were visible in the microstructure (Fig. 54).

The use of bromine and alkaline sodium picrate etches apparently exposed areas from which eutectic carbide disappeared during solid-state cooling. This etching effect has been demonstrated for steels in the case of sodium picrate<sup>(93)</sup> and appears to be effective in cast irons.

Etching in  $\frac{1}{2}\%$  bromine clarifies some of the structural relationships in the mottled areas. Bromine colours pearlite while leaving cementite unaffected. The microstructure in Fig. 55 contains normal ledeburite and some dissociated austenite/cementite areas. Matrix staining is concentrated in the regions between the isolated cementite particles, forming a network which appears to be a ghost image of a normal ledeburite structure. The dark network in this case corresponds to missing areas of cementite in the ledeburite matrix. The isolated cementite particles are situated at nodes of greatest carbide thickness in the ghost ledeburitic structure. This is confirmed at higher magnification in Fig. 56, where a similar dissociated area and network structure has been exposed with boiling alkaline sodium picrate. With this etch, the network appears lighter than portions corresponding to austenite rods, which are darkened.

Further from the chill, the amounts of cementite at ledeburite nodes decreased (Fig. 57), until large areas retained ghosting effects without any cementite being present (Fig. 58). Graphite in such areas often appeared to be compacted, especially in positions bordering or within the network structure.

The last eutectic cementite in the microstructure was associated with the



FIG.56. 1%Si. 1150° ceramic mould.  
Alk.Na.Pic. 58.7mm. x1000.  
Network structure.

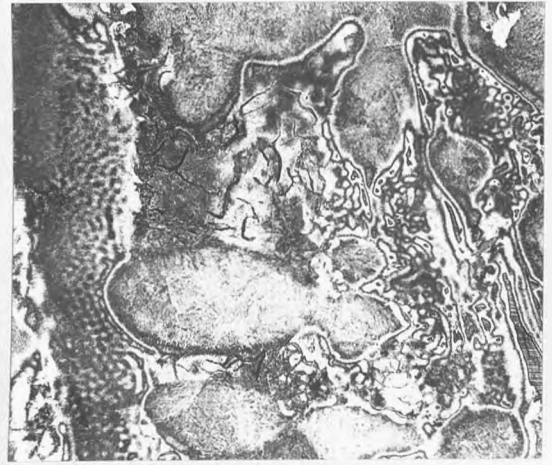


FIG.57. 1%Si. 1150° ceramic mould.  
Alk.Na.Pic. 67.8mm. x160.  
Network structure.

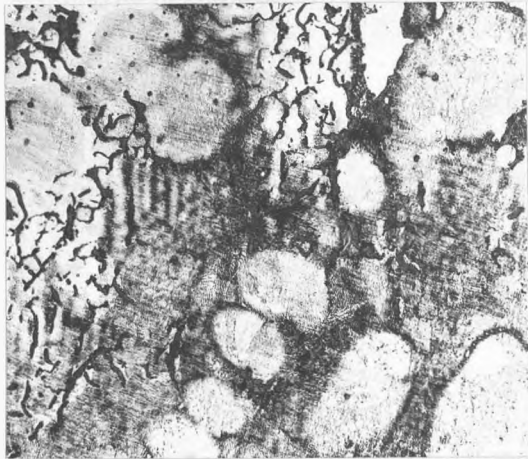


FIG.58. 1%Si. 1150° ceramic mould.  
Br<sub>2</sub>. 74.5mm. x160.  
Network structure.



FIG.59. 1%Si. 1150° ceramic mould.  
Br<sub>2</sub>. 83.6mm. x160.  
Needle network structure.

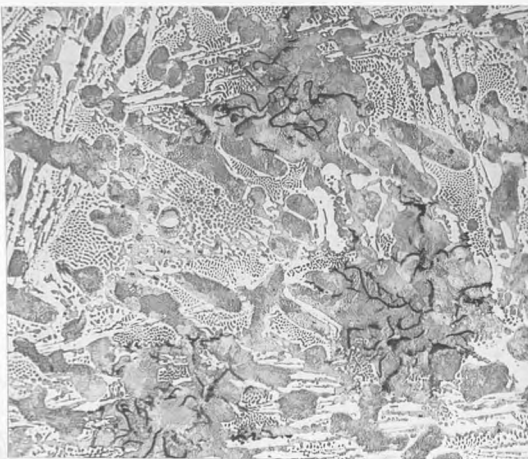


FIG.60. 1%Si. R.T.ceramic mould.  
Nital. 17.6mm. x160.  
First graphite.



FIG.61. 1%Si. R.T.ceramic mould.  
Nital. 32.3mm. x1000.  
Ledeburite colony border.

midribs of cementite needle formations (Fig. 59). These originated from fan-like clusters of cementite plates each of which nucleated a small ledeburite colony. Cementite decomposition resulted in the presence of needle-shaped gaps between graphite colonies, with isolated surviving cementite particles. In the absence of a suitable etching stain, such effects may be undetectable (Fig. 54). Although cementite globules are visible using a nital or picral etch, there is no means of associating them with any pre-existing structure and therefore of accounting for their presence in such numbers.

Room temperature mould castings exhibited the same general structural sequences as those from heated moulds. Initial graphite formations were smaller, occurring under more rapid cooling conditions in the more finely-divided structures near the chill. Small isolated flakes appeared first, often in contact with cementite or austenite dendrite boundaries.

Under the slower cooling conditions further from the chill, the graphite colonies developed into clearly defined rosettes (Fig. 60). The graphite in these rosettes had a radial, interconnected appearance. The outermost flakes penetrated surrounding ledeburite colonies for short distances, and some graphite/cementite contact occurred. Contact zones were narrow and graphite and ledeburite eutectics were more clearly separated than in the heated mould specimens.

Ledeburite colony borders were usually formed from coherent cementite. This coherence was lost, and more dissociated cementite structures were found where penetration by graphite flakes occurred (Fig. 61). A stereoscan view of a similar area after deep etching (Fig. 62), reveals that cementite which appears unconnected in plane section is in fact interconnected in coral-like formation in the vicinity of the tips of graphite flakes. An interesting feature of this figure, shown at greater magnification in Fig. 63, is graphite/cementite contact in the form of short pointed interpenetrating projections. Frederiksson and Hillert<sup>(89)</sup> noted similar structures in their directionally solidified alloys. Light microscopy of a deep etched specimen (Fig. 64) shows a similar interpenetration effect associated with considerable surface contact. An advantage of



FIG.62. 1%Si. R.T.ceramic mould.  
Br<sub>2</sub>. Stereoscan @ 45°. x2600.  
Ledeburite colony border.

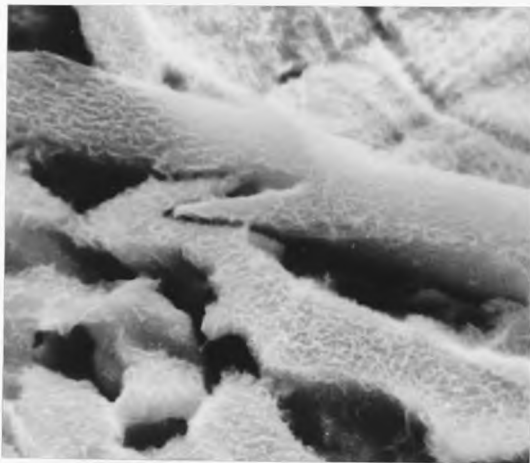


FIG.63. 1%Si. R.T.ceramic mould.  
Br<sub>2</sub>. Stereo @ 45°. x6500.  
Graphite/cementite  
interpenetration.



FIG.64. 1%Si. R.T.ceramic mould.  
Br<sub>2</sub>. x1500.  
Graphite/cementite  
interpenetration.

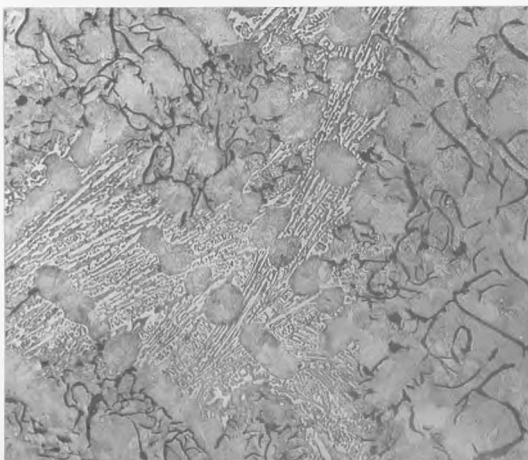


FIG.65. 1%Si. R.T.ceramic mould.  
Nital. 66.8mm. x160.  
Last ledeburite colonies.

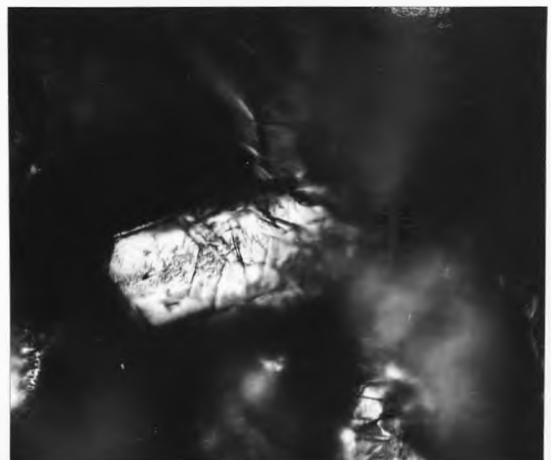


FIG.66. 1%Si. R.T.ceramic mould.  
Br<sub>2</sub>. x1000.  
Graphite flake surface.

light microscopy in such a case is the clear colour definition between the phases involved, a factor absent in scanning electron micrographs.



Cooling through the mould walls before the arrival of the chill wave resulted in growth and impingement of graphite rosettes beyond 21 mm. from the chill. Merging colonies were separated by fine peripheral graphite flakes. As graphite colonies became more extensive, ledeburite was increasingly confined to intercolony areas. The last ledeburite areas retained their characteristic structure, except for limited dissociation and penetration at the borders (Fig. 65). Eutectic cementite in the form of fan-shaped needle clusters noted in the heated mould samples appeared to be absent in room temperature mould castings.

Increased metastable eutectic penetration along the casting axis was a feature of the room temperature mould castings. Graphite colonies started to develop at similar distances from the chill across the casting section. Colony growth and multiplication was more rapid at the mould walls than at equivalent positions in the casting centre. The mottle zone became thinner as the casting edge was approached. Graphite structural sequences were similar within the mottle zone at all positions, except at the very edge of the casting, where graphite flakes tended to be finer and were often aligned between dendrites growing from the mould walls.

Hexagonal surface markings on graphite have been noted by several workers (42, 94, 95). Deep etching, followed by light microscopy revealed similar markings on the coarser flakes of the 1% Si alloy (Fig. 66).

#### 4.2.3.2. 2.04% SILICON ALLOY

The first graphite colonies in the heated mould specimens of this alloy had very much finer flakes than those encountered in the 1.00% Si alloy castings. Fig. 67 shows one of the first graphite colonies which is closely associated with a ledeburite area, forming a common border where graphite and cementite are in contact. The border is marked by a decrease in cementite coherence and

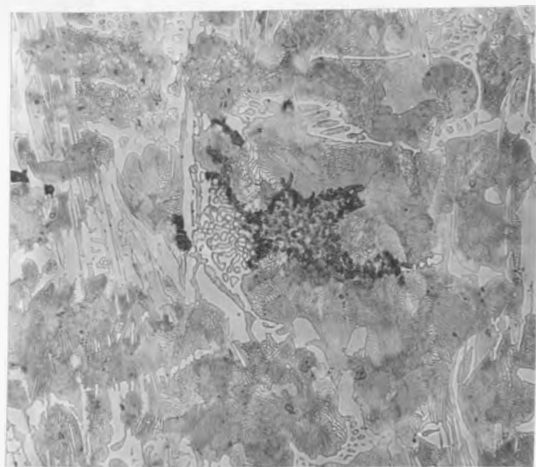


FIG.67. 2.04%Si.1150° ceramic mould.  
Nital. 6.9mm. x400.  
First graphite.

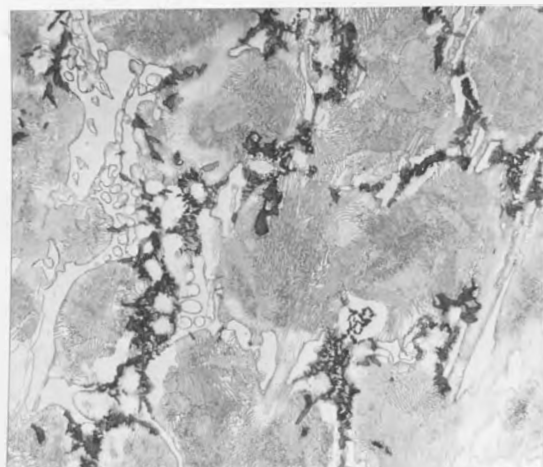


FIG.68. 2.04%Si.1150° ceramic mould.  
Nital. 20.1mm. x400.  
Mottled area.

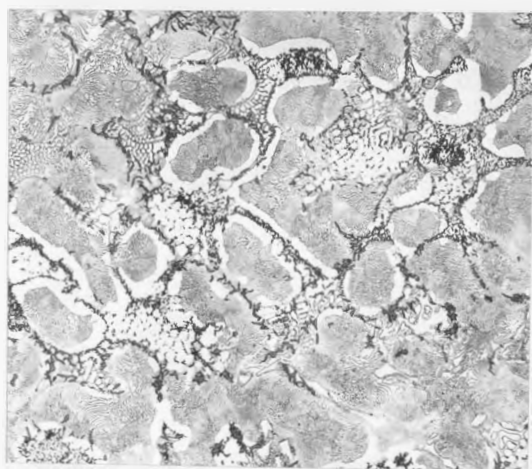


FIG.69. 2.04% Si.1150° ceramic mould.  
Nital. 27.2mm. x160.  
Mottled area.

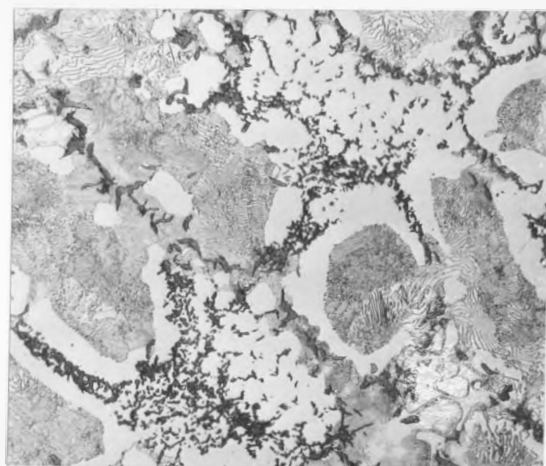


FIG.70. 2.04%Si.1150° ceramic mould.  
Nital. 27.2mm. x400.  
'Honeycombe' structure,

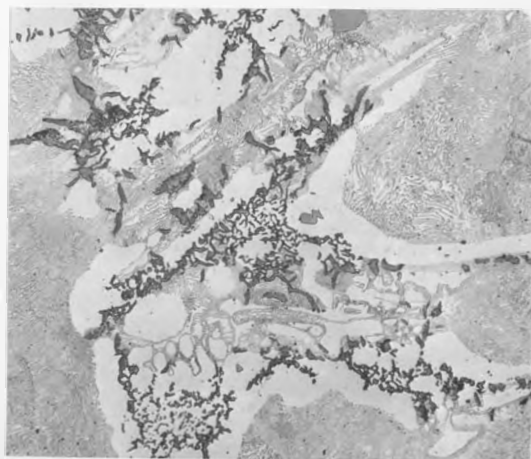


FIG.71. 2.04%Si.1150° ceramic mould.  
Nital. 30.8mm. x400.  
Mottled area.

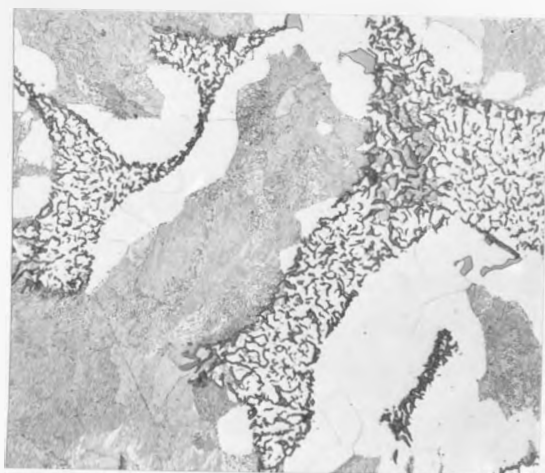


FIG.72. 2.04%Si.1150° ceramic mould.  
Nital. 33.6mm. x400.  
Undercooled graphite.

a compaction of the graphite flakes which form a wall along the interface. The flakes on all sides of the graphite colony show this thickening and are more coherent than the fine curled flakes in the colony interior. Graphite colonies began to merge at 16 mm from the chill, resulting in extensive internal flake coarsening at streamer-like borders. At 20 mm from the chill, mottle was widespread (Fig. 68). The two eutectics were intermixed, losing their clearly defined boundaries. Graphite occurred as compacted flakes, often forming common interfaces with cementite. Some of the graphite colonies contained ferrite areas similar in shape and size to the transformed austenite rods of the adjoining ledeburite eutectic. Graphite colony peripheries showed cementite lath piercing similar to that noted in the 1.00% Si heated mould specimen. Figs. 69 and 70 show an area of the mottled zone at 27 mm from the chill. The ledeburite shows signs of cementite loss in several areas. Graphite in the form of short thick flakes outlines areas which have the characteristic honeycombe ledeburite structure, although little or no cementite may be present. Graphite colonies are most dense at their borders and usually have a ferritic matrix. Ledeburite regions which contain no graphite in plane section may still exhibit 'wasting' of cementite, the original cementite outline being maintained by pearlite. Carbon concentration differences which may outline pre-existing ledeburite structures are indicated by pearlite density variation in Fig. 71. Cementite in this area is retained only at the nodes of the ledeburite colony and along midribs, the remainder of the honeycombe being outlined by pearlite or graphite.

At increasing distances from the chill, lower cooling rates during solidification led to gradual elimination of ledeburite from microstructures. Colonies grew smaller and more isolated, their outline being revealed as needle clusters based on initial cementite plate growth. The last signs of eutectic cementite were at the centres of needles which had largely decomposed to pearlite. The structures involved were similar to those of Fig. 57 for the 1.00% silicon alloy, with the exception of the graphite form, which was much finer in the higher silicon alloy.

'D'-type graphite, shown in Fig. 72, at 33 mm from the chill, was generally coarser but less thick than the initial graphite. Flakes were compact and interconnected at borders with austenite dendrites. The dendrite borders were ferritic, pearlite being present at their centres. Idiomorphic manganese sulphide inclusions were common in these areas.

Rosettes of coarser 'B'-type graphite appeared above 30 mm, among the finer 'D'-type eutectic as in Fig. 73. These colonies consisted of radial interconnected flakes growing from a central nucleus. The coarse flakes were not separated from the fine 'D'-type flakes, but gradually decreased in size with increasing distance from the rosette centre, finally merging with the undercooled eutectic. As the rosettes were spherical and yet contained graphite which appeared continuous with the fine surrounding flakes, it may be that they nucleated and began to develop ahead of the solidification front proceeding from the chill. Before solidification was complete, the growth temperature at the growing edge of the colony could have fallen sufficiently to account for the gradual radial refinement and final merging with the fine graphite of the remaining eutectic.

As the distance from the chill increased, the proportion of rosettes in the microstructure grew until they touched and coalesced, eliminating the last intercolony areas of fine graphite to give a coarse structure. The coarse graphite flakes in the upper part of the bar were long, with smaller curvature and apparent sectional variation than those of the finer eutectic (Fig. 74).

The coarse flakes formed structures in which the outline of the original austenite dendrites was largely obscured by deposition of eutectic austenite, and by the random orientation and wide separation of the graphite. The matrix in such regions was pearlitic with ferrite envelopes around the flakes. Idiomorphic manganese sulphide particles reached large proportions at the slow cooling rates found during solidification in these regions.

Although the extent and position of structural features varied in relation

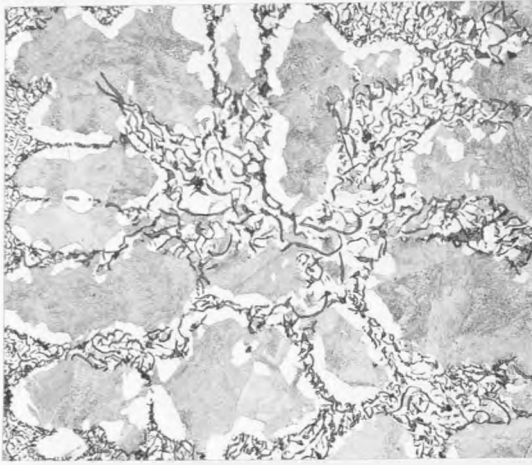


FIG.73. 2.04%Si. 1150° ceramic mould.  
Nital. 40.1mm. x160.  
Coarser rosette graphite.

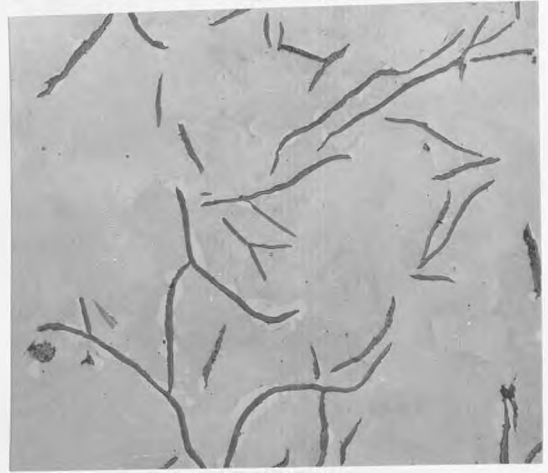


FIG.74. 2.04%Si. 1150° ceramic mould.  
Nital. x160.  
'A'-type graphite.

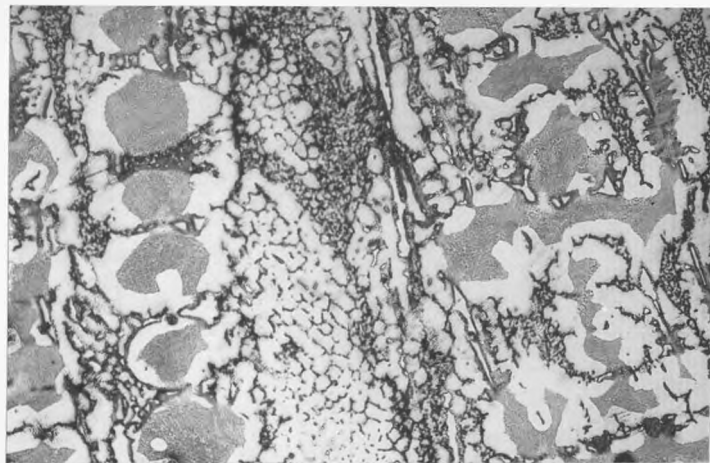


FIG.75. 2.04%Si. R.T.ceramic mould.  
Br<sub>2</sub>/Nital., 45mm. x160.  
Honeycombe structure.

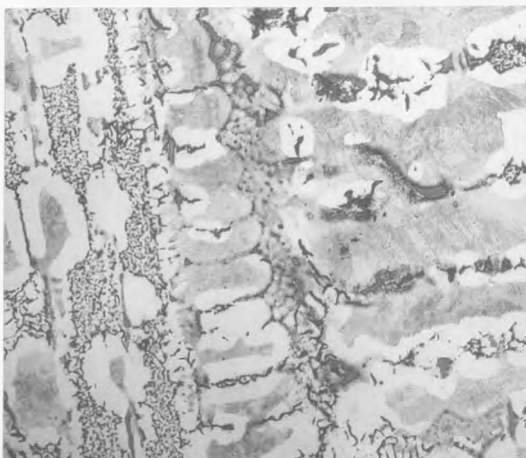


FIG.76. 2.04%Si. R.T.ceramic mould.  
A.Na.P/Nital. 48mm. x160.  
Network structures.

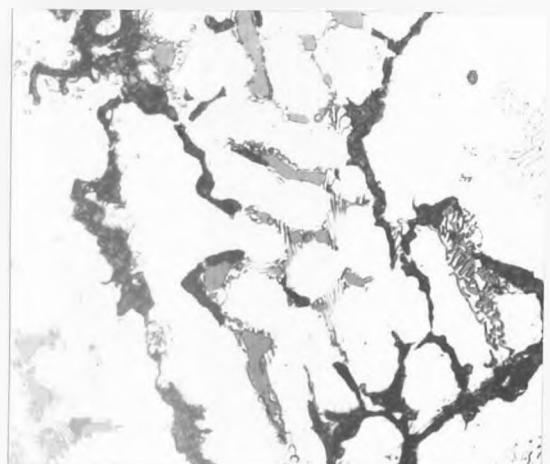


FIG.77. 2.04%Si. R.T.ceramic mould.  
A.Na.P/Nital. x1000.  
Outlining graphite.

to the chill, specimens cast in room temperature moulds exhibited the same range of structures as the heated mould samples. Cementite needle clusters were frequent in mottle regions, associated with ledeburite colonies, which became smaller with increasing distance from the chill.

Metastable eutectic areas in the upper portion of the mottle zone (Fig. 75) once more showed evidence of structural breakdown, with eutectic confined to the nodes of the original ledeburite. Graphite was closely associated with ledeburite in these areas, and occasionally conformed to a honeycombe structure. Graphite flakes in border areas were more continuous than those in colony interiors. Colony borders were often extensively coarsened. The matrix in the vicinity of such graphite areas was generally ferritic, although pearlite occurred around residual cementite particles. More slowly cooled areas further from the chill (Fig. 76), were almost entirely devoid of cementite, but showed 'ghost' ledeburite and cementite needle networks on etching in alkaline sodium picrate followed by nital. The use of this etch technique (Fig. 77) emphasised the outlining role of the graphite in forming a honeycombe structure. Residual cementite was rounded, maintaining contact in many places with the semi-continuous films of graphite. Where cementite was not in direct contact with graphite, the phases were often linked by an intervening pearlite colony. Pearlite also formed networks connecting cementite particles. This may indicate the prior existence of cementite, reflected as residual carbon concentrations in an otherwise ferritic matrix.

#### 4.2.3.3 2.43% SILICON ALLOY

Initial graphite colonies in the heated mould castings (Fig. 78) were similar both in graphite form and relation with surrounding metastable eutectic to those of the 2.04% silicon alloy. As the graphite colonies formed very close to the chill surface they were subject to rapid cooling and exhibited a degree of directionality in common with the metastable eutectic, which contained quantities of elongated cementite plates aligned in the growth direction. Graphite quantities increased with distance from the chill, becoming closely intermixed

with the increasingly ledeburitic metastable eutectic (Fig. 79). Ledeburite in the early stages of mottle retained its structure except in areas where it was immediately bordered by graphite. As the distance from the chill grew and ledeburite quantities lessened, the coherence of eutectic cementite decreased until only a few partly associated areas remained (Fig. 80). Graphite throughout the mottle zone was of the undercooled type, appearing as short curled flakes in plane section, with increasingly coarse and continuous flake forms at colony boundaries.

The nucleation and increase in amount of 'B'-type graphite rosettes occurred in the same way as in the 2.04% silicon samples, although much nearer the chill. A structure consisting of coarser graphite of variable size is shown in Fig. 81, which shows its interdendritic non-directional nature. All graphite in the heated moulds, with the exception of the very first colonies was surrounded by ferrite.

The first graphite colonies in the room temperature mould castings (Fig. 82) were larger than in the heated moulds, as they formed under slower cooling conditions further from the chill. The metastable eutectic still contained considerable quantities of directional plates, and graphite closely associated with these gave an elongated streamer-like appearance to the graphite colonies. A feature of the early graphite forms in both the heated and room temperature mould specimens was the interconnection and compacted nature of the elongated 'streamer' graphite colonies (Fig. 83). Graphite/cementite contact was still frequent, but some streamers ran parallel to cementite needle surfaces without actually coming into contact. Cementite in regions containing graphite showed the loss of structural coherence noted in other samples. A higher magnification view of a ledeburite colony containing graphite (Fig. 84) shows varying degrees of graphite development and cementite coherence within a single microstructural area. Austenite rods are outlined by coherent graphite flakes which appear thinnest at the ends, and thicken towards the centre. Some flakes show signs



FIG. 78. 2.43%Si. 1150° ceramic mould.  
Nital. 0.6mm. x160.  
First graphite colonies.



FIG. 79. 2.43%Si. 1150° ceramic mould.  
Nital. 5.9mm. x160.  
Mottled area.

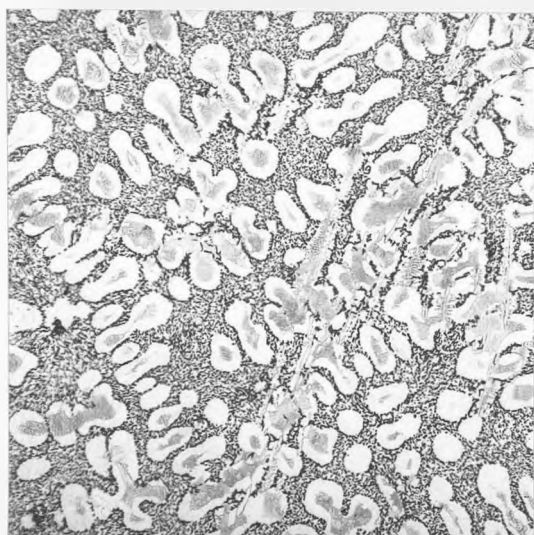


FIG. 80. 2.43%Si. 1150° ceramic mould.  
Nital. 10.1mm. x160.  
Final ledeburite.

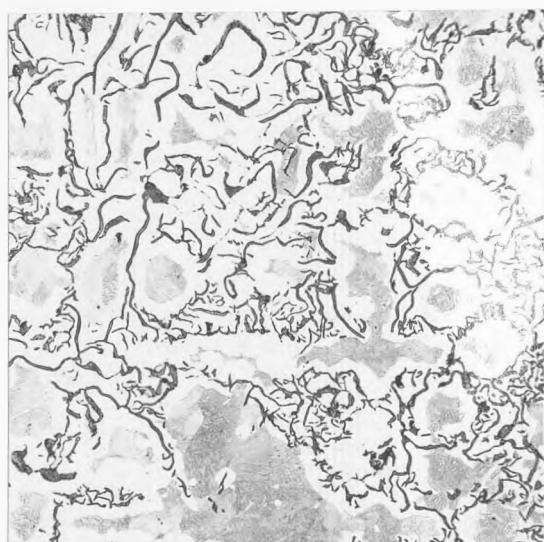


FIG. 81. 2.43%Si. 1150° ceramic mould.  
Nital. 44.6mm. x160.  
Coarser graphite.



FIG.82. 2.43%Si. R.T.ceramic mould.  
Nital. 20.4mm. x160.  
First graphite.

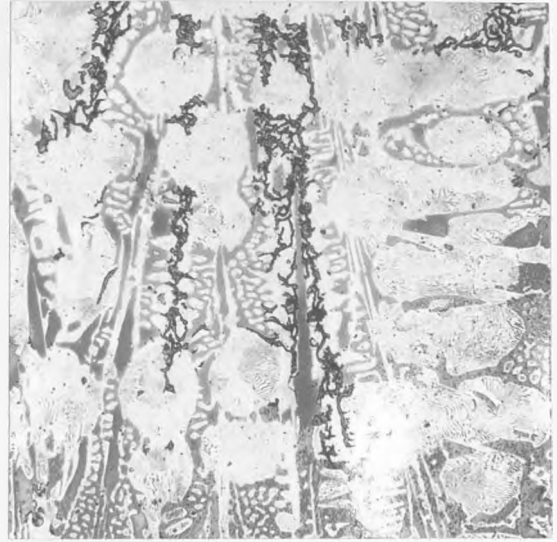


FIG.83. 2.43%Si. R.T.ceramic mould.  
A.Na.P/Nital. 24.2mm. x400.  
Elongated graphite.

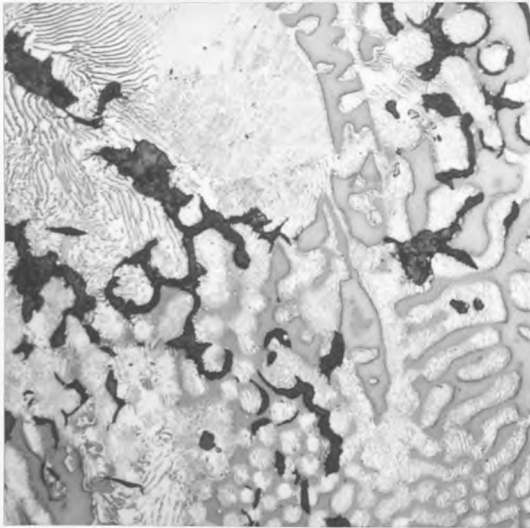


FIG.84. 2.43%Si. R.T.ceramic mould.  
A.Na.P/Nital. 24.3mm. x1000.  
Outlining graphite.

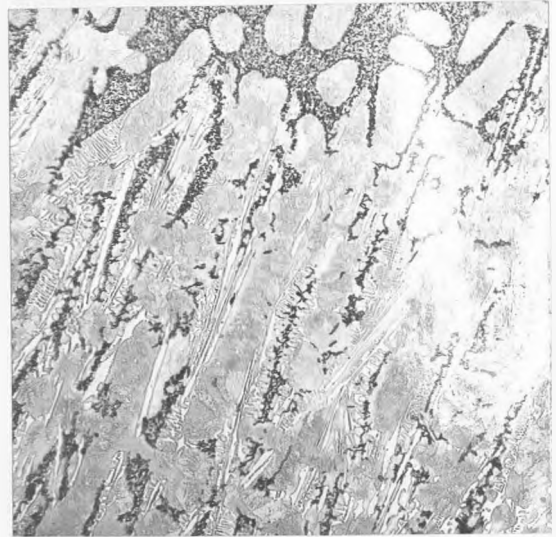


FIG.85. 2.43%Si. R.T.ceramic mould.  
Nital. 35.3mm. x160.  
Graphite streamers.

of penetrating the cementite particles, usually with the pointed flake tips. From this microstructure it appears that whatever process produces the final structures, nucleation and/or growth is highly variable on a microscopic scale. Fig. 85 shows the directionality of graphite streamers associated with plate-like cementite 35 mm from the chill surface. This graphite was similar to that at colony borders nearer the chill, but extended much further along the cementite needles between the large graphite colonies. The needle structures were widespread in the last stage of the mottle zone as in previous samples. The transition from undercooled graphite to coarser radial 'B'-rosettes was similar to that in the 2.00% silicon alloy. The coarse flakes first occurred at the centres of undercooled graphite colonies within the mottle zone, forming a continuous network with the finer graphite. The 'B'-type graphite coarsened further from the chill, spreading toward the colony peripheries.

#### 4.2.3.4 SUMMARY

Increasing silicon content reduced chill and mottle in both heated and room temperature mould castings. The effect of increasing mould temperature in the 1.00% Si alloy was to increase chill and mottle, while similar treatment reduced chill and mottle in the 2.04% and 2.43% Si alloys.

Graphite in the 1.00% Si alloy castings occurred as long coarse flakes. Colonies rapidly acquired a radial structure, with finer flakes at the boundaries. Flake structures at the colony centres coarsened continuously with increasing distance from the chill. Graphite colonies in the higher silicon alloys were initially composed of fine undercooled flakes which coarsened and tended to elongate into streamers at the peripheries. The fine graphite gave way to coarser radial forms which developed at the centres of the undercooled colonies in the upper regions of the mottle zone.

Stable and metastable eutectics were closely associated at stable eutectic colony borders in all alloys. Cementite and graphite in such regions often had common interfaces. Eutectic cementite in such regions tended to become

0.5cm. THERMOCOUPLE.			4.0cm. THERMOCOUPLE.		
TEMP <sup>o</sup> C.	COOLING RATE. °C/min.	ELAPSED TIME. mins.	TEMP <sup>o</sup> C.	COOLING RATE. °C/min.	ELAPSED TIME. mins.
1250	840	0.21	1250	128	0.52
1200	460	0.30	1200	61	1.13
1150	254	0.42	1150	43	1.84
1134-1129	Eutectic Arrest	0.53-0.70	1144-1141	Eutectic Arrest	1.95-3.02
1100	95	0.96	1100	16	4.90
1050	53	1.74	1050	23	11.00
1000	16	3.90	1000	32	12.13
950	16	7.00	950	25	13.60

TABLE 8. Chill/Sand Castings. Thermal Analysis Results.



FIG.86. Chill/Sand Castings. Macrostructures.

dissociated and appeared discontinuous when viewed in plane section.

Graphite colonies were often pierced at the edges by cementite laths aligned with surrounding ledeburite colonies. The amount of eutectic cementite present in the ledeburite and lath areas decreased with increasing distance from the chill. Etching in alkaline sodium picrate or bromine revealed 'ghost' networks which appear to show the position of pre-existing eutectic cementite. These networks were accompanied by continuous graphite flakes similar to those occurring in the colony border areas in association with ledeburite and cementite laths. Graphite colonies in the vicinity had coarsened borders formed by compaction of fine flakes in the 2.04% and 2.43% silicon alloys.

#### 4.3 CHILL/SAND CASTINGS

The object of these experiments was to examine the physical and structural effects of solid chills in sand castings on the three alloys under study. It was hoped that they might provide a link between structures produced under more controlled conditions and those encountered in industrial situations.

##### 4.3.1 THERMAL ANALYSIS RESULTS

Thermal analyses were largely unsuccessful due to thermocouple failure or displacement by inflowing metal. Results were obtained for thermocouples positioned on the casting axis at 0.5 cm and 4.0 cm from the chill surface. Cooling rate data from these positions shown in table 8 is helpful in indicating the influence of the solid steel chill during solidification and subsequent cooling. The results quoted come from a casting in the 2.43% Si alloy, poured at 1440°C. Both thermocouples were situated outside the chill zone in the 2.43% Si casting, but the one at 0.5 cm would have been within those of the 1.00% Si and 2.04% Si alloys.

The thermocouple at 0.5 cm indicates rapid initial cooling under chill influence. The rate decreases in the solidification range, and subsequent cooling at high temperatures in the solid state is slower than in the body of

the casting. Portions of the casting which cool sufficiently rapidly for metastable solidification under chill influence may be subject to very much slower cooling in the solid state. This may produce a self-annealing effect in the chill and mottle zones. The degree to which such processes affect structure is dependent on alloy composition, which determines both cast structure and transformation characteristics.

#### 4.3.2 CHILL/SAND CASTING MACROSTRUCTURES

Macrostructures of the three alloys are shown in Fig. 86. As the steel chill was smaller than the casting diameter, chill formations radiate into the casting section. The extent of chill penetration is indicated in the figure, but more detailed information may be obtained from microstructural measurements (Fig. 87).

Structures occurring at increasing distances from the chill may be divided into a series of bands as in the ceramic mould castings. Clear chill and mottle depths measured along the casting axis increased with decreasing silicon content. A feature of the microstructures was the presence of cementite needles in the outer mottle zone and ghost network structures which formed distinct bands beyond the limit of visible eutectic cementite. These bands were not so evident in the heated mould or room temperature ceramic mould castings, and may indicate differences between the effect of solid and water-cooled chills on microstructure.

#### 4.3.3 CHILL/SAND CASTING MICROSTRUCTURES

As metastable structures and sequences are considered in a later section on the chill casting experiments, results for the chill/sand castings will commence with the first appearance of graphite in the microstructure.

##### 4.3.3.1 1.00% SILICON ALLOY

Structural forms and sequences were largely the same in this casting as those obtained in the heated ceramic mould. Structural changes tended to be

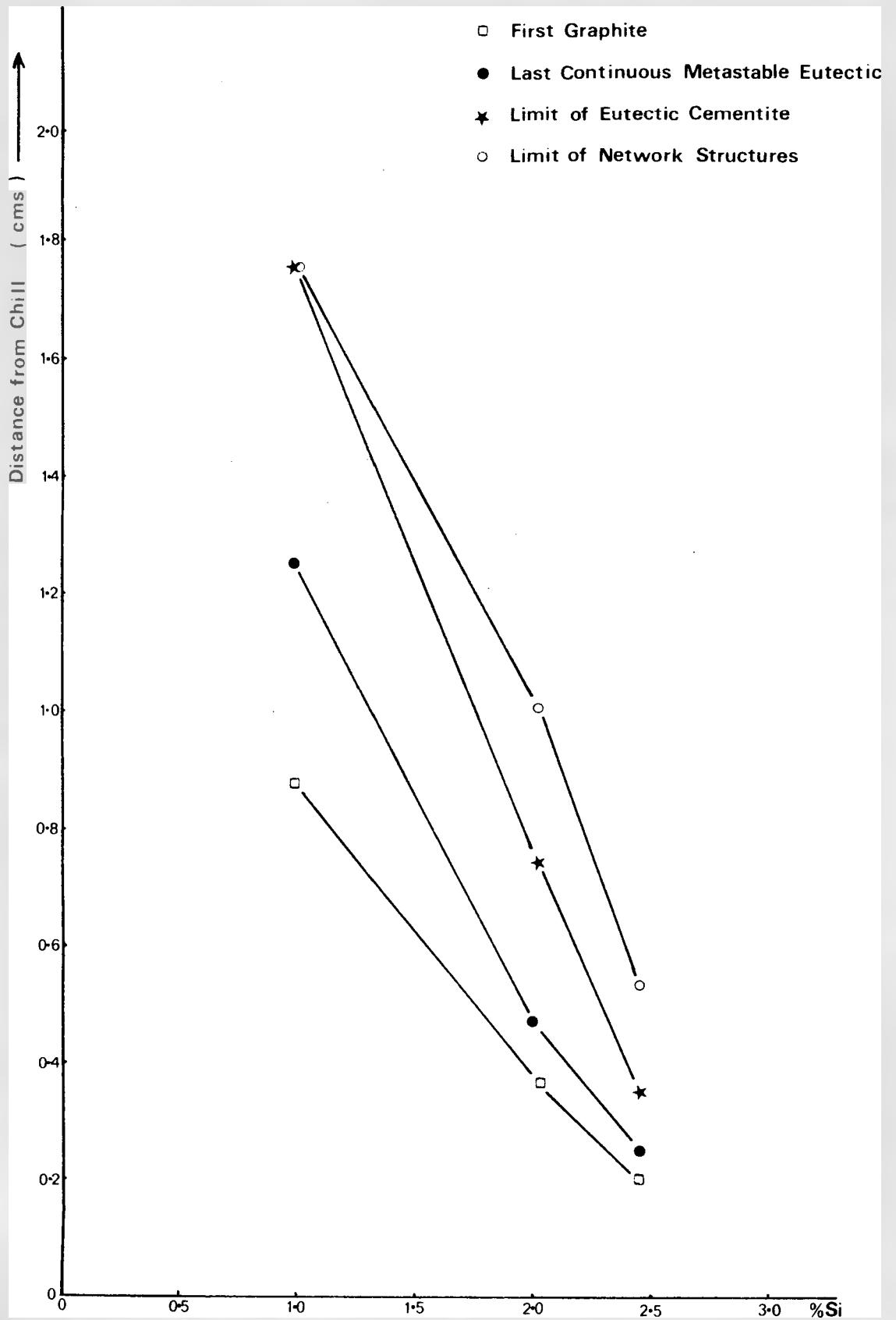


FIG 87 Chill/Sand Castings : Microstructural Measurements

more clearly defined than those of the previous experiment where the depth of chill and mottle was greater.

The first graphite in the microstructure took the form of spherical cells showing the radial structure and peripheral refinement found in the ceramic mould castings. Surrounding ledeburite colonies were dissociated in the border regions, showing evidence of network structures when etched in alkaline sodium picrate solution (Fig. 88).

As the number and size of graphite colonies increased, the peripheral fine graphite areas spread, taking on streamer-like shapes (Fig. 89).

As in previous samples radiating needle clusters of metastable eutectic were associated with streamer graphite. Ledeburite colonies gave way to laths of cementite associated with small amounts of normal ledeburite, which were often dissociated. The needle structures formed a well-defined section of the mottle zone (Fig. 90) extending about 5 cm beyond the massive ledeburite region. The amount of normal or degenerate ledeburite subsidiary to the main cementite laths decreased with increasing distance from the chill, as did the amount of cementite remaining in the needle structure. The outermost needles in the mottle zone were indicated only as networks by alkaline sodium picrate or bromine etching.

The finer streamer graphite colonies often showed continuous coarsened walls (Fig. 91) and contacted or even surrounded cementite particles. Fig. 92 shows a cementite lath surrounded by interconnected graphite, several portions of which form closed loops. The continuous graphite flake above the particle appears coarser than the numerous flakes below. Graphite-cementite contact occurs in several places, via cementite surface irregularities. Such contact appears to be with the sides of graphite flakes (i.e. the basal planes) rather than with the tips. Portions of the cementite near but not in contact with projecting graphite tips appear eroded.

Penetration of cementite particles by graphite flake tips was noted in

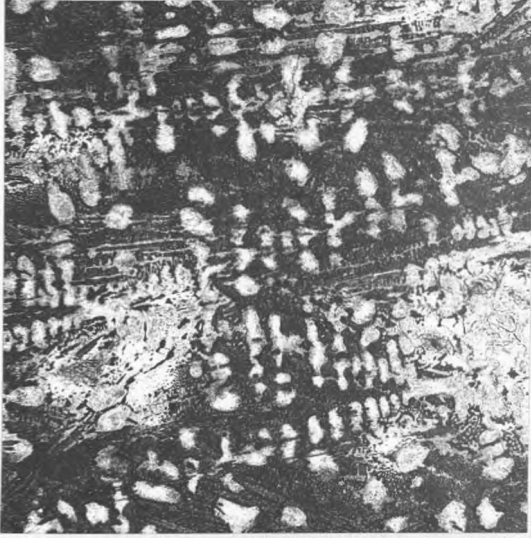


FIG.88. 1%Si. Chill/sand casting.  
Alk.Na.Pic. x60.  
Network structures  
around first graphite.



FIG.89. 1%Si. Chill/sand casting.  
Nital. x160.  
Peripheral streamer graphite.

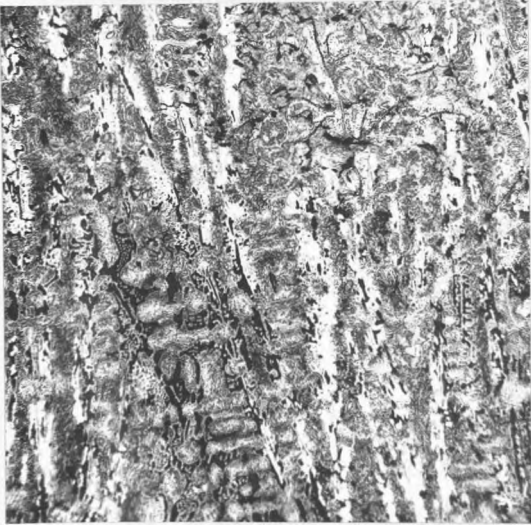


FIG.90. 1%Si. Chill/sand casting.  
Alk.Na.Pic. x60.  
Needle structures.

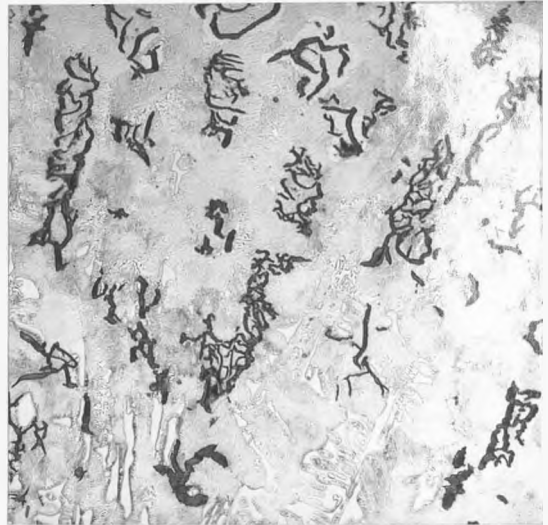


FIG.91. 1%Si. Chill/sand casting.  
Nital. x400.  
Finer graphite colonies.

numerous areas. This is shown in Figs. 93, 94 and 95, which also indicate large areas of contact between the two phases. Common interfaces only appear possible with graphite basal planes: contact with graphite flake tips is nearly always associated with penetration or erosion of the eutectic cementite.

#### 4.3.3.2 2.04% SILICON ALLOY

The first undercooled graphite cells in this alloy were circular (Fig. 96) coarsening into massive graphite at their borders. The compacted or looped flakes were associated with ledeburite areas showing signs of breakdown to network structures. Further from the chill, peripheral graphite was more streamer-like and elongated along the path of cementite needles (Fig. 97). Massive graphite was present, usually as greatly thickened flakes at the borders of the streamer areas. Border ledeburite was represented by cementite at nodes accompanied by network structures (Fig. 98).

Graphite/cementite contact in the streamer areas was often sufficient to produce honeycombe structures involving continuous graphite flakes (Fig. 99). These were associated with or were independent of residual eutectic cementite (Figs. 100 & 101). Fig. 102 shows similarities to Fig. 92 from the 1.00% silicon alloy, in that graphite forms a closed loop around a eutectic cementite particle. Contact between the two phases is by means of projections from the cementite surface. The intermediate area is composed of coarse pearlite, the cementite lamellae being continuous with the eutectic cementite laths. Cementite particles in the vicinity are associated with closely spaced pearlite, which may indicate variations in carbon concentration in the microstructure. Pearlite distributions in Fig. 101 form a network which suggests a pre-existing cementite distribution.

The general pattern of metastable/stable eutectic transition noted in the 1.00% silicon alloy was repeated in the 2.04% silicon casting. Structures progressed from isolated stable eutectic colonies through more directional streamer forms to cementite needle clusters piercing a stable eutectic matrix. The main

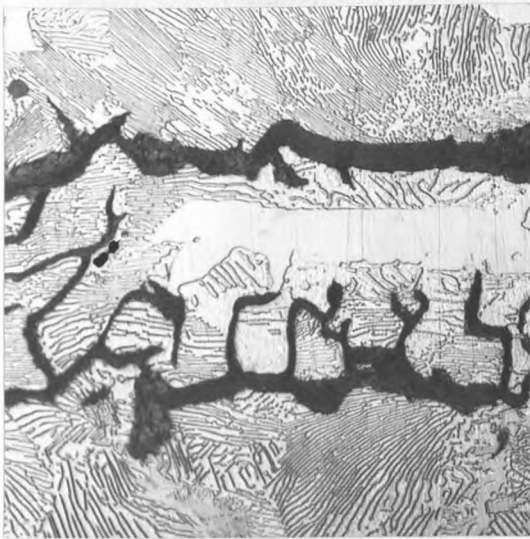


FIG.92. 1%Si. Chill/sand casting.  
Nital. x1000.  
Cementite surrounded  
by graphite.



FIG.93. 1%Si. Chill/sand casting.  
Nital. x1000.  
Graphite/cementite  
contact and penetration.

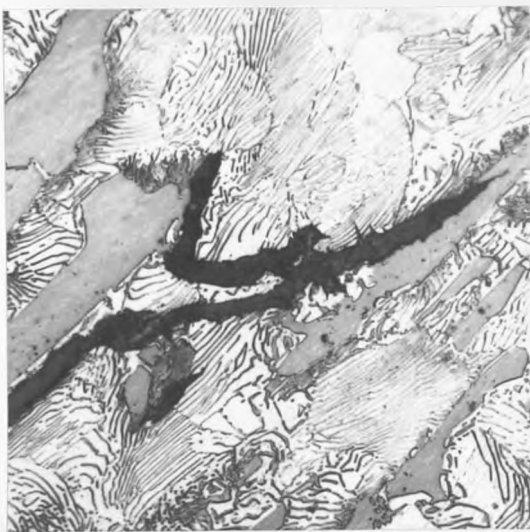


FIG.94. 1%Si. Chill/sand casting.  
Alk.Na.Pic/Nital. x1000.  
Graphite/cementite  
contact and penetration.



FIG.95. 1%Si. Chill/sand casting.  
Br<sub>2</sub>. x1000.  
Graphite/cementite  
contact and penetration.

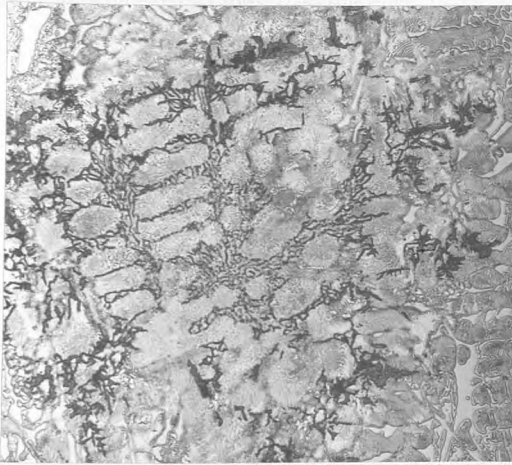


FIG.96. 2.04%Si.Chill/sand casting.  
Nital. x160.  
First graphite.



FIG.97. 2.04%Si.Chill/sand casting.  
Br<sub>2</sub>/Nital. x160.  
Peripheral streamer graphite.

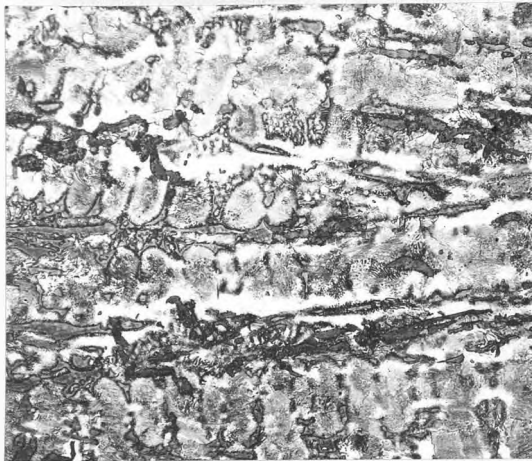


FIG.98. 2.04%Si.Chill/sand casting,  
Alk,Na,Pic/Nital. x160.  
Degenerate ledeburite.



FIG.99. 2.04%Si.Chill/sand casting.  
Nital. x160.  
Continuous streamer graphite.



FIG.100. 2.04%Si. Chill/sand casting.  
Nital. x1000.  
Outlining graphite.

structural difference between the two silicon contents was in graphite form, which was undercooled throughout the mottled zone of the specimen with the higher silicon content.

Network structures were widespread, representing both normal ledeburite (Fig. 103) and cementite needle clusters similar to Fig. 90. Undercooled graphite in these areas showed the border thickening and coherence found in other specimens. Undercooled graphite encountered further from the chill (Fig. 104) was similar to that in the centre of the first graphite colonies (Fig. 96).

#### 4.3.3.3 2.43% SILICON ALLOY

Undercooled graphite cells in this alloy (Fig. 105) were similar to those in the 2.04% silicon casting (Fig. 96). Flakes in the colony coarsened at the periphery, forming closed loops, massive flakes or flake aggregates. The plate-like metastable eutectic lost coherence in the border areas, occurring as isolated cementite particles. Fig. 106 at greater magnification emphasises the compaction and surface irregularity of the peripheral graphite.

The initial region of continuous metastable eutectic with isolated stable eutectic cells, gave way to a more irregular structure characterised by the presence of cementite needles. This region was in turn replaced by spherical undercooled stable eutectic cells intermixed with fine elongated graphite colonies. Fig. 107 shows the transition with the metastable eutectic on the left, and the stable eutectic on the extreme right. The intermediate zone is shown in greater detail in Fig. 108, where spherical stable eutectic cells are surrounded by areas containing stable eutectic pierced by radiating cementite needles and associated ledeburite. As noted by Hillert and Steinhauser<sup>(38)</sup>, the cementite needle cluster alignment appears to be independent of the primary austenite-dendrite lattice.

The mottle zones in this alloy showed extensive and progressive signs of ledeburite and cementite lath decomposition with increasing distance from the



FIG.101. 2.04%Si.Chill/sand casting.  
Alk.Na.Pic/Nital. x1000.  
Outlining graphite.



FIG.102. 2.04%Si.Chill/sand casting.  
Alk.Na.Pic/Nital. x1000.  
Outlining graphite.

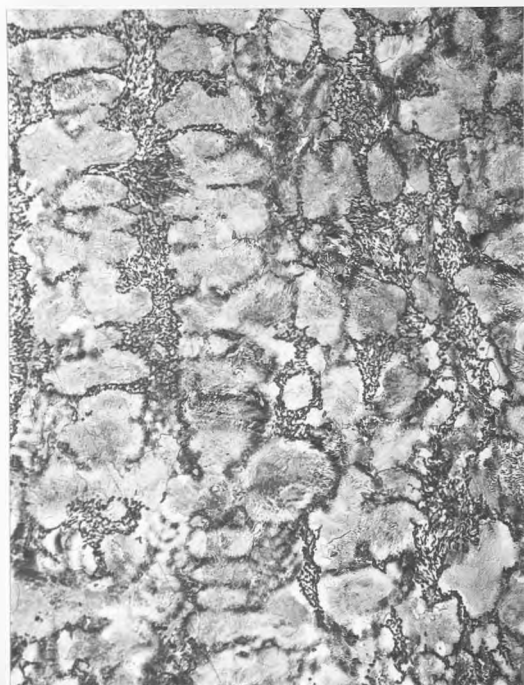


FIG.103. 2.04%Si.Chill/sand casting.  
Alk.Na.Pic/Nital. x160.  
Network structures.

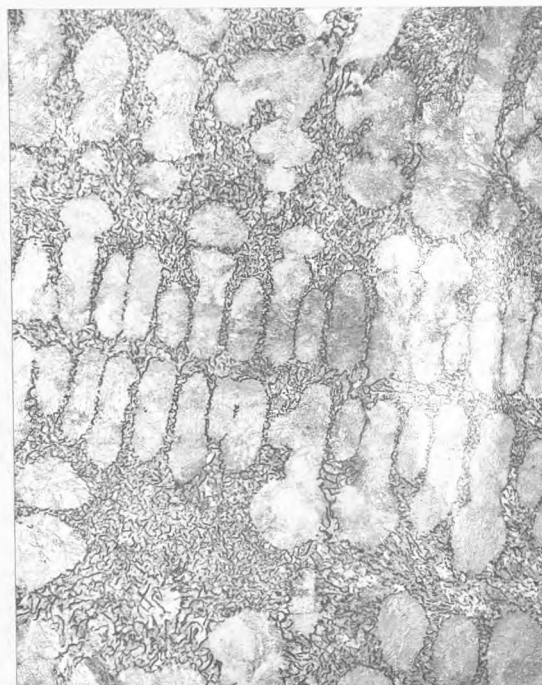


FIG.104. 2.04%Si.Chill/sand casting.  
Nital. x160.  
Undercooled graphite.

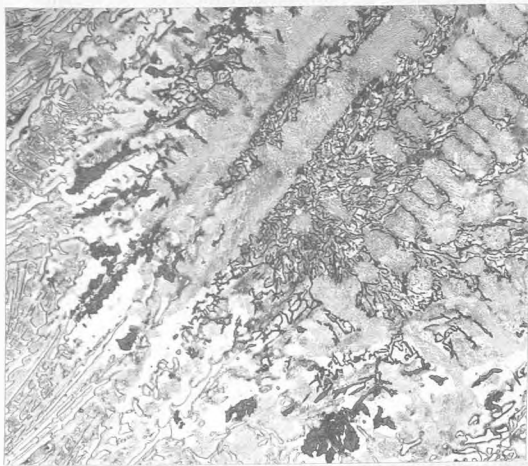


FIG.105. 2.43%Si.Chill/sand casting.  
Nital. x160.  
First graphite.

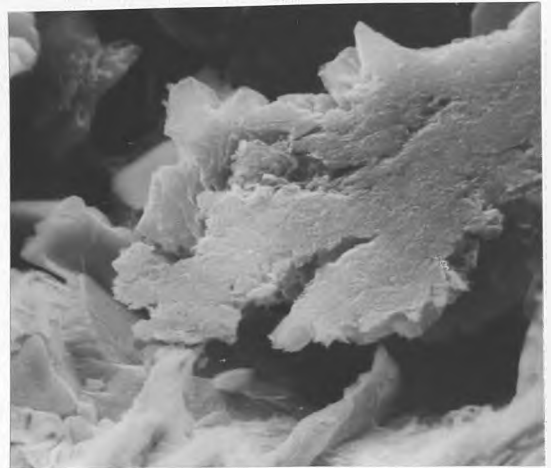


FIG.106. 2.43%Si.Chill/sand casting.  
Br<sub>2</sub>. Stereo @ 45°. x1400.  
Coarse peripheral graphite.

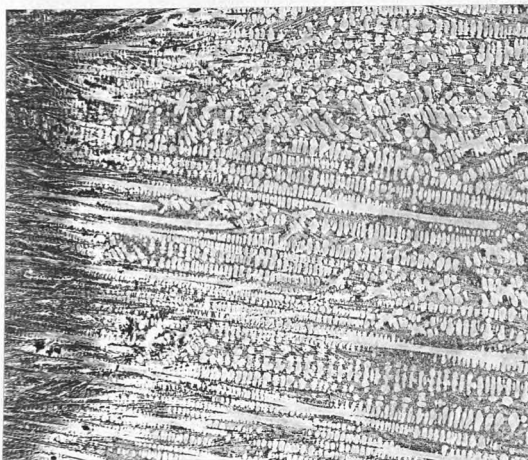


FIG.107. 2.43%Si.Chill/sand casting.  
Alk.Na.Pic./Nital. x30.  
Mottle transition zone.



FIG.108. 2.43%Si.Chill/sand casting.  
Alk.Na.Pic./Nital. x50.  
'Needle' mottle zone.

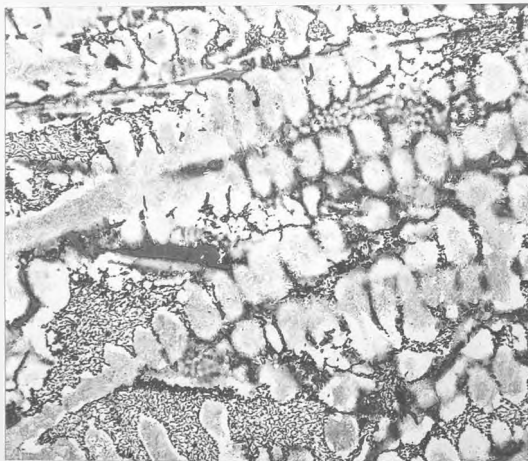


FIG.109. 2.43%Si.Chill/sand casting.  
Alk.Na.Pic./Nital. x160.  
Network structures.

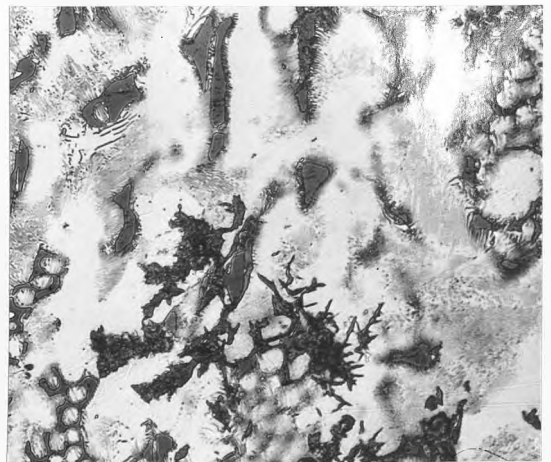


FIG.110. 2.43%Si.Chill/sand casting.  
Alk.Na.Pic./Nital. x400.  
Network structures.

chill. Network structures were widespread (Fig. 109), first occurring in areas containing massive ledeburite colonies. From Figs. 109 and 110, it appears that graphite may or may not be intermixed with the network structures and associated eutectic cementite. Where graphite was absent from the network structure adjacent graphite colonies often developed massive aggregated walls. Graphite found with ledeburite or network structures tended to be more continuous than the surrounding undercooled graphite, and sometimes had extensive common interfaces with cementite.

Fig. 111 shows a mottle area after deep bromine etching to remove ferrite. The area contains cementite in both lath and normal ledeburite forms, all of which show signs of extensive dissolution. Networks of pearlite lamellae outline isolated cementite particles within the ledeburite and cementite laths.

Junctions between normal ledeburite and graphite colonies are shown in Figs. 112 and 113. The graphite is finely-divided, curled and branched and apparently interconnected. Flakes occurring near the interface are thickened and aggregated to form a coherent boundary. (Fig. 114). Ledeburite becomes increasingly dissociated, with less residual cementite as the border with the graphite is approached. The ledeburite near the boundary is clearly outlined by pearlite nucleated by eutectic cementite remaining at nodes in the structure (Figs. 112 & 115). The actual boundary with the coherent graphite is marked by ferritic zones in which no network structure is visible.

Fig. 116 shows a ledeburite/graphite colony boundary, where the graphite is slightly coarser and less deformed than in the previous case (Fig. 113). The thicker peripheral graphite flakes tend to align along the colony boundary to form a coherent interface. The ledeburitic structure is outlined as before, with residual eutectic cementite acting as nuclei for pearlite formation.

With increasing distance from the chill, the amount of eutectic cementite remaining in the microstructure decreased, occurring only as isolated particles

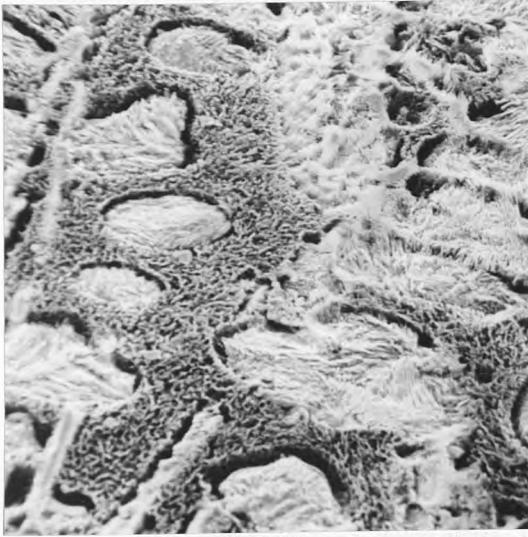


FIG.111. 2.43%Si.Chill/sand casting.  
Br<sub>2</sub>. Stereo @ 45°. x360.  
Mottle area.

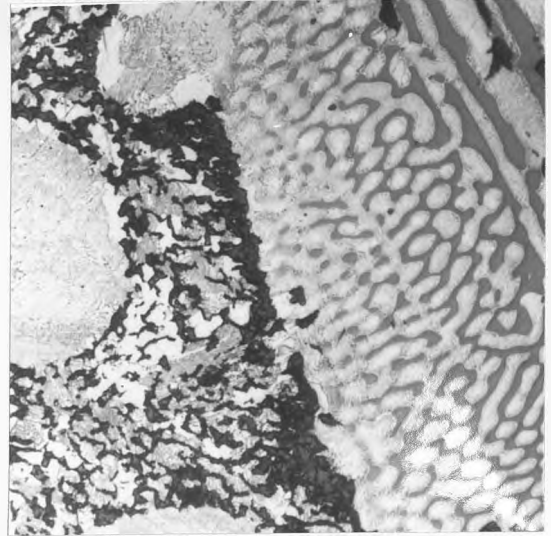


FIG.112. 2.43%Si.Chill/sand casting.  
Alk.Na.Pic./Nital. x1000.  
Ledeburite/graphite  
colony border.

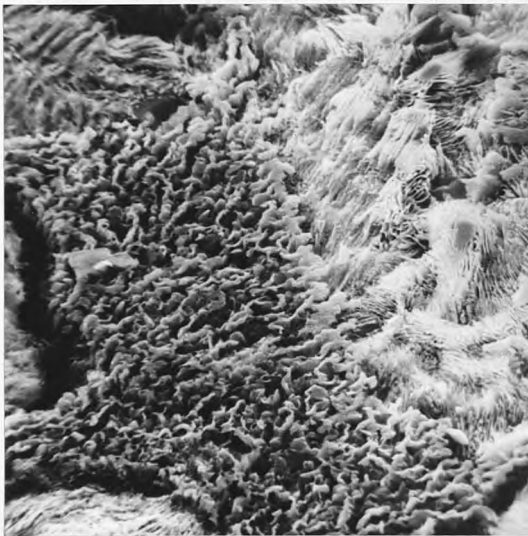


FIG.113. 2.43%Si.Chill/sand casting.  
Br<sub>2</sub>. Stereo @ 45°. x1210.  
Ledeburite/graphite  
colony border.

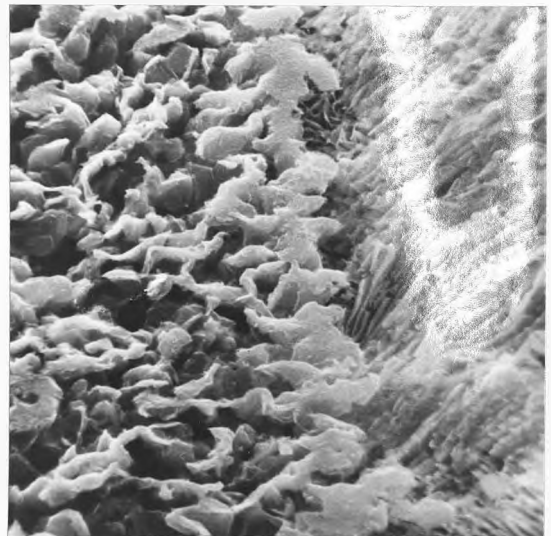


FIG.114. 2.43%Si.Chill/sand casting.  
Br<sub>2</sub>. Stereo @ 45°. x3600.  
Ledeburite/graphite  
colony border.

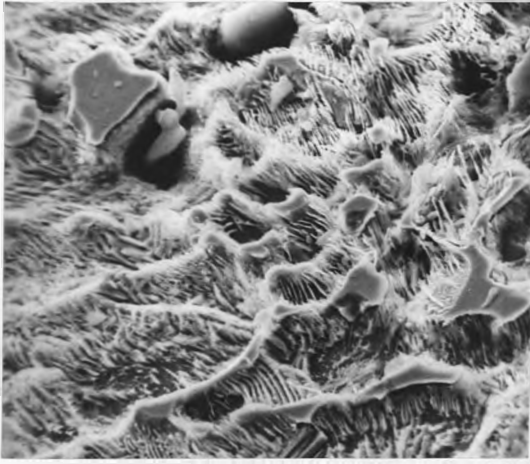


FIG.115. 2.43%Si. Chill/sand casting.  
Br<sub>2</sub>. Stereo @ 45°. x1350.  
Degenerate ledeburite.



FIG.116. 2.43%Si. Chill/sand casting.  
Br<sub>2</sub>. Stereo @ 45°. x1320.  
Ledeburite/graphite  
colony border.

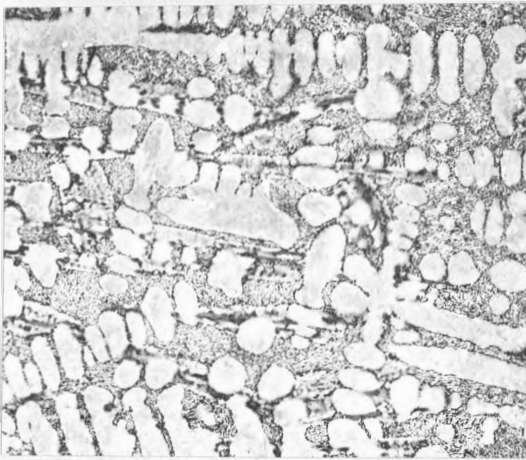


FIG.117. 2.43%Si. Chill/sand casting.  
Alk. Na. Pic./Nital. x120.  
Needle network structures.

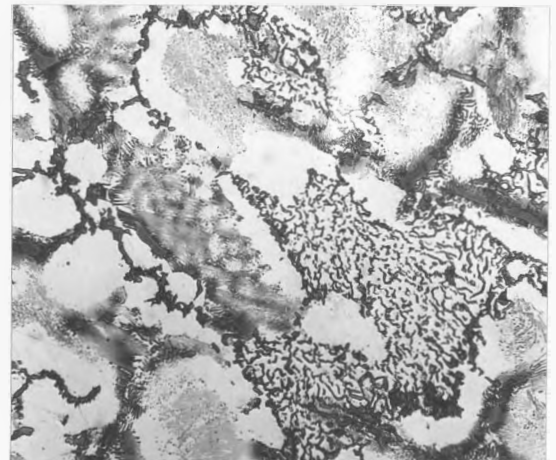


FIG.118. 2.43%Si. Chill/sand casting.  
Alk. Na. Pic./Nital. x400.  
Network structure.

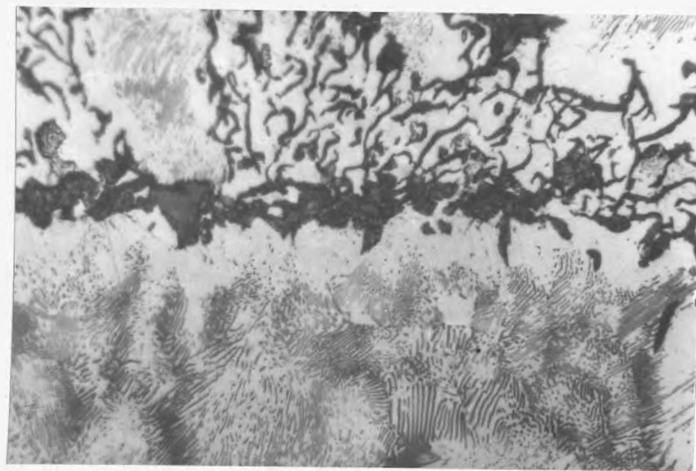


FIG.119. 2.43%Si. Chill/sand casting.  
Alk. Na. Pic./Nital. x1000.  
Network structure.

in the thicker portions of residual networks. Needle clusters were more clearly visible as in Fig. 108, radiating from the chill and intersecting areas of fine stable eutectic. Fig. 117 shows such a needle-cluster area with associated normal ledeburite networks at the outer limits of the mottled zone. Although little eutectic cementite is present, ledeburite networks are clearly indicated by variations in pearlite spacing (Figs. 118 & 119).

#### 4.3.4 SUMMARY

Thermal analysis indicates that portions of the casting near the chill may be subject to initial cooling rates sufficiently rapid to cause metastable solidification. As the solid chill became thermally saturated it grew less effective and cooling rates fall accordingly. The effect such a physical system will have on cast structure depends on the susceptibility of the alloy in question to metastable solidification, and the stability of cementite in chill and mottle areas during slow solid-state cooling.

Increasing silicon contents reduced overall chill penetration while decreasing the distance of first graphite colonies from the chill. Graphite in the 1.00% Si alloy was coarse in colony centres, becoming refined in streamer areas. That in the 2.04% and 2.43% Si alloys was of the undercooled type, becoming coarser at colony borders and more continuous when associated with ledeburite.

Mottled structures in solid chill/sand mould castings may be classified in three successive bands occurring with increasing distance from the chill surface:

1. Mottle in which ledeburite or acicular white eutectic colonies enclose spherical graphite colonies.
2. 'Streamer' mottle in which graphite and cementite are closely intermixed in colonies elongated in the growth direction.
3. Mottle in which stable eutectic colonies are pierced by fan-shaped clusters of cementite needles which may be associated with small areas of ledeburite nucleated on the lath surfaces.

Network structures and associated graphite coarsening occurred in all three mottle regions of all alloys, increasing in amount with increasing distance from the chill. In each alloy, some residual eutectic cementite disappeared before the outer limits of the chill band were reached.

#### 4.4 HEATED METAL MOULD EXPERIMENTS

##### 4.4.1 INTRODUCTION

Thermal analysis and metallography of ceramic mould and chill/sand castings suggested that some of the structures in cast iron mottle zones result from high temperature transformations in the solid state during or after solidification. The object of the present series of experiments was to study high temperature transformation processes in white and mottled structures during slow cooling through limited temperature intervals near the eutectic range.

##### 4.4.2 PHYSICAL CONDITIONS

Thermal analysis showed that physical processes were qualitatively similar in cylindrical, cruciform and plate mould castings. The cooling of a casting in a heated metal mould may be divided into several regions (Fig. 120) commencing with extremely rapid cooling under the chill influence of the mould. The cooling rate slackens as the temperature difference between the casting and mould grows less. At the same time, liberated heat raises the mould temperature, reducing the cooling rate still further until mould and casting reach the same temperature. Both casting and mould then cool slowly until they reach the constant furnace temperature. The final stage of cooling in these experiments was a rapid water quench.

The interaction of these physical conditions with the solidification of the casting, and their influence on microstructure may be controlled by mould design and temperature, holding time at furnace temperatures and alloy composition. For a given alloy, white or mottled solidification is most likely if the eutectic arrest occurs in the initial rapid cooling region. This will be encouraged by lower mould temperatures, low superheating of the melt and small casting size in a given mould material.

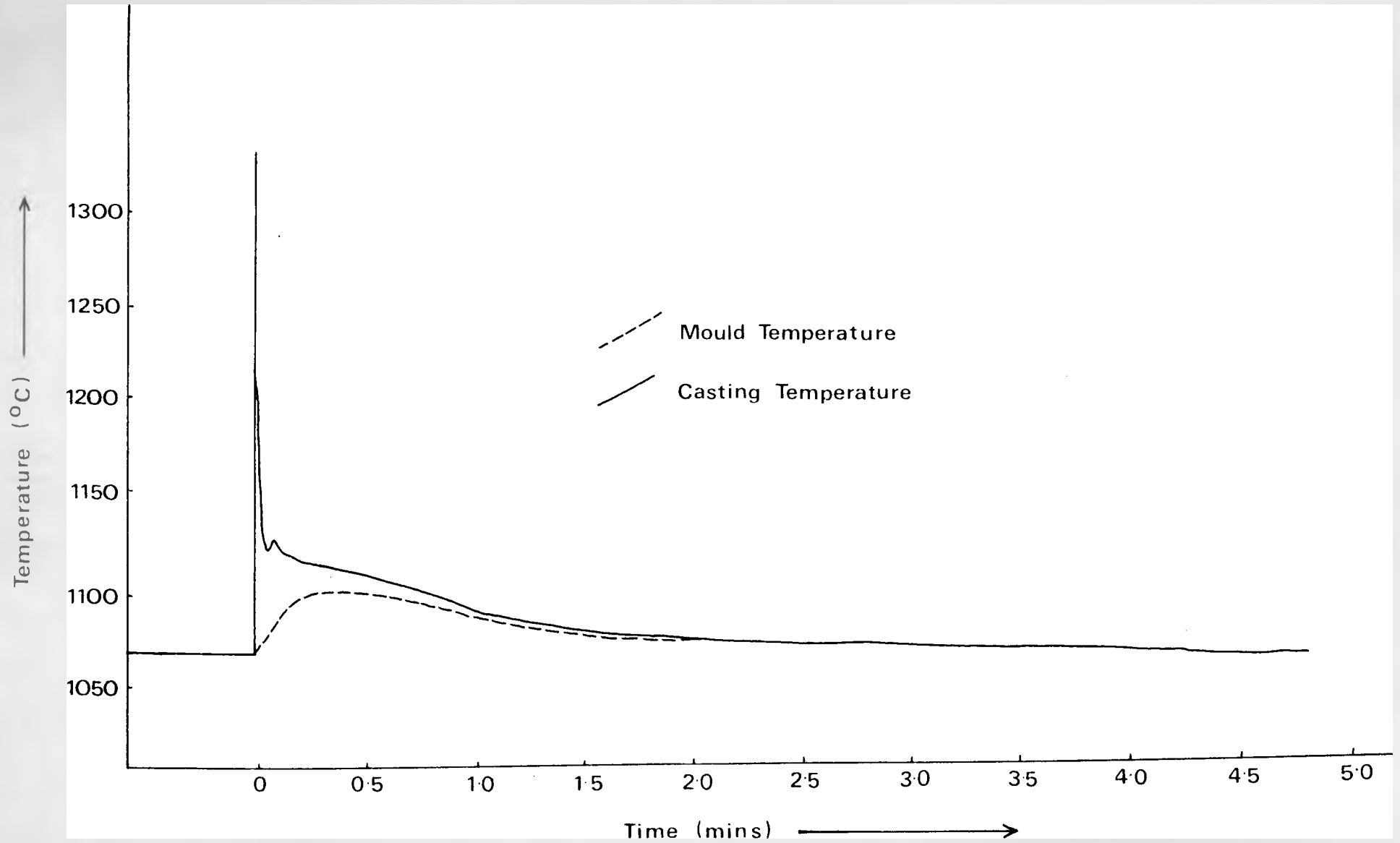


FIG. 120. Cooling Curve in Heated Metal Mould

Initial experiments with cylindrical Ni/20%Cr alloy moulds indicated the desirability of small casting volume/surface area ratios to produce the most rapid initial cooling rates while minimising mould heating and structural heterogeneity in the resulting casting. 3 mm. dia. moulds were satisfactory for 1.00% and 2.04% silicon alloys, enabling chill and mottle production in moulds heated to 1035°C. The greater stability of the graphite eutectic in the 2.34% silicon alloy meant that chill and mottle structures could only be produced in 2 mm. dia. moulds, which had enhanced heat transfer properties and smaller casting thermal capacities.

Cylindrical mould castings showed structural heterogeneity toward the top of the mould, caused by heat input from the downrunner. The main drawback with these moulds was the relatively high volume/surface area ratio, which limited the initial cooling rates and reduced the useful mould temperature range.

Cruciform shape mould castings had lower volume/surface area ratios than the cylindrical mould specimens. This improved heat transfer properties, especially in the thinner sections. The thermal mass of the cruciform mould castings and high pouring temperatures necessary for mould filling resulted in mould temperature rises of up to 85°C. This limited the range of mould temperatures in which metastable solidification could be obtained.

Cruciform moulds were positioned vertically, the 1.5 mm. section being used as a downrunner. This practice encouraged filling of the 0.5 mm. mould section, but resulted in preheating of the 1.5 mm. mould cavity and reduction in its chilling capacity. Cooling of the 1.5 mm. section was also retarded by the metal in the pouring cup.

The tendency to metastable solidification at a given mould temperature increased with distance from the mould centre. This effect was caused by the presence of a heat centre at the junction of the four arms. The inhomogeneity caused by the heat centre was most noticeable in the 2 mm. sections, 1.0 and

0.5 mm. being less affected.

1 mm. plate castings had lower volume/surface area ratios than cylindrical or cruciform mould castings. This, together with the uniform casting thickness and absence of a heat centre, improved casting homogeneity. Figs. 121 and 122 show the variation of cooling rate with temperature for 1.00% and 2.43% silicon alloys cast into 1 mm. plate moulds. Increasing mould temperature resulted in higher cooling rates at a given temperature and consequently higher rates during solidification. Lower mould temperatures in both alloys resulted in high cooling rates during metastable solidification. After solidification, cooling rates remained high until mould and casting reached the same temperature and cooled slowly.

Mould heating in the 1 mm. plate moulds fell within the range 20-30°C for all mould temperatures studied. This became an important factor at higher mould temperatures where the interval between initial mould temperature and the solidification range was small. In such castings, cooling rates before and after solidification decreased due to mould heating. Solidification was followed immediately by slow cooling of both mould and casting to the constant furnace temperature.

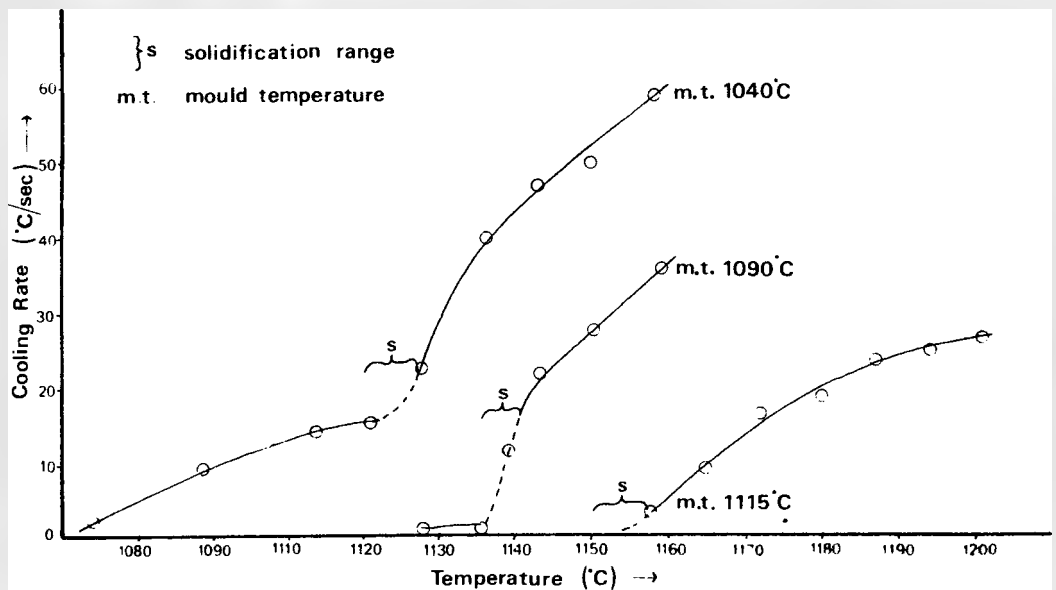
Water quenching produced cooling rates of 20-30°C/sec in the castings. This was sufficient to produce martensite as an austenite transformation product or very fine acicular metastable eutectic in unsolidified regions.

#### 4.4.3 MICROSTRUCTURES

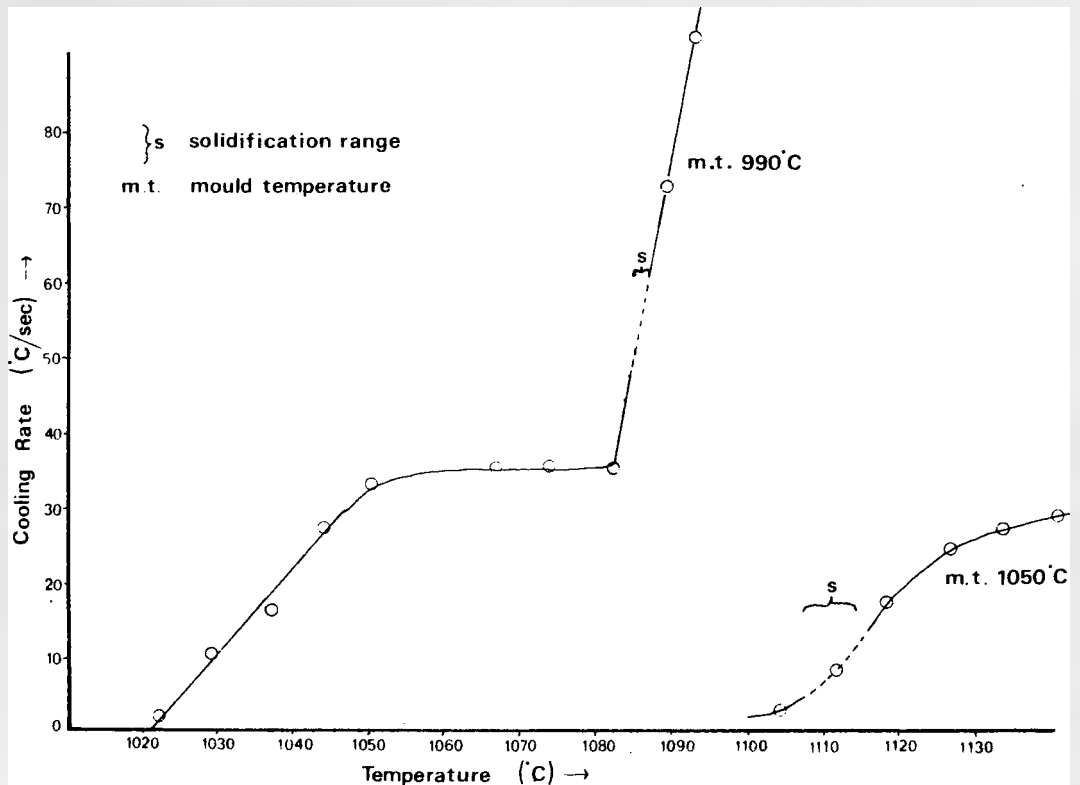
##### 4.4.3.1 1.00% SILICON ALLOY

Table 9 shows the range of metal mould experiments carried out in the 1.00% silicon alloy. Eutectic points are quoted as the temperature ranges from start to the end of the arrest.

Both 3 mm. diameter cylindrical castings solidified with a degenerate metastable eutectic structure. Specimen A quenched after 0.55 minutes was



**FIG 121.** 1% Si ALLOY : 1mm PLATE CASTINGS  
 VARIATION OF COOLING RATE WITH TEMPERATURE



**FIG 122.** 2.4% Si ALLOY : 1mm PLATE CASTINGS  
 VARIATION OF COOLING RATE WITH TEMPERATURE

Expt	Mould Type	No	Mould Temp °C	Time to Quench mins	Temp at Quench °C	Eutectic Arrest °C	Mould Temp Rise °C	Initial Structure
A	3mm Cyl		1015	0.55	1037	-	-	White
B	..		1015	8.0	1015	-	-	
C	1mm Plate	1	1038	-	-	-	21	White
		2	1035	0.85	-	-		
		3	1036	11.4	1037	-		
		4	1034	21.0	-	1116-1113		
D	..	1	1060	1.2	-	-	29	..
		2	1063	4.2	-	-		
		3	-	6.3	-	-		
		4	-	26.5	-	-		
E	..	1	1095	2.0	1101	-	21	..
		2	1090	14	-	1130-1126		
		3	1094	25	-	-		
		4	1090	36	-	1129-1127		
F	..	1	1098	1.3	1096	-	29	Mottled
		2	1098	7.0	1093	-		
		3	1102	14	1100	1120-1115		
		4	1101	30	1098	-		
G	..	1	1115	2.5	1123	-	29	Grey
		2	1125	7.5	-	-		
		3	1114	14	1107	1144-1136		
		4	1115	32	1106	1151-1144		

TABLE 9

1% Si Alloy

Metal Mould Casting Conditions

entirely white, while specimen B which was held in the furnace at  $1015^{\circ}\text{C}$  for 8 minutes showed signs of graphite formation in isolated areas (Fig. 123). The graphite consisted of closely-packed clusters of curled and branched flakes which touched and tended to engulf neighbouring cementite.

The infrequent nucleation or slow growth of graphite was also found in the series of plate castings. Maintaining the casting at  $1030^{\circ}\text{C}$  for over 11 minutes in experiment C produced only infrequent small graphite clusters (Figs. 124 & 125). The graphite consisted of randomly distributed aggregates with irregular outlines and occasional flake offshoots. Eutectic cementite appeared to be less coherent near the graphite and some contact occurred between flakes and isolated cementite particles.

In experiment D, the casting held at  $1060^{\circ}\text{C}$  for 4 minutes had very small amounts of graphite (Fig. 126). The isolated colonies occurred as flake clusters outlining cementite at colony edges. Graphite was most common at the specimen periphery, developing inwards in alignment with the metastable eutectic. After 26 minutes the flakes were coarsened forming aggregated massive areas.

Similar trends were followed in experiment E, with the moulds at  $1090^{\circ}\text{C}$ . Fine peripheral graphite with more massive flakes in the casting body had developed after 14 minutes. These grew in size during furnace holding for 36 minutes (Fig. 127). The alignment and general appearance of the aggregated flakes in Fig. 127 suggests graphite nucleation in porous areas. Fine single crystal offshoots from the main irregular flakes were common (Fig. 128). These extended into the surrounding ledeburite and occasionally contacted cementite particles. Cementite in the vicinity of graphite showed general wasting, only isolated particles remaining at nodes in the eutectic (Fig. 129). Graphite flakes and the wasted cementite particles were frequently surrounded by outlining areas of fine pearlite in an otherwise martensitic matrix.

Preheating moulds to  $110^{\circ}\text{C}$  in experiment F produced mottled structures on

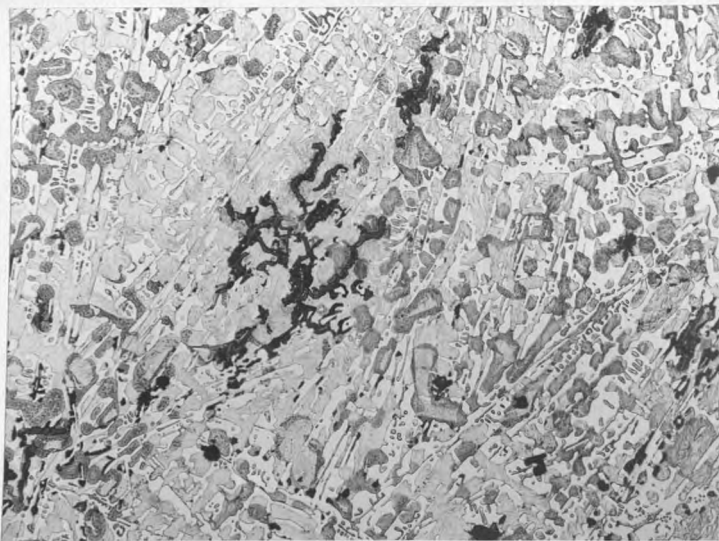


FIG.123. 1%Si. Expt B. 8mins. M.T.1015<sup>0</sup>.  
Nital. x200.  
Graphite cluster.

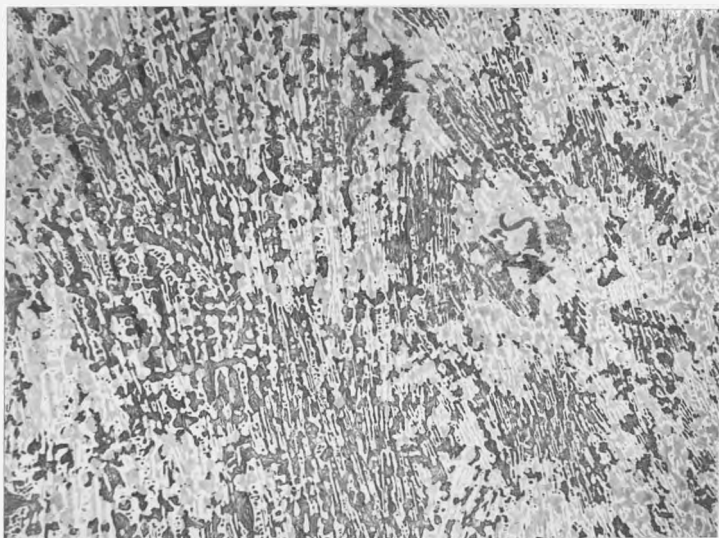


FIG.124. 1%Si. Expt C. 11mins. M.T.1030<sup>0</sup>.  
Picral. x160.  
Aggregate graphite.



FIG.125. 1%Si. Expt C. 11mins. M.T.1030<sup>0</sup>.  
Picral. x400.  
Aggregate graphite.

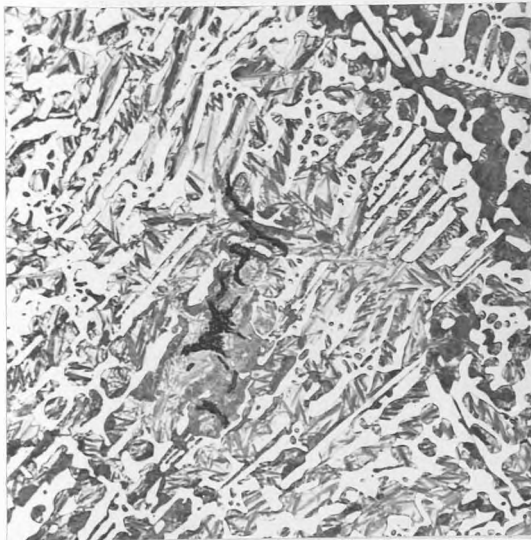


FIG.126. 1%Si. Expt D. x160.  
4mins.M.T.1060°. Picral.  
Flake cluster graphite.



FIG.127. 1%Si. Expt E. x80.  
36mins.M.T.1090°. A.Na.Pic.  
Aligned graphite aggregates.

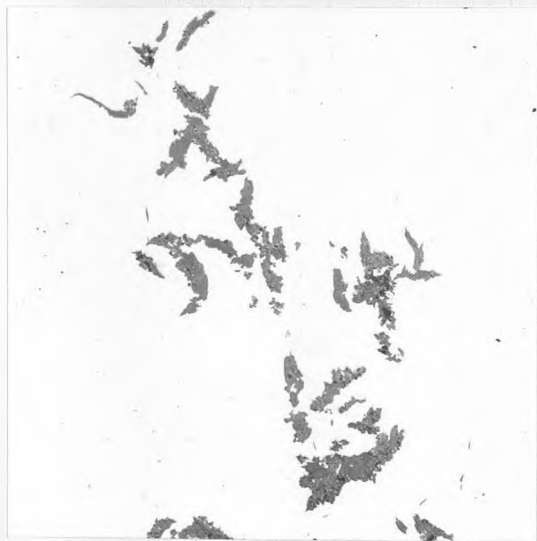


FIG.128. 1%Si. Expt E. x160.  
36mins.M.T.1090°. (unetched)  
Irregular graphite aggregates.

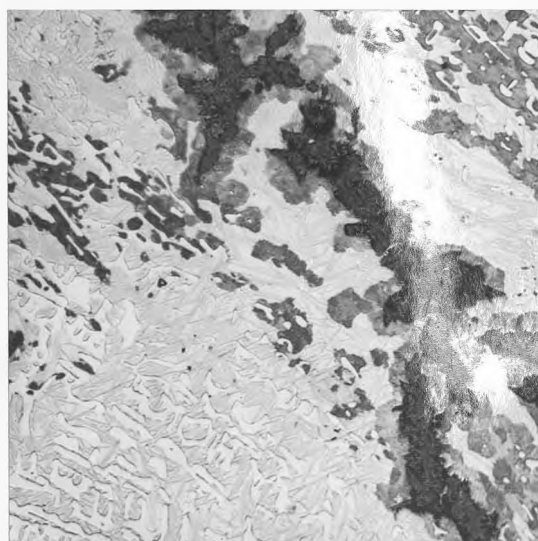


FIG.129. 1%Si. Expt E. x200.  
14mins.M.T.1090°. Picral.  
Wasted cementite in vicinity  
of graphite.

solidification. With such small castings, the amount of mottle produced by solidification under these conditions is likely to vary between specimens. This should be borne in mind when examining castings quenched at different times after pouring.

Graphite colonies were present in all parts of the castings, forming long aligned streamer colonies at the edge and more rounded colonies in the centre (Fig. 130). Graphite flakes coarsened toward colony borders in all specimens, but the development was most marked in those held in the furnace for 7 and 14 minutes. The coarse flakes appeared to be formed by aggregation of small flakes.

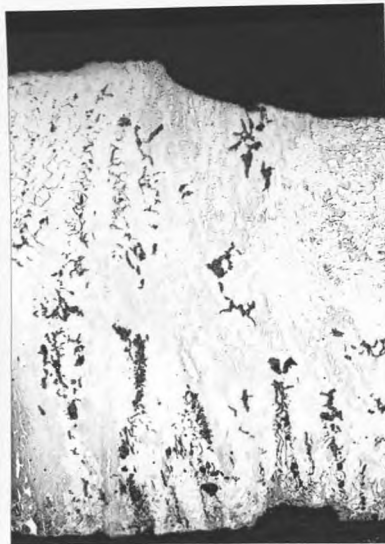
Ledeburite colony peripheries showed signs of structural breakdown in all specimens, the amount of eutectic involved increasing with longer furnace holding times. This is seen more clearly in Figs. 131, 132 and 133, which show graphite colony/ledeburite boundaries in isothermally held specimens. Etching in alkaline sodium picrate defined the border area, showing gradual wasting and dissociation of eutectic cementite until only isolated particles were left near the graphite. The ledeburite colonies were penetrated by streamers of apparently interconnected graphite which was continuous with the finer rounded colonies. The graphite streamers were aggregated when situated outside the light-coloured areas around the cementite. Smoother single crystal graphite flakes occurred within these areas nearer to the original cementite outline.

Specimens cast into moulds at  $115^{\circ}\text{C}$  (experiment G) solidified as the stable eutectic. No eutectic cementite could be detected in the microstructure. Fig. 134 shows an area of interconnected interdendritic flakes typical of these specimens.

From the microstructures it appears that graphite nucleation of growth in the solid state was difficult at mould temperatures below  $1095^{\circ}\text{C}$ . Porosity or the casting surface may be a source of nuclei in such cases. When graphite did form it was coarse and compacted, with irregular surfaces and single crystal projections. With mould temperatures above  $1095^{\circ}\text{C}$ , amounts of graphite increased



FIG.130. 1min.



7mins.



14mins.

1%Si. Experiment F. M.T.1100°. Picral. x40.  
Development of graphite colonies.

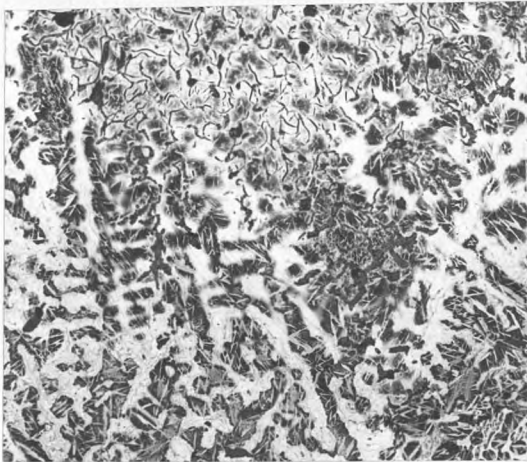


FIG.131. 1%Si. Expt F. x80.  
7mins.M.T.1100°. A.Na.Pic.  
Network structures.

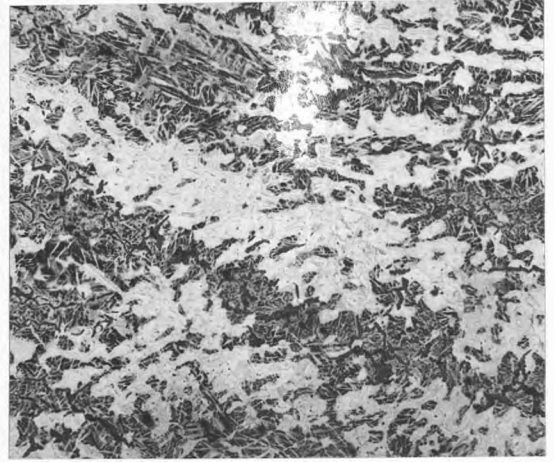


FIG.132. 1%Si. Expt F. x80.  
14mins.M.T.1100°. A.Na.Pic.  
Network structures.



FIG.133. 1%Si. Expt F. x160.  
30mins.M.T.1100°. A.Na.Pic.  
Network structures.



FIG.134. 1%Si. Expt G. x160.  
14mins.N.T.1115°. A.Na.Pic.  
Interdendritic graphite.

forming mottled structures with graphite in the form of circular colonies and directional streamers. Graphite flakes at the colony borders may have acted as nuclei for deposition of carbon provided by cementite decomposition. Graphite deposited in this way coarsened, existing peripheral flakes forming closely spaced crystals or more massive aggregates. Graphite flakes became coarsest where only a few flakes were associated with decomposing cementite, or when the graphite was completely surrounded by metastable eutectic as in the streamers. Graphite/cementite contact was common in border areas as in previous experiments. The graphite flakes in such regions were smoother than the surrounding graphite aggregates.

The course of eutectic cementite decomposition may be revealed by alkaline sodium picrate etching. Cementite became progressively less coherent as border areas were approached. The thicker parts of the metastable eutectic structure were the last to disappear.

#### 4.4.3.2 2.04% SILICON ALLOY

Heated metal mould experiments in this alloy were confined to cylindrical castings (Table 10). The following microstructures are from the body of the castings, away from heterogeneity introduced by the downrunner.

Specimens H and J were cast into moulds preheated to 1017<sup>o</sup>C. Both had mottled microstructures, but graphite form changed during isothermal treatment after solidification. Graphite in specimen H occurred as streamers aligned with the acicular metastable eutectic (Fig. 135). At higher magnification the graphite was seen to be very closely associated with the eutectic cementite (Fig. 136). Etching in alkaline sodium picrate revealed characteristic network structures and isolated cementite particles in the vicinity of the graphite (Fig. 137) and may indicate a certain amount of cementite decomposition in specimen H.

Isothermal treatment at 1017<sup>o</sup>C for 8 minutes (specimen J) produced non-directional graphite aggregates (Fig. 138). Graphite occurred as loosely joined polycrystalline clusters, with no apparent continuity beyond the

Expt	Mould Type	Mould Temp °C	Time to Quench	Temp at Quench
H	3mmCyl.	1017	0.5m	1077
J	..	1017	8.0m	1016
K	..	1033	0.4m	1067
L	..	1039	4.4m	-

TABLE 10.                      2.04% Si Alloy  
Metal Mould Casting Conditions

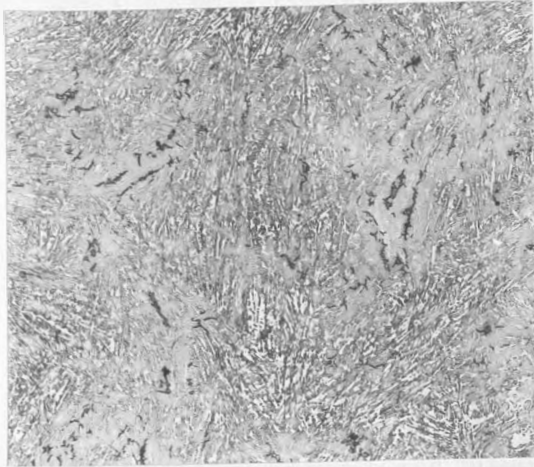


FIG.135. 2.04%Si. Expt H. x80.  
 $\frac{1}{2}$ min. M.T.1017°. Nital.  
 General structure.

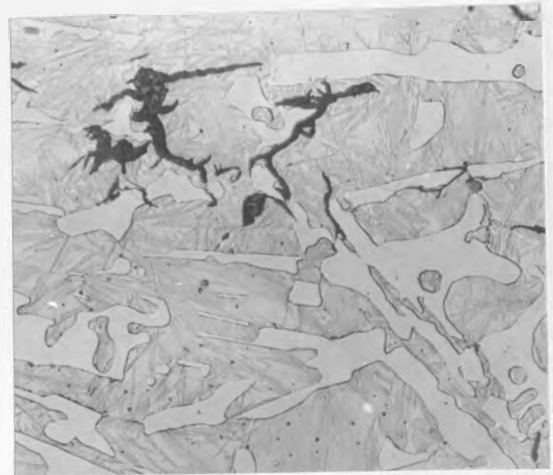


FIG.136. 2.04%Si. Expt H. x1000.  
 $\frac{1}{2}$ min. M.T.1017°. Nital.  
 Outlining graphite.

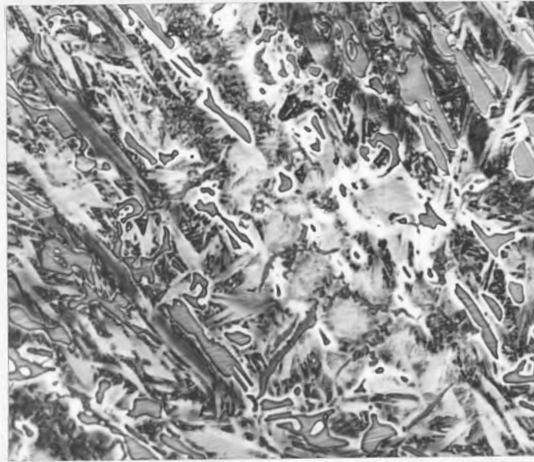


FIG.137. 2.04%Si. Experiment H. x400.  
 $\frac{1}{2}$ min. M.T.1017°. Alk.Na.Pic.  
 Network structures.

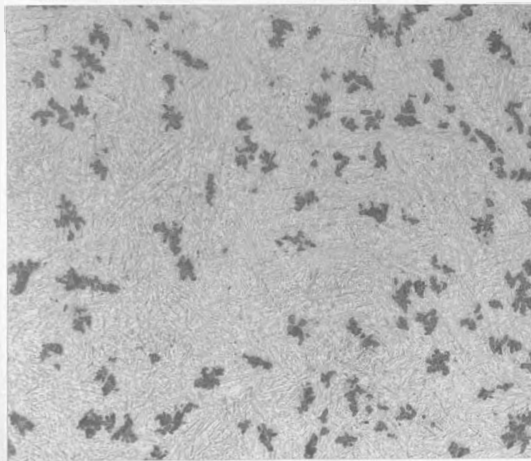


FIG.138. 2.04%Si. Expt J. x80.  
 8mins. M.T.1017°. Nital.  
 General structure.

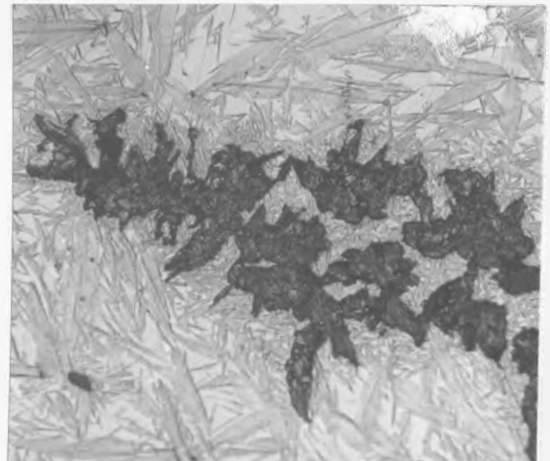


FIG.139. 2.04%Si. Expt J. x1000.  
 8mins. M.T.1017°. Nital.  
 Aggregated graphite cluster.

individual colonies (Fig. 139). Eutectic cementite could not be detected in specimen J using a nital etch. Alkaline sodium picrate (Fig. 140) or bromine (Fig. 141) exposed wasted cementite particles and outlined regions of pre-existing cementite which had decomposed during isothermal treatment. The network pattern revealed by sodium picrate etching (Fig. 142) is comparable with the acicular eutectic of specimen H (Fig. 135).

Specimens K and L were cast into moulds at higher temperatures (Table 10). Graphite in specimen K was of two types (Fig. 143). Very short curled and probably interconnected flakes (Fig. 144) formed colonies closely associated with eutectic cementite at the peripheries. Eutectic cementite laths were aligned with thicker, more continuous flakes. These sometimes surrounded lath sections to form interconnected networks (Fig. 145).

Isothermal holding for 4.4 minutes at 1039°C (specimen L) did not result in the marked changes in graphite morphology noted in the lower temperature specimens (Fig. 146). The amount of fine graphite flakes appeared to increase, forming regions with an aggregated appearance (Fig. 147). Lath outlining flake networks remained although cementite was absent. The flakes appeared generally thicker than in the previous specimen (c.f. Fig. 145) but showed no sign of losing surface regularity and becoming aggregated. Eutectic cementite was not visible in specimen L using nital as an etch. As before alkaline sodium picrate exposed a network structure (Fig. 149) which was similar to the cementite distribution in specimen K (Fig. 143). At high magnification, isolated particles of cementite were visible in some places (Fig. 150).

Comparing specimens H/J and K/L it appears that initial graphite formations were fewer in number at the lower mould temperature. Transformation at the lower temperature resulted in compacted graphite. At the higher temperature, graphite forms altered far less, the amount of fine aggregated graphite increasing during isothermal holding. Cementite dissolution was more rapid at the higher temperature, but was still incomplete after 4.4 minutes with the mould at 1039°C.

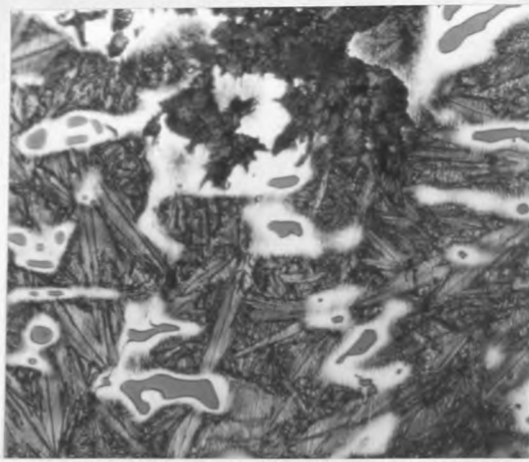


FIG.140. 2.04%Si. Expt J. x1000.  
8mins. N.T.1017°. A.Na.Pic.  
Network structures.

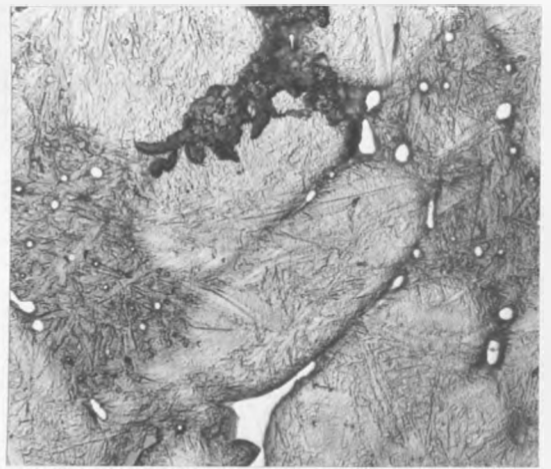


FIG.141. 2.04%Si. Expt J. x1000.  
8mins. N.T.1017°. Br<sub>2</sub>  
Network structures.

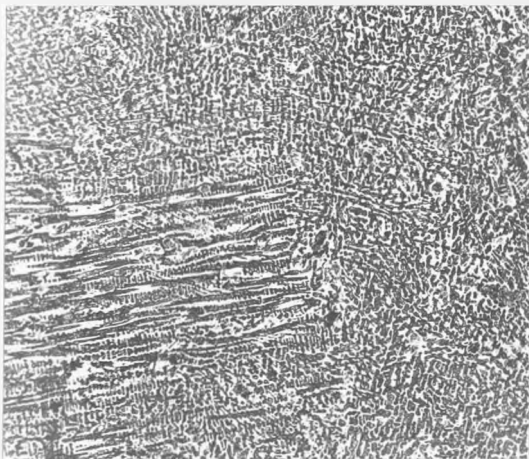


FIG.142. 2.04%Si. Expt J. x80.  
8mins. N.T.1017°. A.Na.Pic.  
Network structures.

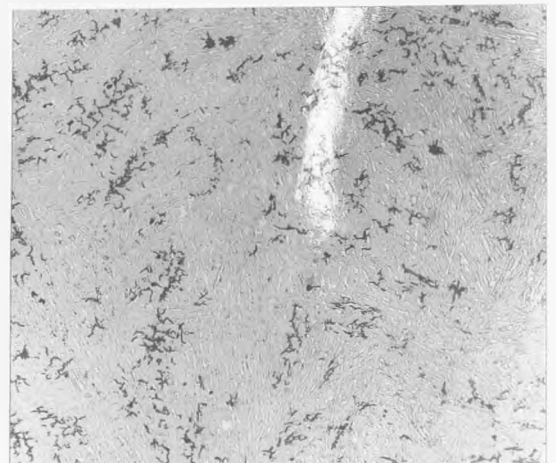


FIG.143. 2.04%Si. Expt K. x80.  
0.4mins. N.T.1033°. Nital.  
General structure.

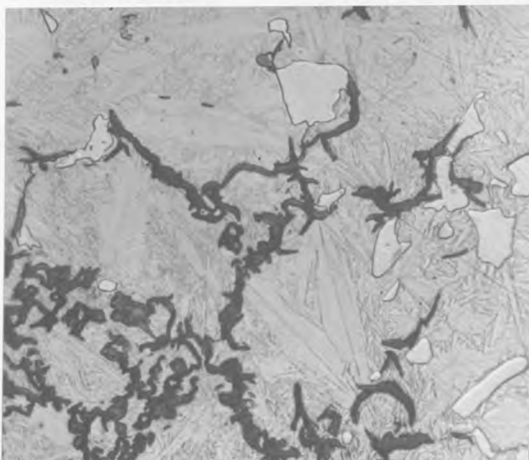


FIG.144. 2.04%Si. Expt K. x1000.  
0.4mins. N.T.1033°. Nital.  
Peripheral outlining graphite.

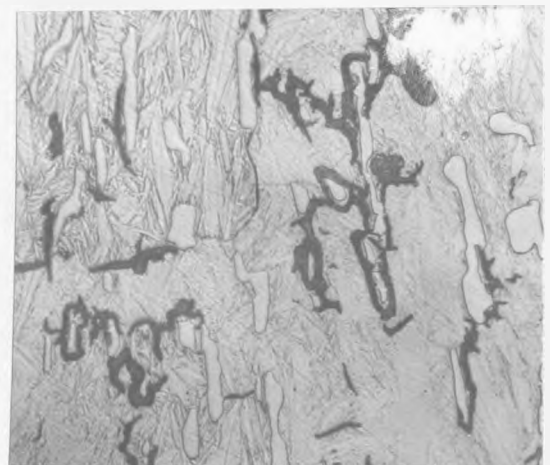


FIG.145. 2.04%Si. Expt K. x1000.  
0.4mins. N.T.1033°. Nital.  
Outlining graphite.

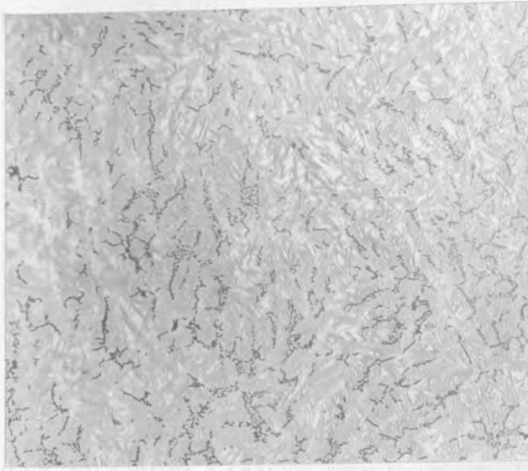


FIG.146. 2.04%Si. Expt L. x80.  
4.4mins.M.T.1039°. Nital.  
General structure.

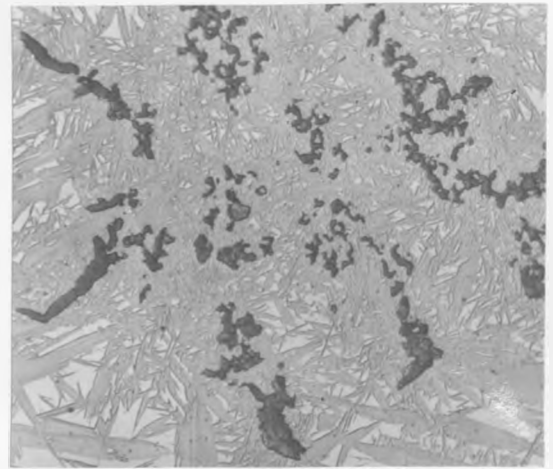


FIG.147. 2.04%Si. Expt L. x1000.  
4.4mins.M.T.1039°. Nital.  
Compacted graphite.



FIG.148. 2.04%Si. Expt L. x1000.  
4.4mins.M.T.1039°. Nital.  
Outlining graphite.

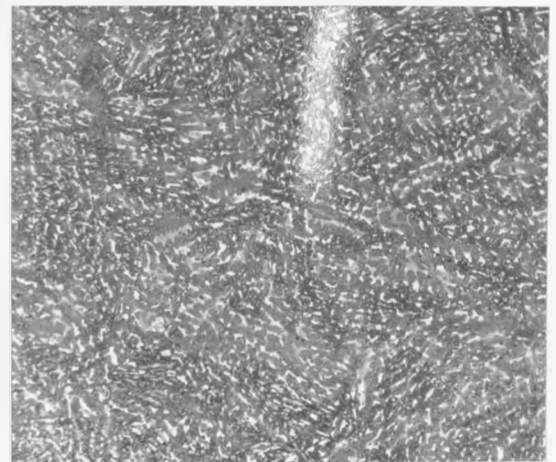


FIG.149. 2.04%Si. Expt L. x100.  
4.4mins.M.T.1039°. A.Na.Pic.  
Network structures.



FIG.150. 2.04%Si. Experiment L. x1000.  
4.4mins. M.T.1039°. Alk.Na.Pic.  
Residual cementite.

#### 4.3.3.3 2.43% SILICON ALLOY

The range of casting conditions covered in this series of experiments is shown in Table 11. Cylindrical mould castings M and N had mottled structures in spite of their relatively low mould temperature. This may have resulted from the low pouring temperatures and use of a grey melting stock. Figs. 151 and 152 show the top portion of cylindrical castings M and N. The influence of the downrunner in producing an inhomogeneous structure is clear. In both cases the upper portions contain undercooled graphite colonies, which give way to more isolated random graphite formations in the body of the casting. Graphite in the body of casting M (mould temperature 1006°C) was of the outlining network type, similar to that shown in Fig. 145. The graphite flakes in the body of casting N (mould temperature 1015°C) were more numerous and aggregated, presumably because of the higher mould temperature and the longer time at the higher temperature. Eutectic cementite in casting N was wasted, and network structures were revealed by etching in alkaline sodium picrate (Fig. 153).

Heated mould casting surfaces were covered with a black surface film containing small whirl structures (Fig. 154). These had well defined centres with radiating arms and concentric markings caused by surface irregularities. Examination at higher magnification showed the surface to be divided by fine cracks into roughly hexagonal areas, similar to those of Fig. 66 found on graphite flakes. The surface film could be easily stripped off, but proved to be insoluble in strong acids. Hughes <sup>(95)</sup> reported the occurrence of similar whirl structures in graphite films formed on the free surfaces of blowholes in iron castings. It appears that the metal mould/casting interface may act as a free surface for graphite formation. This may account for nucleation of graphite at the casting surfaces.

Graphite development at low temperatures in experiment 0 followed the pattern observed in the 1.00% Si alloy (Fig. 156). Graphite appeared to nucleate preferentially at casting edges, forming directional flakes which coarsened into aggregates. Isolated graphite colonies formed in the body

Expt	Mould Type	No	Mould Temp °C	Time to Quench mins	Temp at Quench °C	Eutectic Arrest °C	Initial Structure
M	2mm Cyl		1006	0.25	-		Mottled
N	"		1015	2.0	-		"
O	1mm Plate	1	-	1.0	-		White
		2	992	2.4	1002		
		3	994	5.0	999		
		4	986	10	-	1086-1085	
P	"	1	1040	1.9	-		Mottled
		2	1038	3.9	1027	1089	
		3	1040	6.9	1038	1113-1112	
		4	-	9.9	-		
Q	"	1	1048	0.8	-		"
		2	1049	3.0	-		
		3	1053	13	1050		
R	Cruciform	1	1060	0.5	-		"
		2	-	1.5	-		
		3	1059	6.0	-	1126-1120 (1mm)	
S	"	1	1065	0.5	-		"
		2	1065	1.5	-		
		3	1065	3.0	-		
		4	1066	6.0	-		
T	"	1	1069	0.5	-		"
		2	1072	1.5	-	1132-1128 (1mm)	
U	1mm Plate	1	1070	0.9	-		Grey (Fe <sub>3</sub> C needles)
		2	1063	2.1	-		
		3	1059	3.0	-		
		4	1059	10	-		
V	Cruciform	1	1084	0.5	-		Grey
		2	1083	1.5	-		
		3	1083	3.0	-		
		4	1083	6.0	1082		

TABLE II

2.43% Si Alloy

Metal Mould Casting Conditions



FIG.151. 2.43%Si. Expt M. x30.  
1/2min. M.T.1006°. Nital.  
Top portion of casting.

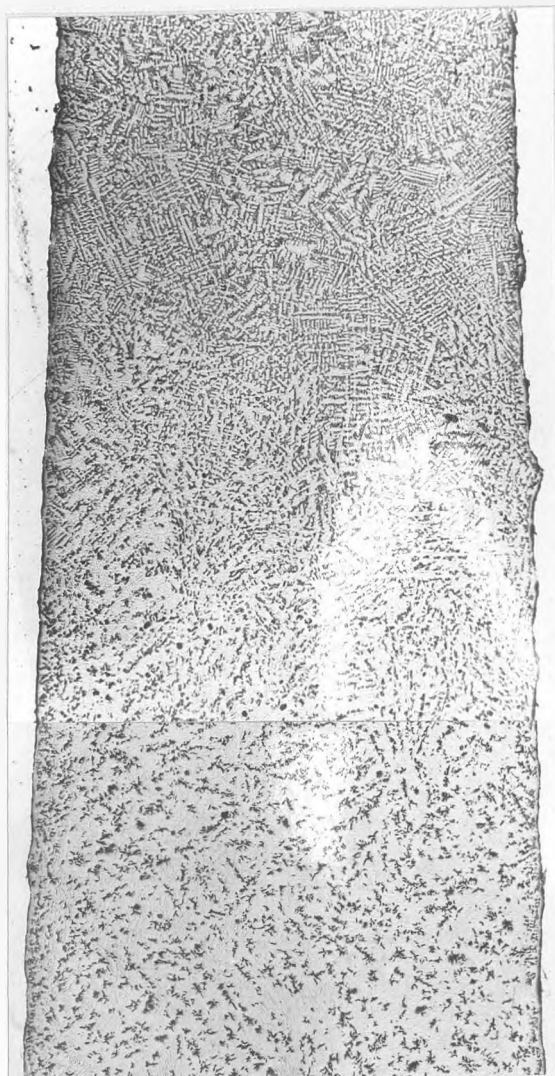


FIG.152. 2.43%Si. Expt N. x30.  
2mins. M.T.1015°. Nital.  
Top portion of casting.

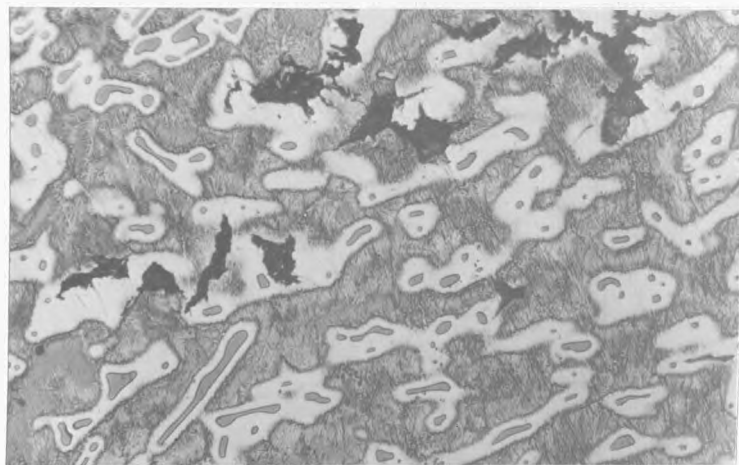


FIG.153. 2.43%Si. Experiment M. x1000.  
2mins. M.T.1015°. Alk.Na.Pic.  
Network structures.

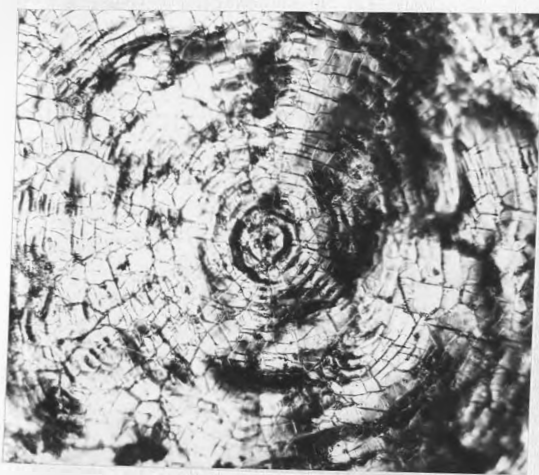


FIG.154. 2.43%Si. Expt B. x100.  
 W.T.1060°. Unetched.  
 Surface whirl structure.

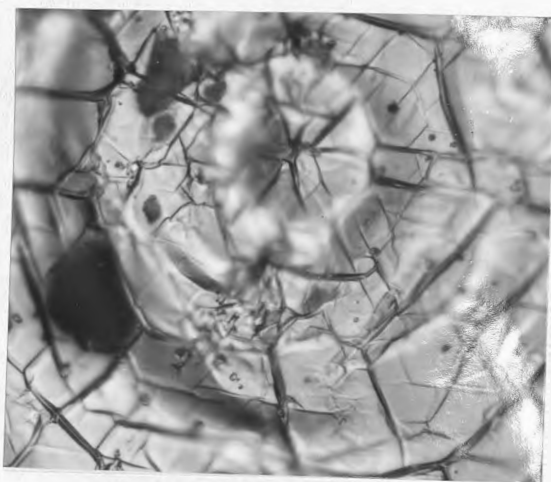


FIG.155. 2.43%Si. Expt B. x1000.  
 W.T.1060°. Unetched.  
 Detail of whirl structure.

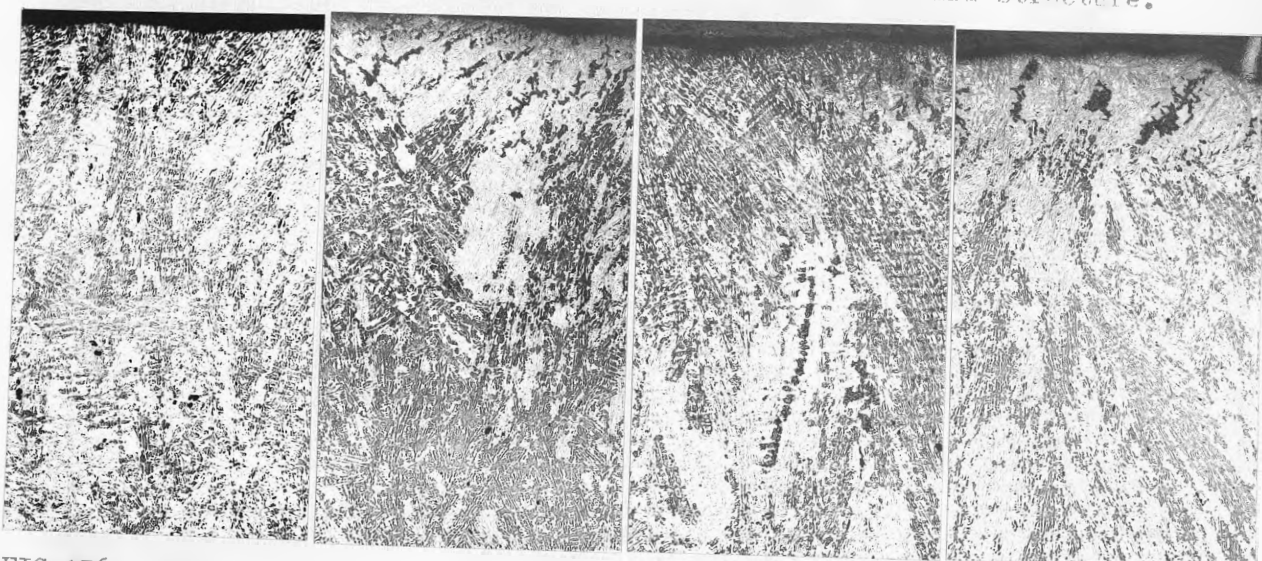


FIG.156. 1min. 2.4mins. 5mins. 10mins.  
 W.T.990°. W.T.992°. W.T.994°. W.T.986°.  
 2.43%Si. Experiment 0. Picral. General views. x80.

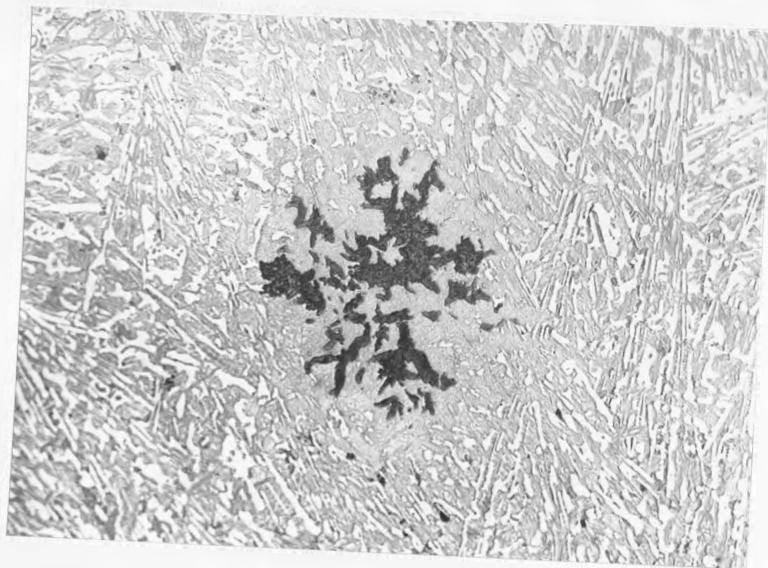


FIG.157. 2.43%Si. Experiment 0. x400.  
 5mins. W.T.994°. Picral.  
 Graphite cluster.

of the casting were sometimes associated with porosity, or were circular with loosely connected coarse flakes (Fig. 157).

Specimens in experiment P with moulds at  $1040^{\circ}\text{C}$  graphitised more rapidly (Fig. 158), being completely graphitic after 10 minutes. During this period, graphite changed from clusters of fine flakes to coarse polycrystalline aggregates (Fig. 159). Etching in alkaline sodium picrate revealed a gradual decrease in eutectic cementite, which was replaced by light coloured network structures on decomposition (Fig. 160). Eutectic cementite was almost completely absent in specimen 4 after 10 minutes at  $1040^{\circ}\text{C}$ . Signs of network structures and wasted cementite were visible in the mottled areas of the specimen quenched after 1.9 minutes (Fig. 161). The graphite occurred in the middle of the network structures which appeared out of focus in relation to the eutectic cementite. The graphite flakes outlined or penetrated regions previously occupied by eutectic cementite (Fig. 162). Fig. 163 shows a similar area in the specimen held at  $1040^{\circ}\text{C}$  for 7 minutes. Although cementite in this structure is largely decomposed, it appears to be preserved when in contact with graphite. The outlining graphite is fairly smooth and continuous, following cementite contours closely.

Fig. 164 shows mottled structures in castings from experiment Q, with the mould at  $1050^{\circ}\text{C}$ . Graphitisation is more rapid than with the mould at  $1040^{\circ}\text{C}$  (c.f. Fig. 158). Graphite formations in experiment Q were often centered on fine interdendritic graphite colonies (Fig. 165). The short curled flakes in these areas contain loops and are joined to more continuous graphite flakes which surround cementite areas. The eutectic cementite which was closely outlined by graphite showed some signs of wasting only 0.8 minutes after pouring (Fig. 166). The outlining role of graphite in the 0.8 minute specimen may be seen from the polished surface, and after etching in bromine (Fig. 167). The development of the outlining graphite after holding at  $1049^{\circ}\text{C}$  for 3 minutes is evident from Fig. 168. After more prolonged isothermal treatment, the outlining

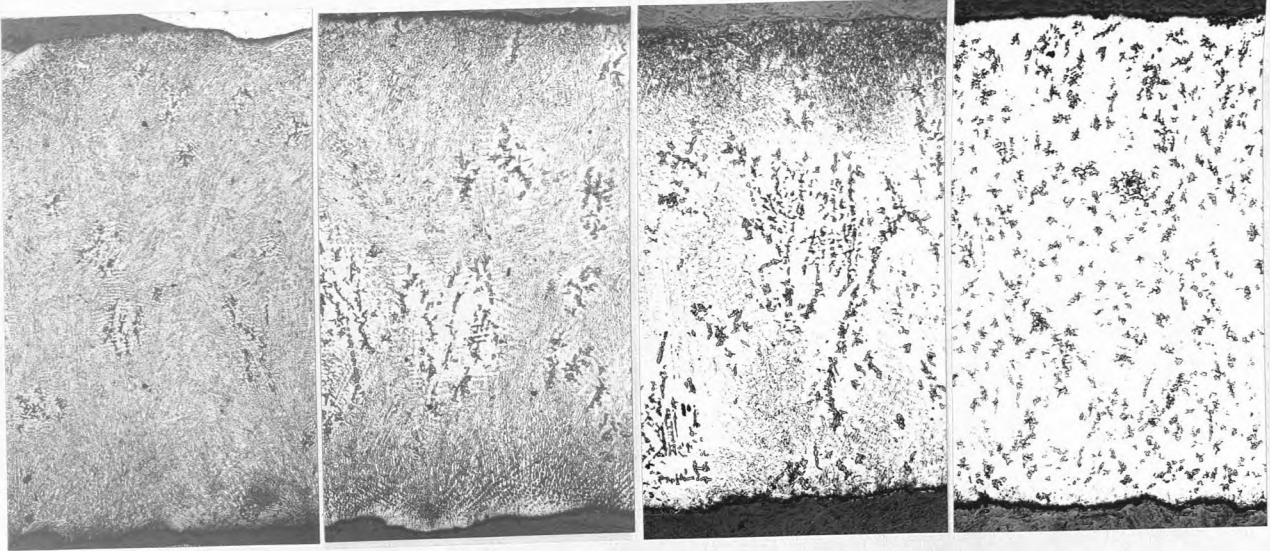


FIG.158. 1.9mins. 3.9mins. 6.9mins. 9.9mins.  
 M.T.1040° M.T.1038° M.T.1040° M.T.1040°  
 2.43%Si. Experiment P. Picral. General views. x60.

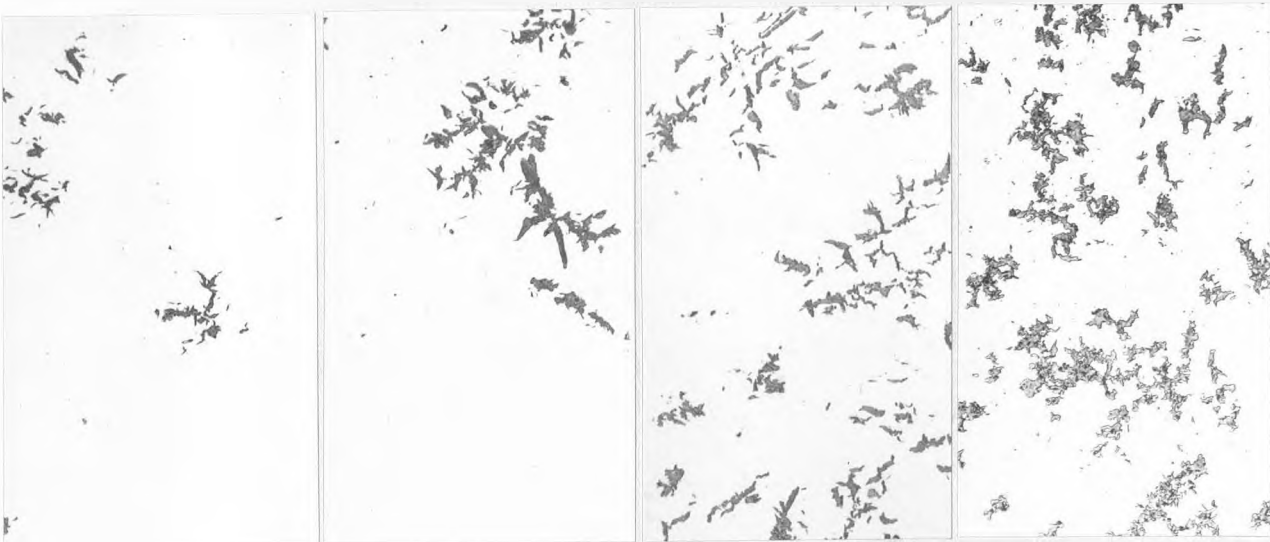


FIG.159. 1.9mins. 3.9mins. 6.9mins. 9.9mins.  
 M.T.1040° M.T.1038° M.T.1040° M.T.1040°  
 2.43%Si. Experiment P. Unetched. Graphite structure. x160.

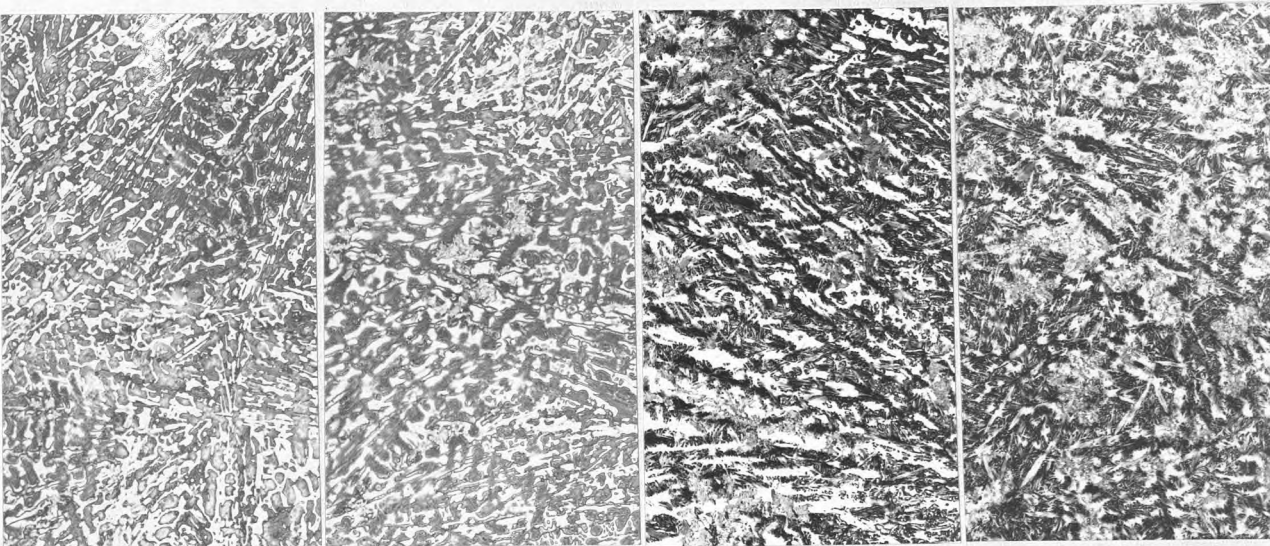


FIG.160. 1.9mins. 3.9mins. 6.9mins. 9.9mins.  
 M.T.1040° M.T.1038° M.T.1040° M.T.1038°  
 2.43%Si. Experiment P. Alk.Na.Pic. Network structures. x160.

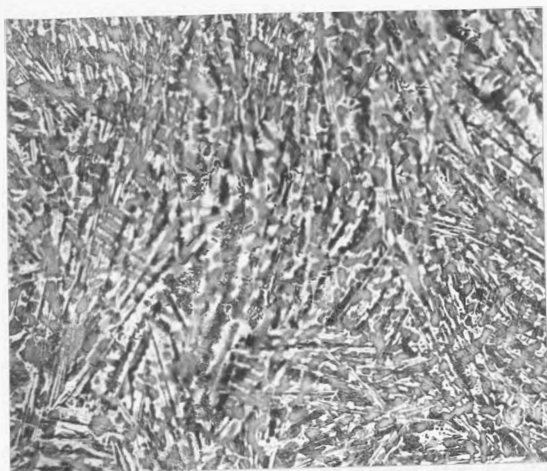


FIG.161. 2.43%Si. Expt.P. x160.  
1.9mins. W.T.1040°. A.Na.P.  
Network structures.



FIG.162. 2.43%Si. Expt.P. x1000.  
1.9mins. W.T.1040°. A.Na.P.  
Graphite & network structures.



FIG.163. 2.43%Si. Expt.P. x1000.  
6.9mins. W.T.1040°. Alk.Na.Pic.  
Outlining graphite.

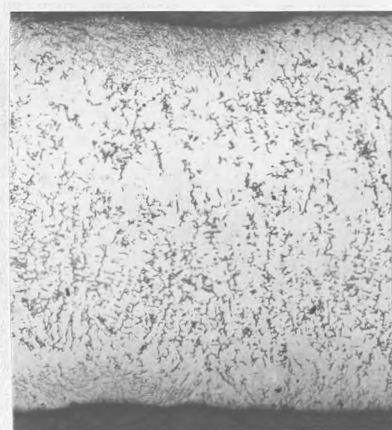
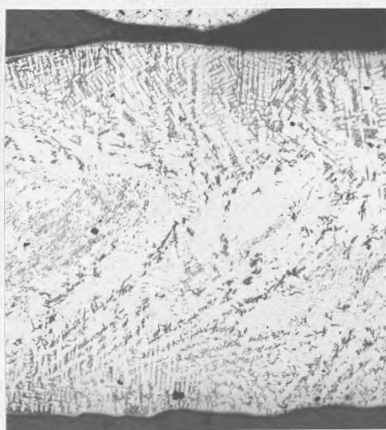
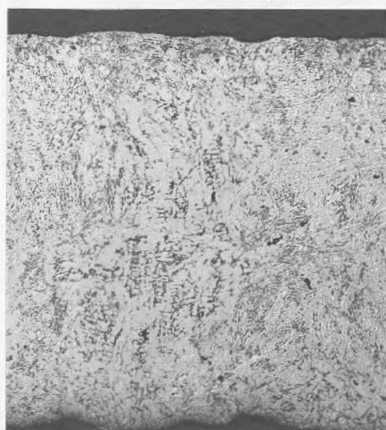


FIG.164. 0.8mins. 3mins. 13mins.  
W.T.1048°. W.T.1049°. W.T.1053°. x40.  
2.43%Si. Experiment Q. Picral. General views.

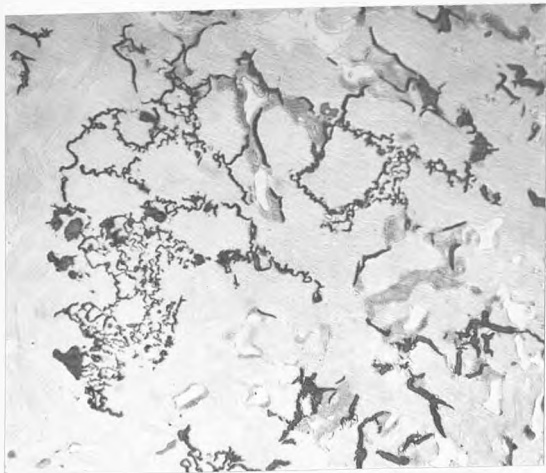


FIG.165. 2.43%Si. Expt Q. x400.  
0.8mins.M.T.1048°. Picral.  
Fine & outlining graphite.



FIG.166. 2.43%Si. Expt Q. x1000.  
0.8mins.M.T.1048°. Picral.  
Outlining graphite.



FIG.167. Unetched. Br<sub>2</sub>. x160.  
2.43%Si. Experiment Q. 0.8mins.M.T.1048°. Graphite/mottle structures.

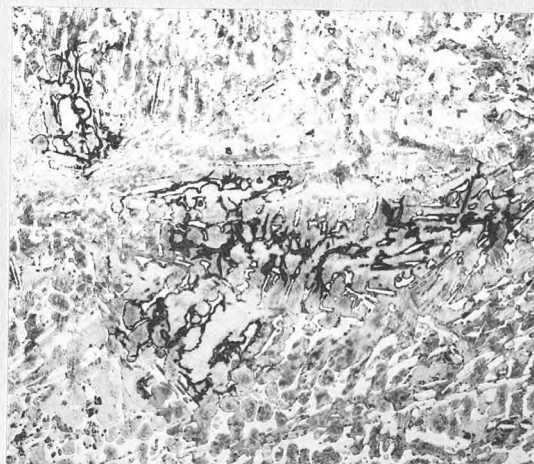
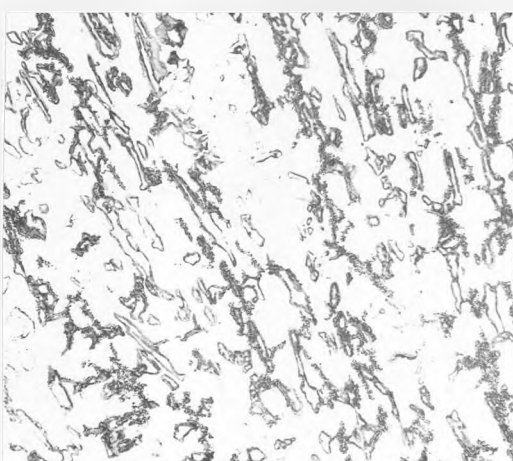


FIG.168. Unetched. Br<sub>2</sub>. x160.  
2.43%Si. Experiment Q. 3mins. M.T.1049°. Graphite/mottle structures.



graphite forms became coarser and more irregular (Fig. 168a). A scanning electron microscope view of an aggregate area (Fig. 169) shows the graphite to be in the form of an interconnected polycrystalline mass, with hexagonal surface markings and sub-units. This may be contrasted with the fine colony graphite (Fig. 170). Very fine graphite was visible at specimen edges, usually outlining cementite laths (Fig. 171). This layer was retained on isothermal treatment (Fig. 172), giving way to coarser graphite toward the specimen centre.

Cruciform mould experiment R produced undercooled graphite colonies in the 2 mm. section, with coarse flakes at the borders. Fig. 173 shows the close association of stable and metastable eutectics at the colony borders in the specimen quenched 30 seconds after pouring. The corresponding network outline is developed in Fig. 174, revealing considerable cementite decomposition in a very short time. Graphite borders tended to be compacted in such areas. Specimens quenched after longer furnace holding had correspondingly more decomposed eutectic cementite (Fig. 175). Graphite outlining such areas was smoother and more continuous than that of the undercooled eutectic.

The increased mould temperature of experiment S (1065°C) produced inhomogeneous castings. Solidification was incomplete in the 1.5 mm. section on quenching after 30 seconds, resulting in the production of fine quenched chill structures in the spaces between rounded stable undercooled eutectic colonies (Fig. 176). At greater magnification the quench structure was easily distinguishable from the metastable eutectic which occurred near the ends of the specimen arms (Fig. 177). The junction between stable and metastable eutectics was marked by fans of short cementite laths which projected into the undercooled areas (Fig. 178). On isothermal treatment the metastable eutectic gave way to network structures and continuous graphite similar to that in specimen R (Fig. 175).

2 mm. mould sections in specimen T solidified as the stable eutectic. 1 mm. sections quenched after 30 seconds contained degenerate metastable

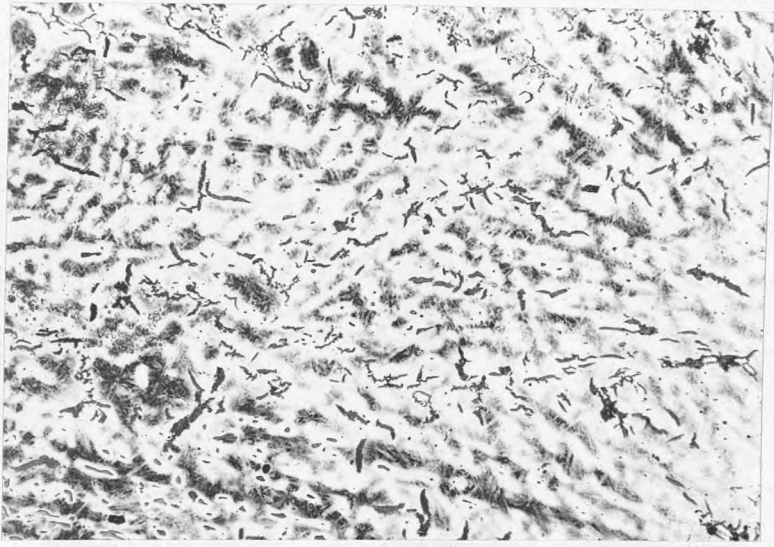


FIG.168a. 2.43%Si. Expt Q. x160.  
13mins. M.T.1053°. Alk.Na.Pic.  
Graphite/network structures.

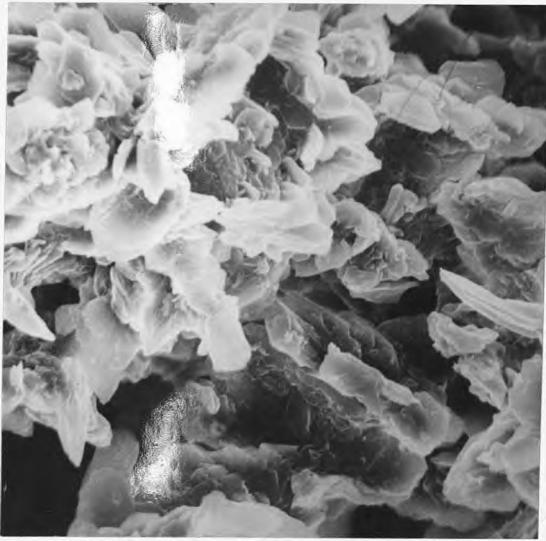


FIG.169. 2.43%Si. Expt Q. Stereo. x1080.  
13mins. M.T.1053°. Br<sub>2</sub>.  
Graphite aggregate.

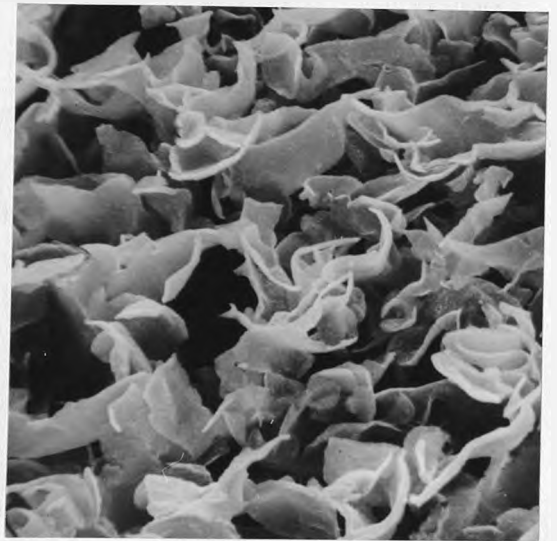


FIG.170. 2.43%Si. Expt Q. Stereo. x1100.  
13mins. M.T.1053°. Br<sub>2</sub>.  
Undercooled graphite.

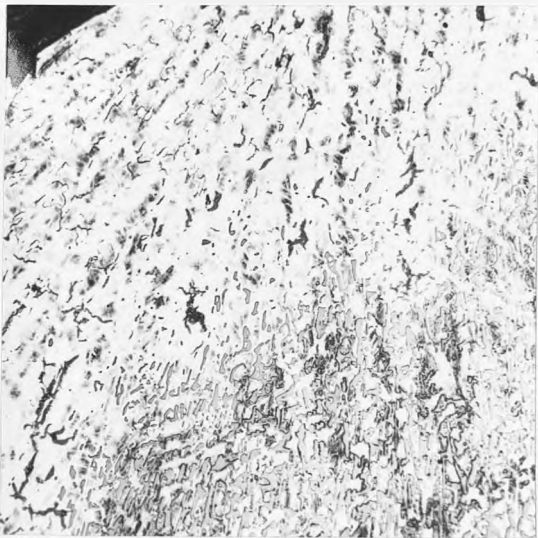


FIG.171. 2.43%Si. Expt Q. x160.  
3mins. M.T.1049°. A.Na.Pic.  
Edge graphite.

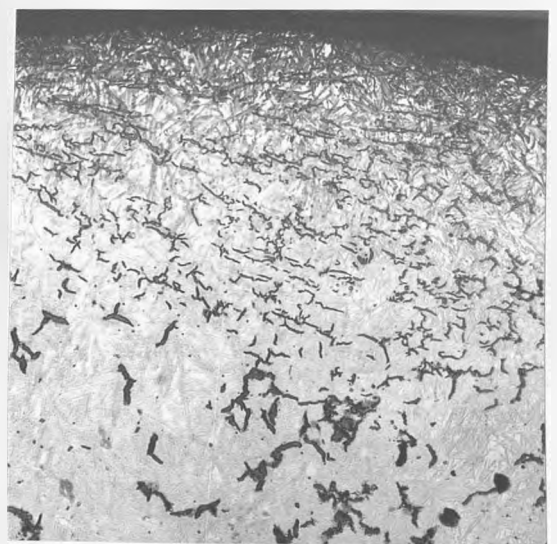


FIG.172. 2.43%Si. Expt Q. x160.  
13mins. M.T.1053°. Picral.  
Edge graphite.

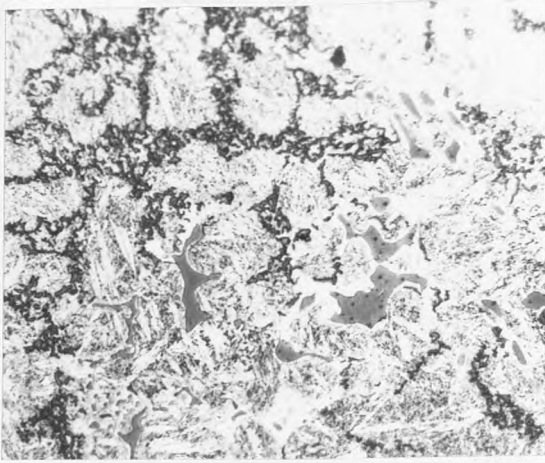


FIG.173. 2.43%Si. Expt R. 2mm.  
0.5mins. M.T.1060°.  
Alk.Na.Pic./Nital. x400.  
Graphite colony periphery.

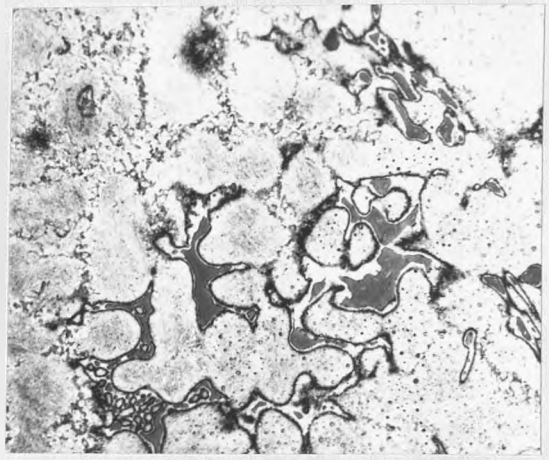


FIG.174. 2.43%Si. Expt R. 2mm.  
0.5mins. M.T.1060°.  
Alk.Na.Pic. x400.  
Network structure corresponding to  
Fig.173.



FIG.175. 2.43%Si. Expt R. 1.5mm.  
1.5mins. M.T.1060°.  
Alk.Na.Pic./Nital. x400.  
Network structures.

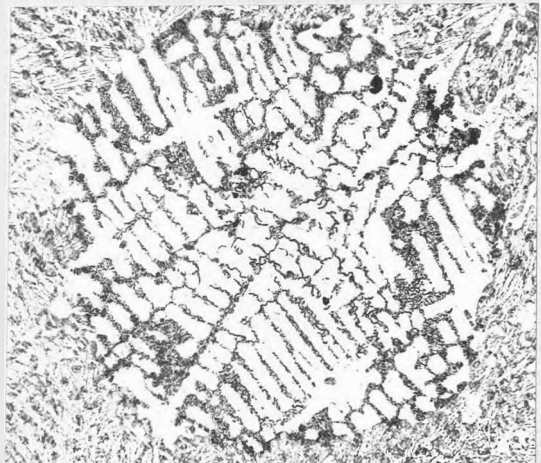


FIG.176. 2.43%Si. Expt S. 2mm.  
0.5mins. M.T.1060°.  
Nital. x100.  
Quenched structure.

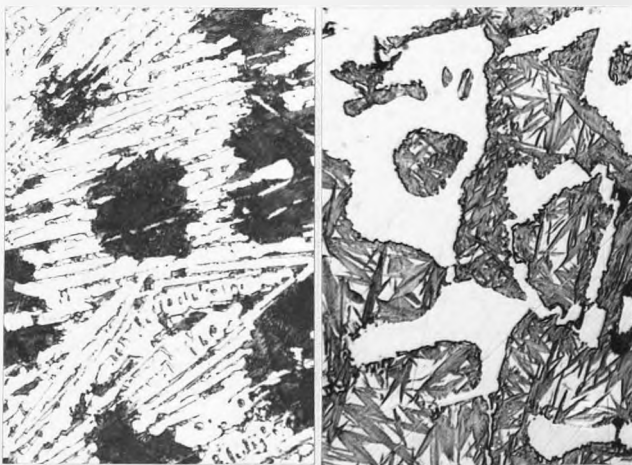


FIG.177. Post-quench. Pre-quench. x1000.  
2.43%Si. Expt S. 2mm. 1min.M.T.1069°.  
Nital. Metastable Eutectic.

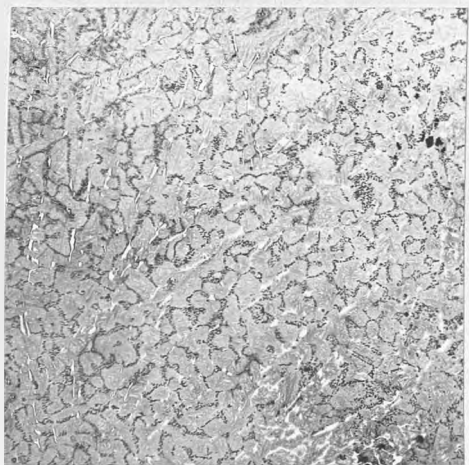


FIG.178. 2.43%Si. Expt S.  
2mm. 1min.M.T.1069°.  
Picral. x80.  
Cementite fans.

eutectic with closely associated fine graphite flakes (Fig. 179/1); The corresponding specimen quenched after 1.5 minutes had a network structure similar to the original eutectic cementite distribution, with more developed fine graphite (Fig. 179/2).

The fan-like cementite lath structures noted in the inhomogeneous zone of experiment S were more regular in the 1 mm. plate castings of experiment U. Figs. 180-183 show the progressive decomposition of cementite laths with isothermal treatment. Even after complete cementite decomposition, the original lath pattern and direction may be seen from the gaps in the undercooled eutectic. This 'piercing' effect is similar to that noted in ceramic mould and chill/sand castings (c.f. Fig. 108). Graphite in the region of laths tended to be more continuous, following the cementite outlines (Fig. 184).

All specimens in the cruciform castings of experiment V with moulds at 1083°C solidified with grey eutectic microstructures.

Mottle structures in the 2.43% Si alloy could be produced over a wide temperature range in the metal moulds. Raising mould temperatures changed the mottle from aggregate graphite formations (experiment O) to less compacted and more closely intermixed structures (experiment P). At higher mould temperatures, rounded undercooled graphite colonies appeared (experiments Q, R, S, T, & U). The larger colonies contained no network structures, but coarsened at the peripheries and were continuous with streamer graphite. The last type of mottle encountered before completely stable solidification took the form of aligned cementite lath clusters which pierced the undercooled eutectic (experiment V).

Decomposition kinetics were slowest in the low temperature regions, but accelerated at higher temperatures, producing progressively finer graphite as the temperature was raised. Graphite colony borders were associated with wasted cementite and network structures in all specimens.

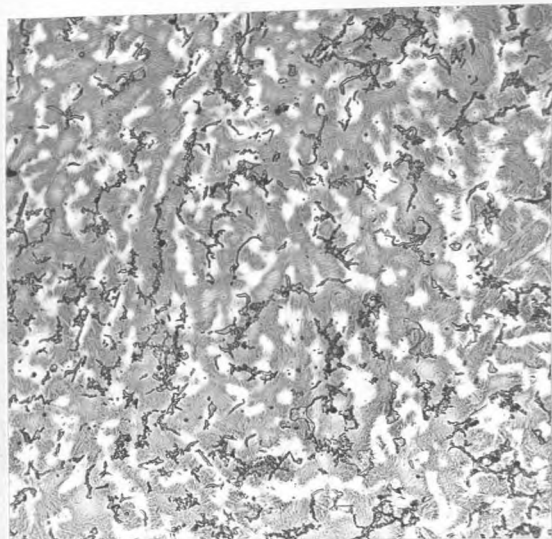


FIG.179. 0.5mins. M.T.1069°. 1.5mins. M.T.1072°. 2.43%Si. Experiment T. 1mm. Alk.Na.Pic. x160. Progress of cementite decomposition.

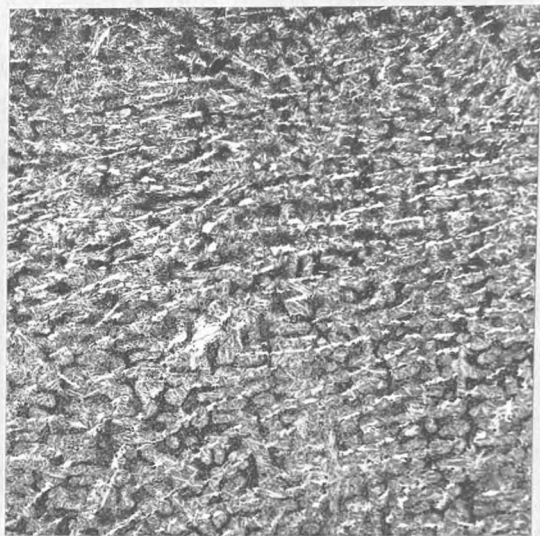
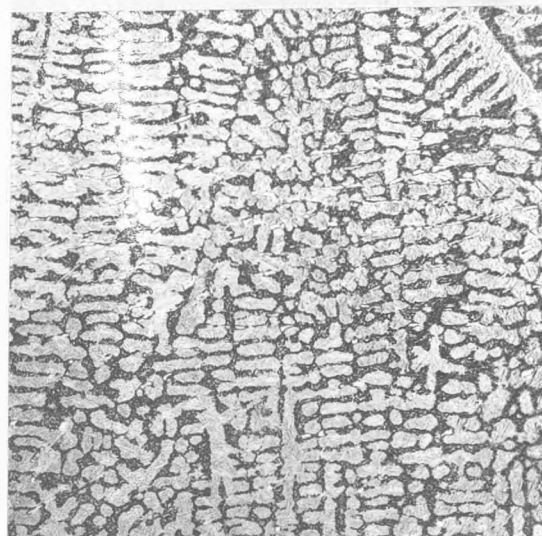
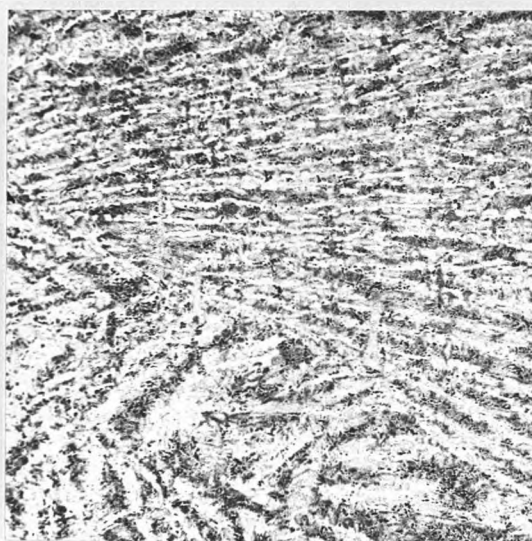
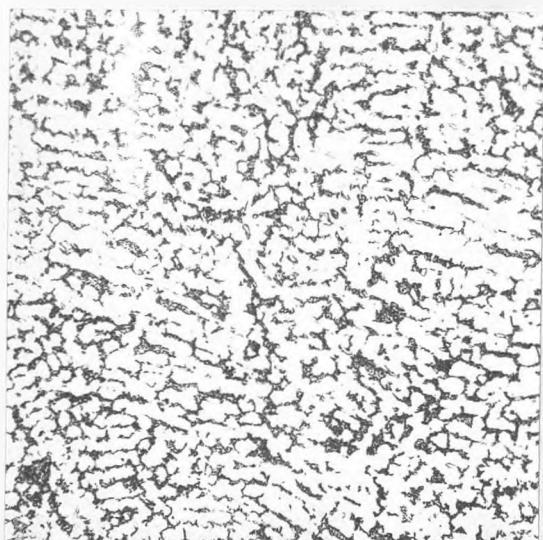


FIG.180. Nital. Alk.Na.Pic. 2.43%Si. Experiment U. 0.9mins. M.T.1070°. x80. Cementite needle structure.



FIG,181. Nital. Alk.Na.Pic. 2.43%Si. Experiment U. 2.1mins. M.T.1063°. x80. Cementite needle structure.

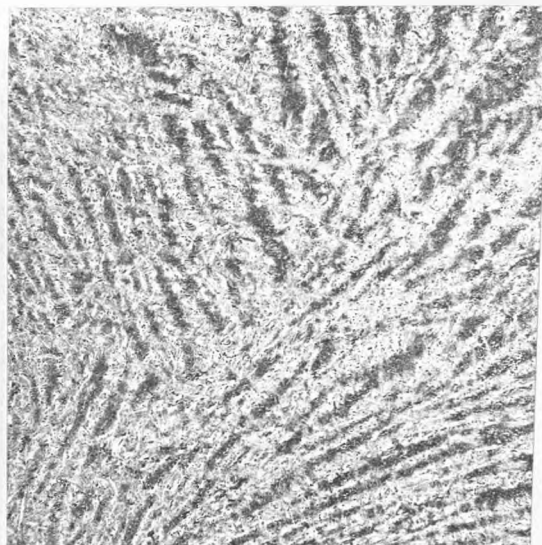


FIG.182. Nital. Alk.Na.Pic.  
2.43%Si. Experiment U. 3mins. N.T.1060°. x80.  
Cementite needle structure.

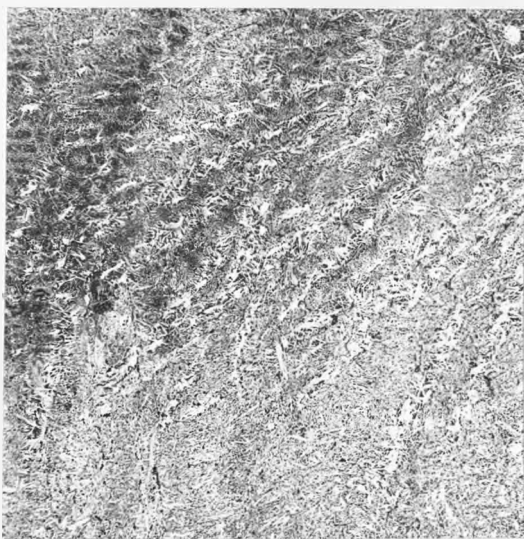
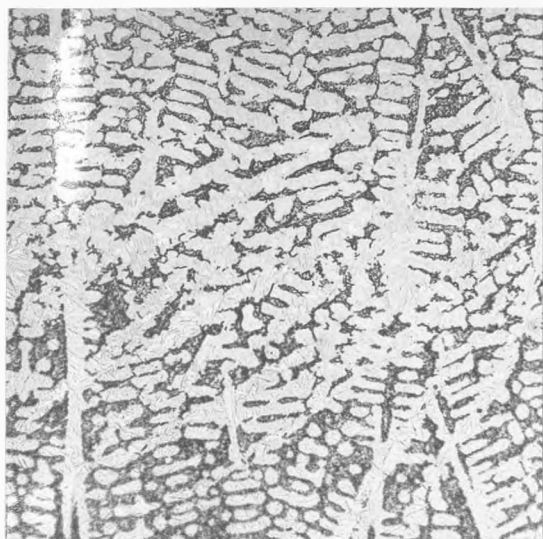


FIG.183. Nital. Alk.Na.Pic.  
2.43%Si. Experiment U. 10mins. N.T.1060°. x80.  
Cementite needle structure.

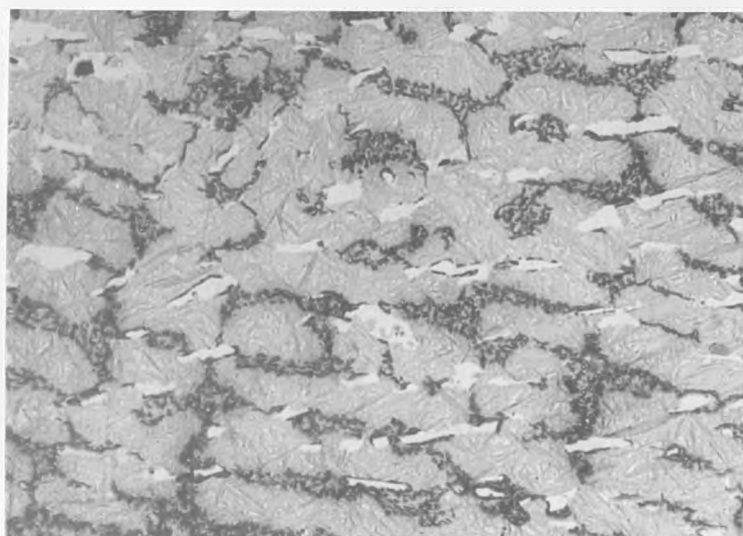


FIG.184. 2.43%Si. Experiment U. x400.  
0.9mins. N.T.1070°. Nital.  
Cementite needles.

#### 4.5 CHILL CASTING EXPERIMENTS

Chill casting experiments were designed to provide more detailed information on structures common to the chill zones of both ceramic mould and chill/sand castings. As the range of chill zone structures was found to be common to all three alloys in the initial experiments, the 2.04% silicon alloy was selected for detailed study.

##### 4.5.1 PHYSICAL CONDITIONS

Cooling rates in chill moulds are dependent on a number of physical factors, including volume/surface ratio of the casting; thermal conductivities of the metal and mould; degree of metal/mould contact; metal superheat and mould temperature. In the present experiments, extreme cooling rates were achieved in the 1 mm. thick flash sections of the chill castings. The 1 cm. diameter cylindrical chill mould sections were subject to lower cooling rates due to their greater volume/surface ratio. Each casting exhibited a range of structures reflecting the change in solidification conditions from the flash surfaces to the slower cooling rates at the centre of the cylindrical sections. This structural range was closely paralleled in the chill zones of the previous experiments.

For constant casting conditions, heat transfer from casting to chill is dependent on the degree of metal/chill contact. Examination of chill specimen surfaces suggested that even in a polished mould the contact is incomplete. Areas on the flash surface coherent with the chill surface, at least during the initial stages of solidification, were surrounded by coarse borders whose structures suggested formation at a lower cooling rate. The degree of contact was not controlled in these experiments, but overall contact areas were approximately equal for castings poured at different superheats.

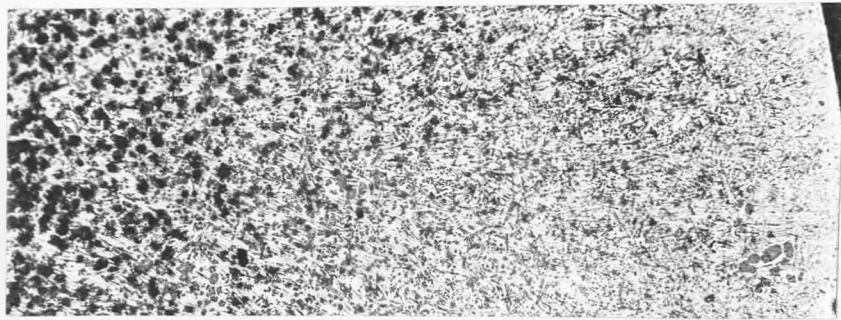
The effect of metal superheat in chill castings was studied in view of its widely known influence on cast iron structure. The wide structural differences which were noted in the present series will be reported and discussed in later sections.

No differences were detected between the surfaces or internal structures of castings poured at  $1400^{\circ}\text{C}$  into chill moulds at room temperature or cooled in liquid nitrogen. All experiments with alloying additions were carried out with room temperature chill moulds, using a  $1400^{\circ}\text{C}$  pouring temperature.

The main difference between the static chill mould and the water-cooled chill of the heated mould series, is that heat extraction by a circulation chill does not diminish with time after casting as it does in the static case. The chilling power of a circulation chill is therefore more sustained than that of a static chill with similar surface and contact area. In the present series of experiments, the small chill castings caused only slight heating of the massive copper mould, and the chilling effect was unlikely to be impaired during the very short solidification period of the samples used.

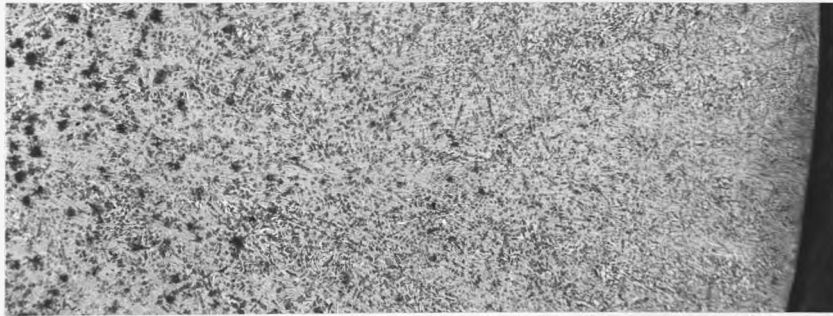
#### 4.5.2 MACROSTRUCTURES

Fig. 185 shows the effect of variations in pouring temperature on the macrostructures of cylindrical chill casting sections. At  $1160^{\circ}\text{C}$  the austenite dendrite structure is coarse and randomly oriented. The presence of very large austenite sections in the lower right hand corner of the photograph may indicate incomplete melting at the pouring temperature. Graphite eutectic colonies, visible as dark round areas are numerous, becoming smaller as the chill surface is approached. Cementite is present as fan-shaped bunches of needles between the austenite dendrites. As the pouring temperature increases to  $1200^{\circ}\text{C}$ , austenite and cementite formations change little, while graphite colonies decrease both in number and size. At  $1300^{\circ}\text{C}$  austenite dendrite form is radically altered, being greatly elongated and more directional. Graphite colonies are visible only on a microscopic scale. As cementite is limited to the interdendritic spaces the fan structure is lost, although needles are still present. Castings at  $1400^{\circ}\text{C}$  and  $1600^{\circ}\text{C}$  are similar to that at  $1300^{\circ}\text{C}$ , with some austenite dendrites passing from at or near the chill to the casting centre.

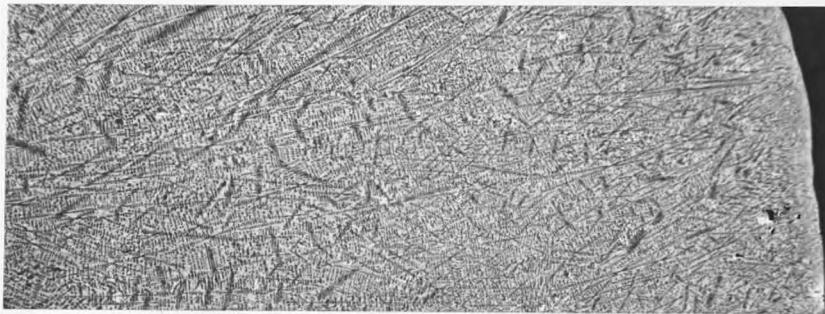


Pouring Temp °C

1160



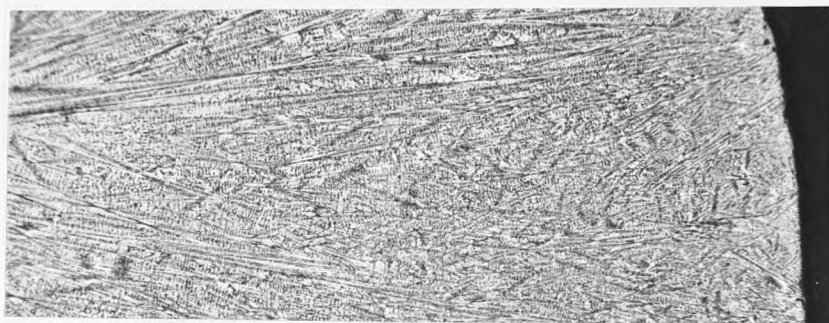
1200



1300



1400



1600

FIG.185. 2.04%Si. Chill Casting Macrostructures.

x25.

#### 4.5.3 MICROSTRUCTURES

The chill casting experiments complement the ceramic and chill/sand casting results by forming an expansion and extension of the non-equilibrium solidification range. Chill structures will be considered as a continuous series from the chill flash surfaces to the normal ledeburite regions at the top of the clear chill zones in ceramic and chill/sand samples.

The use of a chill mould with flat surfaces enabled study of structures at the metal/chill surface, where the conditions of non-equilibrium are greatest. Initial experiments with an unpolished as-machined chill mould produced flash surfaces composed of rectangular arrays of spherulites which appeared star-shaped under polarised light (Fig. 186). At higher magnification (Fig. 187), the spherulites were seen to be centred on irregularities caused during machining of the mould, which accounts for the regularity of the structure.

Polishing the chill mould removed the preferred nucleation sites and produced a more random nucleation distribution (Fig. 188). Spherulites varied widely in size and distribution within each specimen, finest structures being present at the edges of the flash. Casting at temperatures from 1160-1600°C did not appear to affect spherulite formation or distribution, and the flash structures shown are representative of the whole pouring temperature range.

The colour variation between spherulite centres and peripheries in Fig. 188 appeared to indicate a difference in phase or composition with distance from the nucleation site. Spherulite centres were more resistant to discolouration on heat tinting than the peripheral areas. Etching for two hours in 5% picric acid (Fig. 189) appeared to increase visible detail in the central regions, possibly indicating removal of a surface layer. Other parts of the microstructure were heavily attacked. Stereoscan examination of a similar deep etched surface revealed further spherulite detail (Fig. 190). Spherulites appear to grow from a central source, developing radiating arms and cross links which form a web structure. The web centres appear darker than the edges when viewed by

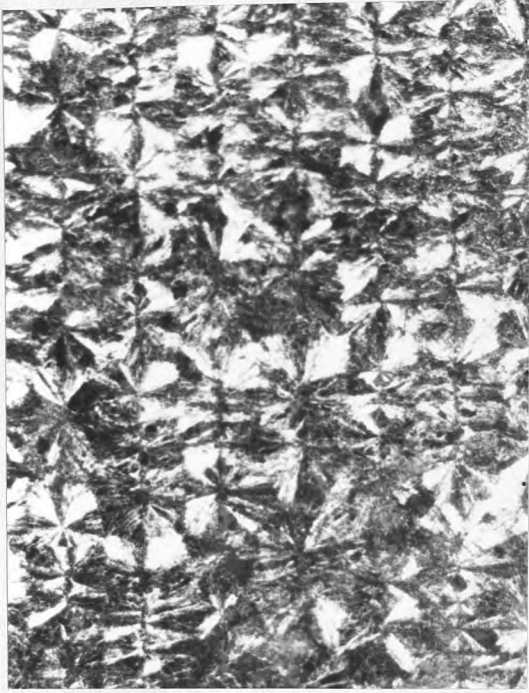


FIG.186. 2.04%Si. Chill Casting.  
Unetched. Xpolar. x160.  
Chill surface, unpolished mould.



FIG.187. 2.04%Si. Chill Casting.  
Unetched. Xpolar. x400.  
As Fig.186. Spherulite centres.

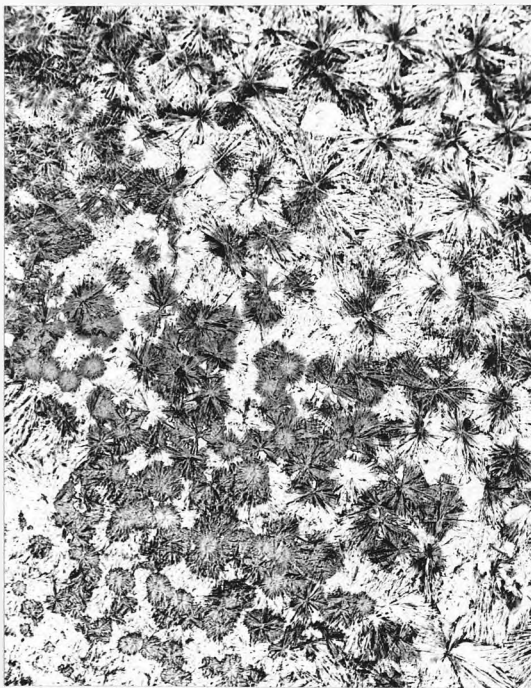


FIG.188. 2.04%Si. Chill Casting.  
Unetched. x160.  
Chill surface, polished mould.

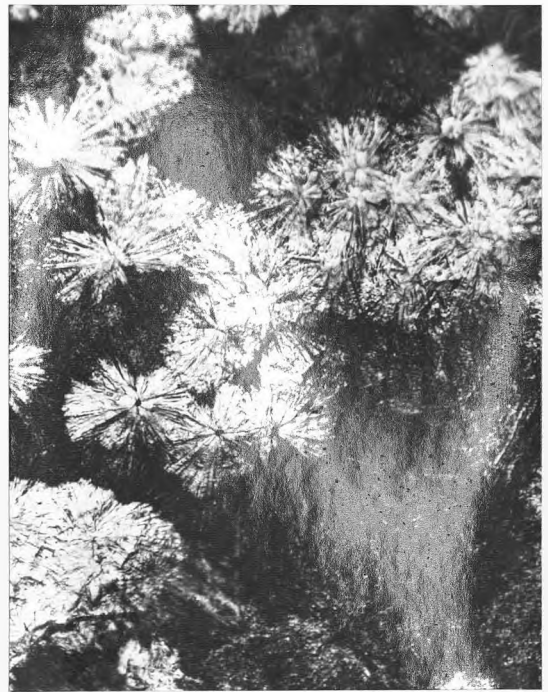


FIG.189. 2.04%Si. Chill Casting.  
Picral. x400.  
Chill surface, polished mould.

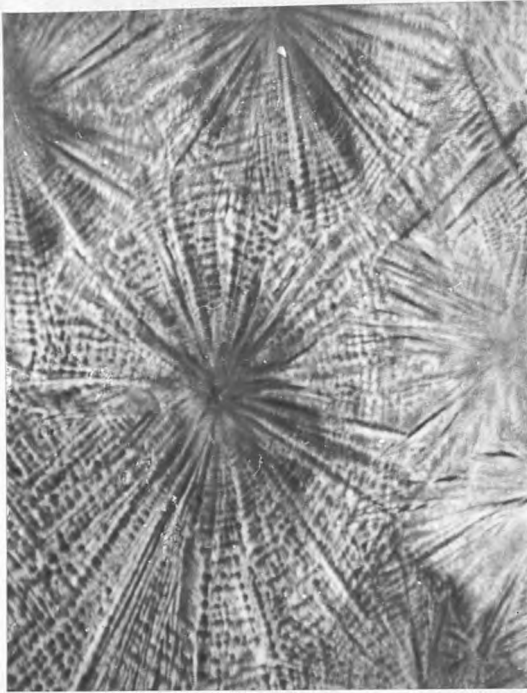


FIG.190. 2.04%Si. Chill Casting.  
Picral. Stereo @45° .x720.  
Surface spherulites.



FIG.191. 2.04%Si. Chill Casting.  
Picral. x1500.  
Spherulite centre.

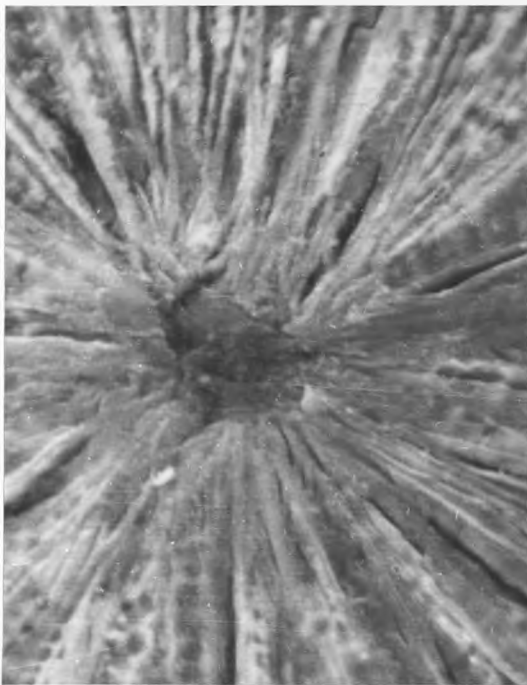


FIG.192. 2.04%Si. Chill Casting.  
Picral. Stereo @45° .x2850.  
Spherulite centre.

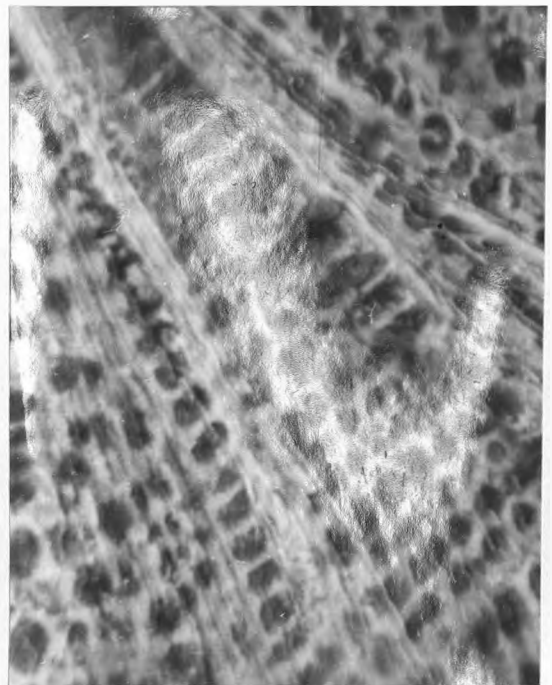


FIG.193. 2.04%Si. Chill Casting.  
Picral. Stereo @45° .x2850.  
Radial structure.

reflected electrons. This colour change is due to increased electron absorption at the centres, and suggests greater concentration of low atomic number elements near the nucleation sites.

An examination of Figs. 189 and 190 shows that etching produces pits at the centres of certain spherulites. Optical examination (Fig. 191) revealed a fine unresolved central structure. This is not apparent in Fig. 192 which is an equivalent view by stereoscan. In both cases, the region around the nucleation site is more coherent than other areas of the web structure, and appears to represent a fusion of the radiating arms.

Fig. 193 is a stereoscan view of a deep etched portion of the unpolished chill face, near a spherulite edge. The two radiating arms included in the picture are composed of very fine unbroken aligned needles. Circular areas of transformed austenite occur as regular arrays between radiating arms, forming the cross links of the web structure.

Polishing and etching the chill flash surface revealed the structure just below the nucleating surface. Figs. 194 and 195 show a spherulite under normal and polarised light. The acicular eutectic structure at the spherulite edges gives way to a more regular honeycombe structure at the centre. At low magnification the regular structure resembles normal ledeburite. The higher magnification view in Fig. 196 shows fan-shaped clusters of cementite laths around areas of transformed austenite. Apart from the cementite discontinuities, the overall resemblance to normal ledeburite is maintained. Austenite transformation products were removed from the chill area of Fig. 196 by etching in hot 5% picric acid for four hours. Stereoscan examination of the remaining cementite (Fig. 197) confirmed its plate-like form. Cementite plates in Figs. 193 and 197 have numerous interconnections, but the extent of single cementite crystals was not determined.

Sectioning perpendicular to the chill face enabled study of the progress of

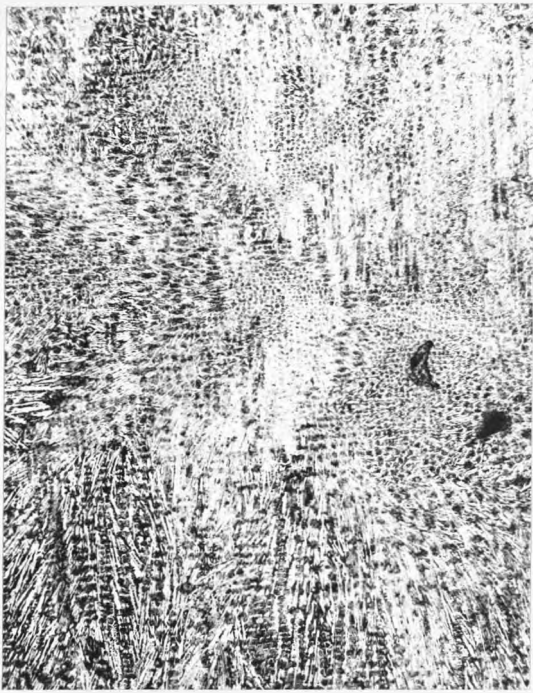


FIG.194. 2.04%Si. Chill Casting.  
Picral. x160.  
Polished surface, spherulite.

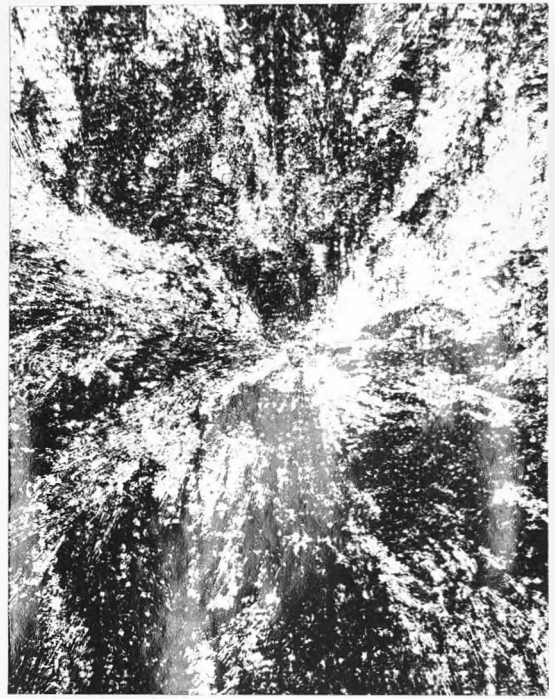


FIG.195. as 194, X polars.

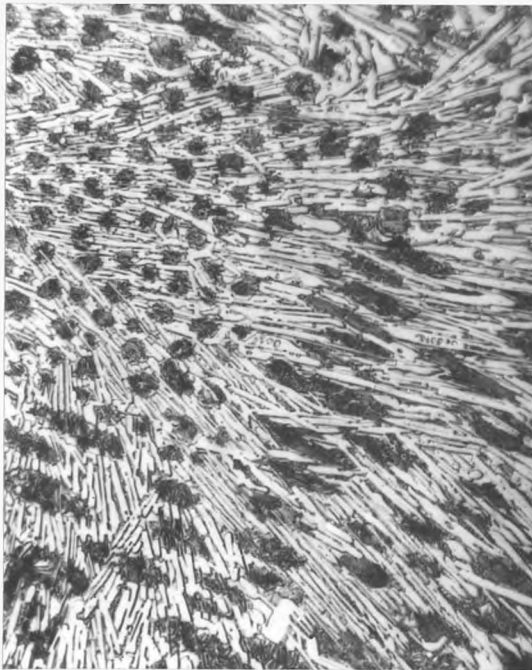


FIG.196. 2.04%Si. Chill Casting.  
Picral. x1000.  
Central detail.

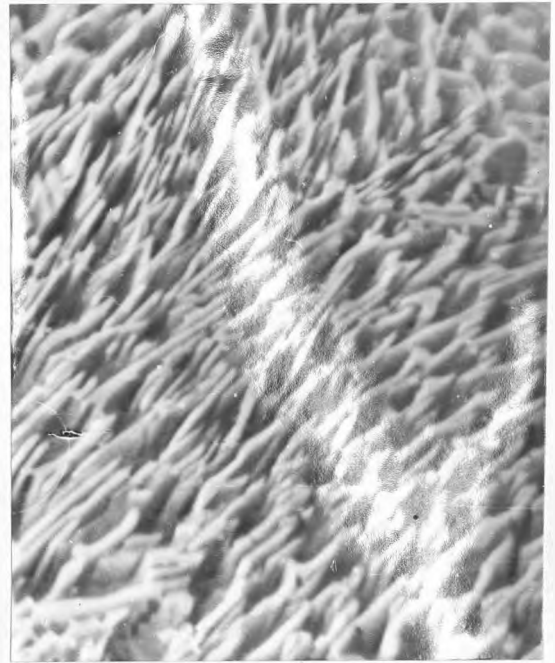
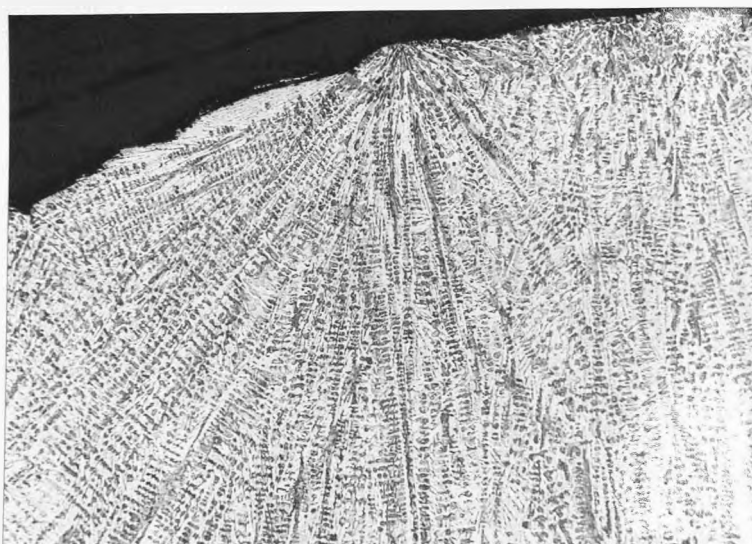


FIG.197. 2.04%Si. Chill Casting. x1720.  
Alk.Na.Pic. Stereo @ 45°.   
Central detail after  
deep etching.

solidification from the surface towards the mould centre. A perpendicular section (Fig. 198) suggests that radiating growth from the nucleating centre is three dimensional and would produce hemispheres in the absence of interference from other growth centres. Radiating growth towards the casting centre was made up of long austenite dendrites, as opposed to the surface structures which appeared to have cementite radiating arms.

The surface structures on either side of the nucleating centre in Fig. 198 represent the two types of surface layers found in chill specimens. On the left of the nucleus is a layer of close packed aligned cementite laths, while the right hand structure is continuous with the matrix. It appears that on the left the section passes through one of the radiating spherulite arms, while the structure to the right is similar to that linking the arms. Closer examination of sections through radiating arms (Fig. 199) revealed two distinct growth forms. The region nearest the chill nucleated at a cementite layer forming the chilled surface. Growth inwards was led by large cementite plates characteristic of hypereutectic alloys. Areas between the 'pro-eutectic' plates are filled by lamellar or degenerate eutectic. Underneath this surface layer, the structure is similar to hypoeutectic acicular white irons and is characteristic of the areas between radiating arms. 'Hypereutectic' surface layers varied widely in thickness, possibly as a result of sectioning effects, and sometimes contained deformed cementite plates as shown in Fig. 200.

Austenite dendrites originating at the chill often continued for long distances into the casting (Figs. 185 & 198). Initially the interstices of the austenite dendrites were filled by acicular eutectic with small quantities of degenerate ledeburite. As distance from the chill increased, the amount of degenerate eutectic rose. Further from the chill in the ceramic and chill/sand mould specimens, eutectic form changed from degenerate to normal. All morphology changes were gradual, mixtures of the various forms occurring in intermediate regions. All types of white eutectic are characterised by cementite form and distribution. Stereoscan examination of deeply etched surfaces may be used in



**FIG.198.** 2.04%Si. Chill Casting.  
Picral. x160.  
Section perpendicular to chill face.

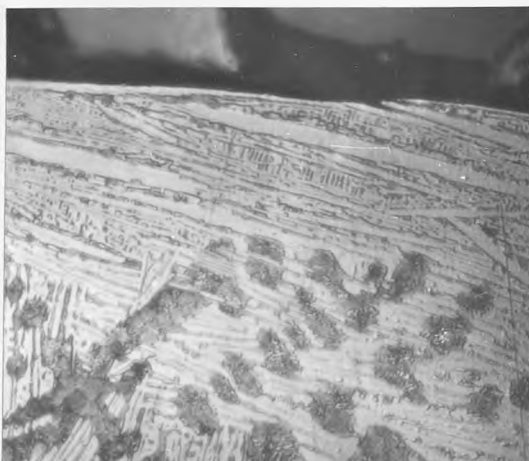


**FIG.199.** 2.04%Si. Chill Casting.  
Picral. x1000.  
Surface detail.



**FIG.200.** 2.04%Si. Chill Casting.  
Picral. x1000.  
Surface detail.

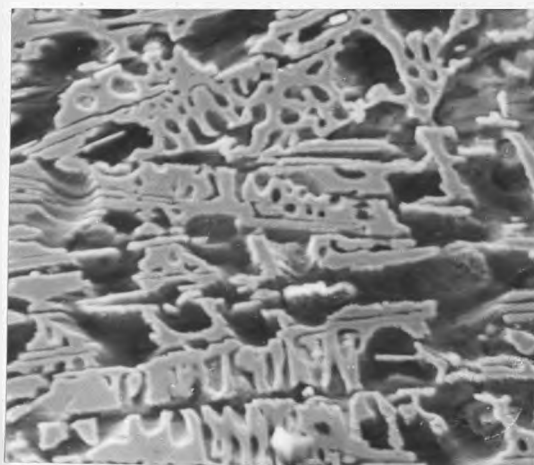


**FIG.201.** 2.04%Si. Chill Casting.  
Picral. Stereo @45°.x760.  
Degenerate/normal ledeburite.

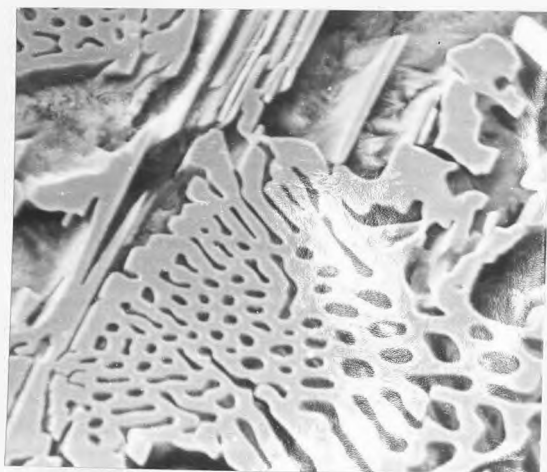


**FIG.202.** 2.04%Si. Chill Casting.  
Picral. Stereo @45°.x710.  
Normal ledeburite.

structural classification. Fig. 201 shows an area where normal and degenerate ledeburite are mixed with eutectic needles. The normal ledeburite of Fig. 202 has intercolony areas corresponding to austenite dendrite sections. Cementite needles, often occurring in clusters appear to pierce the dendrite arms. Stereo-scan examination shows that the needles are in fact laths connected to the eutectic cementite.

#### 4.5.4 ALLOYING EFFECTS IN CHILL CASTINGS

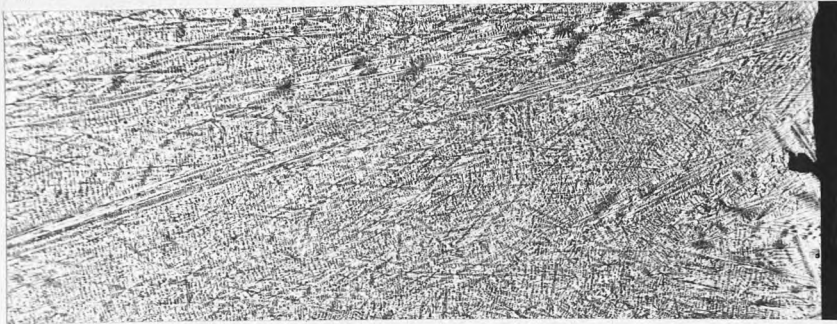
##### 4.5.4.1 MACROSTRUCTURES

Macrostructures of the alloyed chill castings poured at 1400°C are shown in Fig. 203, an unalloyed 2.04% silicon sample being included for comparison. A feature of the series is the gain in regularity brought about by magnesium additions. Competitive growth from the chill face towards the centre is clearly shown, and complex patterns caused by sectioning aligned austenite dendrites are well developed in these specimens. Regularity is not so marked in the tellurium alloyed sample, while the specimen with aluminium additions is less regular than the base alloy. Increases in directionality suggests a parallel with base alloy castings at temperatures greater than 1400°C.

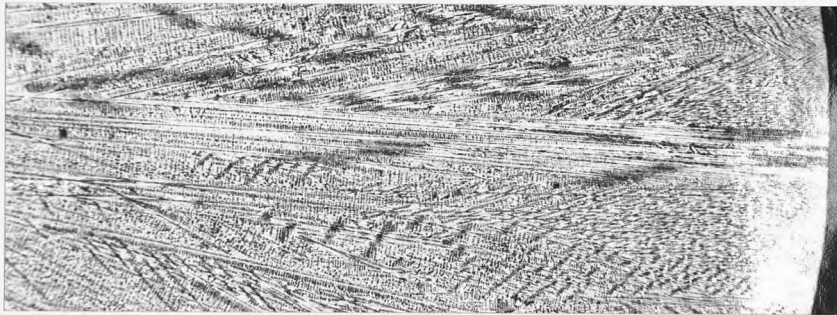
Graphite colonies are just visible in the magnesium bearing casting, while those in the sample with aluminium additions are present to about the extent of the base alloy casting at 1200°C.

##### 4.5.4.2 MICROSTRUCTURES

Flash surfaces in samples with magnesium and chromium additions were similar to those of the base alloy, exhibiting the same spherulite distributions with similar reactions to etching and heat tinting. Aluminium additions gave surface areas with multiple nuclei (Fig. 204); the other surface features being the same as base alloy samples. Alloying with tellurium produced more widespread surface changes, giving large areas where the normal spherulite arrays were deformed into ridges in regular curving patterns (Fig. 205). These ridges were also developed in base alloy castings, but only at pouring temperatures above 1500°C and then in



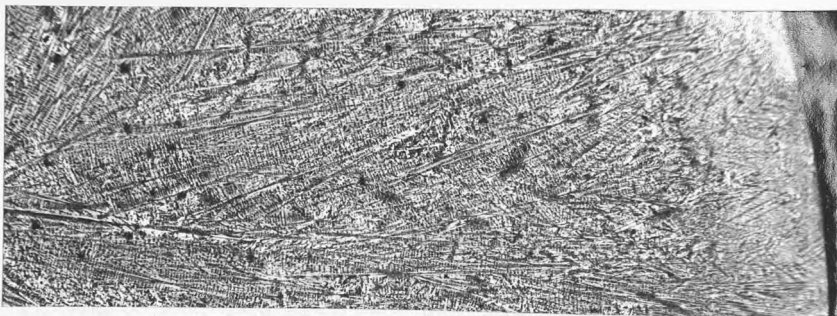
2.04%Si.  
Base Alloy.



+Mg.



+Te.



+Al.

FIG.203. Chill Casting Experiments. Alloying Addition Macrostructures.  
x25.

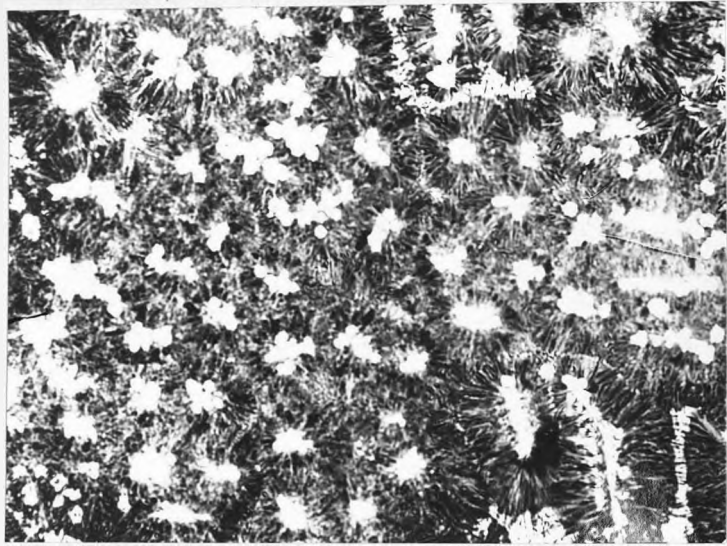


FIG.204. 2.04%Si. Chill Casting. +Al.  
Heat Tinted. x160.  
Multiple spherulite centres.



FIG.205. 2.04%Si. Chill Casting. +Te.  
Unetched. x160.  
Surface irregularities.

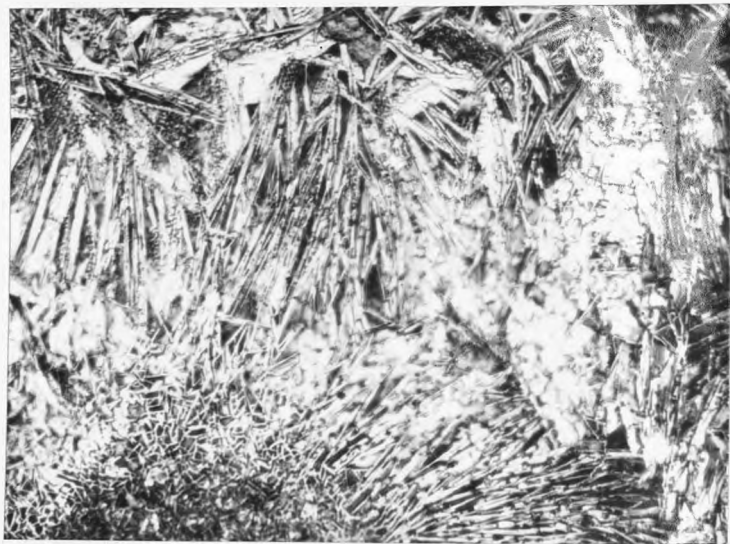


FIG.206. 2.04%Si. Chill Casting. +Te.  
Unetched. x1000.  
Surface irregularities.

quantities far smaller than in the tellurium bearing sample. Areas between spherulites were often irregular, containing random arrays of cementite needles (Fig. 206). The high relief in these areas suggests solidification shrinkage.

The transitions in metastable eutectic structure near the chill surface and throughout the cylindrical sections were similar to the base alloy in all cases.

#### 4.6 HEATED CERAMIC MOULD EXPERIMENTS: ALLOYING EFFECTS

##### 4.6.1 INTRODUCTION

Comparison of the effects of elemental additions to a given alloy is subject to many difficulties, which may be summarised as follows:

(i) Confusion exists regarding inoculation and alloying: inoculants being defined as having an effect on graphite nucleation, while the alloying effect of an element may influence all stages of solidification. In certain cases it may be difficult to determine whether inoculation or alloying effects are operative.

In the present series of experiments a standard procedure was adopted for making pure element additions. Classification of the results of such additions can only be made in general terms, after an examination of overall structural variations and any particular microstructural features.

(ii) Reaction with the atmosphere or evaporation may result in small recoveries. Melting losses were minimised by using rapid melting with additions in the charge centre. This investigation was concerned with the overall effect of given additions on structures formed in the heated ceramic mould experiments. More detailed information on the effect of element concentration would demand extensive analyses together with controlled vacuum or inert gas melting conditions.

(iii) When dealing with an impure alloy under air melting conditions, the possibility of indirect action of an addition by reduction or enhancement of the effect of another element must be considered. In this series, possible reactions and composite effects will be borne in mind, but mechanisms of action

can only be tentatively proposed.

(iv) Differences in atomic weight make comparisons in terms of weight percentage additions difficult to follow. Atomic percent additions were used to ensure the addition of equal atomic concentrations of each element considered.

#### 4.6.2 MICROSTRUCTURAL MEASUREMENTS

Microstructural surveys of the 2.04% Si alloy were extended to cover the alloyed specimens (Fig. 207). The results showed more than one basis for structural classification. Proportions of clear chill and mottle varied with additions. Aluminium reduced the amount of both chill and mottle present in the base alloy. Magnesium, bismuth, titanium, strontium, calcium and tellurium all increased the amounts of chill and mottle, but the position at which graphite first occurred varied widely. Magnesium developed graphite colonies almost on the chill face, while calcium and strontium produced colonies within 1.5 cm. Titanium, bismuth and tellurium inhibited graphite formation, producing large areas of clear chill.

The first rosette graphite was in positions equivalent to the base alloy in castings with aluminium, magnesium, bismuth and strontium, but both titanium and calcium did not form such colonies until all cementite had disappeared. Tellurium additions produced wholly white specimens with isolated graphite colonies near the top of the casting.

The classification of elements as graphitisers or carbide stabilisers becomes difficult if microstructural measurements are considered. If cementite survival in the upper regions of the casting is a criterion, a different series of relative effectiveness is obtained to when the depth of clear chill is considered.

#### 4.6.3 HARDNESS TEST RESULTS

It was hoped that a comparison of hardness values along the bar axis using the chill as a reference zero would enable a graphical comparison of structural variations within the alloyed 2.04% Si specimens. Fig. 208 shows a plot of

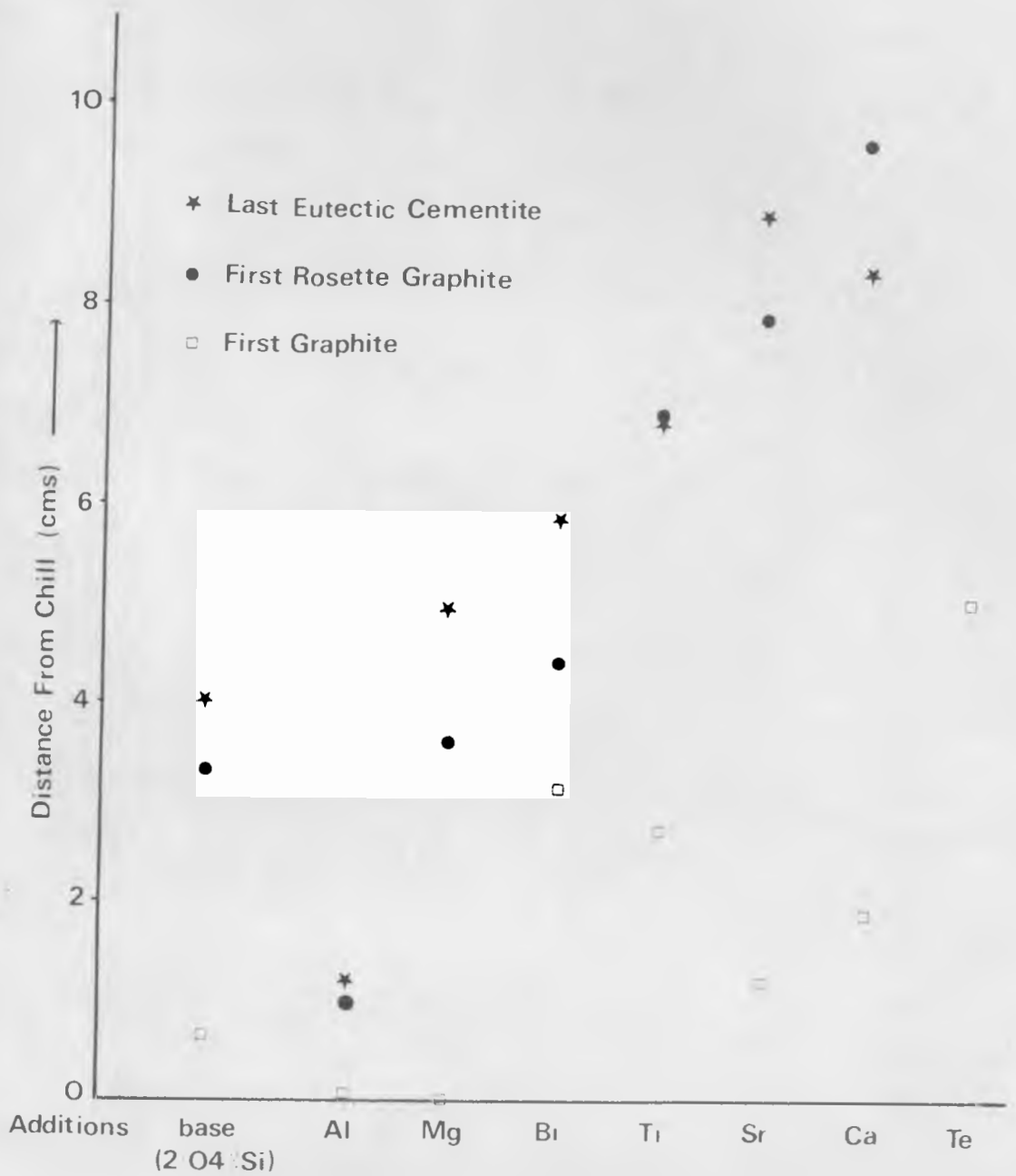


FIG 207. Microstructural Measurements For 2.04% Si Alloy Samples, Cast At 1440<sup>o</sup> Into 1150<sup>o</sup> Ceramic Moulds.

Vickers hardness vs distance from the chill for specimens with added elements, as well as the base alloy for comparison. All specimens were poured at 1440°C into ceramic moulds at 1150°C. The results are given as smooth lines since the large number of points involved makes comparison of curves difficult. Regions in the mottle zone where hardness values were highly variable, are represented by dotted lines which follow a mean path through the scattered points.

Rapid initial softening of the specimen with added aluminium was due to the small clear chill region and rapid development of mottle. After the mottled region, the specimen contained 'D' type graphite in a ferritic matrix with pearlite in the centres of dendrites. This pearlite gave way to ferrite, producing a minimum in the curve. Pearlite formation further from the chill at dendrite centres and the 'A' type graphite matrix, restored the hardness to its final constant value. Remaining samples, with the exception of the one containing tellurium, approached the same hardness as the base alloy after varying amounts of mottle. Mottle zone position and length was highly variable. Transition could be rapid as in the sample treated with bismuth, or gradual as in that with added strontium. The tellurium containing specimen retained its white structure for the whole length of the casting, only softening as the structure coarsened and where isolated graphite colonies were present.

#### 4.6.4 MICROSTRUCTURES

Microstructural measurements and hardness tests have shown the variations in main structural features and phase distribution along the test bars. In many instances, structures encountered were similar to those of the 2.04% Si alloy casting. In the following sections, only structures differing from those of the basic alloy are reported.

##### 4.6.4.1 ALUMINIUM

Microstructures after aluminium addition were similar to those of the unalloyed sample until 10 mm from the chill, where the proportion of ferrite in the microstructures began to increase, giving an entirely ferritic matrix

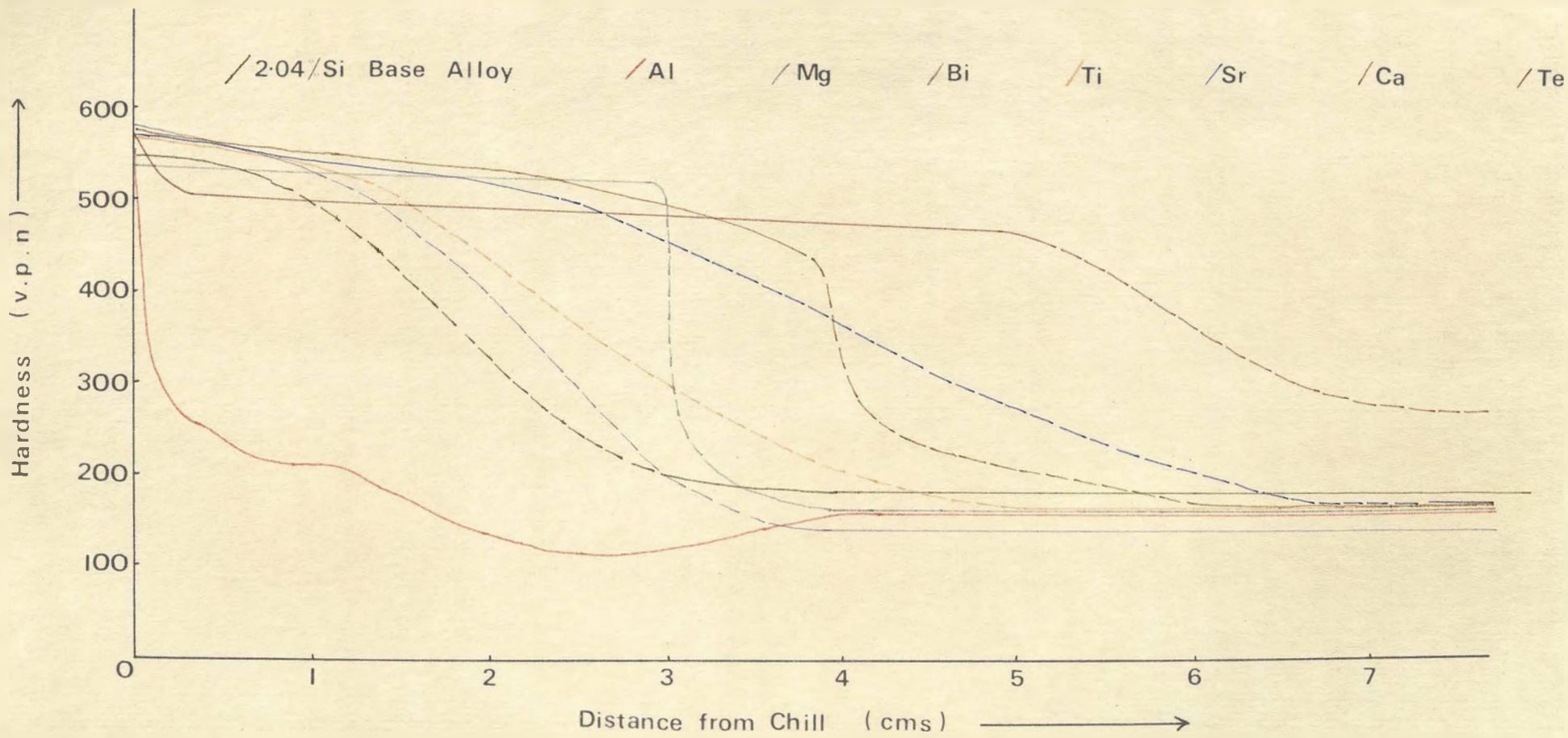


FIG. 208 Hardness Test Results

to the undercooled and rosette graphite eutectics by 13 mm. As ferrite increased in the microstructures, pearlite was segregated to grain boundaries forming equiaxed arrays.

Aluminium additions affected the form and distribution of manganese sulphide which changed from idiomorphs (Fig. 74) to smaller, more numerous rounded particles (Fig. 209). Williams noted this change (Fig. 68), ascribing it to oxygen removal by the aluminium. The surface irregularity of 'A' type graphite flakes was increased by aluminium.

#### 4.6.4.2 MAGNESIUM

Specimens with magnesium additions were similar to the base alloy in both structure and general phase distribution. Clear chill depth was decreased, while mottle penetration was enhanced. The last signs of cementite in the specimens were in the centres of decomposed cementite needles, as in the base alloy. These occurred in aligned clusters at up to 6 cm from the chill.

#### 4.6.4.3 BISMUTH

Bismuth additions produced a large free chill area while increasing overall chill and mottle depth. It may therefore be classified as a carbide stabiliser on both criteria. Structures obtained with bismuth additions were similar to those of the base alloy, graphite formations outlining ledeburite being especially marked.

#### 4.6.4.4 TITANIUM

Titanium produced no marked structural changes in the ledeburite or undercooled graphite regions, but gave an overall carbide stabilising effect by increasing both chill and mottle penetration. Light pink inclusions which were most noticeable in the 'A' type graphite areas were identified as titanium cyanonitride. 'A' type graphite flakes appeared to be slightly coarser than in the base alloy.

#### 4.6.4.5 STRONTIUM

Strontium increased both chill and mottle depth. Structural forms and their relative distributions were similar to those of the base alloy, although the mottled regions had increased amounts of graphite in ledeburitic outlines. Fig. 210 shows such an area, with fine compact graphite flakes outlining a honeycombe area. The flakes were coarsened and joined on the borders with austenite dendrites. More continuous flakes were associated with ledeburite colonies, which had cementite present only at nodes in an otherwise pearlite structure.

#### 4.6.4.6 CALCIUM

Microstructural differences between calcium treated samples and the base alloy were first noticeable in the mottled regions. Graphite formations outlining honeycombe structures were extensive (Figs. 211). The graphite was in association with small amounts of cementite at nodes in the honeycombe structure. Graphite in the ledeburitic regions was continuous with graphite colonies containing short thick flakes characteristic of the undercooled eutectic. The borders of the graphite areas with austenite dendrites were marked by compacted and coarsened flakes, suggesting carbon diffusion from the dendrite centres, followed by deposition on existing graphite. This view is supported by the ferritic borders of the dendrites.

In Fig. 212, short coarse graphite flakes and aggregates are associated with cementite and pearlite. The pearlitic structure appears to outline a pre-existing ledeburite colony. The presence of compact graphite flakes in ferrite areas suggests deposition of carbon on a few nucleation sites.

Cementite lath clusters were present as in the base alloy. They appeared to have developed independently of surrounding austenite dendrites. Some cementite remained at the needle midribs. Carbon diffusion from the needle areas was suggested by densified borders on adjacent undercooled graphite colonies.

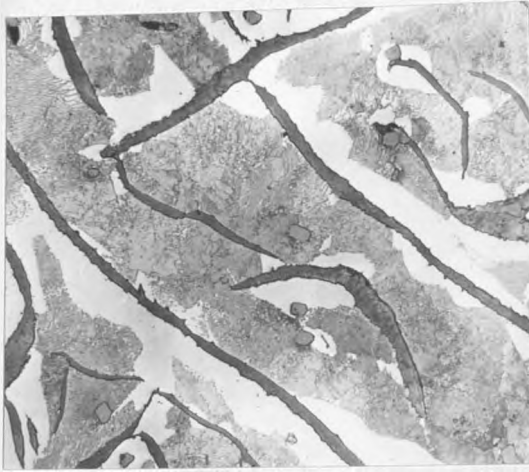


FIG.209. 2.04%Si.1150° ceramic mould.  
+ Al. 84.7mm. Picral.x400.  
Coarse graphite with MnS.

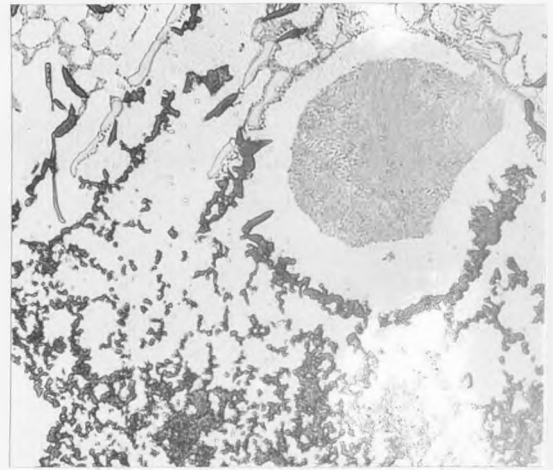


FIG.210. 2.04%Si.1150° ceramic mould.  
+ Sr. 66.2mm. Picral. x400.  
Honeycombe structure.

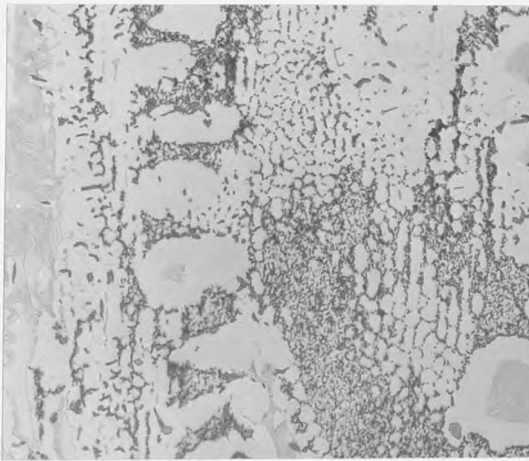


FIG.211. 2.04%Si.1150° ceramic mould.  
+ Ca. 60.4mm. Picral. x160.  
Honeycombe structure.

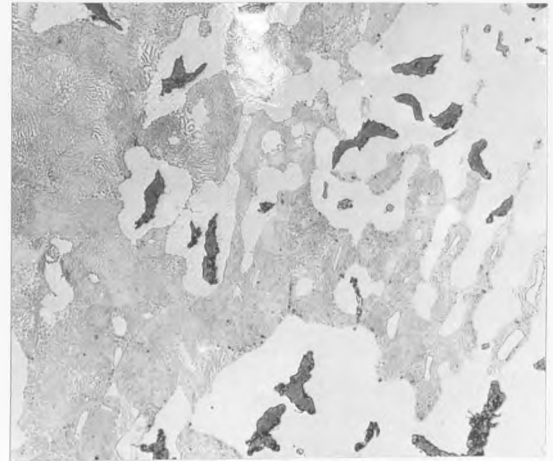


FIG.212. 2.04%Si.1150° ceramic mould.  
+ Ca. 69.3mm. Picral. x400.  
Coarse graphite and  
residual cementite.

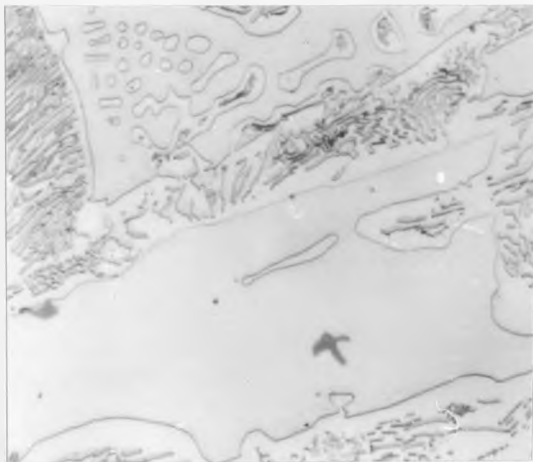


FIG.213. 2.04%Si.1150° ceramic mould.  
+ Te. 68.7mm. Picral.x1000.  
Coarse metastable eutectic.



FIG.214. 2.04%Si.1150° ceramic mould.  
+ Te. 72.3mm. Picral. x400.  
Proeutectoid cementite.

Microstructural measurements (Fig. 207) show that undercooled graphite was stabilised by the addition of calcium, rosette graphite not forming until 20 mm from the end of the mottled zone. Once coarser 'A' type graphite formed, it appeared similar to that of the base alloy.

#### 4.6.4.7 TELLURIUM

Tellurium additions produced the greatest carbide stabilising effect, together with the most marked influence on graphite morphology. Initial differences in structure to the base 2.04% Si alloy were noticeable in the metastable eutectic in the upper portions of the casting. Extensive partitioning of carbon between the eutectic phases is apparent in Fig. 213, where austenite rods have entirely transformed to ferrite and eutectic cementite is surrounded by wide ferrite borders. This may have resulted from ledeburite formation at low cooling rates remote from the chill, producing coarse ledeburite and enabling extensive carbon diffusion during subsequent cooling.

Another feature of the ledeburitic regions was the presence of large numbers of proeutectoid cementite laths in the transformed austenite dendrite regions (Fig. 214). Needles were aligned in three main directions common to adjacent dendrite arms, possibly representing austenite crystallographic planes.

Samples with tellurium additions contained a wide variety of graphite forms in the small mottled areas. Fig. 215 shows such a colony, where flakes outline ledeburitic areas as well as forming masses of interconnected flakes with numerous loops. The graphite types encountered may be divided into five classes:

(i) Fine tangled flakes containing loops (Fig. 215). The compact masses of flakes filled interdendritic spaces in the same way as normal undercooled eutectic.

(ii) Long curled flakes (Fig. 216) which followed the ledeburitic honey-combe structure but frequently deviated from the smooth outline. The flakes

contained many loops and generally appeared between flakes of the first and third categories.

(iii) Smooth flakes which outlined the ledeburitic structure to give loops, or straight flakes where the rods were sectioned longitudinally. This type of structure is shown in Fig. 217. The cementite has entirely disappeared, leaving only the graphite to maintain its original outline.

(iv) Compacted graphite was found in this alloy as short, irregular flakes of comparatively large size (Fig. 217).

(v) Graphite sometimes outlined massive cementite, projecting into the surrounding matrix as spikes with a widmanstätten appearance (Figs. 218 & 219). The form of these flakes suggests growth in pre-existing or growth-assisted cracks at the austenite/cementite borders. An internal crack in the cementite crystal of Fig. 219 continues the line of the graphite flake. Widmanstätten offshoots run parallel to pearlite lamellae in many cases.

In Fig. 220, a cementite needle is bordered by a colony of fine curled and looped flakes. The border graphite is continuous and does not directly contact the eutectic cementite, which appears eroded at the surface. The fine graphite appears to be continuous with smooth graphite loops of type iii which outline a ledeburitic area to the right of the microstructure. The amount of residual eutectic cementite in the ledeburitic area appears to be inversely proportional to the thickness of surrounding graphite flakes. Thin flakes are associated with continuous cementite, while cementite is absent or confined to structural nodes in regions containing thick flakes.

As the austenite rods in the ledeburite are part of a three dimensional structure, the outlining graphite might be expected to be in tubular form. This was confirmed by scanning electron microscopy after deep etching (Fig. 221).

Large rounded inclusions were present in all parts of the tellurium-treated

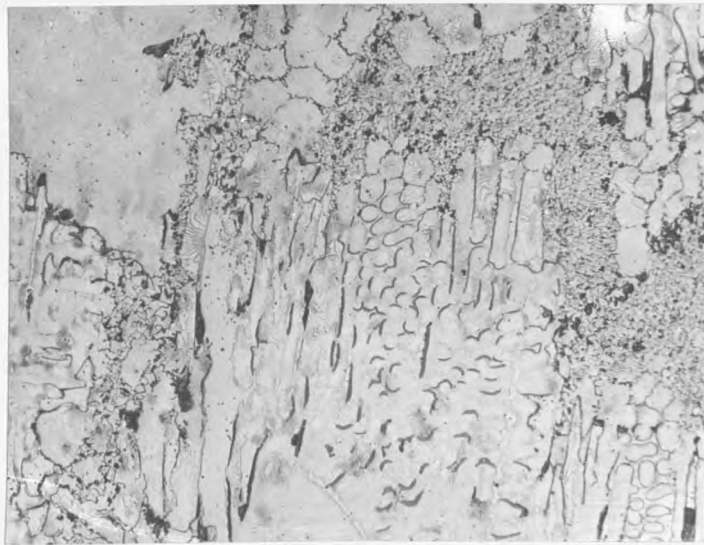


FIG.215. 2.04%Si. 1150° ceramic mould.  
+ Te. 157.9mm. Nital. x160.  
Mottle structure.

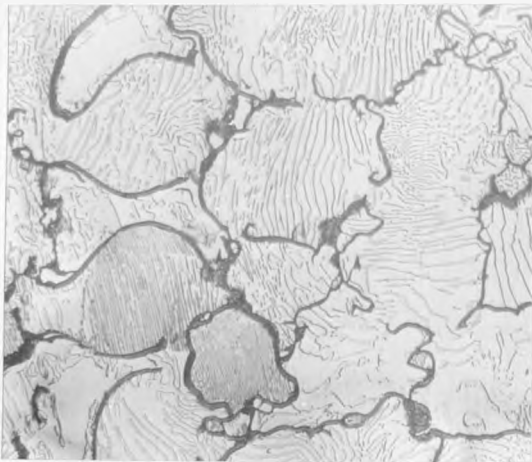


FIG.216. 2.04%Si.1150° ceramic mould.  
+ Te. 100mm. Nital. x1000.  
Curled outlining graphite.

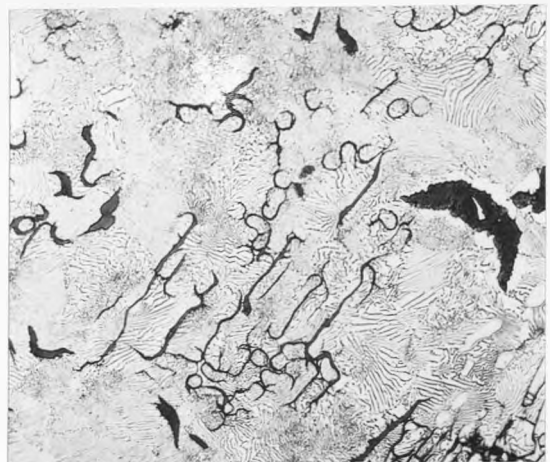


FIG.217. 2.04%Si.1150° ceramic mould.  
+ Te. 157.9mm. Nital. x400.  
Outlining graphite.



FIG.218. 2.04%Si.1150° ceramic mould.  
+ Te. 100mm. Nital. x1000.  
Outlining and widmanstatten  
graphite.

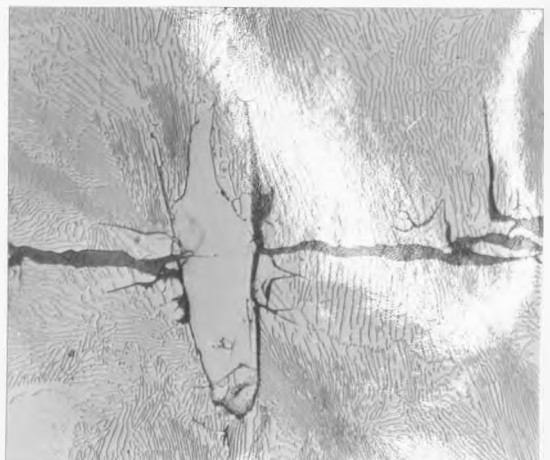


FIG.219. 2.04%Si.1150° ceramic mould.  
+ Te. 100mm. Nital. x1000.  
Outlining and widmanstatten  
graphite.

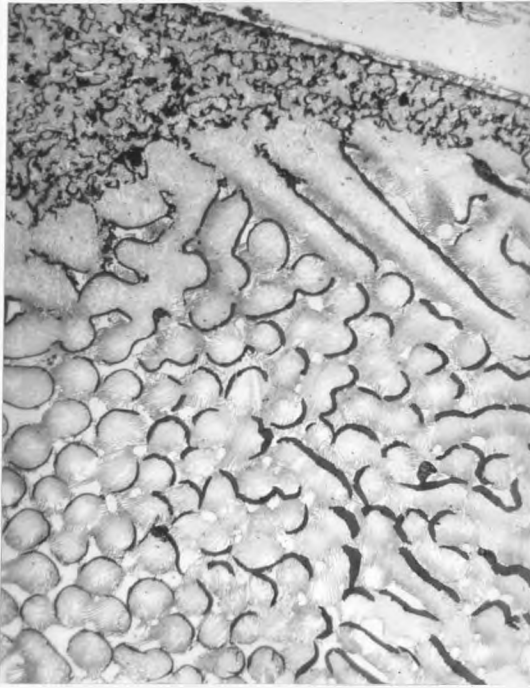


FIG.220. 2.04%Si.1150°C ceramic mould.  
+Te. 121.4mm. Nital. x1000.  
Graphite/ledeburite  
border area.



FIG.221. 2.04%Si.1150°C ceramic mould.  
+Te. 121.4mm. HCl/HF.  
Stereoscan @ 45°. x2400.  
Tubular graphite structure.

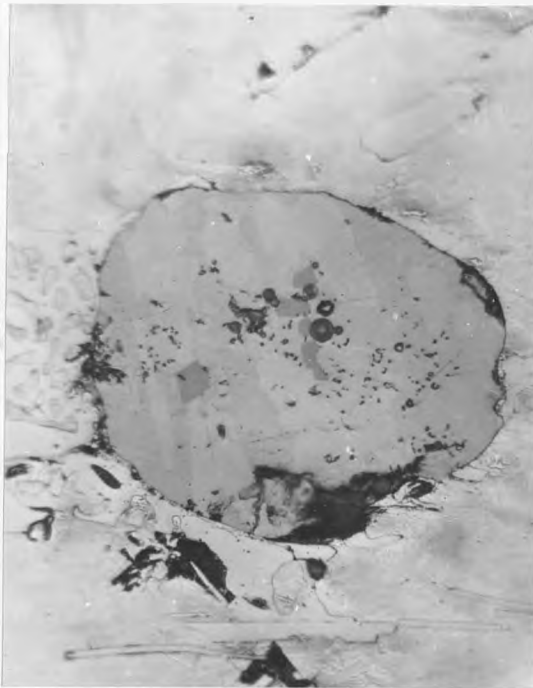


FIG.222. 2.04%Si.1150°C ceramic mould.  
+Te. 84.3mm. Nital. x400.  
Complex inclusion.



FIG.223. as Fig.222, Xpolar.

samples. These bodies were well developed in size even near the chill, suggesting formation in the liquid prior to casting. This was supported by their rounded shape, which was preserved irrespective of the surrounding microstructure. Normal illumination in Fig. 222 reveals three phases. Polarised light examination in Fig. 223 shows four phases: the matrix; one irregular phase; one idiomorphic and one widmanstätten. Microprobe analysis of the inclusions revealed the qualitative composition of the various phases (Fig. 224). A feature of these inclusions was the high concentration of minority elements present in relation to their distribution in the rest of the structure. Unfortunately as the analysis was only qualitative, the exact composition and nature of the separate phases could not be determined. An interesting result of the microprobe analysis was damage to the manganese/tellurium/phosphorus phase by exposure to the electron beam. Fig. 225 shows the result of 2 mins. irradiation at 10 Kv. The damage may be due to evaporation of volatile material when heated by the electron beam under vacuum conditions.

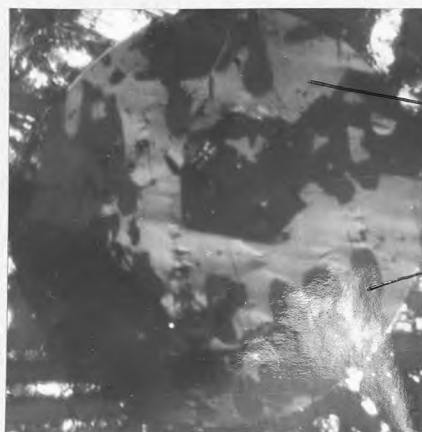
#### 4.6.5 SUMMARY

Addition of pure elements to the 2.04% Si alloy produced wide variations in structural distribution in the heated ceramic mould experiments. Of the elements investigated, only aluminium (graphitiser), calcium and tellurium (both of which acted as powerful carbide stabilisers) had any marked effect on phase morphology. All the others only changed the relative amounts and position in the bar of phases found in the base alloy.



Mn, Si, S.

Te, P.



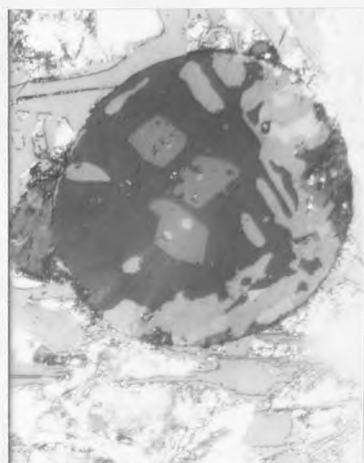
Fe, Te, P.

Mn, Te, P.

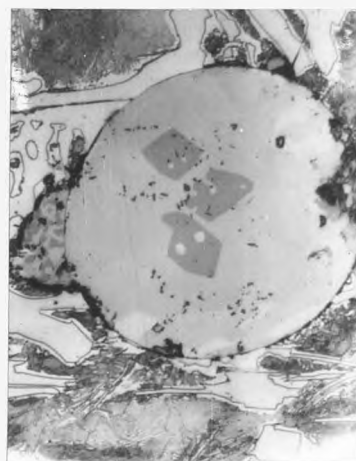
FIG. 224. Normal illumination.

Xpolar.

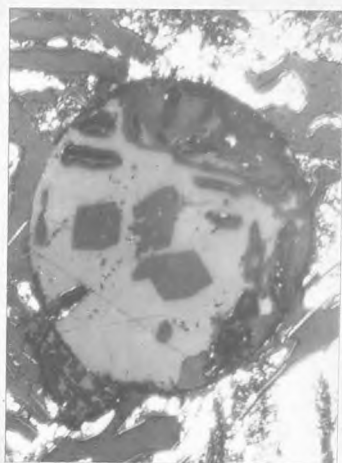
2.04%Si. 1150<sup>o</sup> ceramic mould. +Te. 84.3mm. Nital. x200.  
Complex inclusion. Microprobe Analysis Results.



(a) X polars.



(b) Normal illumination.



(c) X polars.



(d) Normal illumination.

FIG. 225.

2.04%Si. 1150<sup>o</sup> ceramic mould. +Te. 84.3mm. Nital. x200.  
Complex inclusion.

(a)+(b) as polished.

(c)+(d) after 2mins. irradiation by 10KV electrons.

## 5. DISCUSSION

### 5.1 INTRODUCTION

The range of cast iron structures is extremely extensive, especially when considered in microscopic detail. This research has been restricted to a study of microstructural variations in three alloys of similar carbon equivalent, but with varying carbon and silicon contents, subject to a range of cooling conditions both during and after solidification. The microstructural effects of a small range of pure element additions to one of the alloys has also been studied. The major observations of this research will be summarised as a basis for discussing the importance and interdependence of the variables which influence the final microstructure. With this framework it is hoped to provide a hypothesis for explaining typical microstructures of cast irons in terms of constitutional and physical parameters.

Ceramic mould experiments produced a continuous range of solidification and post-solidification conditions from those at the chill face to slow cooling at the top of the casting. No reheating effects were noted from the cooling curves. All parts of the castings were subject to continuous cooling, the cooling rate at any temperature decreasing with increasing distance from the chill. The rate of heat extraction by the water cooled copper chill was similar in all experiments. Structural variations must therefore have resulted from the effects of pouring temperature and mould temperature on the thermal balance within the casting. Increasing the mould temperature to 1150<sup>o</sup>C changed thermal patterns within solidifying and cooling samples, enhancing chill wave penetration, but reducing its intensity.

The use of a solid steel chill of a finite thermal mass in the chill/sand castings resulted in lower cooling rates than in the copper chilled ceramic mould castings. The initially high cooling rates experienced near the chill approached a common level with the body of the casting as the chill became

thermally saturated. Chill and mottle structures were consequently more limited than in the ceramic mould castings.

Macrostructural examination showed a progressive decrease in chill and mottle penetration with increasing silicon content. Preheating ceramic moulds to 1150°C increased chill and mottle in the 1% Si alloy castings, but decreased chill and mottle penetration in the higher silicon alloys.

For a given alloy, solidified in a chill/ceramic or chill/sand mould, structures generally coarsened under the progressively slower cooling rates occurring at increasing distances from the chill. The initially acicular metastable eutectic near the chill surface gave way to increasingly normal and less finely divided ledeburite structures formed at lower cooling rates. Graphite in the 1% Si alloy occurred as coarse flakes which may form radial colonies with finer streamer borders in mottle areas. Graphite flakes were subject to gradual coarsening with increasing distance from the chill. On increasing the silicon content to 2.04% and 2.43%, graphite in mottled regions and stable eutectic areas subject to chill influence during solidification took the form of fine curled undercooled flakes. These regions were bordered by aggregated flakes or more continuous 'streamer' graphite. The gradual flake coarsening with decreasing cooling rate during solidification noted in the 1% Si alloy was more abruptly marked in the higher silicon alloys. Undercooled graphite became interspersed with and finally gave way to coarser rosette forms as cooling rates fell. This tendency to coarser graphite was not noted in the peripheral graphite of the mottle zones in 2.04% and 2.43% Si chill/sand castings, where coarse, aggregated flakes gave way to streamers further from the chill.

Mottle structures in chill/sand or ceramic moulds followed a pattern common to all alloys studied. Graphite occurred initially as isolated colonies which multiplied and grew in size as distance from the chill increased. The graphite colonies coalesced to become the major eutectic form, enclosing metastable

eutectic areas which decreased in size. The last eutectic cementite was in most castings in the form of aligned lath clusters piercing stable eutectic colonies. This was not encountered in room temperature ceramic mould castings in the 1% Si alloy.

Borders between the two eutectic colonies in all alloys contained structures which differed in shape or dispersion from those occurring in stable or metastable colony interiors. Graphite and cementite in such areas were closely intermixed, contact and penetration occurring between the two phases. Eutectic cementite became discontinuous with a generally wasted and isolated appearance, although some form of interconnection was sometimes maintained as a coral-like structure in an austenite matrix. Graphite in border areas was aggregated, or took the form of streamers, or more regular honeycombe structures which followed eutectic cementite outlines.

Mottle areas in all alloys under all casting conditions studied were found to be associated with network structures exposed by etching in alkaline sodium picrate or bromine. These appeared to outline areas of pre-existing eutectic cementite. Isolated cementite particles in the degenerate ledeburite areas were situated at the thickest portions of a structure which may have decomposed subsequent to local solidification. The extent of network structures varied with alloy composition. The compactness and clear definition of the chill and mottle structures in the chill/sand castings enabled measurement of the extent of network structures, beyond the limits of cementite penetration. Such network formations were most extensive in the 2.04% silicon alloy.

Initially rapid cooling followed by varying degrees of isothermal treatment in the heated metal mould experiments enabled study of mottle production and solid-state transformation behaviour in both white and mottled castings. Lower mould temperatures resulted in completely metastable solidification which, when followed by isothermal treatments, produced isolated massive aggregated graphite

forms, characteristic of malleable iron structures. Increasing mould temperatures reduced initial cooling rates and produced mottled structures on solidification. The combination of higher mould temperatures with readily available sites for graphite deposition, resulted in more rapid cementite decomposition. This produced network structures similar to those in the mottled zone of the ceramic and chill/sand castings. Graphite forms resulting from isothermal treatment of mottled structures were coarse at lower temperatures, becoming finer and more continuous as the isothermal treatment temperature was raised.

Increasing the silicon content from 1% to 2.43% enlarged the range of mould temperatures in which mottled structures could be produced and transformed isothermally, from 20°C (1095°-1115°) to over 40°C (1040°-1080°). This enabled production of a greater variety of structures in the higher silicon alloy. The final stages of mottling with cementite laths piercing the graphite eutectic were reproduced in 1 mm plate castings of the 2.43% Si alloy with moulds at 1070°C.

Classification of the effects of 0.2 atomic % pure element additions to 2.04% Si heated ceramic mould castings was found difficult. The sequence of effectiveness of additions in promoting metastable eutectic penetration was different from that for clear chill zone production. This implies that relationships between additions and structure are more complex when considered on a microscopic scale than when the 'macroscopic' graphite promoter or carbide stabiliser classifications are used.

Most elemental additions altered the extent and relative proportions of the structures in the test bars, without affecting phase morphologies. The greatest structural changes were produced by tellurium additions. The small amount of mottling in the tellurium treated specimens contained five distinct graphite forms: interconnected fine flakes; regular and less regular flakes

outlining ledeburite; massive aggregated flakes and widmanstätten graphite. Tellurium additions also resulted in large multi-phase inclusions, containing Te together with S, Si, Mn and P.

Nucleation and growth under chill conditions may lead to radial growth from a point source. The centres and radial ribs of these formations may have structures characteristic of hypereutectic compositions.

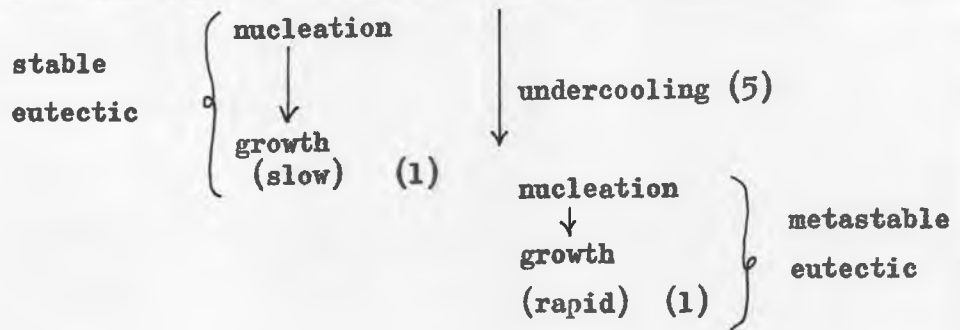
## 5.2 FACTORS AFFECTING CAST IRON STRUCTURE

The factors which may affect cast iron structure during and after solidification are numerous and extremely complex in their interactions. The final structure produced in a given situation is determined by the balance achieved between these interdependent variables. Whatever mode of action is involved, any factor or collection of factors influences the final structure by affecting nucleation and growth of the stable and metastable systems. Some of the factors discussed in the literature which affect nucleation and growth of stable and metastable eutectics are summarised in Fig. 226. Numbers in the figure refer to the reference list. These factors and inter-relationship will be considered together with the results of the present work in the following sections.

## 5.3 MOTTLE FORMATION

Castings which contain both stable and metastable eutectics generally exhibit areas in which the two growth forms are more or less closely associated forming a 'mottled' structure. From the present work, it appears that an extensive range of structures exist, all of which may be classified as 'mottled'. Variation in mottle dispersion and phase morphology occurs with composition and thermal conditions during and after solidification.

Mottled structures have been envisaged as forming in several ways, depending on alloy composition and physical conditions during and after solidification. The main explanations are as follows:



The relative ease of transition between the two eutectics is dependent on the effects of variables on nucleation and growth in the two systems.

Stable Eutectic Nucleation

- Heredity (13,14,15)
- Physical treatments (10,32,33,34)
- Inoculation (23,29)
- Poisoning (36)
- Eutectic equilibrium temperature (4,74)
- Segregation Effects (23,59,75)

Stable Eutectic Growth

- Degree of Stable Eutectic Nucleation (14)
- Undercooling at Growth Front (39)
- Segregation Effects (52,56)
- Relation between austenite and graphite growth rates (43,52)

Metastable Eutectic Nucleation

- Nucleation and Growth Potential of the Stable Eutectic (14)
- Reduction in Proeutectic and Eutectic Austenite Growth Rate (104)
- Separation of Stable and Metastable Eutectic Equilibria (4,74)
- Segregation Effects (55)

Metastable Eutectic Growth

- Segregation (67,68)
- Undercooling at the Growth Front (39)

FIG. 226. FACTORS AFFECTING CAST IRON STRUCTURE.

(1) Mottle may result from metastable eutectic nucleation and growth after undercooling during stable solidification; external physical conditions being uniform<sup>(73)</sup>.

(2) Stable solidification may be interrupted after sudden cooling from an external physical source, e.g. chill<sup>(73)</sup>, or quench<sup>(8)</sup>.

(3) Segregation may cause transition between the eutectics, e.g. metastable eutectic at stable eutectic cell boundaries<sup>(55)</sup>, or possibly inverse chill<sup>(96)</sup>. Alternatively white eutectic solidification may be replaced by grey solidification after segregation, forming indefinite chill<sup>(75,89)</sup>.

(4) Solidification of both eutectics at the same temperature has been postulated, with possibly some degree of co-operation<sup>(14)</sup>.

(5) 'Indirect' mottle formation by solid-state graphitisation of eutectic cementite has been suggested<sup>(49,89)</sup>.

For a given alloy composition, the difference between explanation 1 and 2 lies in the physical conditions under which solidification takes place. Both explanations imply essentially sequential solidification. Mottle results from the overtaking and engulfment of growing stable eutectic colonies by the faster growing metastable eutectic(1). Structures formed in a given alloy by mechanisms 1 and 2 may be similar, provided the undercoolings and growth rates involved do not result in radically different eutectic dispersions or morphologies. In the following discussion, the first mechanism of mottle formation will be referred to as the 'critical cooling rate' hypothesis. The second mechanism, which depends on physical changes imposed from outside the system will be called the 'interruption' mechanism. It will be noted that a pre-requisite for mottle formation by either mechanism is the presence of a sufficiently high cooling rate to cause undercooling into the metastable eutectic region. The value of this parameter depends on alloy composition.

The remaining three sources of mottle may be expected to produce structures distinguishable from the 'critical cooling rate' and 'interruption' types by

reason of distribution or phase morphology.

#### 5.4 PHYSICAL FACTORS

##### 5.4.1 INTRODUCTION

An initial requirement for the interpretation of cast structure is study of the physical factors affecting solidification. Thermal analysis has shown that physical processes in heated and unheated ceramic moulds and chill/sand castings are widely different.

Thermal systems in any mould may be divided into three regions, which govern final structure for a given alloy composition. These are illustrated in Fig. 227 although it must be realised that such regions are not clearly divided and considerable overlap occurs. This is true within a given microstructural area as well as within a given casting, where all three processes may take place simultaneously. The major influence exerted by mould systems is that of heat extraction in terms of its rate and temperature gradient at any given point. The time spent in a given region of Fig. 227 may be critical in determining solidification and post-solidification processes, which influence final structure. The influence of cooling rate in the pre-solidification range was investigated by Williams<sup>(96)</sup>, who concluded that subsequent solidification was independent of this parameter. Even if this is so, pre-solidification cooling may have wide effects on structure by changing mould conditions and affecting cooling in regions II and III. This was found to be especially so in the heated metal mould experiments, as described below.

##### 5.4.2 PHYSICAL INFLUENCES IN SOLIDIFICATION

Cooling conditions through the eutectic solidification range in heated ceramic mould castings appeared to be controlled by the chill rather than by the chill and mould. This would lead to transition between the two eutectic forms and mottle production by the critical cooling rate mechanism. Structural transitions under such conditions would reflect the response of an alloy to progressively

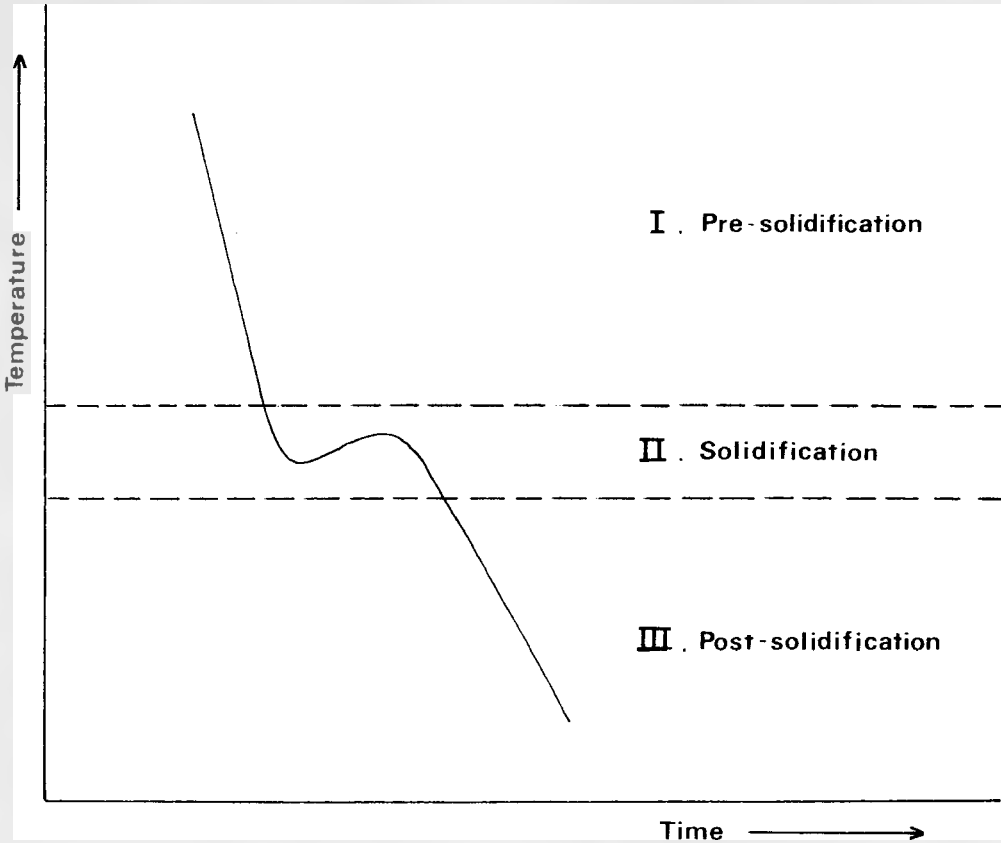


Fig 227. Thermal Regions governing Cast Structure .

[ schematic ]

decreasing cooling rates more clearly than in castings where competition might occur between mould and chill as means of heat extraction.

Room temperature ceramic mould castings solidified under the combined influence of the chill and mould. The region close to the chill, which solidified entirely under chill influence was subject to cooling rates which decreased with increasing distance from the chill. Further from the chill, cooling through the mould walls initiated solidification before arrival of the chill wave.

Solidification structures in these castings reflected a combination of critical cooling rate and interrupted solidification<sup>(73)</sup> as means of producing a stable-metastable eutectic transition. The relative degree of effectiveness of these mechanisms depends on alloy composition. Mottled zones in the room temperature ceramic moulds were subject to relatively rapid cooling through the latter part of the solidification region (Fig. 227). This is likely to produce different structures to those formed in heated moulds where solidification region cooling is slower.

Transition between eutectic structures during solidification in chill/sand moulds may occur as a result of chill wave interruption of stable system solidification or by the critical cooling rate mechanism. In these experiments, the thermal mass of the chill was limited while cooling conditions in the casting body were slow (Table 8). The structural transition along the casting axis above the chill appeared to result from solidification at a critical cooling rate under the influence of the chill wave. The interrupted solidification mechanism may have applied in regions to the side of the chill surface (Fig. 33), where initial stable system solidification took place under the influence of the sand mould. The intensity of the chill effect in chill/sand castings was much less than in either type of ceramic mould.

Heated metal mould castings were subject to continuous cooling at a range of cooling rates prior to and during solidification. Mottle formed by solidification

in such cases would form by the critical cooling rate mechanism. An important physical factor in solidification in heated metal moulds was mould heating during superheat loss and recalescence in the solidifying alloy. On a macroscale this effect limited the upper mould temperature at which castings solidified in the initial rapid cooling portion of the cooling curve (Fig. 120). Temperatures above a certain level resulted in very slow cooling through the eutectic region and always gave grey solidification in the alloys studied. Initial cooling rates in the rapid cooling region were also affected by mould temperature (Figs. 121, 122). The mould temperature at which the initial cooling rate was reduced enough to produce a completely grey solidification structure was highly sensitive to alloy composition (Tables 9 & 11). This effect gave an indication of the susceptibility of alloys to metastable solidification.

On a microscopic scale, the thermal interaction of solidifying eutectic cells may influence both solidification and solid-state processes. In the present series of experiments many interesting structural effects were associated with the borders of stable eutectic colonies in the mottle zone. The size of these areas is such that accurate prediction or interpretation of structural processes may not be possible from thermal arrest data. The problem of thermal analysis in such systems becomes acute, when it is realised that apart from any problems of accuracy or sensitivity the thermocouple itself may alter solidification or transformation processes.

#### 5.4.3 POST-SOLIDIFICATION PROCESSES

If post-solidification or 'secondary' mottle occurs, (mechanism 5) its form and extent in a given alloy will depend on the physical conditions both during and after solidification<sup>(87)</sup>. The amount of time spent at elevated temperatures is inversely proportional to the cooling rate through the temperature range in question (Fig. 227). In these experiments, post solidification cooling at any given point in the chill and mottle zones was most rapid in room temperature

ceramic mould castings (Fig. 46). Corresponding positions cooled at much lower rates in heated mould specimens. Thermal saturation of the solid steel chill in chill/sand castings resulted in very slow cooling conditions throughout the chill zone (Table 8). A cooling rate of  $16^{\circ}\text{C}/\text{min.}$  through  $1000^{\circ}\text{C}$  was recorded at a distance of 0.5 cm from the chill. This point was within the limits of network structures in all chill/sand castings (Fig. 87).

Heated metal mould results should be interpreted in the light of the 'composite' nature of the cooling process after solidification. Isothermal treatment in heated metal moulds was preceded by slow cooling after solidification from the temperature attained by mould and casting to the furnace temperature (Fig. 120). The rate of cooling before isothermal conditions were reached decreased with increasing furnace temperatures (Figs. 121 & 122).

## 5.5 COMPOSITIONAL INFLUENCES ON SOLIDIFICATION

### 5.5.1 INTRODUCTION

Solidification in a given physical situation is governed by alloy composition and its prior history. Compositional effects in commercial cast iron solidification are obviously extremely complex, involving many elements exerting both individual and composite influences. Elemental effects may be divided into two main classes. The first group is based on the thermodynamic effect of an element on the relative stability of stable and metastable eutectic systems. The second depends on direct influence on nucleation and growth processes. In the case of thermodynamic influence, structures obtained should not be exclusive to alloys containing the particular alloying element, and should be no different from structures produced by other means. In the case of direct influence on nucleation and growth, structures may conform to the normal structural range of cast iron, but abnormal morphologies can form which are characteristic of the influence of a particular element or group of elements. In each case, it must be remembered that the influence of an element may be exerted indirectly by reason of its

reaction with one or more other elements. An element may also influence structure by a combination of the 'thermodynamic' and 'direct' mechanisms outlined above.

### 5.5.2 THE EFFECT OF SILICON

The present work is concerned with the effect of variations in silicon content on structures produced by a range of different solidification conditions. Silicon content at constant carbon equivalent appears to have a major effect on graphite morphology, clear chill and mottle formation.

Hillert<sup>(43)</sup> and Dvidjev<sup>(52)</sup> considered stable eutectic morphology in terms of the growth rates of austenite and graphite, which in themselves are temperature dependent (Fig. 18). Graphite morphology differences between alloys and within a given alloy may result from differences in growth temperature. Growth at different undercoolings may account for the appearance of both rosette and undercooled graphite eutectic colonies in 2.04% and 2.43% Si alloy castings, and coarse graphite in 1.00% Si alloy specimens. Patterson and Ammann<sup>(32)</sup> suggested that changes in graphite form could be due to nuclei of varying chemical composition becoming effective at different undercoolings. In these requirements, all types of graphite colony nucleation appeared to occur at or near austenite dendrite surfaces. This may support Lakeland and Hogan's theory of nucleation<sup>(59)</sup>, but the actual nature of the nuclei involved is uncertain. Direct inoculation effects due to variations in silicon content were minimised in the present series of experiments by sand casting and rapid remelting between alloy preparation and final casting.

Segregation may affect carbon deposition from the melt, retarding growth and causing changes in eutectic morphology. Variations in flake distribution across graphite eutectic rosettes have been attributed to inverse silicon segregation<sup>(43)</sup>. The possibility of interaction between silicon and minority elements e.g. sulphur<sup>(97)</sup> or oxygen<sup>(98)</sup> is yet another structural influence which

may result from changes in silicon content.

An approach to explanation of structural variations between alloys with different silicon contents may be made using Oldfield's work on the effect of Si on stable and metastable equilibria<sup>(4)</sup>. Solidification in ceramic or chill/sand moulds is a sequential process, which in the alloys studied commences at the chill with metastable eutectic nucleation and growth. The depth to which this eutectic form predominates or continues at all is determined by a competition process with the stable eutectic. This competition commences at any point in the bar as soon as the stable eutectic nucleates and starts to grow, whether under the influence of the chill, or by heat extraction through the mould walls. A factor which affects chill depth and final microstructures is the time advantage for nucleation and growth which may be given to the stable eutectic by reason of its higher equilibrium temperature. In alloys where the equilibria are narrowly spaced, stable eutectic nucleation from a given number of nucleation sites may be followed by undercooling into the metastable eutectic region at relatively slow heat extraction rates. This may be the case in the 1.00% Si alloy of these experiments. The occurrence of finer flakes at colony borders in this alloy may indicate a certain amount of undercooling and more rapid branched growth before metastable solidification<sup>(73)</sup>. The great disparity in growth rate between graphite solidifying at only moderate undercooling and the metastable eutectic will effectively halt further stable eutectic growth<sup>(1)</sup>.

Alloys with higher silicon contents and a wider separation between the stable and metastable eutectics<sup>(4)</sup> are able to undercool more during stable eutectic solidification before initiation of metastable growth. This may enable increased nucleation<sup>(32)</sup> and more rapid growth by highly branched undercooled flakes to compensate more effectively for heat extraction<sup>(5)</sup>. Flake refinement during undercooled growth may be due to an increased growth advantage of austenite compared with graphite as temperature falls<sup>(43,52)</sup>. From these considerations

it will be seen that a higher cooling rate is necessary to cause metastable eutectic nucleation and growth as silicon content is increased.

### 5.5.3 SOLIDIFICATION IN CERAMIC AND CHILL/SAND MOULDS

Clear chill depth decreases with increasing silicon in heated ceramic mould castings (Fig. 49a). This follows the enhancement of stable eutectic nucleation and growth potential brought about by the increased separation of the eutectic nucleation and growth ranges. The same mechanism may be responsible for the decrease in the extent of the mottle zone with increasing silicon. Final eutectic cementite in these castings reflects the minimum improved cooling rate at which metastable solidification is possible under chill influence. Under conditions of directional eutectic solidification with no eutectic nucleation ahead of the chill wave, graphite at any part of the specimen will nucleate during cooling under chill influence and grow at rates determined by the undercooling. Metastable eutectic nucleation in these circumstances is continuous, resulting from propagation of fast-growing cementite plates at low undercoolings<sup>(1)</sup>. If the disparity between the case of stable and metastable nucleation is removed, the formation of a mottled structure may be possible at lower heat extraction rates, than under conditions where cementite nucleation is necessary. This mechanism may account for results in 1% Si heated ceramic mould castings, where mottled structures were produced at cooling rates lower than those resulting in completely grey solidification in the body of unheated ceramic mould castings. The occurrence of such an effect is subject to changes in graphite nucleation and growth potential imposed by composition. In the higher Si alloys, the more favourable nucleation/<sup>and</sup> growth conditions prevented such an effect occurring.

The formation of rosette graphite with coarse flakes in the higher silicon alloys may indicate sufficiently low heat extraction rates for appreciable coarse flake growth before increased undercooling and flake refinement at colony peripheries. The difference in position of such rosettes in 2.04% and 2.43% Si

alloys implies a difference in nucleation or growth potential. This could result from the increase in the stable eutectic equilibrium temperature with increasing silicon<sup>(4,99)</sup> giving more favourable conditions for graphite nucleation followed by slow growth during cooling under chill influence.

Changes in pouring temperature of 2.04% Si heated ceramic mould castings gave results in agreement with previous work<sup>(16)</sup>. Variation in occurrence of rosette graphite may be interpreted in terms of graphite nucleation by superheating<sup>(16,32)</sup>. This could lead to greater undercooling followed by nucleation and growth of undercooled graphite in the specimen poured at the higher temperature. In the present series of experiments, melts were poured at the maximum temperature reached during the melting cycle. In such a case it is not possible to separate nucleation effects from the changes in cooling conditions caused by varying pouring temperature.

Room temperature ceramic mould castings are subject to generally higher cooling rates during solidification and during subsequent solid state cooling than specimens cast in heated moulds (Fig. 46). Initial graphite colonies in the 1% Si castings are rounded (Fig. 60), as opposed to the more elongated colonies formed by the critical cooling rate mechanism in heated mould specimens (Fig. 50). Colonies also form closer to the chill under more severe chill conditions than in heated mould castings. This would suggest the formation of initial graphite colonies ahead of the chill wave, followed by interruption of stable solidification to give a mottled structure. The interruption mechanism would continue to operate until solidification according to the stable system in the casting body was complete before arrival of the chill wave.

Initial graphite in the 2.04% and 2.43% Si alloy room temperature mould castings probably formed by the critical cooling rate mechanism under direct chill influence (cf Figs. 44 & 49a). Solidification to form mottled structures by the critical cooling rate mechanism in these alloys would have continued until the point was reached where graphite growth occurred in the body of the

casting before the chill wave arrival. Subsequent mottle would have resulted from interruption of stable eutectic growth. This point may be represented by the occurrence of rosette graphite, formed under slow cooling conditions (Fig. 49a). Increased cooling rates in the higher silicon alloys would initially cause increased undercooling with correspondingly enhanced radial growth rates and flake branching. This could be followed by further undercooling and metastable solidification if the heat extraction rate was high. The increased mobility of graphite growing in undercooled form in these alloys would lead to greater growth competition between stable and metastable eutectics during the final stages of solidification especially at points near the end of the mottle zone. The last stages of chill effect in the higher silicon alloys cast in room temperature ceramic moulds may be seen as undercooled graphite development beyond the extent of metastable eutectic.

Processes of mottle formation in chill/sand castings appear to have been similar to those in heated ceramic mould specimens. The relative structural distributions in the different alloys reflect the reaction of different compositions to cooling under the influence of a chill with limited thermal mass (cf Figs. 49a & 87).

A feature of solidification in chill sand moulds and all ceramic mould specimens except the 1.00% Si room temperature ceramic mould castings, was the formation of cementite needle clusters, surrounded by stable eutectic (Figs. 59, 80, 90, 97 & 108). These formed in the upper regions of the mottle zone and at colony borders with the metastable eutectic. Initial propagation of cementite as plates was followed by slower sideways growth (Fig. 23)<sup>(43)</sup>. Under conditions of low undercooling for cementite growth the graphite eutectic may be able to compete with the growing ledeburite. Latent heat liberation by growing graphite colonies and the large heat contribution from needle propagation or the initial stages of sideways ledeburite growth<sup>(1)</sup>, may also increase the growth advantage of graphite. Under these circumstances, structures may develop in which the initial plates of

cementite are overgrown by stable eutectic during sideways growth. The occurrence of such structures may therefore depend on the relation between sideways growth of ledeburite and the radial growth rate of graphite colonies under the thermal conditions in question. The absence of such structures in 1.0% Si room temperature ceramic mould castings is to be expected, since coarse flake graphite will not be able to compete with ledeburite developing under the relatively rapid cooling conditions imposed by the chill wave. A degree of growth competition may occur between ledeburite and the coarse graphite of the 1.0% Si alloy under slow cooling conditions in the upper region of the chill zones of heated ceramic mould or chill/sand castings (Figs. 59, 90).

In all castings of the higher silicon alloys, the greater undercooling necessary for metastable eutectic growth favours competitive growth between ledeburite and undercooled graphite. This may occur under more rapid cooling conditions than in the low silicon alloy.

#### 5.5.4 SOLIDIFICATION IN HEATED METAL MOULDS

Previous arguments regarding the relative ease of stable and metastable eutectic solidification in alloys with different silicon contents are supported by heated metal mould results. Tables 9 & 11 show that increasing the silicon content from 1.00% to 2.43% reduced the mould temperature levels at which mottled solidification occurred. The range of mould temperatures between totally white and totally grey solidification was increased from 20°C (1095° - 1115°) at 1.0% Si to 40°C (1040° - 1080°) at 2.43% Si. Interpreting metal mould temperature as an indication of the rate of cooling through the eutectic solidification range, it may be seen that increasing silicon enables totally grey solidification at much greater cooling rates than are possible in the low silicon alloy.

Results from heated metal mould experiments support the mechanism of growth competition between cementite and graphite for production of cementite needle structures. This form of mottle was found in 2.43% Si alloy castings, cast into

metal moulds preheated to 1059°C - 1070°C; 21° - 10°C below the mould temperature at which castings solidified totally grey (Figs. 180-184). Such needle structures were not found in 1% Si alloy castings when moulds were preheated to 1100°C; 15°C below the mould temperature for grey solidification. The relatively rapid cooling rates during solidification in these castings (Fig. 121) may preclude growth competition between coarse graphite flakes and the metastable eutectic.

## 5.6 INDIRECT GRAPHITE FORMATION

### 5.6.1 INTRODUCTION

Previous work on high temperature solid-state transformations in cast iron has largely relied on the techniques of quenching during solidification<sup>(8,23,29,87)</sup> or reheating samples cooled to room temperature after casting<sup>(62,80,86,87,88)</sup>. Although such techniques are important in determining solidification processes or in duplicating the conditions of malleabilising, they fall short of reproducing behaviour after solidification in actual castings in several respects.

The interrupted solidification experiments of Hultgren et al<sup>(8)</sup> were intended to test the indirect theory of undercooled graphite formation. As decomposition of an initially ledeburitic structure to undercooled graphite was supposed to occur extremely rapidly at temperatures just below the eutectic, experimental times and temperatures were arranged accordingly. Results obtained by quenching during or immediately after the eutectic arrest are not strictly comparable with the structures found in the chill and mottle zones of real castings. In the latter case, transformation may take place during considerable time intervals over a continuously falling temperature range, both during and after solidification.

Reheating experiments have been carried out in extensive studies of malleablising<sup>(62,80)</sup> as well as in the study of indirect graphite formation<sup>(86,87,88)</sup>. The cooling and reheating stages may cause changes in stresses between micro-structural phases, lattice defects, matrix transformations, gas contents and

segregation patterns. These may affect subsequent transformations and lead to a false picture of high temperature transformations in real castings. A feature common to most reheating experiments has been the use of completely white iron samples (with pearlitic or martensitic matrix) as starting material. This practice may be questioned, in the case of indirect graphite formation studies, since high temperature transformation processes appear to be most marked in regions solidifying with mottled structures.

From the present work it appears that if secondary mottle occurs, it forms after solidification, during continuous cooling with all the physical and chemical conditions that this implies. The final cast structure must be viewed as an integration of solidification and solid-state processes.

#### 5.6.2 CEMENTITE DECOMPOSITION

Before considering secondary mottle formation, we must examine the formation and occurrence of network structures in eutectic cementite. Hultgren<sup>(93)</sup> and more recently Charbonnier and Margerie<sup>(53)</sup> used alkaline sodium picrate to reveal areas of cementite decomposition in heat treated steel or cast iron. The latter workers<sup>(53)</sup> related the etching effects to silicon depletion and manganese concentration in areas previously occupied by cementite. In the present work, chemical heterogeneities have been exposed by etching with alkaline sodium picrate or bromine, sometimes followed by nital. Network structures have been revealed at all levels of mottle zones in all alloys, with both pearlitic and martensitic matrices. The networks were shown by colour effects (Figs. 56,90,108,141,174) or pearlitic distributions (Figs. 71, 77, 101,111, 112, 113, 119). They were often, but not always, associated with residual cementite.

Heated metal mould experiments using high temperature isothermal treatments have enabled production of network structures closely resembling as-cast eutectic cementite distributions (Figs. 160,179,174,180-183). Such networks remained after all trace of eutectic cementite had vanished. This supports the findings of Charbonnier and Margerie<sup>(53)</sup>, who found that isothermal treatments resulted

in only slow homogenisation of chemical heterogeneities in regions previously occupied by cementite.

Segregation patterns revealed by etching may be slightly distorted on a microscopic scale by small amounts of diffusion at high temperatures in the solid state. This may be indicated in Fig. 175 where outlining graphite, which presumably bordered the eutectic cementite, is shown as being totally within the network outline. To eliminate possible errors, network structures should be compared with similar areas of untransformed metastable eutectic wherever possible.

Eutectic cementite may remain at various sites in the ledeburitic structure during decomposition:

- (a) at points of greatest thickness in the original eutectic cementite,
- (b) at points most removed from graphite nucleation sites,
- (c) in areas where carbide stabilising elements have concentrated or graphitising elements have become depleted by segregation during solidification.

In practice, a combination of all three conditions for cementite retention will probably determine final distribution. In many areas, residual cementite decreased in amount as adjacent graphite colonies were approached (Figs. 112 & 116), suggesting a combination of (a) and (b) above.

### 5.6.3 COMPOSITIONAL EFFECTS

The silicon content of cementite and its effect on cementite decomposition has been the subject of controversy. Some authors<sup>(100)</sup> have reported that cementite contains little or no silicon. Others maintain that not only does the silicon content of cementite vary with composition, but it has the effect of reducing cementite stability at high temperature<sup>(101)</sup>. Segregation of silicon in the austenite of ledeburite has been shown to be high, especially at cementite/austenite interfaces<sup>(3,53)</sup>. This phenomenon has been used to predict a decrease in cementite stability with increasing silicon content, using thermodynamic

arguments<sup>(102)</sup>. The effect of silicon is said to be exerted in austenite rather than in the cementite by increasing the free energy of formation of cementite. The effect of silicon during first stage malleablising has been attributed to an increase in nucleation rate. Effects on growth rate are said to be slight<sup>(80)</sup>. This viewpoint has been challenged in view of the possible silicon content of cementite<sup>(103)</sup>. Results from malleablising studies may not be strictly applicable to the alloys and conditions under consideration, in view of the compositional and physical differences involved.

In the present series of experiments, increasing silicon content appeared to reduce the stability of the metastable eutectic, under given physical conditions. The effects found in a given casting depend on the balance between solidification structures, carbide stability and physical conditions. The distribution of network structures in chill/sand castings illustrates this point. Fig. 87 shows that eutectic cementite was retained at the extremity of the mottle zone in the 1% Si alloy, although surrounded by network structures. Fig. 228 summarises schematically the effect of silicon in chill/sand mould castings. The gradients of the 0-100% decomposition lines indicate variation in cementites stability with composition. Deep chill and mottle penetration found in the 1.0% Si alloy results in slow cooling at high temperatures for large amounts of the metastable eutectic. This factor is balanced by high cementite stability, resulting in relatively incomplete decomposition at the extremity of the chill mottle zone. Lower silicon alloys solidify with less chill and mottle, but have apparently reduced cementite stability, producing large network areas in regions close to the chill. A degree of balance between chill susceptibility and cementite stability may be detected in the occurrence of maximum network structures free from eutectic cementite in the 2.04% Si alloy. The increased chill depth in this alloy may not be fully offset by a corresponding increase in cementite stability, giving rise to an increase in network structures formed by total cementite decomposition at the limit of the mottle zone.

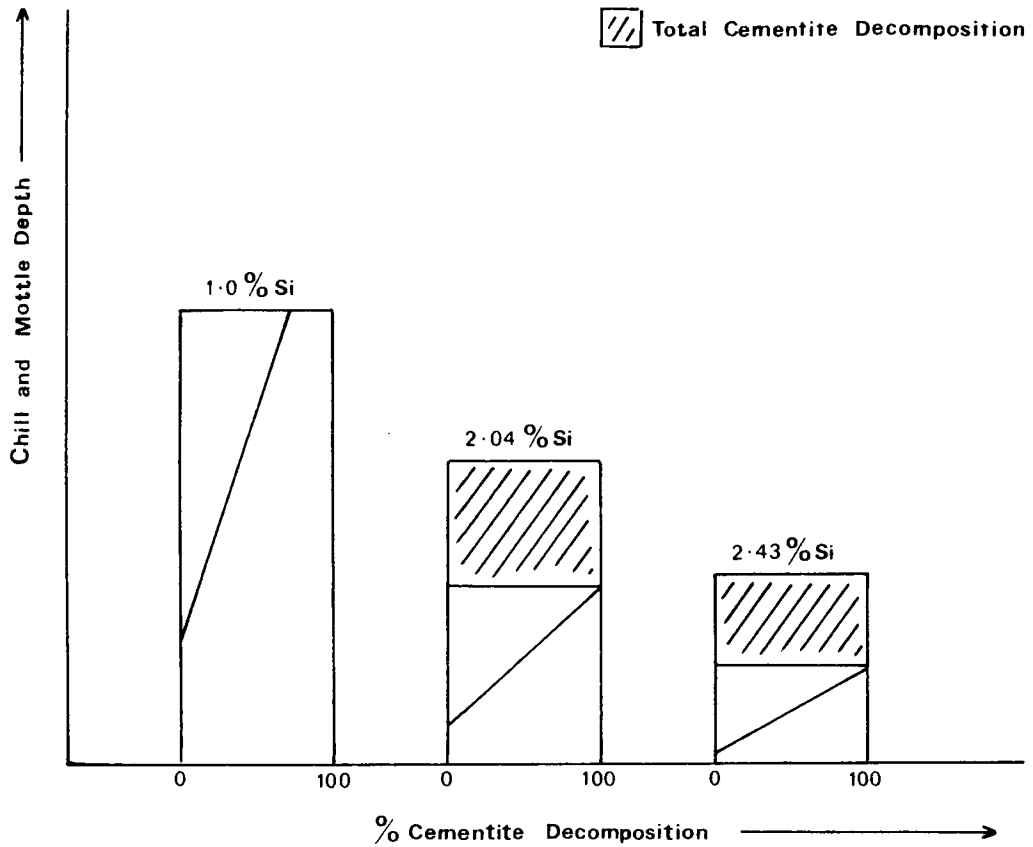


**Fig. 228.** Balance between Solidification and Post-solidification Processes in Chill/Sand Moulds.

[schematic]

Heated metal mould experiments confirmed the general finding that increasing silicon content decreased metastable eutectic stability. In spite of the variations in metastable eutectic morphology and distribution between alloys, the mode of decomposition to form network structures remained similar in all cases.

#### 5.6.4 GRAPHITE NUCLEATION

A pre-requisite for the decomposition of cementite and growth of graphite during solid-state transformation is the formation of a suitable graphite nucleation site. Favoured sites may exist at structural heterogeneities, such as phase interfaces, grain boundaries and free surfaces<sup>(78)</sup>. Apart from free surfaces, such as porosity<sup>(94)</sup> the most favoured sites for graphite deposition appear to be austenite/cementite interfaces<sup>(77)</sup>.

The 'spontaneous' nucleation of graphite at austenite/cementite interfaces is difficult in continuously-cooled castings<sup>(104)</sup>. Such nucleation if at all possible, will be favoured during slow cooling through high temperatures<sup>(87)</sup> as in the outer limits of mottle penetration. It is in these areas, however, that maximum amount of eutectic graphite is available for further carbon deposition and solid-state growth. Nucleation of graphite during cooling through lower temperature ranges is slow or confined to free surfaces and porosity, (Experiments A-E, O. Figs. 123-129, 156, 157.). In real castings these conditions may apply in the lower portions of the mottle zone near the chill. During continuous cooling of mottled structures, the availability of graphite formed during solidification increases as the ease of 'spontaneous' graphite nucleation increases. The presence of graphite formed by solidification may therefore remove the problem of 'fresh' graphite nucleation, at least in the immediate area.

The decomposition process in mottle zones of ceramic and chill/sand castings appears to be highly inhomogeneous. Undecomposed, decomposing and fully decomposed eutectic cementite may be found in close proximity. (Figs. 55,69,110). From the present work, it appears that network structures and the various stages

of cementite wasting are generally associated with adjoining stable eutectic colonies. As the structures involved are three-dimensional, areas of cementite decomposition without apparent relation to graphite may adjoin graphite out of the planar section.

#### 5.6.5 GRAPHITE GROWTH

If secondary mottle structures are closely associated with primary mottle formations, the division between the two forms may not be easily distinguishable. Graphite may form over a continuous range of temperatures, from the start of eutectic solidification, to below the eutectoid. Within a casting solidifying with a mottled structure graphite will form over a range of temperatures from a variable number of nuclei. Undercooling and growth rate will vary during the solidification of an individual eutectic cell, in response to physical and chemical factors resulting from both internal and external sources. Solidification structures in the alloys studied have been classified as flake graphite varying from fine undercooled to coarse A-type flakes. In a real casting containing a mottled zone, the inherent variability of the growth process may continue into solid state transformations. The nature of these reactions in a given casting will depend on the relative dispersion and morphology of the two eutectics, as well as on the stability of eutectic cementite under the physical conditions operating. All these factors are dependent on alloy composition.

Forms of graphite which are of interest from the secondary mottle point of view are found at borders between stable eutectic colonies and ledeburite or network structures. Cementite/graphite contact has been shown to exist at all stages of mottling in the alloys studied. In each case, graphite appeared to conform to eutectic cementite outlines, except where piercing by graphite flake tips occurred. The degree of outlining varied with silicon content, being least in 1.0% Si alloy castings. The more extensive honeycombe structures in higher silicon alloys exhibited a variety of graphite dispersions suggesting different conditions of initial formation or subsequent history. Graphite/cementite

contact was encountered in heated metal mould castings at the highest temperatures for mottle production (Figs. 131, 166-168, 184). This tends to confirm their high temperature origin. Although graphite/cementite contact and out-lining structures could generally be related to areas of cementite degeneration and network structures, they do not necessarily form entirely in the solid state. Graphite films resulting from solidification or co-precipitation from the liquid could act as nuclei for subsequent graphite deposition and cementite decomposition to produce network structures. As the structures under consideration are continuous with both stable and metastable eutectics, several hypotheses may be suggested for their formation. These are outlined below, together with observations as to their possibility under given circumstances. The mechanisms involved are shown schematically in Figs. 229-235.

The presence of considerable amounts of graphite/cementite contact in a given area would appear to preclude straightforward growth competition between the two eutectic forms. If competitive growth occurred, cementite and graphite should be separated by austenite, except perhaps for limited contact between graphite flake tips and eutectic cementite.

Austenite/graphite/cementite ternary structures could form by direct solidification at a solid/liquid interface (Fig. 229). This hypothesis appears unlikely in view of the problem of matching phase growth rates and segregation patterns at the growth front while maintaining the normal ledeburite structure over considerable areas.

An alternative possibility is that the liquid between austenite rods involved in ledeburite solidification approaches the composition of cementite and then precipitates cementite and graphite concurrently (Fig. 230). Under these circumstances, continuing growth of the austenite, accompanied by complete divorcement of the graphite could account for the structures observed<sup>(104)</sup>. This mechanism, which is likely to be highly dependent on composition and segregation within the

ledeburite, could produce graphite/cementite contact over large areas. Graphite deposition might be favoured at cementite/austenite interfaces.

Graphite in the honeycombe regions could nucleate at favoured sites on austenite/cementite interfaces within the ledeburite structure, possibly very soon after the passage of the growth front<sup>(89)</sup>(Fig. 231). Subsequent graphite growth at high temperature would be favoured by attachment of carbon atoms at flake tips<sup>(105)</sup>, producing crystals with close packed basal-plane surfaces with minimum surface energy. Formation along cementite/austenite boundaries could minimise strain energy caused by graphite deposition by enabling creep deformation of austenite and cementite. Polygonisation of the graphite crystals would enable curvature to follow cementite/austenite interface contours, outlining the eutectic cementite structure. Under these circumstances, graphite particles would not necessarily be interconnected or continuous with adjacent graphite colonies formed during solidification.

Solid-state decomposition immediately after solidification could commence at borders with stable eutectic colonies (Fig.232). Graphite formed in the process could penetrate the ledeburite structure along cementite/austenite interfaces. This would produce a completely interlinked graphite skeleton surrounding decomposing cementite. An alternative process, which would not depend so heavily on graphite penetration of the ledeburite structure involves cementite decomposition and deposition of graphite films along the austenite interface. These films could develop into flakes by graphite deposition normal to the basal plane (Fig.233). During subsequent cooling, carbon might be provided by cementite decomposition and deposition from supersaturated austenite. Any hypothesis which relies on graphite nucleation and growth in the solid state at cementite/austenite interfaces is liable to be highly dependent on segregation, which may affect graphite growth or the kinetics of cementite decomposition<sup>(3,102,91)</sup>. The applicability of such mechanisms can only be determined by study on a microscopic scale.

A problem with either method of solid state graphite formation is the production of graphite/cementite contact. Although cementite interfaces are preferred sites for graphite nucleation<sup>(3,77)</sup>, continuing growth of graphite demands cementite dissolution. Consequent austenite production would then separate the two phases. In many cases, outlining graphite occurs in regions from which cementite has totally or partially disappeared (Figs. 56, 70, 75, 99, 110). In these areas, graphite could develop along the outline of the eutectic cementite while causing its simultaneous decomposition (Fig. 234). Coherence of the developing graphite with the original cementite austenite interface implies favoured growth along the original cementite outline rather than along the cementite interfaces developing in the course of decomposition. This might be favoured by segregation factors affecting cementite stability along the original interface<sup>(102)</sup>.

When cementite and graphite are present in the same structure, cementite borders may appear irregular as if eroded (Figs. 83, 93, 99, 102, 145). The outlining graphite may form branches which approach the cementite more closely than the main outlining flake. In Fig. 92, direct contact between cementite and graphite occurs by means of projecting spurs of cementite. The cementite surface between spurs appears eroded. From the present series of experiments, cementite in contact with graphite appears to have a higher stability than that in other areas (Figs. 84, 92, 99, 100, 110, 163). This may result from the absence of austenite with associated segregation<sup>(102)</sup>, acting as a sink for iron atoms liberated by the decomposition process. Graphite/cementite contact areas may therefore be crystallographically coherent or stabilised by some other mechanism, possibly segregation.

Coherence between graphite and cementite could result from carbon deposition in the solid state from supersaturated austenite (Fig. 235). This process would presumably be dependent on segregation patterns within the ledeburite structure. Once stable graphite films nucleated they could develop by growth at basal plane edges and by flake thickening. Graphite at such interfaces would be able to grow

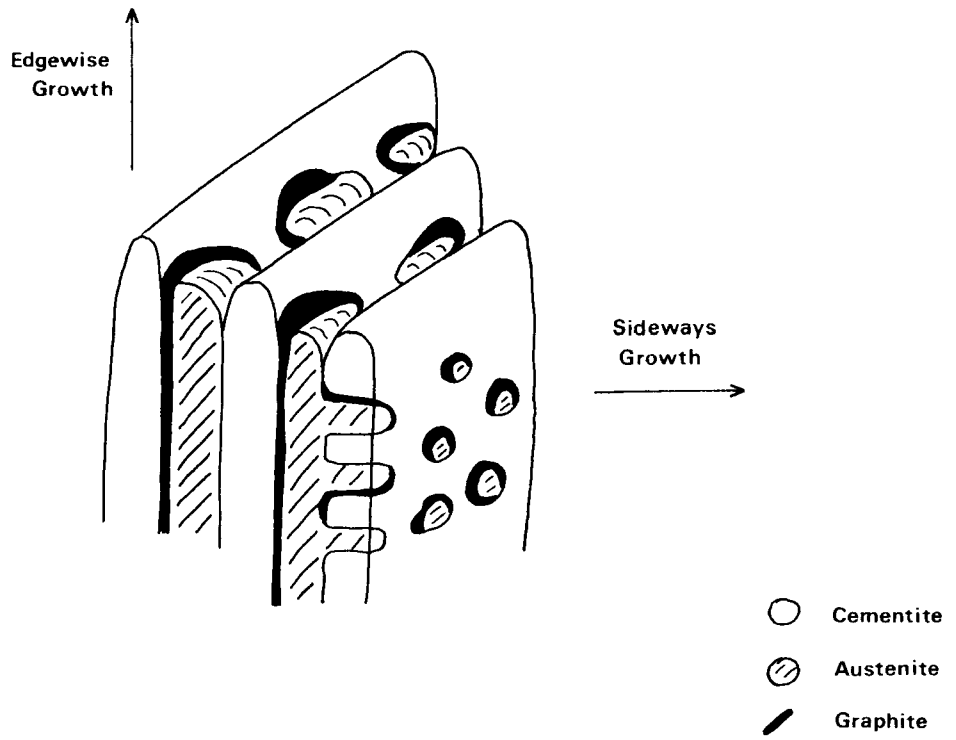


FIG. 229. Cementite/Austenite/Graphite Ternary Solidification.

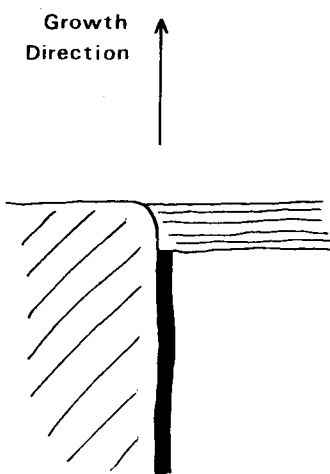


FIG. 230. Graphite/Cementite Coprecipitation.

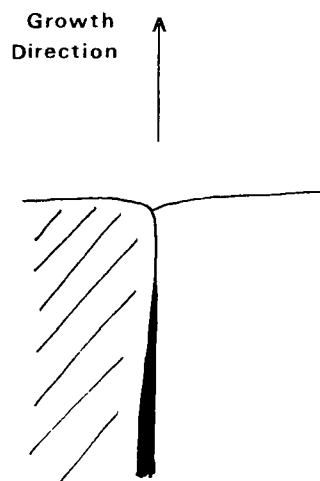


FIG. 231. Decomposition following Growth Front.

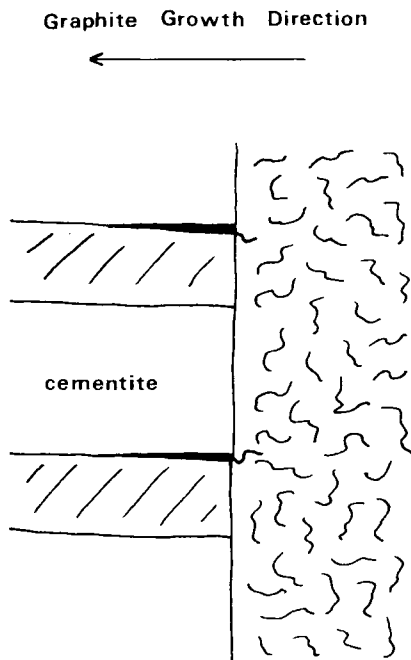


FIG. 232. Graphite Penetration of Ledeburite.

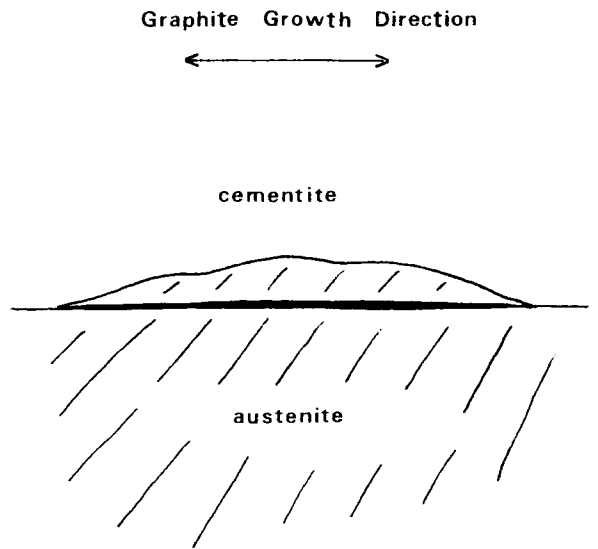


FIG. 233. Graphite Growth and Cementite Decomposition.

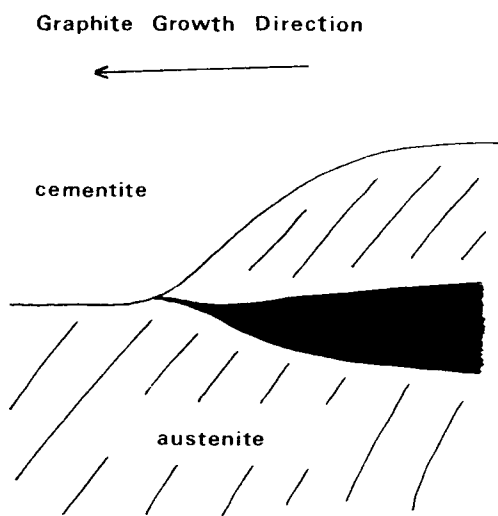


FIG. 234. Graphite Growth and Cementite Decomposition.

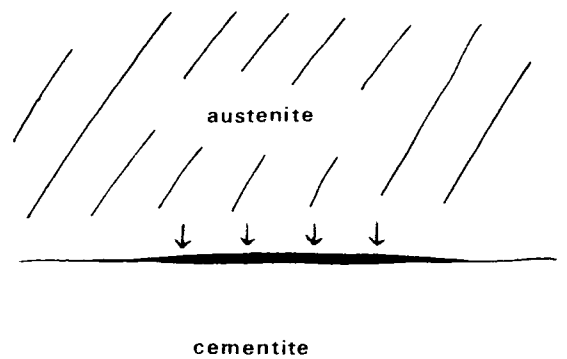


FIG. 235. Nucleation of Graphite by Carbon Deposition from Austenite.

at the expense of neighbouring cementite not in contact with its surface, resulting in an inhomogeneous decomposition process (Figs. 84,102,110).

From the present work, it appears that solid state graphite in continuously cooled samples generally nucleates and grows on or in close proximity to graphite structures formed by solidification. Whatever the means of graphite nucleation just before or after final solidification, subsequent growth may occur by deposition of graphite from austenite at lower temperatures. This will in turn allow decomposition of cementite to form network structures.

Graphite encountered in the mottle areas of the castings studied exhibited structures which reflect the total thermal history of the sample at the position in question. Unless cooling is interrupted, as in the present series of heated metal mould experiments, graphite formed during and immediately after solidification will be overlaid by graphite forming at lower temperatures. Decomposition and corresponding graphite development in the solid state under given physical and chemical conditions may be dependent on position within a mottle area and on the relative dispersion of the two eutectics within that area. Graphite flakes in the peripheries of stable eutectic colonies surrounded by ledeburite may be exposed to greater amounts of carbon deposition than areas within the graphite border, where amounts of decomposing cementite are less (Fig. 96). Flakes within the borders of such graphite colonies may tend to retain their shape during prolonged solid state cooling, while flakes at colony peripheries become coarse and even aggregated (Figs. 97, 105,106,109). A different type of graphite growth may be found in the upper regions of mottle zones, especially in areas containing cementite needles. In these areas, cementite laths are surrounded by graphite and secondary sideways development of ledeburite may be limited. Carbon deposition on existing graphite may produce thickened border flakes, which may become coherent enough to form aggregated walls around needle areas (Figs. 70,91,112-114). Aggregation of flakes during slow cooling appears to be more likely when inter-flake distances are small, as in the undercooled graphite areas of 2.04% and 2.43% Si alloys.

The morphology of graphite formed in the solid state is dependent on temperature<sup>(106)</sup> and alloy composition<sup>(80)</sup>. An additional factor in the present case is the morphology and characteristics of the mottle structures and graphite nucleation substrate. Results from heated metal mould experiments indicate that growth by carbon deposition at graphite flake tips increases more rapidly with temperature than growth normal to the basal plane (cf Figs. 125 & 131; 157, 159 & 168a, 179). This is in agreement with previous work on malleablising<sup>(106)</sup>.

The increase in the ease of solid state graphitisation with increasing silicon was accompanied by a refinement of solid state graphite in the metal mould experiments (Figs. 132, 179). This result is contrary to work on malleable irons<sup>(80)</sup>. The change in morphology with increasing silicon may result in part from the limitation of the heated mould method in studying high temperature processes in alloys where stable and metastable nucleation ranges are closely spaced. As graphite formed by solidification may act as a nucleation substrate for solid state growth, a source of the difference may lie in refinement of the stable eutectic during solidification. Hultgren and Ostberg<sup>(105)</sup>, however, reported that graphite form during malleablising is not dependent on nucleation so much as the subsequent growth conditions, which in turn vary with temperature, composition and annealing atmosphere. An alternative possibility is that decreased cementite stability in alloys with higher silicon content may enable refined rapid growth from the multiple undercooled flake nucleation centres.

#### 5.6.6 SUMMARY

Final structures in chill/sand and ceramic mould castings of the alloys studied appear to result from a series of transformations both during solidification and in the solid state. Solid state decomposition of eutectic cementite may be revealed as 'network' structures by the appropriate etching technique. The form and occurrence of such networks depends on alloy composition. This not only determines chill and mottle depth and hence the physical conditions under which the mottle zone cools, but markedly affects cementite stability. Increasing silicon content decreases chill penetration, but at the same time decreases

eutectic cementite stability and may lead to a greater amount of decomposition in the mottle zone.

Graphite formed by deposition of carbon from austenite appears to nucleate on or near graphite formed during solidification. Growth at high temperatures either during or soon after solidification may give rise to a wide range of mottle structures in which graphite/cementite contact may occur. Cementite in contact with graphite appears to be stabilised during solid state transformations. Graphite encountered in the mottle zones of the castings studied may represent the result of successive graphite depositions both during solidification and over a range of temperatures in the solid state. The extent to which a particular graphite form predominates at any point in the microstructure may depend on both compositional and structural factors. Alloy composition determines cementite stability under the physical conditions in question, as well as affecting graphite form and the relative morphology of the two eutectics. The interruption of transformations in the heated mould experiments enabled study of the production of network structures. The technique also provided information regarding variation of graphite growth morphology and cementite stability in limited high temperature ranges. This avoided some of the structural complications produced by continuing decomposition and graphite deposition on existing structures during continuous cooling. The decrease found in cementite stability with increasing silicon content and temperature is in agreement with previous results<sup>(101,102,87)</sup>. Changes in graphite morphology with increasing temperature follow tendencies observed in previous work<sup>(105)</sup>, while the general refinement of solid state graphite with increasing silicon contradicts certain malleablising literature<sup>(80)</sup>.

#### 5.7 INFLUENCE OF SOLUTE ELEMENTS OTHER THAN SILICON

In view of the difficulties in comparing elemental additions set out in Section 4.6.1, classification of elemental effects can only be made in general terms, outlining possible interactions and influences on nucleation and growth. The classification of elements as graphite promoters or carbide stabilisers has

been shown to be more complex in heated ceramic mould castings than would be suggested by examination of fracture surfaces. A more concise classification could be based on clear chill depth, which is a measure of the ease of graphite nucleation and growth at high cooling rates; and the depth of cementite penetration into the test bar, which indicates the extent to which carbide solidification is stabilised. These parameters do not follow the same pattern in the elements used in this study. The microstructural measurements of Fig. 207 show the relative effects of additions to be (in increasing order):

depth of clear chill: Mg; Al; Base alloy (2.04% Si); Sr; Ca; Ti; Bi; Te.

depth of mottle; Al; Base alloy; Mg; Bi; Ti; Sr; Ca; Te.

Only the ferritic matrix structures of the aluminium treated specimens and the graphite forms of the samples with tellurium additions were not found at any point in the base alloy castings. The other elemental additions only influenced the relative extent and distribution of structures found in base alloy specimens. These effects will only apply at the concentrations and under the conditions being studied.

The graphitising effect of aluminium was as noted in other publications. A feature of the structure was the change in sulphide inclusion shape, from the idiomorphs of the base alloy (Fig. 74) to more rounded forms (Fig. 209). This transition was noted by Williams<sup>(68)</sup> who postulated reaction with oxygen to account for the graphitising effect of aluminium. The full role of oxygen in determining cast iron structures is however by no means clear<sup>(94)</sup>.

The promotion of a ferritic matrix in regions containing undercooled graphite may be due to reaction of aluminium with nitrogen, an element which has been shown to be a carbide stabiliser<sup>(107)</sup>. Formation of aluminium nitride may effectively remove nitrogen from solution in the metal<sup>(108)</sup>. Amounts of pearlite in the matrix further from the chill may result from coarsening of austenite and graphite which increases the diffusion distance for carbon deposition.

Tellurium is an extremely powerful carbide stabiliser. Nieswaag & Zuithoff<sup>(58)</sup> confirmed its surface activity, reporting a strong decrease in iron surface tension on alloying with tellurium. This was considered to result in the adsorption of tellurium at the growing tips of graphite flakes, thus impeding the addition of carbon atoms from the melt. The effect was said to be the same as a decrease in the diffusion coefficient in Jackson & Chalmers' equation (p.9), namely a refinement of the graphite eutectic. The retardation of graphite growth rates enabled undercooling to produce metastable solidification.

The direct influence of tellurium on graphite growth was questioned by Heine<sup>(104)</sup>, who attributed its marked carbide stabilising effect to depression of the growth temperature of austenite during both proeutectic and eutectic solidification. If austenite growth is retarded under given physical conditions, the melt may only reach eutectic composition and begin to solidify after undercooling below the temperature at which metastable eutectic may be nucleated.

Film, lacy and Widmanstätten graphite in tellurium-treated castings were said to result from solid-state graphitisation<sup>(76)</sup>. This effect was especially noticeable at silicon contents above 2%<sup>(104)</sup>. Graphite morphologies found in the tellurium-treated heated ceramic mould castings (Figs. 215-219) were similar to those listed by Loper & Heine<sup>(76)</sup>. The concentration of the various graphite forms into limited areas of mottle containing interconnected graphite (Fig. 215) may indicate a relationship between the various growth forms. Such mottled areas may result from a single nucleation event and transition from fine curled flake masses through curled outlining flakes to graphite films with decreasing temperature of formation. The process of forming these structures might be exactly analogous to that operating in the mottle zone of the base alloy castings, with graphite forming in both liquid and solid states. If the fine curled flake masses form during eutectic solidification, the highest temperature decomposition product would appear to be the curled flakes loosely outlining the ledeburite structure at the flake mass borders (Fig. 216). This could result from high temperature

decomposition, where growing graphite follows the cementite/austenite surface which recedes by cementite solution. The resultant graphite would be kinked as shown in the figure. Loops could form by graphite encirclement of cementite particles which subsequently decomposed. The interdependence between graphite film thickness and the amount of residual cementite in the outlining areas of Fig. 220, suggests solid-state graphitisation, but does not reveal whether the film nucleated in the liquid or solid states. The continuity of graphite in these regions implies uniform interface nucleation or growth conditions within restricted areas.

The presence of large multiphase inclusions in all parts of tellurium-treated specimens indicates formation in the liquid phase by reaction of tellurium with Mn, Fe, P, Si and S. The behaviour of tellurium in forming inclusions resembles that of selenium. Gagnebin<sup>(109)</sup> investigated the effect of selenium additions on inclusions in steel castings. He concluded that selenium promoted sulphide rejection from solution before solidification was complete. In cast irons, selenium is largely removed from solution by reaction with manganese forming selenides<sup>(104)</sup>. The effect of tellurium in removing large amounts of minority elements from solution should be remembered in assessing its final effect on microstructure and casting properties.

### 5.8 NUCLEATION AND GROWTH AT CHILL SURFACES

The physical and chemical properties of structures occurring at casting surfaces may be of considerable practical importance. An interesting feature of this work has been the structural variations occurring near chill surfaces.

Zhukov et al<sup>(110)</sup> have recently published results from pure eutectic Fe-C, melted under argon and cast into 4 mm cylindrical chill moulds. A layer near the casting surface contained primary cementite needles aligned parallel or at very shallow angles to the chill. The primary cementite laths were separated by thin layers of austenite. The austenite films nucleated austenite dendrites which supplanted cementite as primary phase at positions removed from the casting

surface. Non-faceted cementite growth was noted in several areas, giving rise to bent primary crystals.

Structures similar to those of Zhukov et al<sup>(110)</sup> were noted in the present work (Figs. 199 & 200). An important difference between the results was the distribution of areas containing primary cementite. These formed a continuous layer at the casting surface in the eutectic alloy<sup>(110)</sup>, but were limited to spherulite centres and radial arms in the hypoeutectic (C.E. 4.0) alloy of the present work. This may indicate the need for greater undercooling to form primary cementite at reduced carbon content. Zhukov et al cited Lakeland and Hogan's theory of the coupled zone concept as applied to iron-carbon alloys<sup>(44)</sup> as being contrary to their experimental results. Lakeland & Hogan, however, only considered the stable austenite-graphite eutectic system in their work and did not extend it to cover the metastable system. Zhukov's work and the present result suggest that the coupled zone for metastable eutectic growth may be positioned differently to that of the stable system.

The influence of pouring temperature on chill casting structure (Fig. 185) agrees with the work of Hughes on chill effects<sup>(73)</sup>. This has been outlined before in relation to eutectic solidification, but is equally applicable to austenite dendrite solidification under chill influences.

Specimens with added tellurium poured at 1400°C had surface (Fig. 205) and internal (Fig. 203) structures which were found in base alloy castings poured at higher temperatures. This supports the depression of proeutectic and eutectic solidification temperatures by tellurium addition, since depression of the solidification temperature in a chill casting will have an effect equivalent to raising superheat.

## CONCLUSIONS

1. A continuously decreasing cooling rate through the eutectic solidification range can be obtained by using hot ceramic moulds with a water cooled copper chill. Chill and mottle depths within such castings provide a clearer guide to solidification behaviour of cast irons than could be produced in castings where competition between chill and mould cooling may result in discontinuous heat flow situations.

2. Increasing silicon content at constant carbon equivalent changes graphite morphology in the mottle zone from coarse to undercooled flakes, while decreasing susceptibility to metastable solidification. Increased separation between stable and metastable eutectic nucleation temperatures with increasing silicon may enable refined graphite growth at greater undercooling without metastable eutectic formation.

3. Eutectic cementite decomposition occurring in the transition zone between the stable and metastable eutectics may be revealed as network structures by etching in alkaline sodium picrate or bromine.

4. The processes determining final cast structures in the mottle zones of the alloys and cooling systems studied do not cease with solidification. Cast structures of many cast irons must be viewed as the product of a continuous process which commences with solidification and continues during cooling in the solid state.

5. Cementite decomposition in the mottle zone during continuous cooling after solidification appears to be often closely associated with graphite formed during solidification.

6. Increasing silicon content at constant carbon equivalent reduces chill and mottle depth in a given cooling situation. It also decreases eutectic cementite stability and increases the probability of secondary mottle formation under given

solid state cooling conditions.

7. Metastable eutectic nucleation and growth under conditions of high temperature gradient and cooling rate at the chill surface differ from those found in the body of the casting. Solidification commences at the chill surface, producing structures with centres and radial arms consisting of primary cementite needles with interspersed degenerate eutectic and austenite films. These regions give way to acicular metastable eutectic with primary austenite in areas between radial arms and at positions removed from immediate chill influence.

## REFERENCES

- Ref.  
No.
- 1 HILLERT. M.  
'RECENT RESEARCH IN CAST IRON'  
GORDON & BREACH. N.Y. 1968.
  - 2 BRIGHAM, R., PURDY, G. & KIRKALDY, J.  
J. PHYS. CHEM. SOLIDS. 1967. Suppl. 1. 161.
  - 3 LEVI, L. & STAMENOV. S.  
RUSSIAN CASTINGS PRODUCTION. 1967. (5). 221.
  - 4 OLDFIELD, W.  
B.C.I.R.A. JOURNAL. 1962. 10. 17.
  - 5 OLDFIELD, W.  
B.C.I.R.A. JOURNAL. 1960. 8. 177.
  - 6 SNAGOVSKI, V., LUCHIN, L., MALIK, I. & TARAN. N. YU.  
SBORNIK. TRUDOV. INST. CHERN. MET.  
MINISTERSTVA. CHERN. MET. SSR. 1970. 38. 71.
  - 7 DRAPAL, S.  
SLEVARENSTVI. 1969. (11). 443
  - 8 HULTGREN. A., LINDBLOM, Y. & RUDBERG. E.  
J.I.S.I. 1954. 176. 365.
  - 9 SAMARIN, A.  
J.I.S.I. 1960. 200. 95.
  - 10 IVANOV. D.  
T.A.F.S. 1962. 70. 871.
  - 11 VERTMAN, A. & SAMARIN, A.  
PROC. ACAD. SCI. of the U.S.S.R.  
(PHYS. CHEM. SECT.) 1960. 134. 895.
  - 12 NAKAGAWA, Y. et al.  
TRANS. JAPAN INST. METALS. 1968. 9.(1) 62.
  - 13 WILLIAMS, W.  
METALLURGIA. 1955. 51. 273.
  - 14 BOYES, J. & FULLER, A.  
B.C.I.R.A. JOURNAL. 1964. 12. 424.
  - 15 PATTERSON, W.  
T.A.F.S. 1962. 70. 176.
  - 16 PIWORWASKY, E.  
T.A.F.A. 1926. 34. 914.
  - 17 HUGHES, I.  
J. AUST. INST. METALS. 1965. 10. 4.

- 18 LAKELAND, K.  
B.C.I.R.A. JOURNAL. 1964. 12. 634.
- 19 KOVES, G. & MONDOLFO, L.  
J.I.S.I. 1964. 202. 424.
- 20 LOPER, C. et al.  
'RECENT RESEARCH IN CAST IRON'  
GORDON & BREACH. N.Y. 1968.
- 21 MASSARI, S. & LINDSEY, R.  
T.A.F.A. 1941. 49. 953.
- 22 SCHNEBLE, A. & CHIPMAN, J.  
T.A.F.A. 1944. 52. 113.
- 23 EASH, J.  
T.A.F.A. 1941. 49. 887.
- 24 LUX, B. & TANNENBURGER, H.  
T.A.F.S. 1962. 70. 129.
- 25 KIEL, O. VON et al  
ARCH. FUR. EISENHUTTENWESEN. 1934. 7. 579.
- 26 LUX, B.  
MODERN CASTINGS. 1964. 45. 222.
- 27 ZUTHOFF, A. & KORTMULDER, R.  
GIESSEREI. 1964. 14. 135.
- 28 LUX, B.  
**32nd** INTERNAL FOUNDRY CONGRESS. WARSAW. 1965.
- 29 MORROGH, H. & WILLIAMS, J.  
J.I.S.I. 1947. 155. 321.
- 30 LOPER, C. & TAKIZAWA, N.  
T.A.F.S. 1964. 72. 520.
- 31 MORROGH, H.  
BRITISH FOUNDRYMAN. 1960. 53. 221.
- 32 PATTERSON, W. & AMMANN, D.  
GIESSEREI. 1959. 23. 1247.
- 33 GITTUS, J.  
J.I.S.I. 1959. 192. 118.
- 34 PATTERSON, W. BRAND, H.  
GIESSEREI. 1963. 15. 137.
- 35 BHATTACHARJEE, A. & BANERJEE, P.  
FOUNDRY. 1970. 98. 1058.
- 36 MASCRE, C.  
MEM. SCI. REV. METALLURGIE. 1971. 68. 131.
- 37 LUX, B.  
'RECENT RESEARCH IN CAST IRON'  
GORDON & BREACH. N.Y. 1968.

- 38 HILLERT, M. & STEINHAUSER, H.  
JERNKONTORES ANN. 1960. 144. 520.
- 39 CHALMERS, B.  
'PRINCIPLES OF SOLIDIFICATION'  
Pub. J. WILEY. 1964. Ch. 6.
- 40 WILKINSON, M. & HELLAWELL, A.  
B.C.I.R.A. JOURNAL. 1963. 11.(4). 439.
- 41 ORON, M. & MINKOFF, I.  
'RECENT RESEARCH IN CAST IRON'  
GORDON & BREACH. N.Y. 1968.
- 42 MINKOFF, I. & LUX, B.  
A.F.S. CAST METALS RESEARCH JOURNAL. 1970. 6.(4).181.
- 43 HILLERT, M. & SUBBA RAO, V.  
'SOLIDIFICATION OF METALS'  
J.I.S.I. LONDON. 1968.
- 44 LAKELAND, K. & HOGAN, L.  
'SOLIDIFICATION OF METALS'  
J.I.S.I. LONDON. 1968.
- 45 ROLL, F. GESSEREI. 1928. 15. 1270.
- 46 BUNIN, K. LIT. PROIZV. 1953. 4. (9) 21.
- 47 OLDFIELD, W. & MORROGH, H.  
IRON & STEEL. 1959. 32. 431 & 479.
- 48 MORROGH, H.  
J.I.S.I. 1968. 206. 1.
- 49 GADGIL, V. & KONDIC, V.  
BRITISH FOUNDRYMAN. 1969. (OCT) 392.
- 50 A.S.T.M. STANDARD SPECIFICATION. 1947. A.247.
- 51 GUNNARSON, S.  
BRITISH FOUNDRYMAN. 1958. 61. 279.
- 52 DJIDJEV, J.  
35th INTERNATIONAL FOUNDRYCONGRESS  
KYOTO. OCT. 1968.
- 53 CHARBONNIER, J. & MARGERIE, J.  
'RECENT RESEARCH IN CAST IRON'  
GORDON & BREACH. N.Y. 1968.
- 54 MERCHANT, H.  
T.A.F.S. 1962. 70. 973.
- 55 MERCHANT, H.  
'RECENT RESEARCH IN CAST IRON'  
GORDON & BREACH. N.Y. 1968.
- 56 GARBER, S.  
J.I.S.I. 1955. 179. 147.

- 57 HEISTERKAMP, F. & LCHBERG, K.  
ARCHIV. FUR. EISENHUTTENWESEN. 1966. 37. 813.
- 58 NIESWAAG, H. & ZUITHOFF, A.  
34th INTERNATIONAL FOUNDRYCONGRESS. PARIS. 1967.
- 59 LAKELAND, K. & HOGAN, L.  
'RECENT RESEARCH IN CAST IRON'  
GORDON & BREACH. N.Y. 1968.
- 60 LIPSON, H. & PETCH, N.  
J.I.S.I. 1940. 142. 95.
- 61 PETCH, N.  
J.I.S.I. 1944. 149. 42.
- 62 BROWN, B. & HAWKES, M.  
T.A.F.S. 1951. 59. 181.
- 63 BRIGHAM, R. et al  
CANADIAN MET. QUART. 1964. 3. 239.
- 64 OKAMOTO, T. & MATSUMOTO, H.  
IMONO. 1970. 42.(2). 104.
- 65 FULLER, A. & HUGHES, I.  
B.C.I.R.A. JOURNAL. 1958. 7. 288.
- 66 BUNIN, K.  
METAL SCIENCE & HEAT TREATMENT. 1961. 9,10. 384.
- 67 MORROGH, H. & TUTSCH, P.  
J.I.S.I. 1954. 176. 382.
- 68 WILLIAMS, W.  
J.I.S.I. 1950. 164. 407.
- 69 SCHEIL, E. & POHL, D.  
ARCH. FUR. EISENHUTTENWESEN. 1955. 26. 105.
- 70 RICKARD, J. & HUGHES, I.  
B.C.I.R.A. JOURNAL. 1961. 9. 11.
- 71 LEVI, L. & STAMENOV, S.  
RUSSIAN CASTINGS PRODUCTION. 1967.(5). 221
- 72 MALINCHKA, Ya.N.  
RUSSIAN CASTINGS PRODUCTION. 1963.(1). 23.
- 73 HUGHES, I.  
B.C.I.R.A. JOURNAL. 1957. 7. 10.
- 74 DILEWIJINS, J. & DEFRANCO, C.  
33rd INTERNATIONAL FOUNDRY CONGRESS. DEHLI. 1966.
- 75 KAMENSKY, R. & PISKOR, J.  
SLEVARENSTVI. 1967 (12). 496.
- 76 LOPER, C. & HEINE, R.  
T.A.F.S. 1961. 69. 583.

- 77 WALKER, B. & KONDIC, V.  
J.I.S.I. 1962. 200. 1037.
- 78 TKACHENKO, F.K.  
RUSSIAN CASTINGS PRODUCTION. 1962.(5). 235.
- 79 TKACHENKO, F.K. & TKACHENKO, T.  
RUSSIAN CASTINGS PRODUCTION. 1966.(4). 173.
- 80 BURKE, J. & SWINDELLS, N.  
'RECENT RESEARCH IN CAST IRON'  
GORDON & BREACH. N.Y. 1968.
- 81 BARANOV, A.  
RUSSIAN CASTINGS PRODUCTION. 1967.(2). 96.
- 82 HULTGREN, A. & OSTBERG, G.  
J.I.S.I. 1954. 176. 351.
- 83 MITSCHKE, R. et al  
GIESSEREI-FORSCHUNG. 1969. 21. 73.
- 84 HUGHES, I.  
'SOLIDIFICATION OF METALS'  
J.I.S.I. LONDON. 1968.
- 85 MORROGH, H.  
B.C.I.R.A. JOURNAL. 1955. 5. 655.
- 86 BERMAN, A. & KONDIC, V.  
J.I.S.I. 1954. 176. 385.
- 87 HARRIS, J. & KONDIC, V.  
FOUNDRY TRADES JOURNAL. 1957. 102. 267 & 311.
- 88 OLDFIELD, W.  
B.C.I.R.A. JOURNAL. 1959. 7. 844.
- 89 FREDRIKSSON, H. & HILLERT, M.  
BRITISH FOUNDRYMAN. 1971. 64.(2). 54.
- 90 MORROGH, H.  
J.I.S.I. 1941. 207.
- 91 MORROGH, H.  
J.I.S.I. 1946. 154. 399.
- 92 LARSON, W. et al  
MODERN CASTINGS. 1959. 35. 48.
- 93 HULTGREN, A.  
T.A.S.S.T. 1929. 16. 227.
- 94 HUGHES, I.  
T.A.F.S. 1969. 77. 121.
- 95 GADGIL, V.  
M.Sc. THESIS. INDUSTRIAL METALLURGY.  
BIRMINGHAM UNIVERSITY. 1969.
- 96 WILLIAMS, W.  
B.C.I.R.A. JOURNAL. 1952. 4. 403.

- 97 VASCHENKO, K. & RUDOI, A.  
T.A.F.S. 1962. 70. 855.
- 98 DRUYAN, M.  
RUSSIAN CASTINGS PRODUCTION. 1969. (12). 550.
- 99 HEINE, F.  
A.F.S. CAST METALS RESEARCH JOURNAL. 1970.(JUNE).49.
- 100 OWEN, W.  
J.I.S.I. 1951. 167. 117.
- 101 SATO, T. et al  
J. JAPAN INST. METALS. 1955. 19.(5).445.
- 102 PHELPS, W.  
'RECENT RESEARCH IN CAST IRON'  
GORDON & BREACH. N.Y. 1968.
- 103 SANDOZ, G.  
'RECENT RESEARCH IN CAST IRON'  
GORDON & BREACH. N.Y. 1968. P.475.
- 104 HEINE, R.  
A.S.M. TECHNICAL REPORT. 1969. P.9-41.3.
- 105 HEINE, R.  
PRIVATE COMMUNICATION.
- 106 HULTGREN, A. & OSTBERG, G.  
J.I.S.I. 1954. 176. 351.
- 107 DAWSON, J. et al  
B.C.I.R.A. JOURNAL. 1953. 4. 540.
- 108 MOUNTFORD, F.  
BRITISH FOUNDRYMAN. 1965. 59. 141.
- 109 GAGNEBIN, A.  
T.A.F.S. 1947. 55. 277.
- 110 ZHUKOV, A. et al  
IZV. AK. NAUK. SSSR METALLY. 1970. NOV.-DEC. (6). 176.